2013-01-01

Depositional Setting And Sequence Stratigraphic Analysis Of The Lower Permian Lower Hueco Formation On The Western Margin Of The Orogrande Basin, South Central New Mexico

Jonathon Eric Stautberg
University of Texas at El Paso, jestautberg@miners.utep.edu

DEPOSITIONAL SETTING AND SEQUENCE STRATIGRAPHIC ANALYSIS OF THE LOWER PERMIAN LOWER HUECO FORMATION ON THE WESTERN MARGIN OF THE OROGRANDE BASIN, SOUTH CENTRAL NEW MEXICO.

JONATHON ERIC STAUTBERG

Department of Geological Sciences

APPROVED :

Katherine A. Giles, Ph.D., Chair

Richard P. Langford, Ph.D.

Greg H. Mack, Ph.D.

Benjamin C. Flores, Ph.D.

Dean of the Graduate School

DEDICATION

This work is dedicated to all of my family and friends who supported my desire for science and enabled me to furthered my education in a field that I am so passionate towards.

DEPOSITIONAL SETTING AND SEQUENCE STRATIGRAPHIC ANALYSIS OF THE LOWER PERMIAN LOWER HUECO FORMATION ON THE WESTERN MARGIN OF THE OROGRANDE BASIN, SOUTH CENTRAL NEW MEXICO.

BY

JONATHON ERIC STAUTBERG, B.S.

THESIS

Presented to the Faculty of the Graduate School of

The University of Texas at El Paso

In Partial Fulfillment

of the Requirements

for the Degree of

MASTER OF SCIENCE

Department of Geological Sciences

THE UNIVERSITY OF TEXAS AT EL PASO

December 2013

ACKNOWLEDGMENTS

I would like to begin by thanking the Institute of Tectonic Studies for Salt-Sediment Interaction at the University of Texas at El Paso, as well as the American Association of Petroleum Geologists William J. Barrett Family Grant, the Southwest Section of the American Association of Petroleum Geologists, and the Geological Society of America for providing generous funding for this research project.

Most of all I want to acknowledge Dr. Katherine Giles for her undeniable expertise in sedimentology and stratigraphy, providing the necessary tools and support for myself to complete this project and develop into a research scientist and a professional geologist. I thank you dearly for the education you have provided me with and the avenues that are now open for my career. I would also like to acknowledge Dr. Greg Mack for being an exceptional teacher, geologist, mentor, and friend while we traversed across the peaks and valleys of the Robledo Mountains, measuring sections, collecting samples, and helping me become the geologist and person I am today. I have no doubt in my mind that working with you two was one of the best choices I have ever made, and feel incredibly lucky to have had this opportunity.

In addition I would like to thank Dr. Richard Langford and Dr. Tim Lawton, two exceptional geologists that sparked questions and expanded my curiosity towards all aspects of geology, science, and life through being exceptional educators. Also, this would not be possible without the help of all of the students I worked with and taught at both the University of Texas at El Paso and New Mexico State University. In particular I thank Sean Gaynor, Evey Gannaway and Bill Schellenbach for the lifelong memories and friendships that we now share. Special thanks also go out to Nila Matsler for providing unlimited logistical help over the past few years.

Lastly, I thank my parents, Frank and Kathy, and brother Eugene for the years of love and support for anything and everything I chose to peruse. I am incredibly grateful for this and words cannot express my feelings towards you guys. Finally, I thank my girlfriend of 4 years, Mallorie, for putting up with me living 800 miles away and still supporting all of my decisions. Regardless, my education and future would not be possible without the help from not only the people mentioned here but everyone I have worked with and learned from over the past 25 years. Thank you everyone.

ABSTRACT

On the western margin of the Orogrande Basin in south-central New Mexico, eight outcrop datasets, in the form of measured stratigraphic sections from the lower interval of the Lower Permian Lower Hueco Formation were analyzed in regard to depositional facies distribution and sequence stratigraphy. Based on petrographic analysis of 247 samples and associated field relationships, 11 depositional facies are recognized: 1) quartz sandstone, 2) quartz siltstone and shale, 3) fenestral dolomudstone, 4) microbial intraclast packstone, 5) dolomudstone, 6) green-algal packstone to grainstone, 7) ostracode foram wackestone, 8) oolitic packstone, 9)fossiliferous packstone and grainstone, 10) fusulinid packstone and grainstone, 11) phylloid algal bafflestone. The spatial and temporal distribution of these lithofacies was used to develop 4 depositional facies associations that describe their relative position on the Wolfcampian depositional profile: 1) shoreface siliciclastics, 2) supratidal carbonate, 3) intertidal carbonate, and 4) subtidal carbonate. Waltherian transitions between these lithofacies and subsequent depositional facies associations suggests this margin of the Orogrande Basin existed as a shallow marine carbonate ramp, deepening to the east during the early Wolfcampian. Phylloid algal bioherms form thin, isolated buildups locally concentrated in the Robledo Mountains while the remaining depositional ramp is dominated by wide facies belts of supratidal carbonate, intertidal carbonate and subtidal carbonate environments. Deposition of these lithofacies was mainly controlled by changes in relative sea level with little effect from local subsidence as compared to the eastern margin of this basin.

Sequence stratigraphic analysis of this region shows two distinctive third-order depositional sequences (Sequence 1 and Sequence 2) within the lower member of the Hueco Limestone. Sequence 1 is bounded at its base by a regionally extensive Type 1 sequence

boundary that represents a regional unconformity at the Pennsylvanian-Permian boundary across the Orogrande Basin. Highstand systems tract deposition during Sequence 1 are characterized by thick fourth-order highstand systems tracts composed of aggradational and progradational peritidal carbonate cycles with very thin to absent transgressive systems tracts composed of 1 or 2 subtidal carbonate cycles. The upper boundary surface of Sequence 1 is also a Type 1 sequence boundary that forms a distinctive erosive unconformity with an incised valley filled with estuarine marine siliciclastic in the Robledo Mountains.

Sequence 2 in the lower Hueco member begins with fluvial incision forming an incised valley on the shelf and early transgressive estuarine shoreface siliciclastics backfilling the incised valley during the late stage of sea-level lowstand. Phylloid algal bioherms are only present in one stratigraphic interval in Sequence 2 and represent transgressive deposits related to increased rates of sea-level rise and initial development on antecedent topographic highs created by differential compaction of lowstand shoreface siliciclastics. Sequence 2 is characterized by transgressive and highstand subtidal carbonate and subtidal carbonate bioherm cycles, suggesting higher average sea level compared to Sequence 1. Peritidal cycles are still present but are confined to exposures in the Robledo Mountains to the west. Sequence 2 is also capped with another Type 1 sequence boundary with fluvial incision from the overlying sequence. The fluvial incision is consistent with another incised valley filled with late lowstand estuarine shoreface siliciclastics. These shoreface siliciclastics represent the transition into the upper interval of the lower Hueco member of the Hueco Limestone in the Robledo Mountains.

TABLE OF CONTENTS

LIST OF FIGURES

Page

LIST OF PLATES

Chapter 1

INTRODUCTION

Phylloid algal buildups are organic carbonate accumulations or "reefs" that were globally abundant in shallow marine environments during the Carboniferous and Permian. In particular, these carbonate buildups are common in the Midcontinent and Southwestern United States and have been well studied in both outcrop and subsurface studies (e.g., Heckel and Cocke, 1969; Heckel, 1972; Erxleben, 1975; Wermund, 1975; Toomey, 1976, 1981; Wahlman, 2002, and others). However, despite their abundance during the late Paleozoic, the growth morphology and depositional controls that led to large scale phylloid algal buildups are yet to be fully understood. What is understood however, is that secondary porosity from algal plate dissolution permits these buildups to form widespread petroleum reservoir rocks in the United States (Permian and Paradox basins), Russia (Russian Platform and Ural Trough), and Kazakhstan (Pricaspian Basin) (Wahlman, 2002). Because of their importance to hydrocarbon exploration and production, an increased understanding of the depositional controls on and stratigraphic distribution of phylloid algal buildup development is needed.

New work focused at studying outcrop exposures through petrographic analysis, lithofacies interpretation, and depositional environment distribution, will enhance the understanding of the spatial and temporal evolution of phylloid algal buildups within the associated stratigraphic architecture. This would prove useful for developing more effective hydrocarbon exploration and production strategies in regions where phylloid algal buildups and adjacent stratigraphy represent the targeted reservoirs. Additionally, understanding these controls provides more insight into regional tectonic and stratigraphic evolution of the basins containing

phylloid algal builds and the evolution of reef communities through time. Consequently, this research focuses on determining the depositional controls on Lower Permian phylloid algal mounds on the western margin of the Orogrande Basin in both New Mexico and west Texas. Detailed description and interpretation of depositional lithofacies associations and a regional sequence stratigraphic framework provide the necessary criteria to recognize these controls.

1.1 Phylloid Algal Buildups

Wahlman (2002) classified late Paleozoic carbonate buildups into five main types: 1) phylloid algae, 2) calcareous sponge and algae, 3) palaeoaplysina, 4) fenestrate bryozoan and *Tubiphytes*, and 5) siliceous sponge and bryozoa. Phylloid algae and paleoaplysinid have become recognized as the reef builders of the late Paleozoic and petroleum exploration in strata of this age has increased the need for detailed petrographic studies of algal buildups, as they constitute some of the major petroleum reservoirs worldwide (Grammer et al, 2009; Baars and Torres, 1991). The term phylloid algae was proposed by Pray and Wray (1963) to describe all platy or leaf-like forms of calcareous algae present during the late Paleozoic that have little preservation of their internal fabric required for identification (Scholle and Ulmer-Scholle, 2003). In North America, buildups of Permian phylloid algae are found in the mid-continent region along with the Permian and Paradox basins. Most of these buildups represent boundstones or bafflestones of disarticulated calcified plates of phylloid algae that grew upright on the sea floor as small leaf-like structures (Figure 1A). Because of exposure to wave and tidal current energy, these upright structures collapsed and were fragmented on the sea floor, which eventually built up into mound shaped bioherms (Scholle and Ulmer-Scholle, 2003). Construction of phylloid algal buildups is currently considered to be through *in situ* growth of calcareous algae with sediment trapping and baffling coeval with precipitation of early marine cements leading to preservation of the buildup

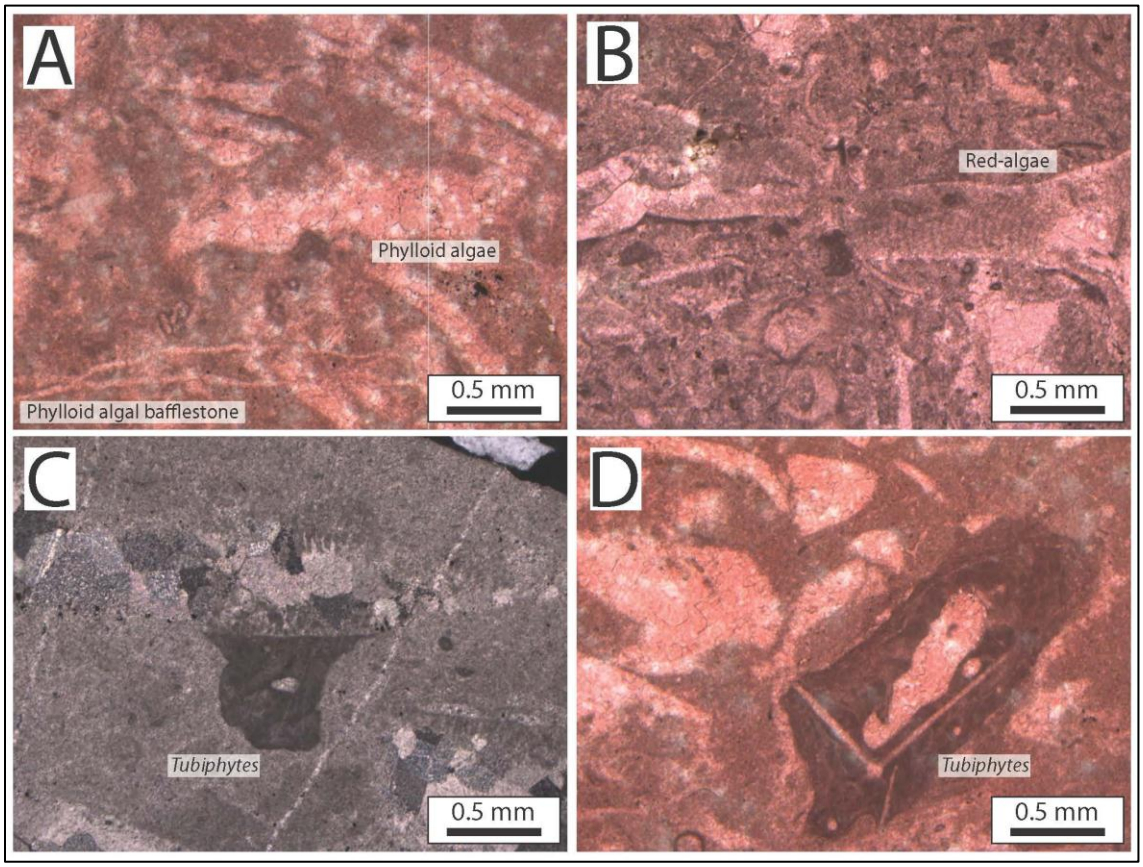

Figure 1: Types of Permian Algae in the Lower Hueco Limestone, Robledo Mountains.

A). Phylloid algae, stained, plane light. B) Laminar red algae, stained, plane light. C) *Tubiphytes* encrusting on a plate of phylloid algae, unstained, cross polarized light. D) *Tubiphytes* encrusting algae filled with calcite microspar, stained, plane light.

(Wahlman, 2002). When the buildups form discrete massive carbonate bodies with topographic relief, they are referred to as bioherms. When they form tabular sheets they are referred to as biostromes. Phylloid algal bioherms typically formed "patch reefs" or small interconnected mound complexes on a broad carbonate shelf, at or near the shelf margin (Toomey, 1991; Wahlman, 2002; Grammer and Ritter, 2009). In the Permian Basin of west Texas and southern New Mexico, outcrops of upper Paleozoic bioherms are typically found on steep, high relief,

prograding carbonate platforms, that were additionally supported by microbial growth and pervasive early-marine cementation (Kenter et al., 1997).

Within phylloid algal bioherms, other types of algae are also common such as laminar and encrusting forms. Laminar encrusting red algae is interpreted as an encruster or binder within bioherms and not a sediment baffler like the upright growing phylloid algae (Figure 1B). Encrusters are important organisms in reef construction because they serve as binders to hold the bioherms components together (Wahlman, 2002). The most common taxon of red algae in the Permian is *Archaeolithophyllum lamellosum*, which was an ancestral coralline red alga with well-defined internal cellular structure and conceptacles (Johnson; 1946, 1956, Wray; 1977). The growth habit of this type of algae is laminar and encrusting rather than leaf-like, and has a thin wavy appearance. *Tubiphytes* is another form of encrusting algae and consists of irregularly rounded, encrusting masses with thick, dense micritic walls and a central tubular canal that is usually filled with sparry calcite cement (Figure 1C and D) (Wahlman, 2002). *Tubiphytes* is also one of the most important encrusters in the late Paleozoic reef community because of its abundance and broad distribution and is very abundant in the Permian and Orogrande Basins.

Phylloid algal bioherms have been classified as either isolated mounds or large amalgamated banks. Mounds tend to be massive to faintly bedded, have a convex downward top, and a flat base. This geometry would have been produced along shelf margins or on the tops or flanks of paleotopographic highs on carbonate shelves (Wilson, 1975). Phylloid algal mounds represent concentrated growth under more normal marine conditions and therefore are best developed at or near shelf margins where a consistent supply of normal marine seawater is available (Wahlman, 2002). In addition to these conditions, the massive character of phylloid algal mounds results from rapid localized growth along with continuous submarine cementation.

Also, mounds can form stacked complexes if they are exposed to periodic sea-level rise leading to increased accommodation space. Occasionally, mounds are found in laterally linked complexes, but this relationship is rare (Wahlman, 2002).

Phylloid algal banks are much larger than mounds, have a more tabular to lens shape, and are internally well bedded (Toomey, 1976; Ball et al., 1977). Large banks typically grew on broad seafloor topographic highs at very shallow depths where seawater temperatures and salinities might have been elevated enough to exclude most normal marine biota (Wahlman, 2002). In both mounds and banks, phylloid algae acted as bafflers, trapping sediment, while encrusting red algae bound the internal structure together.

In the Hueco Mountains of southern New Mexico and west Texas, Stoklosa et al. (1998) described lower Permian phylloid algal mounds on the eastern margin (Sacramento shelf) of the Orogrande basin (Figure 2). Mounds here are interpreted to form at a distinctive shelf margin with a pronounced shelf-slope break. These mounds are associated with recurrent shelf margin erosion and abrupt facies changes landward of the mounds. Also, dramatic bed thickness changes occur over short distances adjacent to these mounds (Simo et al., 2001). One the western margin of the Orogrande Basin (Robledo Shelf) phylloid algal mounds are present in correlative lower Permian strata but this margin is interpreted as a low-angle ramp and not a high-relief platform with a pronounced shelf-slope break (Mack and James, 1988; Kues and Giles, 2004). Further to the east along the Eastern Shelf of the Midland Basin (Figure 2), Toomey and Winland (1973) describe a Desmoinesian shelf-margin bank complex that is 11 miles long and up to 3 miles wide. Six different carbonate lithofacies are recognized within this complex, suggesting dramatic facies changes within this complex, landward of the shelf margin. This bank is near the end of a 125-mile-long chain of shelf-margin buildups that make up the Nena Lucia Field in which the

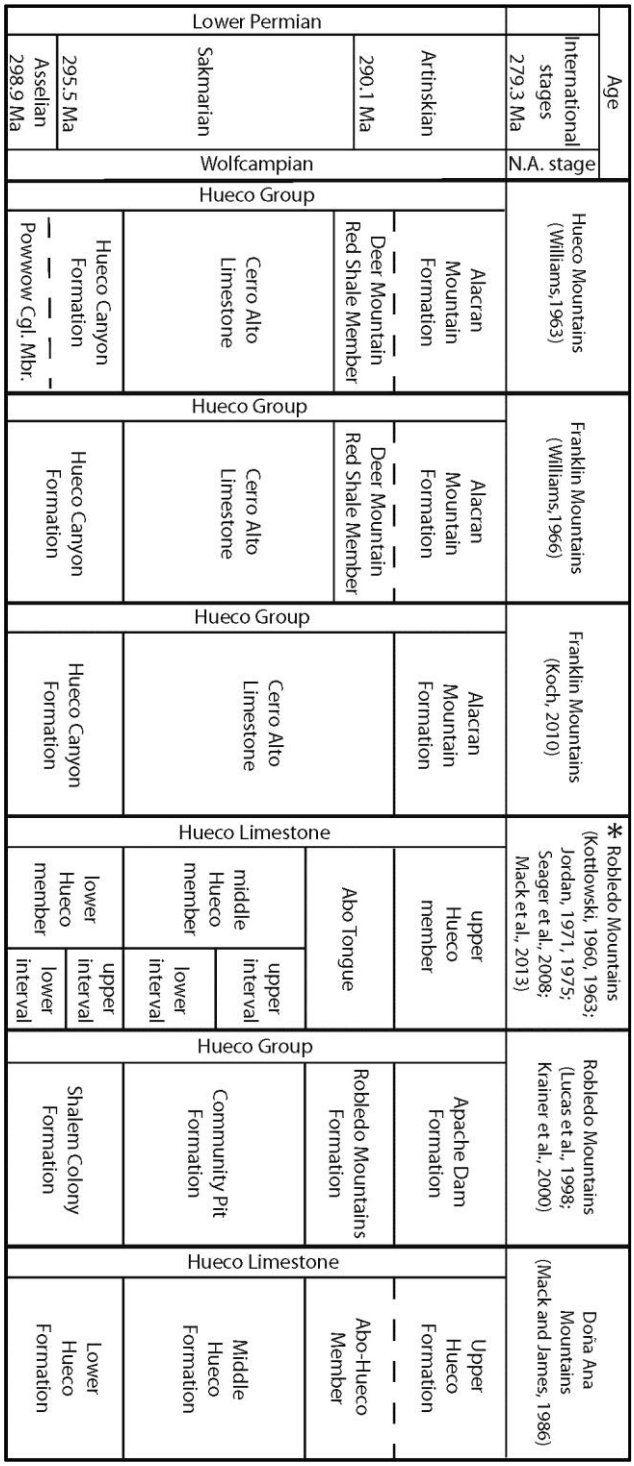

Figure 2: Stratigraphic Nomenclature for the Lower Permian Hueco Limestone.

*Indicates the nomenclature for the Robledo Mountains used in this study.

massive shelf-margin phylloid algal buildups are the primary producers. In the northern part of the Midland Basin (Figure 2), the Missourian Horseshoe Platform contains phylloid algal mound complexes that are found adjacent to shelf margin to upper slope submarine carbonate debris flows, suggesting development at a steep shelf margin (Schatzinger 1983). In all three of these areas, phylloid algal buildups are associated with rapid facies changes, thickness variations, and development along an erosive shelf margin with a steep slope above the adjacent basin.

Giles and Soreghan (1999) proposed another mechanism for phylloid algal mound construction based on Pennsylvanian Wilson mound in the Sacramento Mountains of New Mexico. In their model, plates of algae were transported by tidal energy and deposited in interconnected mounds. Grammer and Ritter (2009) followed up on this theory by comparing these phylloid algal mounds in the Paradox Basin of Utah to modern sand waves off the coast of Florida. They concluded that to form in this manner, mounds would have been confined to areas where tidal energy was concentrated and where algae could be transported from more basinal sources. However, this would only apply for interconnected mound complexes and not isolated bioherms or biostromes. Regardless, determining the depositional controls and mechanisms that produce phylloid algal bioherms are essential for understanding the stratigraphic architecture where these organic carbon accumulations are found.

1.2 Research Objectives

This study of phylloid algal bioherms focuses on depositional and stratigraphic analysis in the lower interval of the lower Hueco member of the Lower Permian (Wolfcampian) Hueco Limestone on the western margin (Robledo shelf) of the Orogrande Basin (Figure 2) (Mack et al., 2013). The analysis is based on detailed field and petrographic work that describe lithofacies and stratigraphic relationships and interpretations of depositional environments and regional

sequence stratigraphy. Results will test the hypothesis that the Robledo shelf geometry existed as a platform style with a pronounced shelf-slope break during early Permian time. The presence of phylloid algal buildups and associated shallow marine environments are used to define the shelf and shelf margin's position and facies associations are used to interpret the depositional geometry.

The primary objectives of this project are to 1) determine the lithofacies and depositional environments, 2) compile, correlate, and build a sequence stratigraphic framework for the lower interval of the lower Hueco member of the Hueco Limestone, 3) understand how sedimentation rates, subsidence, and eustatic sea-level changes affected sedimentation and depositional environments on the Robledo shelf, and 4) compare these interpretations to previous work completed in adjacent regions of the Orogrande and Permian basin.

1.3 Hueco Group Stratigraphy

Stratigraphic nomenclature for upper Paleozoic stratigraphy in the Orogrande Basin has changed considerably since its initial designation over 100 years ago. In particular, the name Hueco Limestone was originally proposed for Carboniferous strata located in the Hueco Mountains and trans-Pecos Texas region by Richardson (1904). Over the next 30 years, various regional stratigraphic names were applied to the strata in the Hueco Mountains such as the Magdalena and Manzano groups (Beede, 1920) then the Gym Limestone (King and King, 1929). King (1934) identified three subdivisions of the Gym Limestone and later applied the name Hueco Limestone to the Lower Permian stratigraphy in this area (King, 1934). Using the Hueco Mountains Stratotype, King, et al. (1945) divided the Hueco Limestone into three informal subdivisions: the lower, middle, and upper. Williams (1963) elevated the Hueco Limestone to Group status and redefined these informal subdivisions into 3 formations with members. In

ascending order the formations of the Hueco Group are: the Hueco Canyon, Cerro Alto Limestone, and Alacran Mountain (Figure 2). The basal unit of the Hueco Canyon Formation is the Powwow Conglomerate Member. The Powwow conglomerate overlies an angular unconformity that truncates progressively older formations southward in the Hueco Mountains (King et al., 1945). It is also important to note that the Alacran Mountain Formation contains the Deer Mountain Red Shale Member, which correlates to part of the Abo Formation to the north (Williams, 1963). In 1966, Williams extended these names to exposures of the Hueco Group in the Franklin Mountains to the west. Later studies to the north in the Robledo and San Andres mountains (Seager, et al., 1976; Seager, 1981; Mack and James, 1986; Mack et al., 1988, Mack et al., 2013) applied the older "divisions" and not the formal "member" names defined by Williams (1963 and 1966).

In the Robledo and Doña Ana mountains, mapping and biostratigraphic studies continued to use the older informal nomenclature: lower, middle, and upper members (Seager et al., 2008). These studies added the informal Abo Tongue and Abo-Hueco member, which lie between the middle and upper members and are correlative to the Abo Formation to the north and the Deer Mountain Red Shale Member to the south (Figure 2) (Kottlowski, 1960, 1963; Williams, 1963, 1966; Jordan, 1971, 1975; Seager et al., 1976; Mack and James, 1986; and Wahlman and King, 2002). Lucas et al. (1998) has applied formal names to the informal members of the Hueco Group in the Robledo Mountains and in ascending order are: Shalem Colony Formation, Community Pit Formation, Robledo Mountains Formation, and Apache Dam Formation (Figure 2). However, because these informal names are not present on the only published geologic map for the Robledo Mountains (Seager et al, 2008), this study will continue to use the nomenclature of the Hueco Group in the Robledo Mountains as originally defined by Kottlowski (1960) that

was used for geologic mapping. Stratigraphic subdivisions described by Mack et al., (2013) are also applied to these stratigraphic intervals (Figure 2).

1.4 Geologic Setting

Upper Paleozoic strata preserved in western North America record the stratigraphic and structural evolution of the Ancestral Rocky Mountains and associated basins. During this period of time, progressive westward suturing of the Laurasian landmass to the paleocontinent Gondwanaland formed the Ouachita-Marathon orogenic belt in Oklahoma and Texas, and provided the structural setting for the development of the Ancestral Rocky Mountains foreland to the orogenic belt (Graham et al., 1975; Kluth and Coney, 1981; Ross, 1986; Algeo, 1992). The majority of basins associated with the uplifts of the Ancestral Rockies were situated at equatorial tropical to subtropical paleo-latitudes, with carbonate production centered around the south and western margins of Laurentia (Ross and Ross, 1988). This margin of Laurentia contains all of the Ancestral Rocky Mountain uplifts and basins which are represented by surface exposures and subsurface data and most are major areas of hydrocarbon production today (Kluth and Coney, 1981; Ross and Ross, 1985; Kues and Giles, 2004) (Figure 3).

1.5 The Permian Basin Complex

Directly adjacent to the Ouachita-Marathon orogenic belt in west Texas and southern New Mexico, a series of basins began to develop that were separated by structural shelves created by syndepositional faulting related to Permian tectonism (Ross, 1986; Wahlman, 1988). These structural shelves allowed massive carbonate platforms to develop in shallow marine environments between the paleocoastlines and deep basins (Cys and Gibson, 1988). This large

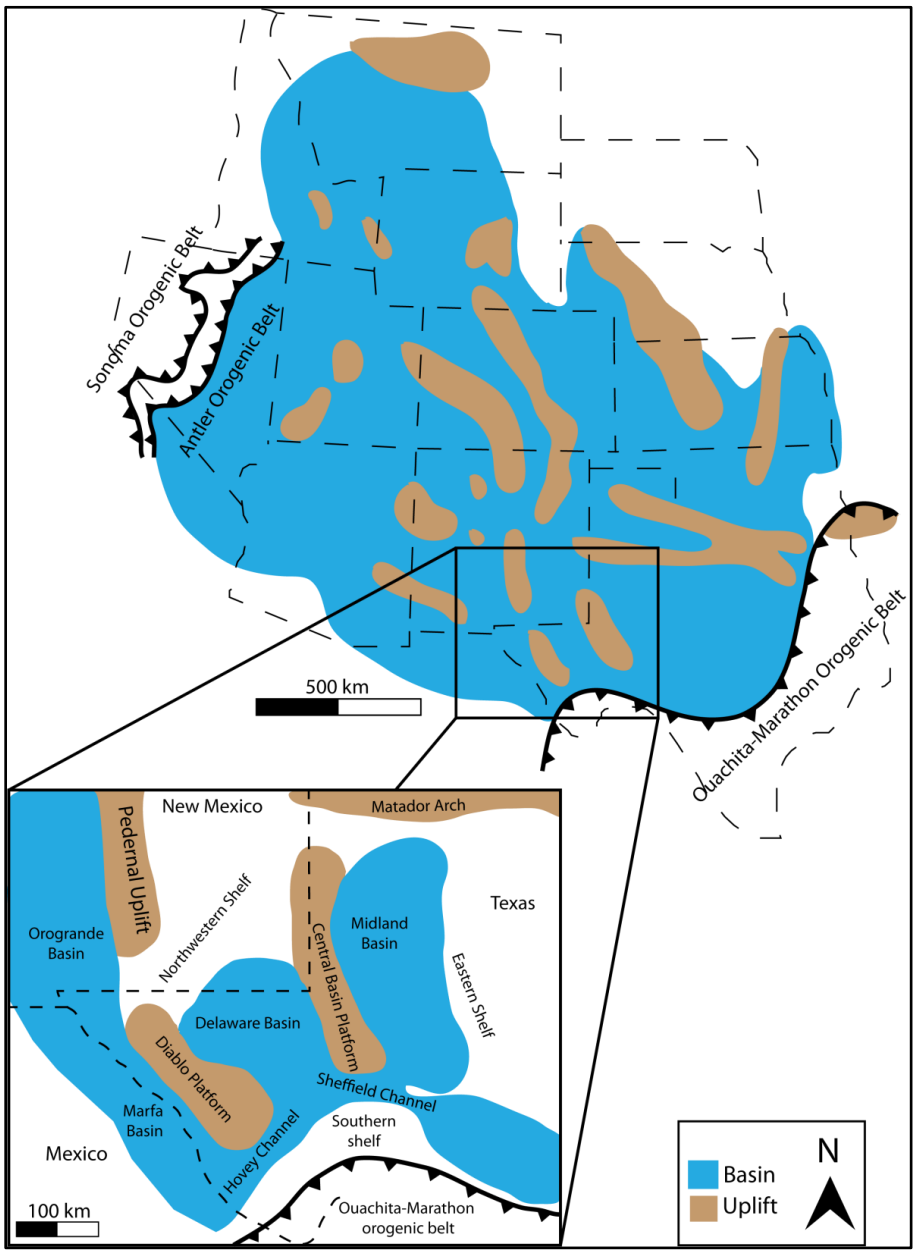

Figure 3: Ancestral Rocky Mountains Basins and Uplifts.

Location of basins and uplifts associated with the Ancestral Rocky Mountain development across western North America. Highlighted in the pulled out map are the geographic features of the Permian Basin Complex and adjacent regions. Modified from Cys and Gibson (1988), Kottlowski et al. (1988), and (Kues and Giles (2004).

grouping of basins and carbonate platforms in west Texas and southern New Mexico is aptly named the Permian Basin Complex. From southwest to northeast across the Permian Basin Complex, the primary paleogeographic elements are: the Hovey Channel, Southern Shelf, Marfa basin, Orogrande Basin, Diablo Platform, Sheffield Channel, Delaware basin, Northwest Shelf, Pedernal Uplift, Central Basin Platform, Midland basin, and Matador Arch (Figure 3).

Structural highs, such as the Diablo and Central Basin platforms, were isolated from the adjacent subsiding basins and allowed for large scale deposition of shallow marine carbonates throughout the entire Permian. Associated with these structural highs were shelf margin organic carbonate buildups that were able to develop because the topographic relief that caused abrupt environmental gradients between the shelves and basins (Wahlman, 1988). One of these highs, the Diablo Platform, was the southern extension of the Pedernal uplift and was a stable carbonate shelf throughout the Pennsylvanian and Permian (Cys and Gibson, 1988). The Orogrande Basin borders this region to the northwest (Figure 3).

The late Paleozoic is known for its distinctive sedimentary cycles driven by glacio-eustatic sea-level fluctuations. In particular, strata of this age was deposited as part of the Absaroka Megasequence driven by the large-scale continental glaciation of Gondwana, similar to the Pleistocene "icehouse climate" (Sloss, 1963; Wanless and Cannon, 1966; Heckel, 1977; Veevers and Powell, 1987; Vail et al., 1991; Crowell, 1999). As a result of this glaciation, the late Paleozoic is considered an "icehouse climate" for its large amplitude sea-level fluctuations, extreme stratal cyclicity, and high-relief carbonate reefs and banks in tropical settings (Read, 1995; Lehrmann and Goldhammer, 1999). Strata that these characteristics were derived from are located globally but exposures in western Texas and southern New Mexico are most relevant to

understanding local hydrocarbon production. Many outcrop and subsurface studies in the Permian Basin were completed for this reason but outcrop exposures to the west remain less studied.

1.6 The Orogrande Basin

Located in south central New Mexico and west Texas, the Orogrande Basin formed adjacent to the Permian Basin Complex during the Pennsylvanian and early to mid-Permian (Kues and Giles, 2004). During the late Mississippian to early Pennsylvanian (Morrowan), initial tectonism in the Ouachita-Marathon orogenic belt partitioned the large and regionally extensive precursor Tobosa basin into a series of basins divided by local uplfits (Cys and Gibson, 1988). In particular, the Pedernal and Diablo Platform uplifts developed, which separated the Orogrande Basin from the Permian Basin to the east (Figure 3). Further tectonism during Morrowan and Atokan time increased the rate of basin subsidence, providing abundant accommodation space for deposition of large volumes of siliciclastics from the adjacent Pedernal uplift (Pray, 1961; Wilson, 1988; Algeo et al., 1991). Additionally, carbonate deposition began on the eastern margin of the Orogrande Basin during the early Atokan, mainly as open marine and lagoonal environments with abundant phylloid algal buildups (Connally and Stanton, 1983).

Carbonate and siliciclastic deposition continued into Atokan time, when major marine transgression spread marine environments from the Orogrande Basin into northwest New Mexico (Kues and Giles, 2004). Throughout the Atokan period, marine carbonate deposition continued around the entire basin margin on low angle and distally steepened ramps. Shallow marine limestones and subordinate phylloid algal banks developed on these ramps while the center of the basin was filled with shales and thin carbonates (Jordan, 1975; Wilson and Jordan, 1983; Mack and James, 1986; Mazzullo and Reid, 1987; Candelaria, 1988; Mazzullo, 1995).

Maximum transgression during the Desmoinesian resulted in open marine carbonate deposition across New Mexico and west Texas (Kues and Giles, 2004). Despite widespread transgression, only relatively thin (~70m) carbonate deposits are found on the Robledo shelf as compared to the thicker (128-151m), massive carbonate beds in the surrounding basin (Kottlowski and Seager, 1988; Seager and Mack, 1991). Renewed tectonism and uplift during the Missourian provided source areas for the large volumes of siliciclastics shed in to the adjacent, rapidly subsiding Orogrande Basin (Kues and Giles, 2004). Consequently, this rapid sediment influx almost filled the entire Orogrande Basin to sea level during the Missourian resulting in widespread, thin shallow marine carbonate successions interbedded with shallow-marine siliciclastics (Harbour, 1972; LeMone, 1982).

Rapid downwarping of the Orogrande Basin continued into the Virgilian along with increased glacio-eustatic sea-level fluctuations estimated at 100 m or more (Soreghan and Giles, 1999a, b). Consequently, cyclic siliciclastics and carbonates were deposited in fluvial, deltaic, and shallow marine environments as sandstones and biostromal limestones. Large phylloid algal bioherms formed on the tectonically active shelf along the eastern margin of the Orogrande Basin in the present day Sacramento Mountains (Soreghan and Giles, 1999a). However, near the end of the Virgilian, thick accumulations of gypsum were deposited in the southern part of the basin, related to lowering eustatic sea-level and possible temporary isolation of the Orogrande Basin from the open ocean (Kottlowski et al., 1956; Kottlowski and LeMone, 1994). The transition from the end Pennsylvanian (Virgilian) to the Permian (Wolfcampian) is marked by a major eustatic sea-level fall and lowstand.

Wolfcampian strata in the Orogrande Basin are representative of marine transgression induced by a glacio-eustatic rise sea-level rise that followed the major lowstand at the

Pennsylvanian-Permian boundary (Kues and Giles, 2004). Marine strata associated with this transgression began to onlap and overlap highlands that were being eroded during the waning stages of Ancestral Rocky Mountain uplift. These thick marine sequences are the Hueco Group and are found in the Hueco, Franklin, Organ, and Robledo mountains (King, 1934; Williams, 1966; Kottlowski and Seager, 1988). To the northeast in the Sacramento Mountains, correlative Lower Permian strata consists of rapid lateral facies changes from mudstones to limestones to sandstones and conglomerates, and local shelf-margin phylloid algal buildups (Laborcita Formation; Wilson, 1975). Additionally, the Permian marks a significant climatic shift from the Pennsylvanian icehouse climate dominated by glacio-eustatic sea-level fluctuations to a more temperate, less humid climate (Ross and Ross, 1990, Heckel, 1986; 1994; Mack, 2003). This change continued into the Leonardian leading to a more arid, green house climate. Consequently, lower Permian strata records an important transition in Earth's climate history which is preserved in the Hueco Limestone of southern New Mexico and west Texas.

1.7 Previous Work on the Lower Member of the Hueco Limestone on the Robledo Shelf

Numerous researchers have studied the Hueco Limestone in order to address a variety of different problems. The first work was mainly focused on characterizing and defining Wolfcampian stratigraphy in this region. King et al. (1945), Kottlowski et al. (1956), Williams (1963; 1966), Jordan (1971, 1975), Seager et al. (1976), Seager (1981), and others used regional mapping and widely spaced measured stratigraphic sections to construct the general stratigraphic framework of Wolfcampian strata in the Orogrande Basin. However, these studies were focused at regional lithostratigraphic and biostratigraphic correlation, not detailed facies and depositional environment interpretations. One of the first detailed lithostratigraphic studies was completed by

Jordan (1975) in order to correlate Wolfcampian stratigraphy from the east (Laborcita Formation) to the west side (Hueco Limestone) of the Orogrande Basin. This study constructed the first regional correlation for all Wolfcampian age sediments in the Orogrande Basin and was aimed at showing the general distribution of outcrops (Figure 4). These correlations were derived from broad regional lithostratigraphic relationships, buts provided a framework base to begin detailed sequence stratigraphic studies across the entire basin. Harbour (1972) completed a geologic map of the northern Franklin Mountains and used work from King et al. (1945), and Williams (1961, 1966) to understand the lower Hueco stratigraphy in the Franklin Mountains. However, no detailed petrographic analysis, interpretations, or depositional environments had been completed at this point.

To the north, Seager et al. (1976), Seager and Mack (1991, 1998, 2008) provided stratigraphic descriptions and measured stratigraphic sections of the lower Hueco while completing detailed geologic mapping in the Garfield, McLeod Tank, and Leasburg quadrangles. All of these studies were focused on regional geologic understanding and not specifically looking at the lower Hueco. Consequently, no detailed petrography and sequence stratigraphy has been done for the lower Hueco. However, Wahlman and King (2002) completed a detailed fusulinid biostratigraphic study of the Lower Hueco Limestone in the Robledo Mountains in order to better determine the Pennsylvanian-Permian boundary horizon within this stratigraphy. This work better constrained the position of the Pennsylvanian-Permian boundary in the area and resulted in the placement of the Bursum Formation in the latest Virgilian.

The most recent study completed in this area (Koch, 2010) compared a general sequence stratigraphic framework for the entire Hueco Group across the Orogrande Basin utilizing oxygen and carbon isotope variations in order to make interpretations about paleoclimate change during

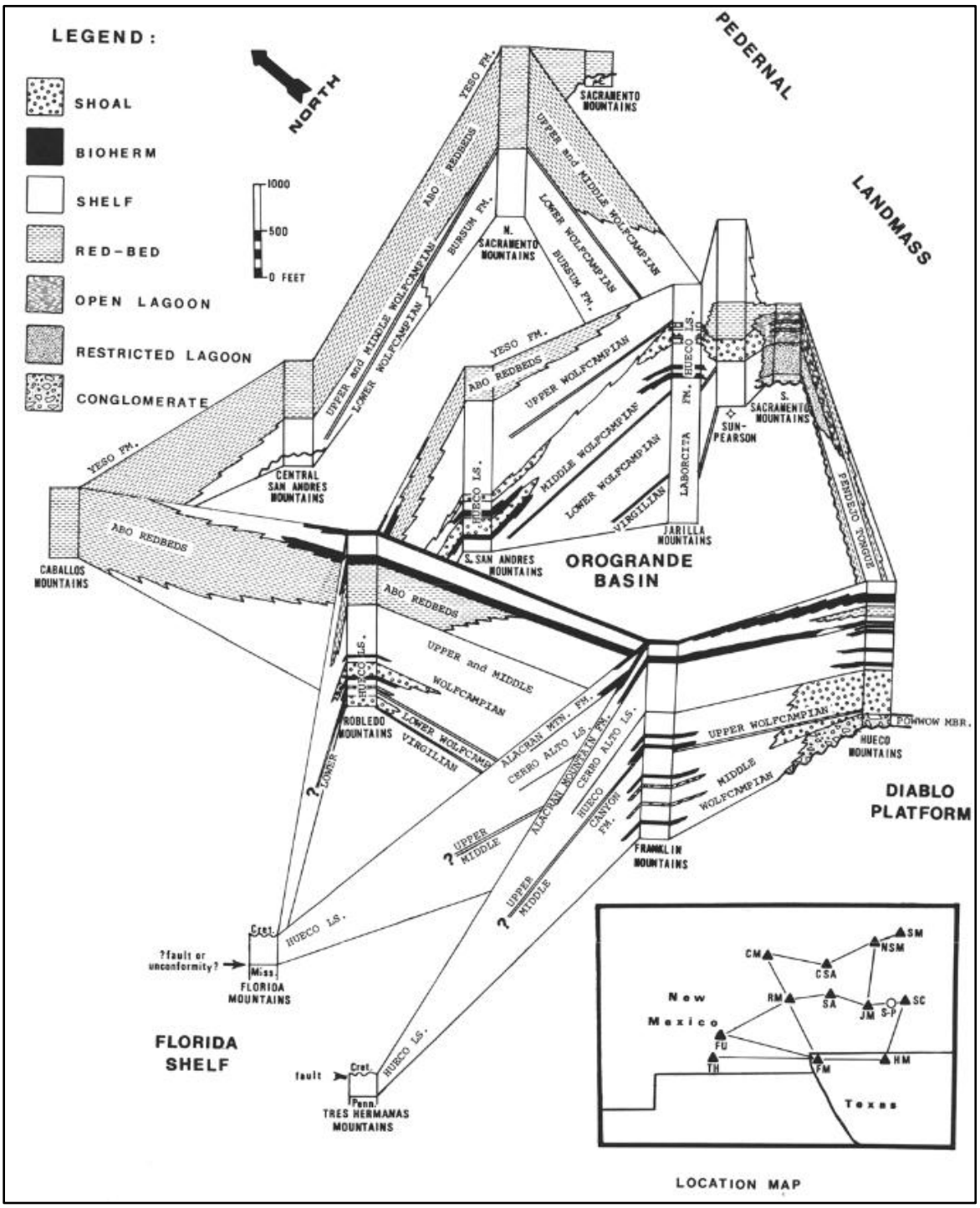

Figure 4: Wolfcampian Fence Diagram of the Orogrande Basin. Regional stratal correlations between mountain ranges in the Orogrande basin from one of the first major stratigraphic studies completed in this area. From Jordan, 1975.

the early Permian. Measured stratigraphic sections and subsurface cores from across the Orogrande Basin were used to complete a general sequence stratigraphic framework for all upper Pennsylvanian and lower Permian stratigraphy. However, only one section was from the Franklin Mountains and no data was used from the Robledo Mountains. Additionally, this study was not focused on detailed petrography and depositional environment interpretation, but it did provide constraints on sea-level changes during the late Pennsylvanian and early Permian that will be compared to the sequence stratigraphic framework completed in this study.

1.8 Methods

In order to construct a sequence stratigraphic framework for the lower Hueco Limestone on the Robledo shelf, the correct lithofacies associations and depositional environments need to be interpreted and formed into a depositional profile. Five stratigraphic sections were measured in the Robledo Mountains of south central New Mexico near the city of Las Cruces. An additional three stratigraphic sections were completed in the Franklin Mountains, north of El Paso, Texas. These stratigraphic sections represent all major outcrop exposures of the lower Hueco strata across the paleo-Robledo shelf (Figure 5). These measured stratigraphic sections form a northwest to southeast trending transect across the shelf and provide the regional scale for this project. The current distance between the furthest northwest stratigraphic sections (Limonite Mine, Robledo Mountains) and the furthest southeast (Tom Mays Park, Franklin Mountains) represents a distance of approximately 70 kilometers (Figure 5). The location of stratigraphic section represents a slightly oblique transect of the paleoshoreline to shelf margin transition.

1.8.1 Outcrop and Petrographic Analysis

Each stratigraphic section was completed using a 1.5 m Jacobs staff along with a Brunton compass for accurate attitude measurements. Multiple attitude measurements were taken

throughout each section to ensure proper stratigraphic thickness. In addition, a handheld GPS unit provided UTM coordinates (NAD 84) at the base and top of each section. Measured stratigraphic sections are detailed in Appendix A. Hand samples were collected at each major change in lithology for hand sample and petrographic analysis. When phylloid algal bioherms were present, samples were collected from both the base and top of the mound core, and one from each flank, where available. Additionally, multiple samples were collected from beds containing abundant fusulinids for proper fusulinid identification and for fusulinid biostratigraphic correlation. From these stratigraphic sections, 247 hand samples were made into thin sections for petrographic analysis (Plate 3), and at least one sample from each identified lithofacies was made into a polished slab.

Samples made into thin section were analyzed using a Leica DM750 petrographic microscope for their depositional and diagenetic lithologic attributes. This data was compiled in an excel spreadsheet for each measured stratigraphic section and used to interpret lithofacies assemblages (Appendix B). These lithofacies provide a means for correlation across the 70km transect and allowed for interpretation of regional depositional environments. By determining the geographic position of depositional environments (landward vs. basinward), a depositional profile of the Robledo shelf was constructed to understand the Wolfcampian depositional geometry.

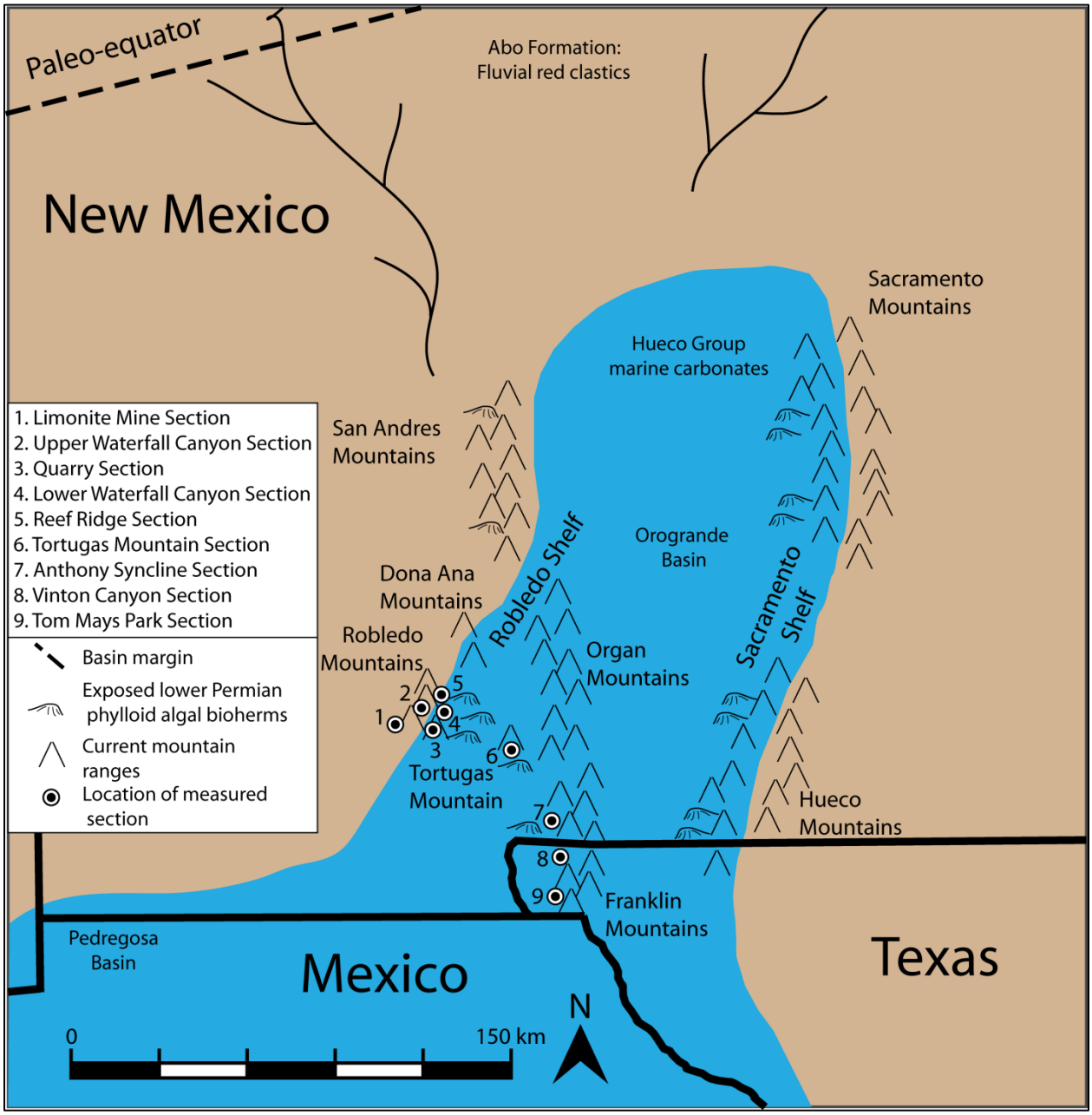

Figure 5: Location of Outcrop Exposures in the Orogrande Basin.

Schematic early Permian paleogeography of southern New Mexico and west Texas showing the position of the Orogrande Basin, current mountain ranges, and location of measured sections used in this study. Basin margin modified from Jordan, (1975) and Kues and Giles (2004).

1.8.2 Sequence Stratigraphy

Lithofacies and depositional environments, determined from outcrop and petrographic analysis, from each stratigraphic section were analyzed for their stratigraphic stacking patterns. These vertical successions of interpreted depositional lithofacies were placed into parasequences and parasequence across the Robledo Shelf. Between parasequences and parasequence sets are distinctive specific stratal surfaces, such as flooding, regressive, or ravinement surfaces, which were identified in each section from both field and petrographic observations (i.e. scour surfaces, sedimentary structures, lag deposits, condensed sections, and concentration of glauconite grains). The stacking pattern and nature of significant surfaces were used to define sequences and systems tracts within sequences. This framework was used to make interpretations on relative rates of sea-level fluctuation, subsidence rates, and how these factors controlled the spatial and temporal distribution of environments across the Robledo shelf.

1.8.3 Biostratigraphy

The majority of measured stratigraphic sections did not have a correlative stratigraphic basal or upper contact because of extensive Quaternary alluvium cover, dip-slope erosion that grades back into alluvium, or where truncated by faults. Consequently, lithographic and sequence stratigraphic correlation alone could not be completed accurately. To ensure all sections were early Wolfcampian and effectively correlate across this region, fusulinid biostratigraphy was utilized to augment the sequence stratigraphy. Fusulinids were used because of their abundance, diversity, and visibility, which makes them the most widely used index fossils in the Orogrande-Permian Basin region (Wahlman and King, 2002).

Each stratigraphic section that contained packstones or grainstones with abundant fusulinids were heavily sampled to ensure thin sections would contain adequate numbers of

fusulinids. At least five thin sections from each bed were made into thin sections and sent to Dr. Greg Wahlman (Wahlman Geological Services, LLC) for proper taxonomic identification. These identifications were compared to regional and global fusulinid zones that allowed for specific chronostratigraphic placement of the stratigraphy.

1.9 Stratigraphic Sections

Outcrops from the lower interval of the lower Hueco member are located across a broad geographic area of southern New Mexico and west Texas. To achieve the goals of this project, outcrop data needed to be collected from stratigraphic sections of the lower Hueco on the western margin of the Orogrande Basin. Consequently, potential stratigraphic sections were identified in the Robledo Mountains of southern New Mexico, Tortugas Mountain adjacent to Las Cruces, New Mexico, and the Franklin Mountains around El Paso, Texas (Figure 5). Discussed below are the location and characteristic of the nine stratigraphic sections listed from northwest to southeast position along a paleoshoreline to basin transect.

1.9.1 Robledo Mountains Sections

Located in south central New Mexico, the Robledo Mountains represent a wedge-shaped upper Cenozoic horst block of Paleozoic sedimentary rocks and Cenozoic clastic, volcanic, and intrusive rocks, all of which are tilted about 15 degrees to the south (LeMone et al., 1975; Seager et al., 2008). Outcrop exposures of the lower interval of lower Hueco member of the Hueco Limestone are mainly located in the central part of the range and comprise both the eastern and western sides of the range (Figure 6). Upper Paleozoic rocks are found in numerous different fault blocks caused by multiple episodes of structural deformation in the area, such as Laramide, Basin and Range, and Rio Grande Rift tectonic influences (Seager and Mack, 1986, Seager, 2004; Mack, 2004; Smith, 2004; and others). Consequently, most stratigraphic sections in the

Robledo Mountains are bounded by faults or form the tops of ridges, making it difficult to document lateral relationships of beds in most areas. However, this complex faulting does allow for multiple stratigraphic sections in a small area to represent different stratigraphic intervals.

Five measured sections were completed across the fault blocks of the Robledo Mountains that form a west to east transect across the center of the range and are all located in different fault blocks (Figure 6). Section locations were identified through field reconnaissance based on local geologic maps to ensure each section was completed within the lower Hueco Formation (Seager et al., 2008). One of these stratigraphic sections in the southeastern part of the Robledo Mountains lies within the borders of the Prehistoric Trackways National Monument, which was recently designated a National Monument by the 111th United States Congress in 2009. Stratigraphic section descriptions and locations are listed below from west to east.

Limonite Mine Section

Located on the western flank of the Robledo Mountains, this measured stratigraphic section forms the footwall fault scarp of the Western Robledo fault. Limonite mineralization and exploration pits are common along this fault and provide the basis for the name of this section. Strata here dip 16º to the southeast with a strike of 015º. Utilizing previous regional interpretations of paleogeography, this stratigraphic section represents the most landward deposition of the eight stratigraphic sections used in this study. An important aspect of this section is that it has a conformable basal contact with the Pennsylvanian Bursum strata below, one of the few sections that exhibit this relationship in the area (Appendix A.1). Regionally, the basal contact is defined by a board sub-aerial angular unconformity separating the Powwow Conglomerate above (Hueco Canyon Formation) from the underlying Pennsylvanian strata (King and King, 1929; King et al., 1945; Williams, 1963, 1966). However, little evidence of this large

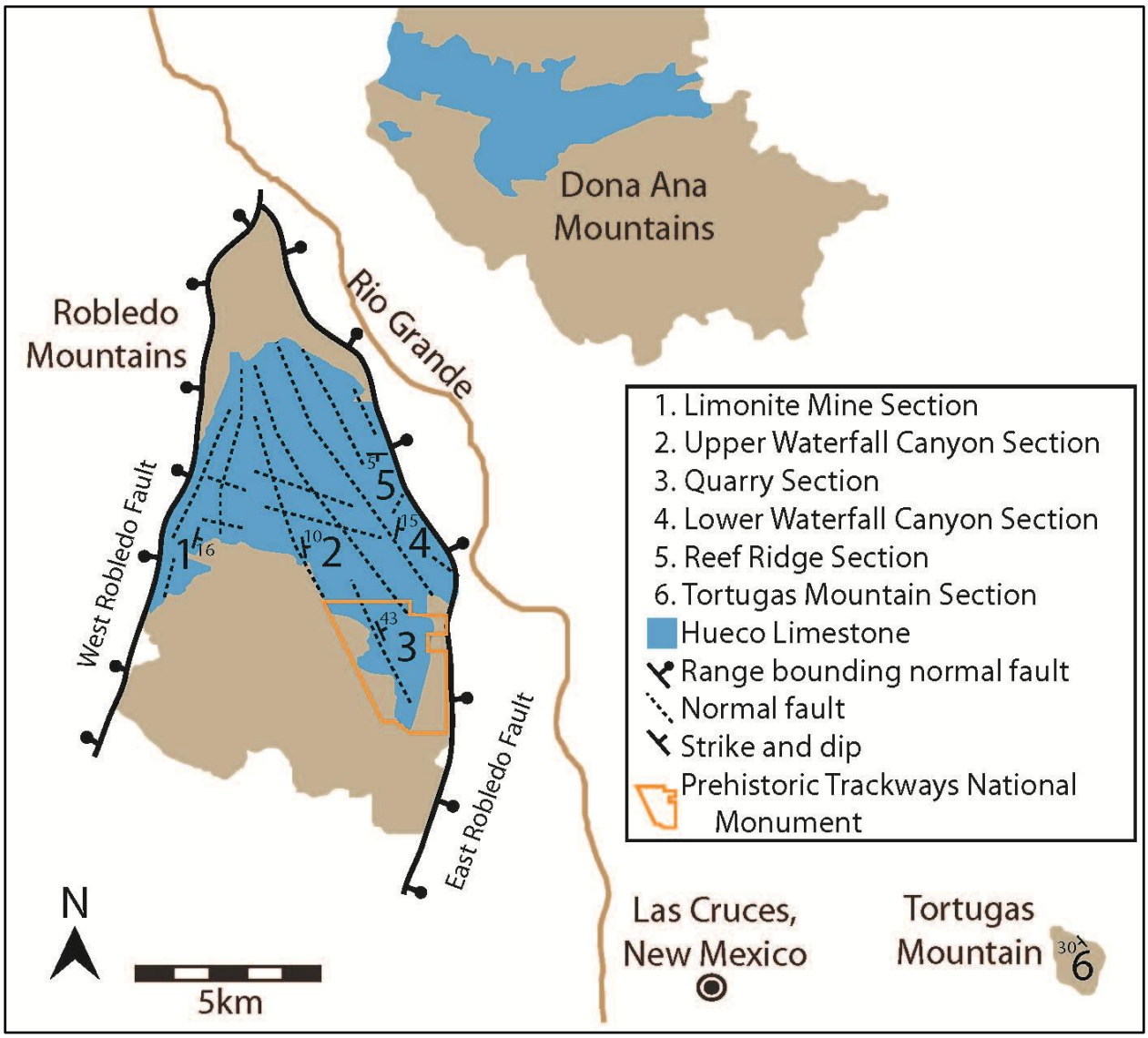

Figure 6: Location of Measured Sections in the Robledo Mountains and Las Cruces Region.

Schematic map showing outcrop exposures of the Hueco Limestone (Seager and Hawley, 2008) and locations of measured stratigraphic sections used in this study.

scale basal Permian unconformity is observed in the Robledo Mountains and the Powwow Conglomerate is rarely found on the Robledo shelf. The top of this section is located geographically to the northeast across a small normal fault with displacement to the east. This

stratigraphic section was completed as a composite section by tracing distinctive marker beds across the fault and to an adjacent hillside (Appendix A1). The upper most bed in this section is a thick, laterally continuous sandstone that represents a marker bed for the transition from the lower to middle intervals of the lower Hueco member of the Hueco Limestone (Durr, 2010; Mack et al., 2013). Consequently, this stratigraphic section contains both a basal and upper contact and is the only nearly complete stratigraphic section of lower Hueco member in the Robledo Mountains.

Upper Waterfall Canyon Section

The Upper Waterfall Canyon Section represents the shortest stratigraphic section (31m) within the lower interval of the lower Hueco member measured in this study and is located near the center of the Robledo Mountains (Figure 6). Exposures dip 10º to the southwest and strike 347º. This section is located almost due east of the Limonite Mine Section but is within a different fault block. Much of the lowermost and uppermost parts of this section are truncated by a sill of the Tertiary Robledo Rhyolite (Appendix A.2). The upper part of this section was added by traversing a small hillside west of the base of this section in order to add the sandstone marker bed that represents the transition between the lower and middle Hueco members. Overall, this section only preserves a thin interval of lower Hueco strata from the uppermost parts but contains valuable fusulinid biostratigraphic beds and the upper sandstone marker bed, which permits correlation to the Quarry and Limonite Mine sections respectively.

Quarry Section

The Quarry Section is located south east of the Limonite Mine and Upper Waterfall Canyon sections and is near the eastern flank of the Robledo Mountains. This section lies within the Prehistoric Trackways National Monument and was also completed as a composite section

from two adjacent hillsides (Figure 6 Appendix A.3). A composite section in this location ensured most covered intervals would be filled in and accurate bed thicknesses were obtained. Beds dip 43º to the southwest and strike at 340º. This section represents the upper half of the lower interval of the lower Hueco member in the Robledo Mountains and is about 90 m thick. Particularly, this section contains a thick sequence of marine siliciclastics at its base, a low relief phylloid algal bioherm above the siliciclastics, and is capped by the regional siliciclastic marker bed between the lower and upper intervals of the lower Hueco member. Consequently, correlation between these sections was completed through lithographic correlation of the upper siliciclastic marker bed and a few fusulinid biostratigraphic beds.

Lower Waterfall Canyon Section

The Lower Waterfall Canyon Section is located on the eastern flank of the Robledo Mountains, almost due east of the Upper Waterfall Canyon and Limonite Mine sections (Figure 6). Dips are very shallow here, about 5º to the southeast and strike at 017º. This section sits in the hanging wall of the East Robledo Fault to the east and is bordered by a westerly dipping normal fault to the west (Appendix A.4). The base of this section starts deep within the canyon on a slope of poorly exposed mudstones and shales, below a phylloid algal bioherm. This section ends 20 m above the massive cliffs forming the top of the exposed stratigraphy in this location and preserves a total of 55 m of the lower interval of the lower Hueco member. Because this section lacks the contact with the Pennsylvanian strata below, lithographic correlations were used to determine what part of the lower Hueco member this section represents.

Reef Ridge Section

The Reef Ridge Section is the furthest northward section used in this study and is also found on the eastern flank of the Robledo Mountains, northwest of the Lower Waterfall Canyon

Section (Figure 6). Similar to the Limonite Mine Section, this area contains the contact with the Pennsylvanian Bursum Formation strata below but only represents half of the exposed lower interval of the lower Hueco member in the Robledo Mountains. Beds in this area dip shallowly to the south (< 5 degrees) and appear to strike obliquely east west. However, this section contains a small phylloid algal bioherm complex at the top that can be traced laterally across the canyon to the south (Appendix A.5). Unfortunately, a small normal fault (roughly five meters of displacement to the west) does cross cut this section but distinct marker beds were found on both sides of the fault, so it did not decrease the quality of this stratigraphic section. Additionally, the East Robledo Fault is located to its east, placing this section in a horst block similar to the Lower Waterfall Canyon Section.

1.9.2 Franklin Mountains

Three measured stratigraphic sections were completed on a north-south transect across the western escarpment of the Franklin Mountains (Figure 7). Based on the regional paleogeography (Jordan, 1975; Wilson, 1977), all of these sections represent deposition in a more distal part of the Robledo shelf but the north-south transect parallels the paleoshoreline. Additionally, these stratigraphic sections are slightly thicker than what is observed in the Robledo Mountains to the northwest. The particular location for these stratigraphic sections was chosen from field reconnaissance based on the local geologic map of the Franklin Mountains (Harbour, 1972). Additionally, previously completed studies by both Williams (1966), and Koch (2010) were used for comparison with both the Tom Mays Park and Vinton Canyon sections.

Anthony Syncline Section

This stratigraphic section is located on the western limb of the Anthony Syncline in the northern Franklin Mountains directly on the border with Texas and New Mexico (Figure 7).

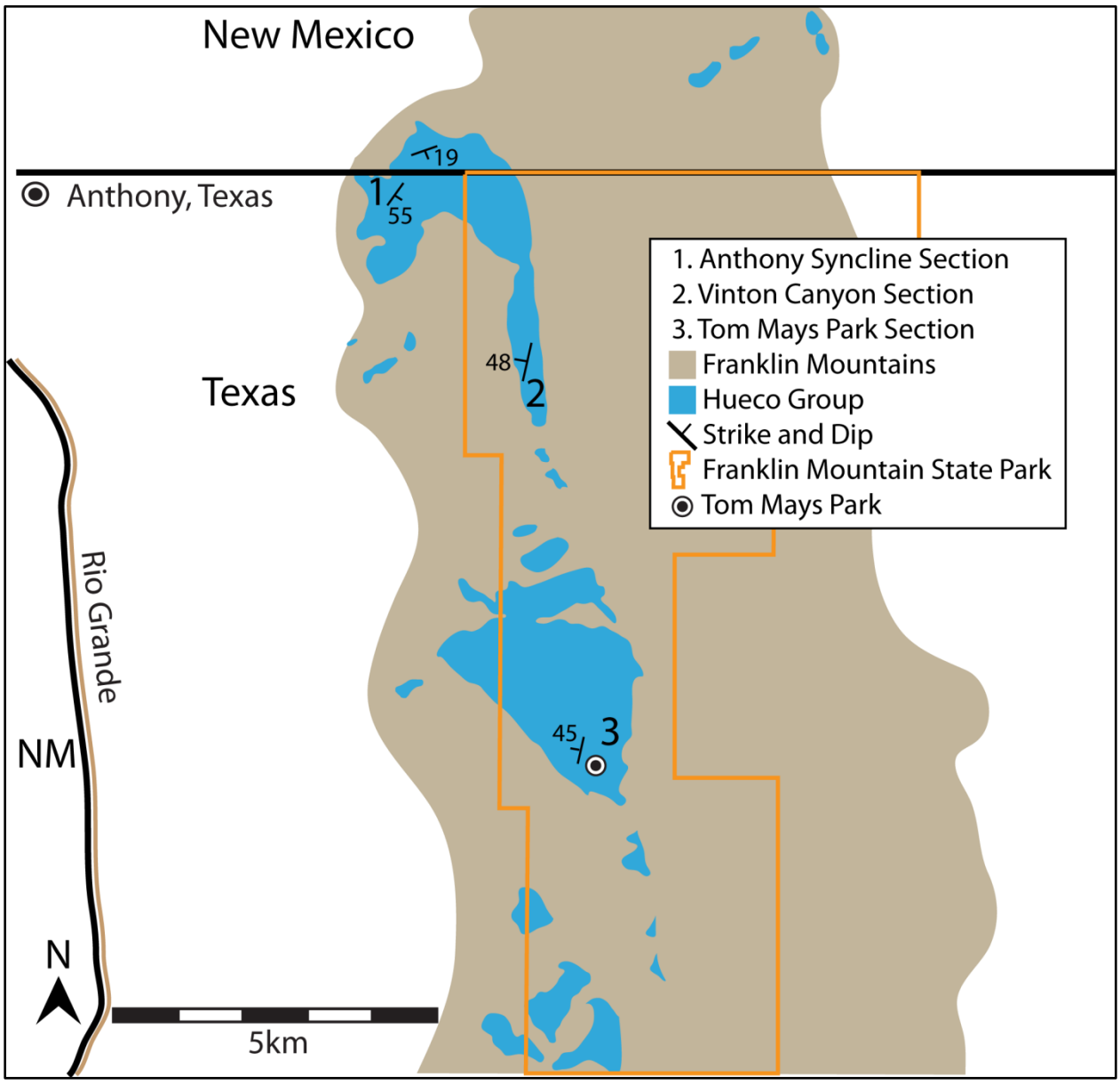

Figure 7: Location of Measured Sections in the Franklin Mountains.

Schematic map showing the location of measured stratigraphic sections from the Franklin Mountains used in this study. Three measured stratigraphic sections were obtained from the western flank of the Franklin Mountains. Two of these three lie in the Franklin Mountain State Park and the third is located directly on the border between Texas and New Mexico, east of the town of Anthony, Texas.

Strata here dips 55º to the southeast and strikes at 035º. This section was measured along a small road that traverses the hillside perpendicular to strike, providing very good exposure of almost all beds (Appendix A.6). The upper part of this section was completed on the dip-slope moving into the center of the syncline. Similar to the Limonite Mine Section, this section also contains conformable basal contact with the Pennsylvanian Panther Seep strata below and also forms a conformable contact with the middle Hueco member (Cerro Alto Formation) above (Figure 2). Two stratigraphic sections used in this study from the Franklin Mountains display this relationship. Additionally, the lower part of this section contains abundant fusulinid beds that were used for regional biostratigraphic correlation.

Vinton Canyon Section

The Vinton Canyon Section is also located in the northern Franklin Mountains but south of the Anthony Syncline Section. Exposure of this section is along a north south trending horst block just west of the Franklin Mountains and in the northern Franklin Mountains (Figure 7). Beds dip 48º to the southwest and strike at 010º. The base of this section on the eastern side of this horst block is covered by Quaternary alluvium but the upper part contains the contact with the overlying middle Hueco member (Cerro Alto Formation), providing a suitable level for correlation (Appendix A.7). This strata was also compared to previously completed stratigraphic studies from this area by Toomey (1991), where a measured section was completed on the same horst block. Also, thin sections and field reports were used from previously completed petrographic studies by the New Mexico State University Department of Geological Science Carbonate Depositional Environments and Petrology class. This provided an additional 51 thin sections that were compared to thin sections made during this study. Petrographic results are located in Plate 3.

Tom Mays Park Section

This stratigraphic section represents the furthest southward outcrop dataset used in this study and is located on the western side of the Franklin Mountains in the center of Tom Mays State Park (Figure 7). Beds in this area dip on average 45º to the west and strike at 012º. Similar to the Anthony Syncline Section, this section also has a conformable basal contact with the underlying Pennsylvanian Panther Seep Formation and a conformable upper contact with the middle Hueco member above (Cerro Alto Formation) (Appendix A.8). Exposures in this section are found along the western side of the main park road and some parts of the lower and upper Sunset Trails, as described by the park map. This stratigraphic section follows a very similar transect to previous studies completed in this area by Williams (1966), Toomey, (1991), and Koch (2010). This study chose this classic transect in order to compare results to the previous studies for both broad-scale stratigraphic interpretations (Williams, 1966) and paleoclimate data (Koch, 2010) to make more accurate conclusions on Wolfcampian sedimentation in the Orogrande Basin.

1.9.3 Tortugas Mountain

Tortugas Mountain Section

The Tortugas Mountain Section is located due east of Las Cruces, New Mexico (Figure 6) on the small horst block called Tortugas Mountain that is mapped as undifferentiated Permian limestones due to their extensive dolomitization and silicification (King and Kelley, 1980). This location would provide a stratigraphic section directly east (basinward) of the Robledo Mountains. A short stratigraphic section was measured on the south west flank of this horst block, near the Observatory Road (Appendix B). Beds here dip on average 30º to 40º to the southwest and strike at 340º. Outcrop exposures are heavily dolomitized and silicified, making

outcrop and petrographic analysis much more difficult than all other stratigraphic sections utilized in this study. Despite this, a well formed red-algal bioherm is present in the lower part of this section along the Observatory Road. However, because of extensive faulting and hydrothermal alterations related to the Organ Mountain Caldera, exact placement of these outcrop exposures in the lower Hueco stratigraphic framework is dependent on fusulinid biostratigraphy.

Previous studies by King and Kelly (1980) found fusulinid assemblages on the eastern flank of Tortugas Mountain that resembled assemblages classified in the "Permian" Bursum Formation but also stated that the upper stratigraphy resembled that of the Hueco and contained no fusulinids. Wahlman and King (2002) completed a fusulinid study in the Robledo Mountains that moved the Permian Bursum Formation into the latest Virgilian. Fusulinid samples collected for this study were focused on determining the age of strata exposed on the western flank of Tortugas Mountain.

Field reconnaissance was able to locate small exposures of silicified fusulinids within a dolomitized carbonate bed near the base of the western flank of Tortugas Mountain. Biostratigraphic analysis of fusulinids (Wahlman 2013, personal communication) indicates a late Pennsylvanian (Virgilian) age as determined from the inflated species *Triticites creekensis.* No other fusulinid species were found in this section. Based on these results, the stratigraphic section measured at Tortugas Mountain now appears to be related to the late Pennsylvanian Burusm Formation and was not included in this study. Data for this stratigraphic section can be found in Appendix B and fusulinid results will be discussed in the following chapters.

Chapter 2

RESULTS

2.1 Lithofacies of the Lower Hueco Member of the Hueco Limestone

Outcrop and polished hand sample observations of lithologic and sedimentological features augmented by petrographic analysis of 247 thin sections were used to determine the lithofacies observed in the lower interval of the lower Hueco Limestone member exposed in the Robledo and Franklin mountains. Petrographic attributes from thin section analysis are summarized in chart form in Plate 3. Eleven distinct lithofacies were identified: 1) quartz sandstone, 2) quartz siltstone and shale, 3) fenestral dolomudstone, 4) microbial intraclast packstone, 5) dolomudstone, 6) green-algal packstone to grainstone, 7) ostracode foram wackestone, 8) oolitic packstone, 9) fossiliferous packstone and grainstone, 10) fusulinid packstone and grainstone, and 11) phylloid algal bafflestone. The lithofacies were subsequently grouped into genetically similar related depositional facies associations. The depofacies associations are listed below according to their relative position on a marine depositional profile: 1) supratidal carbonate, 2) intertidal carbonate, 3) subtidal carbonate, and 4) shoreface siliciclastics.

2.1.1 Supratidal Carbonate Depositional Facies Association

This depositional facies association only contains one lithofacies, fenestral dolomudstone. Supratidal facies were deposited in a near shoreline environment, landward of areas that experience high wave energy and were mainly sub aerially exposed with periodic inundation. Characteristics of this environment include sedimentary structures that suggest evidence of sub-aerial exposure in arid environments and mineralization related to very saline

and brackish water conditions, similar to documented characteristics of arid sabkha deposits on the Trucial Coast in the Middle East (Shinn, 1983).

Fenestral Dolomudstone

Outcrop and Petrographic Characteristics

Fenestral dolomudstone are confined to exposures in the Robledo Mountains, with the majority occurring in the Limonite Mine Section (Figure 5 and 6) (Appendix A.1). However, these beds are also common within the upper parts of the Quarry Section with the best exposure of this lithofacies occurring in the Upper Waterfall Canyon Section. Outcrops form both laterally continuous yellow, tan, and white ledges or poorly exposed slopes, which can also be used as marker beds because of the abundant float concentrated on a small slope. Weathered outcrops range in color from yellow, tan, white, and gray with fresh surfaces usually appearing light gray, tan, pink, or dark red (Figure 8A-E). Most outcrops are thin to medium bedded (0.1 - 0.5 m), with some beds up to 1.0 m thick. Many beds contain wavy laminations associated with stromatolitic algal mats (Figure 8B-E). Stromatolites are common within this lithofacies and occur as both digitate and laminated forms (Figure 8C, 8E, and 9A). Brown and dark gray chert nodules are abundant in thicker bedded intervals within this lithofacies and in particular in the upper Limonite Mine Section (Figure 8A).

Localized beds of highly brecciated thin wavy laminated flat pebble conglomerates composed of brecciated stromatolites occur interbedded within most stromatolitic intervals (Figure 8B and 8C). Flat pebbles range in size from 0.5 to 2.0 cm on their long axis and are only a few millimeters thick. Arrangement in the matrix is usually chaotic, but occasionally flat rip-up pebbles are found in oriented, imbricated orientations. Fenestral vugs range in diameter from 1-5

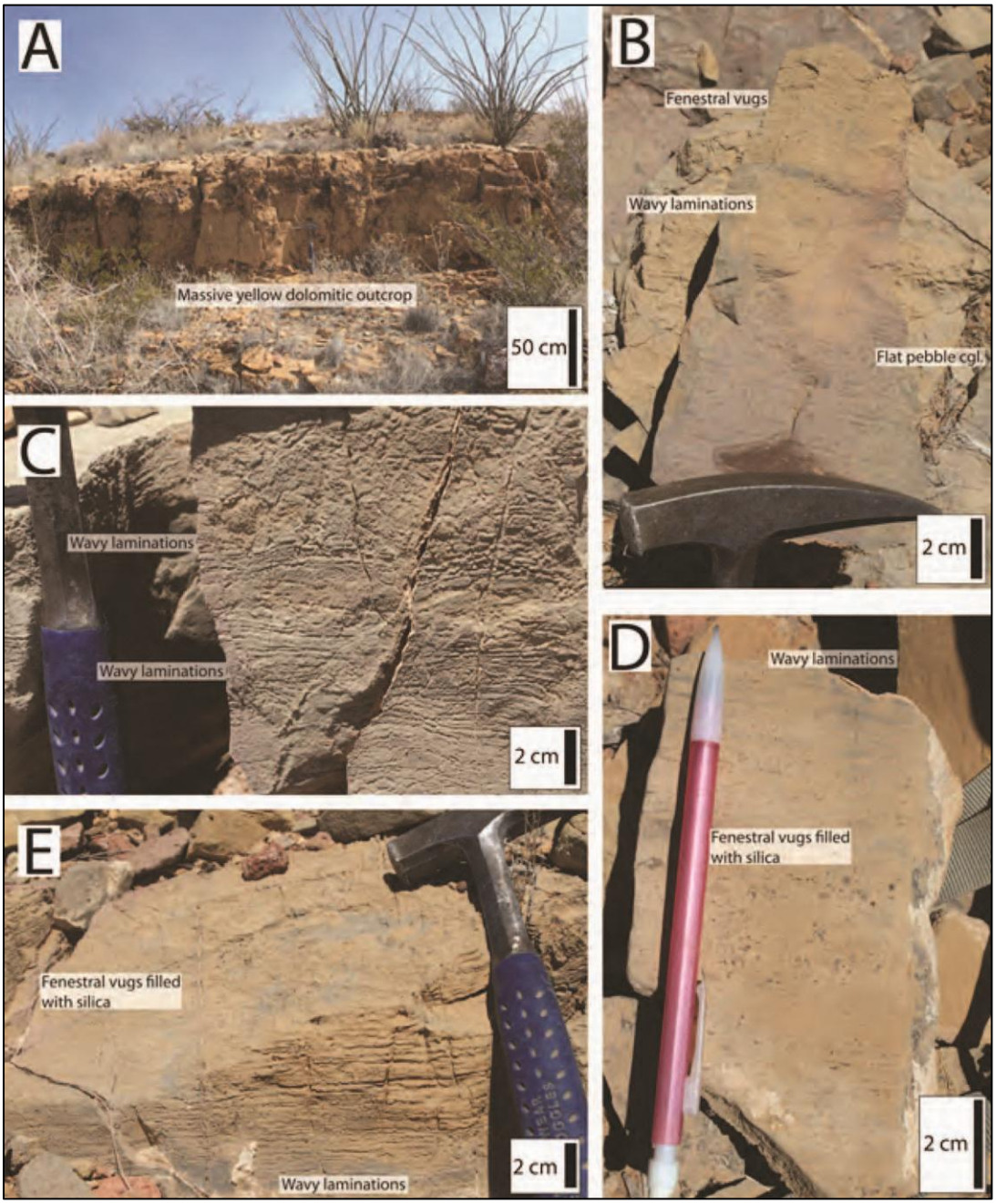

Figure 8: Outcrop Photographs of Fenestral Dolomudstone.

A) Yellow fenestral dolomudstone with chert nodules, Limonite Mine Section B) Flat pebble conglomerate and fenestral dolomudstone, Upper Waterfall Canyon Section. C) Brecciated algal mats, Upper Waterfall Canyon Section. D) Fenestral dolomudstone, Limonite Mine Section. E) Brecciated, dolomitized stromatolitic laminations, Upper Waterfall Canyon Section.

mm ovals and are typically filed with sparry calcite or silica cements (Figure 8D). Larger vugs occur interlaminated with stromatolites while vugs are less common where stromatolitic mats are brecciated and form flat pebble conglomerates. Brecciation on the top bedding plane is also common along with desiccation cracks (Figure 8D and 8E).

Some exposures of the monomict flat pebble conglomerates form light gray ledges that are heavily mottled and brecciated (Figure 9B). The heavily mottled and brecciated ledges are composed of dark gray monomict intraclasts suspended in a light gray matrix that have either been ripped up and transported very short distances or brecciated in place (Figure 9B). Both the dark gray clasts and light gray matrix are composed of a similar mudstone with no distinctive petrographic difference besides outcrop color. Only two conglomerate beds are observed in the Limonite Mine Section and each is overlain by a thin dolomudstone interval. These flat pebble conglomerates are much larger than what is observed interbedded with stromatolitic mats. A similar bed is observed in the Reef Ridge Section and is almost identical to what is observed in the Limonite Mine Section (Figure 9B) (Appendix A.1). Also, similar to the Limonite Mine Section, this bed is overlain by a thin dolomudstone interval. These beds appear to represent a disrupted zone below sub aerially exposed brecciated, laminated stromatolites.

Overall, fenestral dolomudstone beds are non-fossiliferous, but some beds contain encrusting and uniserial forams or ostracodes. Fine-grained quartz sand is also common within this facies, but is found either sparsely throughout the matrix or concentrated in darker micritic stromatolitic laminations (Figure 10A). Intraclasts are usually composed of peloids and dense microcrystalline calcite mud and ooids only have one or two laminae of growth and as a result are very small (< 0.5 mm) (Figure 10B). Large oncoid-shaped grains are also present, but are typically heavily micritized (Figure 10C). Very dense microcrystalline calcite forms clotted

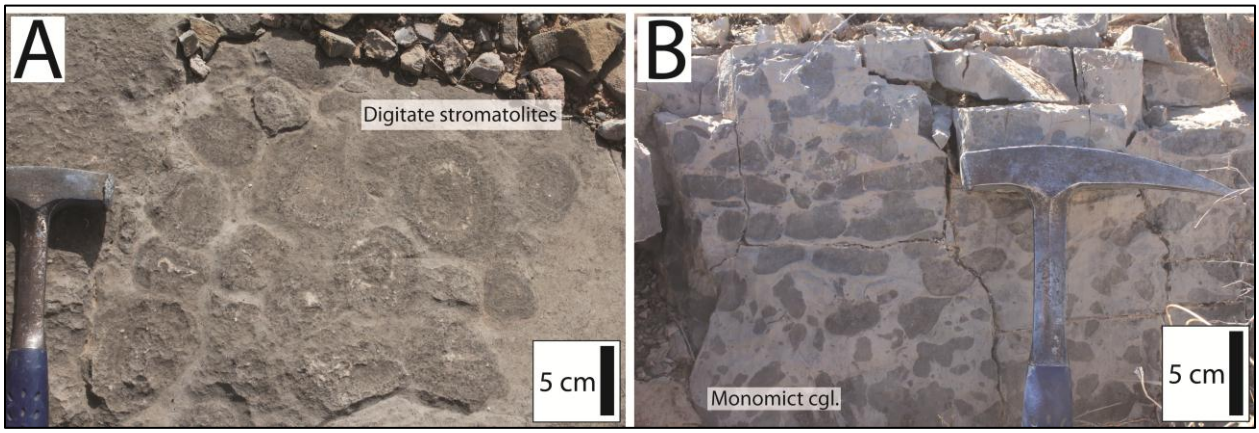

Figure 9: Outcrop Photographs of Fenestral Dolomudstones.

A) Plan view of digitate stromatolites, Limonite Mine Section. B) Large monomict flat pebble conglomerate, Reef Ridge Section.

textures throughout the matrix and represents brecciated fragments of stromatolitic mats that suggest long term sub aerial exposure (Figure 10C and 10D). Peloids occur frequently throughout the matrix but are bounded within the dense, clotted microcrystalline calcite.

The most distinguishing petrographic characteristic of this lithofacies is the dense microcrystalline calcite matrix and heavy micritization of both skeletal and non-skeletal grains. Some of these beds are completely dolomitized but the majority still effervesce when exposed to hydrochloric acid without being scratched. Non-fabric selective dolomitization is common throughout these beds. Quartz cement is common in beds and is typically found filling fenestral vugs. However, occasionally quartz cement is found filling intercrystalline porosity in highly dolomitized samples (Figure 10A and 10B). Calcite microspar and spar is also common filling fenestral vugs and interparticle porosity with a drusy mosaic geometry (Figure 10A and 10D).

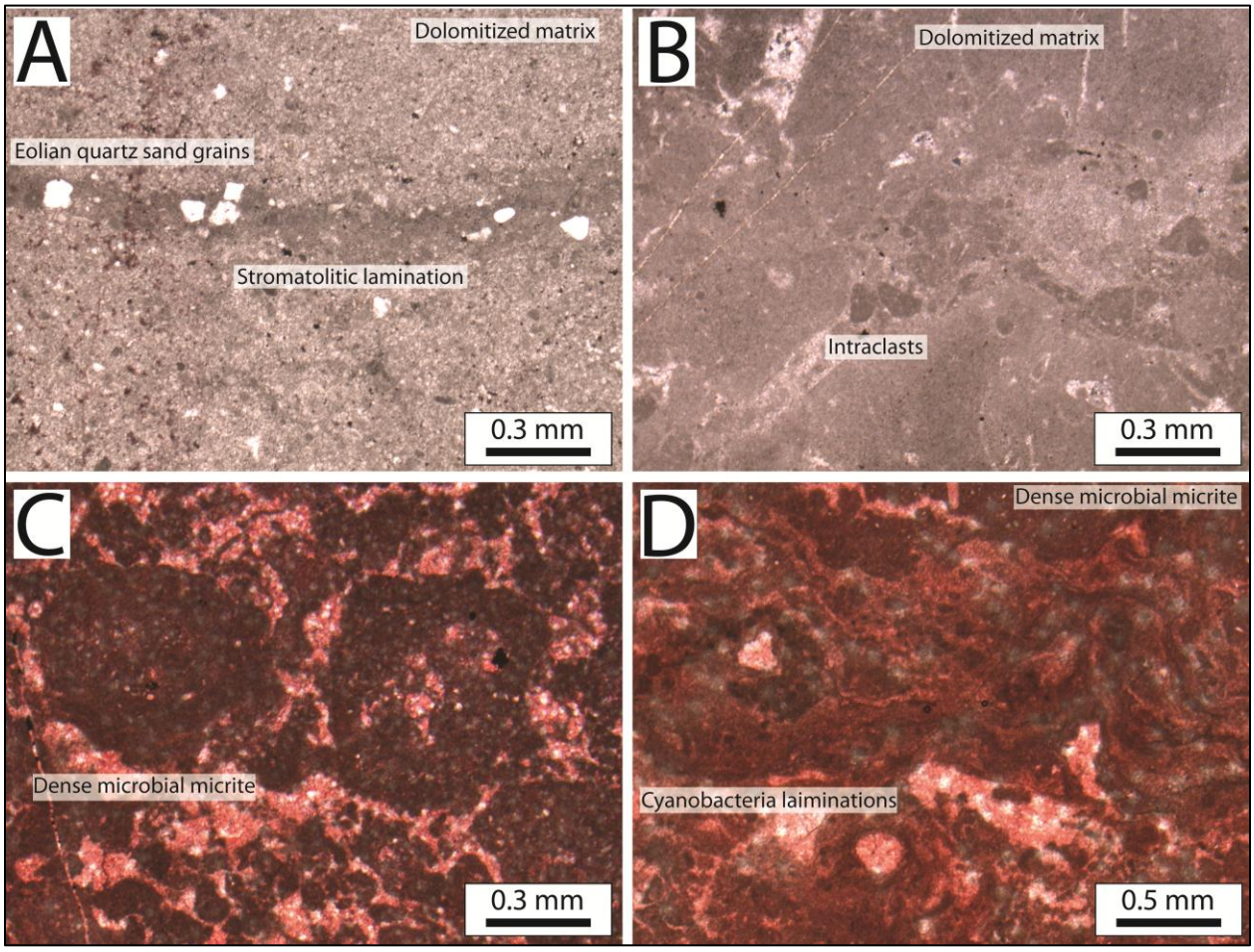

Figure 10: Photomicrographs of Fenestral Dolomudstone.

A) Dolomitized stromatolitic lamination with trapped eolian sand, stained, plane light. Sample LH-92. B) Dolomitized matrix intraclasts, stained, cross polarized light. Sample LH-107. C) Dense cyanobacteria clotted matrix, stained, plane light. Sample LH-101. D) Dark, wavy cyanobacteria laminations and clottings, stained, plane polarized light.

Fenestral dolomudstones are confined to the Robledo Mountains and are not present in the lower Hueco strata in the Franklin Mountains. Their occurrence is at the top of shoaling upward cycles of intertidal and supratidal lithofacies. Additionally, these beds are easily correlated between closely spaced stratigraphic sections based purely on lithologic

characteristics, suggesting a broad geographic distribution in more proximal environments along the paleoshoreline.

Depositional Environment Interpretation

Three key factors were considered when making environmental interpretations for fenestral dolomudstones: 1) pervasive dolomitization, 2) inter-laminated stromatolites with local brecciation and flat pebble conglomerates, and 3) fenestral vugs within the heavily laminated intervals. *In-situ* dolomitization was first recognized on carbonate tidal flats by Deffeyes et al. (1965), Shinn et al., (1965), Wells (1962), and Illing et al. (1965) in the Netherlands Antilles, Bahamas, and Persian Gulf respectively. All of these authors confirm that dolomite can form in the supratidal zone on tidal flats as sea water is brought to the surface by capillary action or from storm induced flooding. Evaporation leaves highly concentrated brines that allow dolomite to precipitate. In addition to this dolomitization process, Illing et al. (1965) found stromatolitic algal laminae underlying the upper most supratidal deposits, with very fine-grained peloidal muds sitting below the algal laminations. A similar relationship observed in the Upper Waterfall Canyon Section of the Robledo Mountains as seen in Figure 8C and 8E. Similar beds are also observed in the Limonite Mine and Quarry Sections.

Stromatolites are another common feature along coastlines across the world and throughout the geologic record. Stromatolites present in the lower Hueco strata of the Robledo Mountains are both flat, laminated forms and vertically-stacked hemispheroids, which are both a product of variations in sedimentation rates and wave/tidal energy (Logan et al., 1965). These digitate and thinly laminated mats would have grown within the supratidal and high intertidal environments (Shinn 1983). Also, small quartz sand grains within darker laminations in a dolomite matrix (Figure 10A) represent sediment trapped by cyanobacteria mats during dust

storms, which is typical of arid sabkha environments (Shinn, 1983). Brecciation and flat pebble conglomerates are also commonly interbedded among both laminated and digitate stromatolitc beds. These conglomerates appear to represent destruction of algal mats during high energy storms that temporally inundate the tidal flat (Cressman, 1976). As the storm surge regresses, the fragile mats are disrupted and deposited as randomly oriented fragments within a muddy matrix (Figure 8B, 8C, and 9B).

Fenestral vugs are common throughout intervals with algal laminations and are often filled with calcite spar or silica cements (Figure 8D, 10C and 10D). These vugs form from the shrinkage of sediment surrounding gas bubbles within algal mats as the gas bubbles escape to the air and represent reliable indicators of supratidal environments when found in muddy rocks (Fischer, 1964; Tebbutt, 1965; Shinn, 1983) In every outcrop exposure with laminated stromatolites and flat pebble conglomerates in the Robledo Mountains, fenestral vugs are commonly interlaminated between thin algal laminations (Figure 8B-E). Based on these factors, fenestral dolomudstones found in the lower Hueco member of the Hueco Limestone are considered to have developed on a supratidal flat similar to a modern day sabkha environment. Pervasive dolomitization, the presence of eolian dust, and brecciation of stromatolitic beds also suggest these environments were very arid as described by Shinn (1983).

2.1.2 Intertidal Carbonate Depositional Facies Association

Lithofacies within this category are: microbial intraclast packstone, dolomudstone, green-algal packstone to grainstone, and ostracode foram wackestone to packstone. All of these lithofacies are found in a narrow zone parallel to the paleoshoreline and mark a distinct transition

from supratidal facies that are often sub aerially exposed, to the shallow marine subtidal zone that is never sub aerially exposed. These rocks show evidence of restricted environments with both low and high tidal and wave energy, with sedimentary structures indicative of strong tidal influences, and heavily reworked storm deposits. Additionally, their relative position to each other could be interchangeable depending on paleogeography and local topographic relief. The exact characteristics that describe how and where these rocks formed during the early Wolfcampian are described below in order from most landward to most seaward.

Microbial Intraclast Packstone

Outcrop and Petrographic Characteristics

Outcrop exposures of microbial intraclast packstones form discontinuous, poorly exposed benches that weather light gray to light brown and are thin bedded (< 0.5 meters thick) (Figure 11A-F). Fresh surfaces are also light gray or slightly light blue to yellow. Microbial intraclast beds thin laterally and my represent thin, shallow channels that transition laterally into dolomudstone and fenestral dolomudstone. Locally, these beds are interbedded with thin (10 to 20 cm), tan to yellow dolomudstone and light brown sandstone. Outcrop exposures of these beds contain elongate (2 to 5 cm) carbonate intraclasts, elongate (5 to 10 cm) rip-up fenestral dolomudstone intraclasts, laminated stromatolitic intraclasts, chert pebbles, ooids, fine-grained sand, and abraded fossil fragments (Figure 11A, 11B and 11C). Some beds appear wavy laminated, indicative of local stromatolitic growth (Figure 11E). Moderate to high angle planar cross-beds are also observed, but because of poor outcrop exposure it is difficult to determine the paleogeographic transport direction (Figure 11F).Additionally, small chert pebbles and large granules are abundant throughout the coarse-grained, intraclast-rich intervals (Figure 11B, 12A, and 12B).

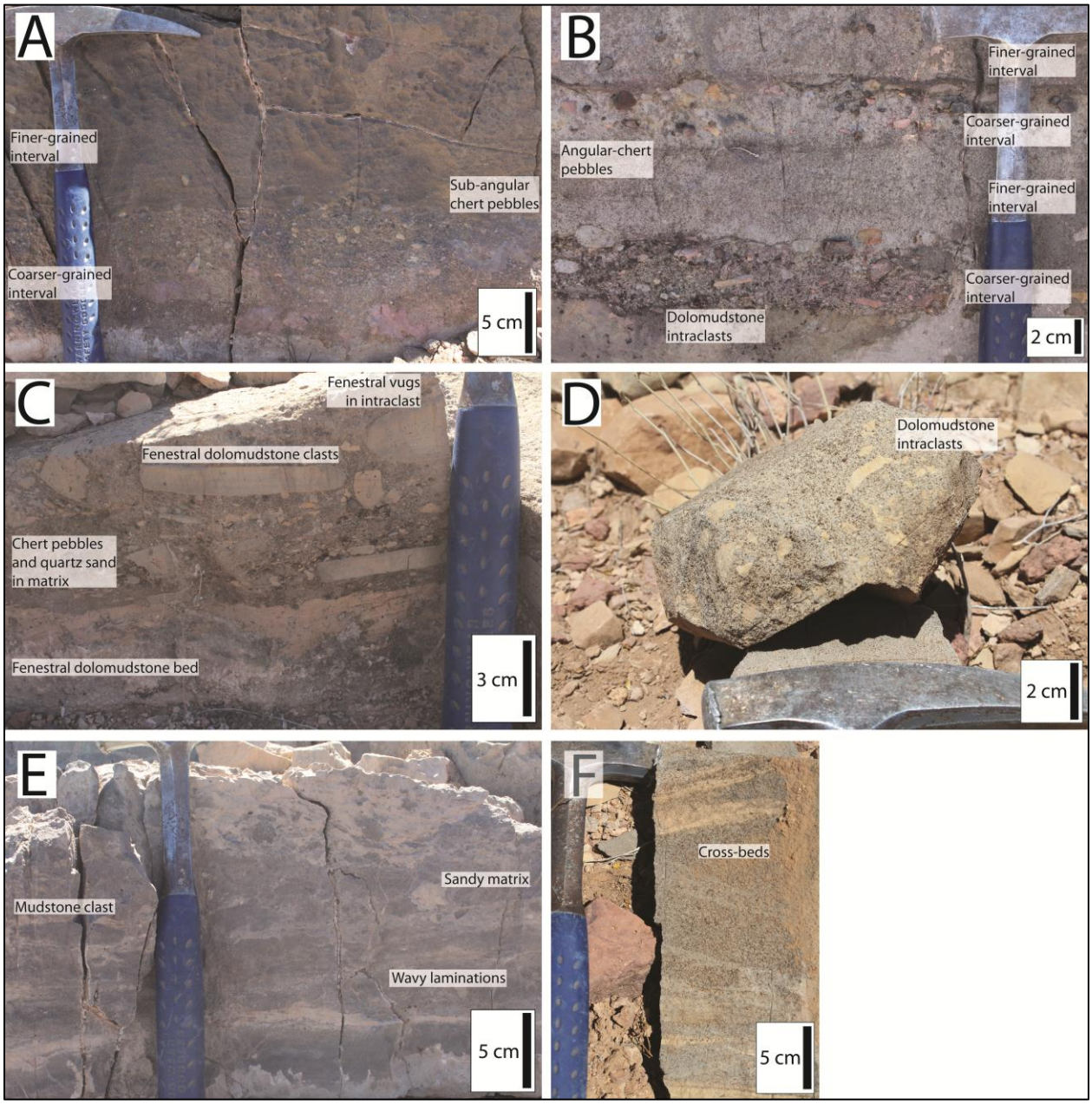

Figure 11: Outcrop Photographs of Microbial Intraclast Packstone.

A) Thin granule to pebble lag interbedded with a laminated sandy mudstone, Reef Ridge Section. B) Chert pebble lag, Reef Ridge Section. C) Rip-up clast conglomerate, Reef Ridge Section. D) Tan dolomudstone clasts within a light gray sandy oolitic packstone, Upper Waterfall Canyon Section. E) Rip-up stromatolites in a sandy packstone, Reef Ridge Section. F) Cross bedded sandy oolitic packstone, Upper Waterfall Canyon Section.

Fine-grained intervals appear to contain quartz sand and non-skeletal grains, but no large (> 2 cm) intraclasts or extraclasts. In the Upper Waterfall Canyon Section, these beds contain abundant fine-grained quartz sand and large, yellow dolomudstone intraclasts that appear to be sourced from the dolomudstone bed that directly underlies this bed (Figure 11D, 12C, and 12F). Overall, exposures of microbial intraclast packstone contain coarse-grained lithic debris derived from all adjacent lithofacies interbedded with finer-grained sandy intervals, amalgamated into one coarse-grained deposit.

The majority of grains within these beds are non-skeletal but skeletal grains include disarticulated and abraded fragments of crinoids, echinoids, bryozoan, brachiopods, bivalves, gastropods, sponges, encrusting forams, and ostracodes (Figure 12C-F). In thin section, small peloids (<0.2mm) are abundant along with 0.5 to 2 mm intraclasts that are also heavily micritized (Figure 12F). Dense microbial microcrystalline calcite is found coating most grains and appears to act as a binder with sparry calcite cement holding the grains together. Blocky calcite microspar and spar are very abundant filling interparticle and intraparticle porosity. Small patches of large dolomite rhombs are present, representing localized non-fabric selective dolomitization of carbonate mud matrix.

The Reef Ridge Section contains the majority of this lithofacies, but each section in the Robledo Mountains contains a few thin beds (Appendix A.1-A.5). However, slight variations do occur across these stratigraphic sections including slight changes or non-existent sedimentary structures, changes in dominant rock forming grains, changes in intraclast lithology, and color changes based on grain types. These spatial and temporal changes within this lithofacies suggests that subtle differences in depositional setting were present across the intertidal flats of this region.

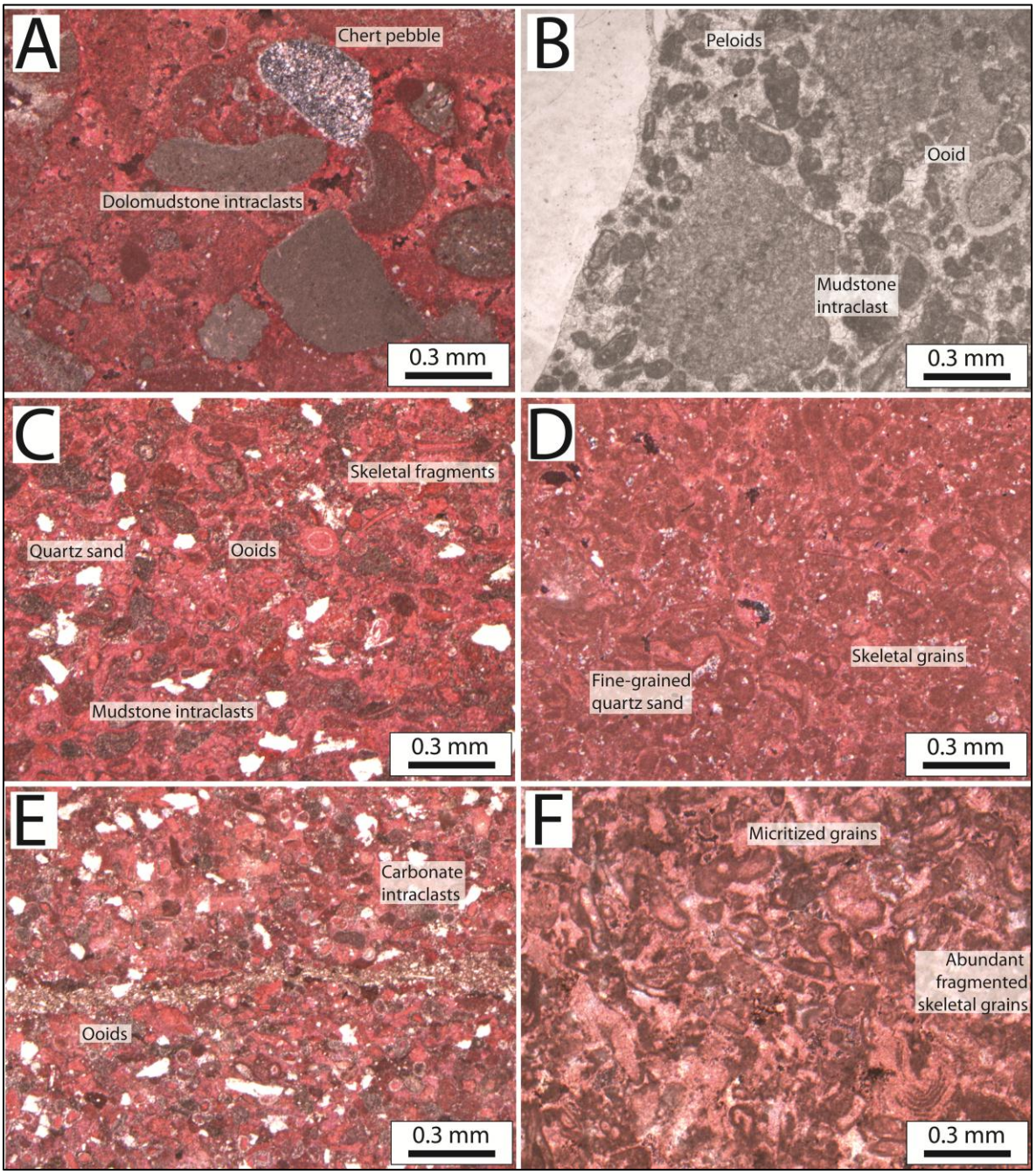

Figure 12 Photomicrographs of Microbial Intraclast Packstone.

A) Dolomudstone intraclasts, stained, cross polarized light. Sample LH-126. B) Peloids and mudstone intraclasts, unstained, plane light. Sample LH-99. C) Sandy oolitic packstone, stained, plane light. Sample LH-130. D) Micritized skeletal grains and peloids, stained, cross polarized light. Sample TM-11. E) Sandy oolitic packstone, stained, plane light. Sample LH-132. F) Micritized and abraded skeletal grains, stained, plane light. Sample LH-36.

Depositional Environment Interpretation

Two different types of depositional environments could be responsible for creating these beds. Based on the very heterogeneous mixture of non-skeletal and skeletal grains, these beds could either be deposited infrequently in the intertidal zone by large storms or slowly by small intertidal channels. Carbonate dominated tidal channels have been described in areas of the Trucial coast and the Bahamas that contain cross bedding, abundant skeletal and non-skeletal grains, and a distinctive down cutting into the underlying strata (Evans et al., 1969; Kendall and Skipwith, 1969; and Bathurst, 1975; Shinn, 1983;). In both areas the observed sedimentary structures and sequences that resemble those of siliciclastic fluvial systems but the presence of burrowing is the main difference between both (Shinn, 1983). These channels cross cut and traverse similar lithofacies to what has been described in the previous sections. Similar beds and sedimentary structures have been observed in the upper interval of the lower Hueco member of the Hueco Limestone in the Robledo Mountains (Durr, 2010; Mack et al., 2013). Consequently, outcrops that contain these characteristics are considered to represent a channelized deposit that transports a very heterogeneous mixture of grain types.

Based on the abundance of skeletal and non-skeletal grains, these beds could have also been formed by large storms that would have temporally inundated the intertidal and supratidal flats. As storm surge retreated from the coastline, it may have channelized or scoured into the underlying sediments producing carbonate storm deposits, often called tempestites. Previous studies have documented tempestite deposition with a particular influence on hummocky cross-stratification being a distinguishing feature (e.g., Hamblin and Walker 1979; Kreisa 1981; Dott and Bourgeois, 1982; Leckie and Walker, 1982; Swift et al. 1983; Craft and Bridge, 1987). In all of these studies, storm deposits contain a similar grouping of sedimentary structures such as

hummocky cross-stratification, ripple cross-laminae, scape burrows, couplets of fine- and coarse-grained laminae, abundant mixes of skeletal and non-skeletal grains, and intraclasts sourced from the underlying facies that are deposited during storm surge retreat (Kresia, 1981; Myrow and Southard, 1996; Seguret et al., 2001; Mohseni and Al-Aasm, 2004). However, no hummocky cross-stratification has been observed in this lithofacies in the Robledo and Franklin mountains. Despite this, the abundance and diversity of grain types suggests that these grains were sampled from areas landward and basinward of where they were deposited. Consequently, microbial intraclast packstones represent small, localized channel deposits related to major storm surge inundation and retreat in supratidal and intertidal environments.

Dolomudstone

Outcrop and Petrographic Characteristics

At outcrop scale, dolomudstone beds have a similar appearance to supratidal fenestral dolomudstone based on their color and composition but other characteristics, such as non-algal laminations and increased faunal diversity, suggests these beds formed in a restricted lagoonal depositional setting. Dolomudstone can be found in both the Robledo and Franklin mountains but are most abundant in the Robledo Mountains. Weathered outcrop exposures form thin tan, yellow, light gray, pink, light blue, or white ledges (0.2 - 1.0 m thick) that are laminated and usually cap thicker, more massive mudstone and wackestone intervals. Fresh surfaces usually appear a darker version of the weathered surface, with some beds having a reddish brown hue in the fresh matrix (Figure 13A-F). Thin, medium- to fine-grained, well-sorted sand laminations are occasionally observed but are confined to exposures in the Robledo Mountains. Overall, these beds lack significant sedimentary structures, but thin, sandy laminations are present in almost every exposure of dolomudstone in this region (Figure 13A-D). Small rounded burrows are

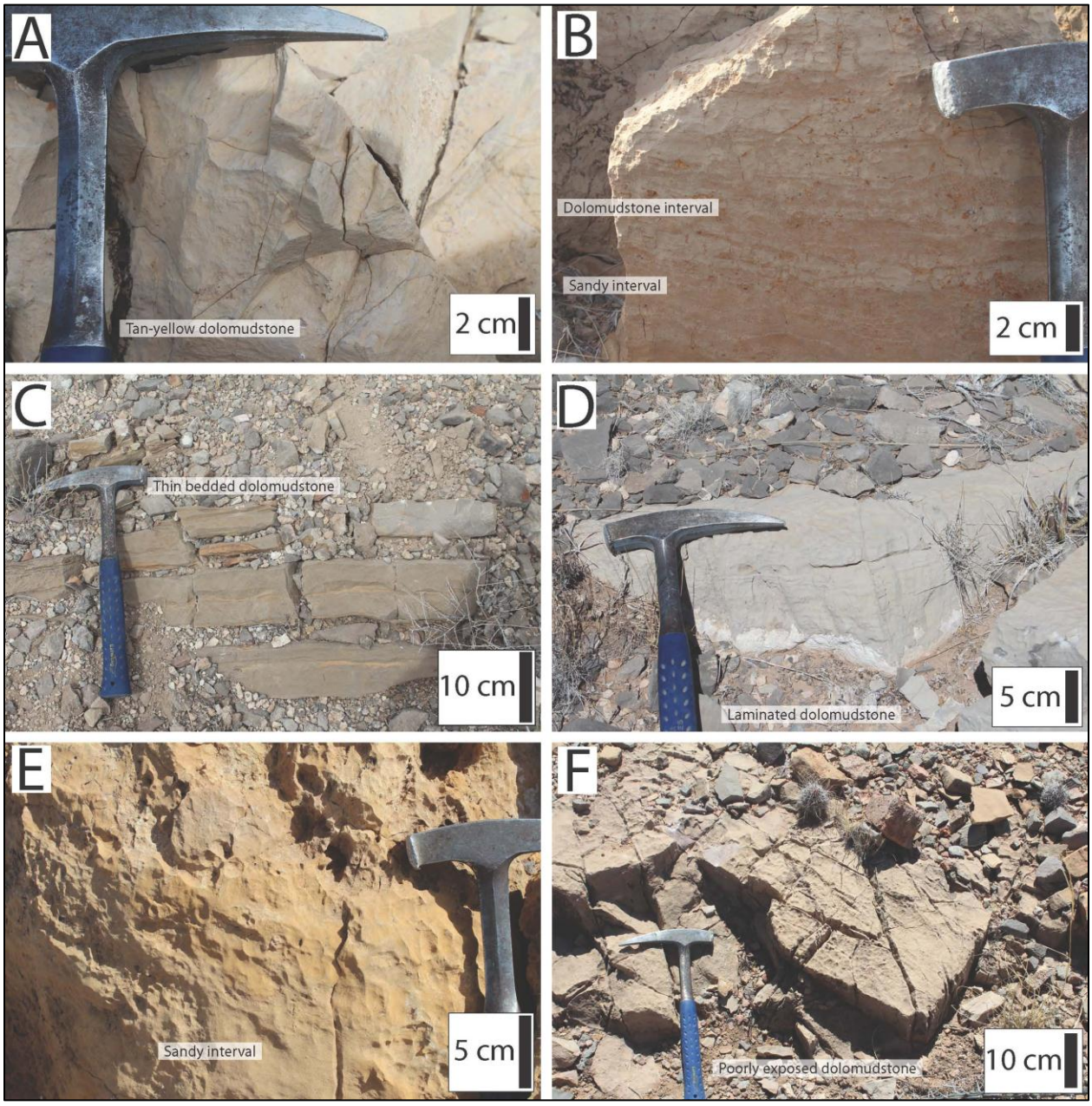

Figure 13: Outcrop Photographs of Dolomudstone.

Massive dolomudstone, Tom Mays Park Section. B) Laminated and partially brecciated dolomudstone, Limonite Mine Section. C) Thin bedded dolomudstone, Vinton Canyon Section. D) Laminated dolomudstone, Tom Mays Park Section (TM-12). E) Yellow sandy dolomudstone, Limonite Mine Section. F) Tan dolomudstone, Upper Waterfall Canyon Section.

occasionally found on bedding planes and typically the upper bedding plane appears brecciated (Figure 14B).

This facies contains more skeletal and non-skeletal grains than the fenestral dolomudstone lithofacies. Non-skeletal grains are the most abundant and consist of pellets, peloids, oncoids, intraclasts, authigenic quartz crystals, intraclasts, and fine-grained quartz sand (Figure 14A-D). Intraclasts have darker rims of very finely crystalline dolomite (<500 microns) while their centers are usually less dolomitized (Figure 14A-C). Chert is fairly common within these beds and forms small, dark brown elongate nodules that are usually less than 20 cm on their long axis. Skeletal grains are rare, mostly ostracode and bivalve fragments. *Tubiphytes* fragments, crinoid columnals, and encrusting forams, are present but are also locally disarticulated, abraded, and micritized (Figure 14D).

The matrix of these beds consists of microcrystalline calcite and dolomicrite (Figure 14A - F). Dolomite crystals are very small (<500 microns) because they likely formed by recrystallizing microcrystalline calcite crystals. Dolomitization appears to be non-fabric selective as it has altered both the matrix and non-skeletal grains to the same degree. However, the rims of grains can be identified from the darker, finer-grained dolomite crystals that compose them. Silica cements occur rarely and but calcite cements are abundant in small vugs, fractures, and interparticle porosity as both microspar and spar, but no common geometric arrangement of the blocky calcite crystals exists (Figure 14C, 14D, and 14F). Exposures in the Franklin Mountains are more micritic compared to beds found in the Robledo Mountains, a likely result of much less non-fabric selective dolomitization.

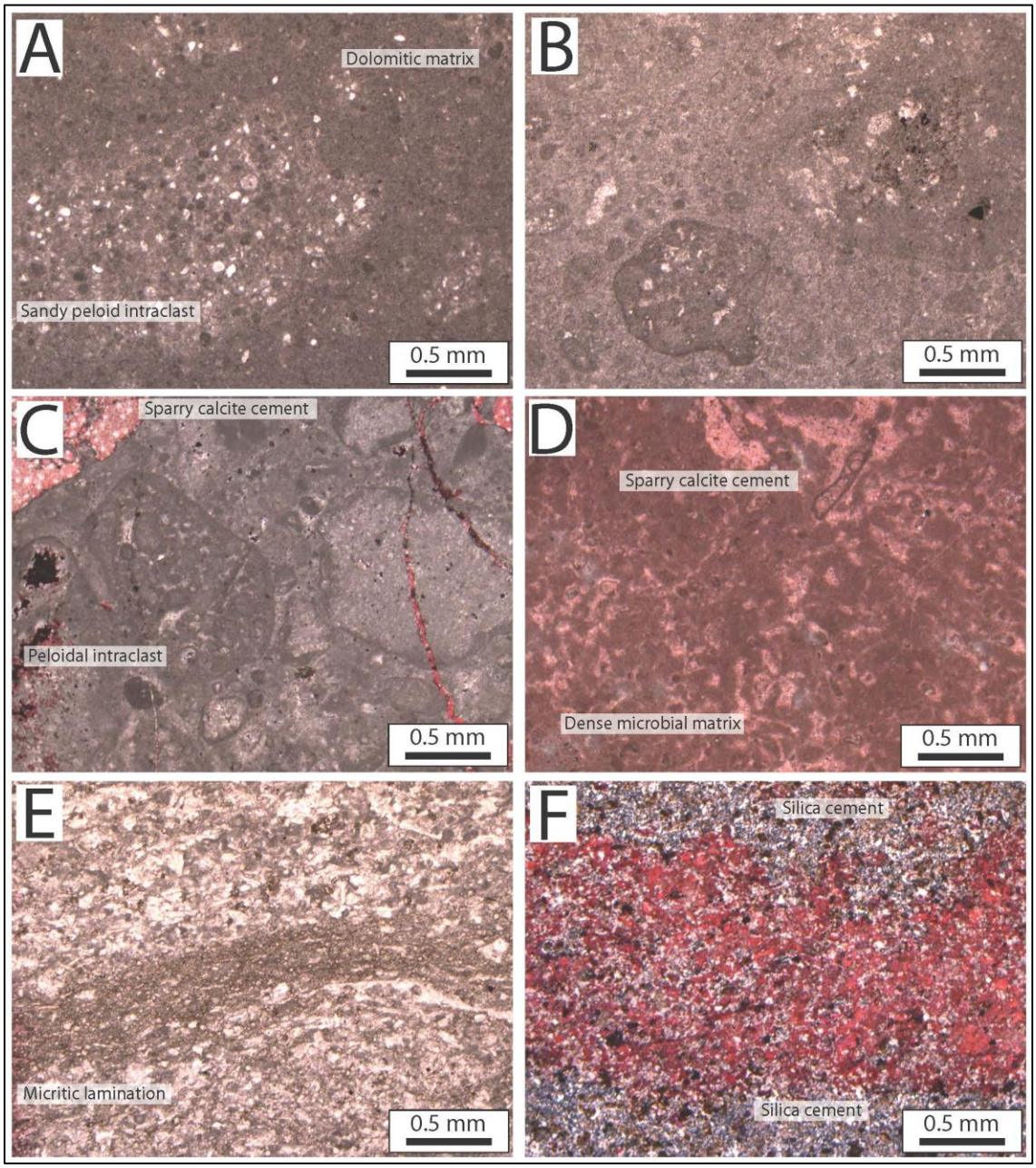

Figure 14: Photomicrographs of Dolomudstone.

A) Sandy, intraclast dolomudstone, stained, plane light. Sample TM-12. B) Dolomitized intraclasts, stained, plane light. Sample TM-5. C) Dolomitized peloidal intraclasts, stained, plane light. Sample LH-91. D) Dense microbial micritic matrix, stained, cross polarized light . Sample LH-15. E) Laminated dolomudstone, unstained, plane light. Sample VC-9. F) Laminated dolomudstone with silica cement, stained, cross polarized light. VC-9.

Similarly to the fenestral dolomudstone, dolomudstone is predominately found in the Robledo Mountains and rarely found in the lower Hueco strata of the Franklin Mountains. In the Robledo Mountains, these exposures are typically bounded within shoaling upward cycles between fenestral dolomudstone above and intertidal facies below. However, in the Franklin Mountains, dolomudstone is only found as thin laterally continuous beds bounded by subtidal facies above and below. Occasionally, other intertidal environments are found below dolomudstone. In these sections, dolomudstone forms the cap to shoaling-upward cycles while in the Robledo Mountains dolomudstones comprise the middle parts of these cycles.

Depositional Environment Interpretation

Based on the characteristics described above, dolomudstones appear similar to fenestral dolomudstones but lack many features observed in them. Unlike the fenestral dolomudstones, these dolomudstones appear to form in association with saline brine evaporation and is not formed by *in-situ* dolomitization on supratidal flats (Deffeyes et al. 1965; Shinn et al., 1965; Wells 1962; and Illing et al., 1965). Environments that experience periodic hypersaline conditions from a decrease in water circulation from sea-level changes or development of a barrier or shoal have potential to form conditions that would allow for dolomite precipitation at the sediment-water interface (Enos, 1983). These conditions would lead to a restricted faunal diversity, such as observed in the lower Hueco dolomudstones. The laminated appearance of these beds could also be the result of reduced circulation in this restricted environment, resulting in a lower energy regime that would allow finer-grained sediment to slowly settle out of the water column.

Enos (1983) identifies restricted shelfal lagoons and bays based on the style of shoaling upward cycles where basal muddy carbonates with low diversity are overlain by supratidal fenestral dolomudstones or other adjacent intertidal facies. Additionally, the muddy low energy restricted environments may contain facies mosaics of random transitions related to minor sea-level changes in shallow environments that create substantial changes in depositional environments (Enos, 1983; Laporte, 1967). Thin dolomudstone beds observed in the lower interval of the lower Hueco member are always interbedded with supratidal and intertidal deposits (microbial intraclast packstone, ostracode foram wackestone, and oolitic packstone). Based on this relationship, along with the low faunal diversity, abundant non-skeletal grains, and dolomitization, it appears that this lithofacies is characteristic of a restricted lagoon environment that led to very saline to hypersaline water chemistries and deposition of laminated and massive dolomudstone.

Green-algal Packstone to Grainstone

Outcrop and Petrographic Characteristics

This lithofacies is only found in three stratigraphic sections in both the Robledo and Franklin mountains (Limonite Mine, Lower Waterfall Canyon, and Tom Mays Park sections respectively) and beds have very different physical characteristics at each outcrop. Beds in the Limonite Mine Section (Appendix A.1) weather light gray while the beds in the Lower Waterfall Canyon and Tom Mays Park sections are dark gray on both fresh and weathered surfaces. In all places these beds form small resistant, laterally continuous ledges between 0.5 and 1 m thick. The basal parts have a mottled, heavily bioturbated appearance and contain few ooids (Figure 15A-D). Muddy bioturbated beds grade into grain-rich beds that contain abundant abraded, disarticulated bivalves and are often interbedded with laminated dolomudstone (Figure 15D). The upper bedding plane

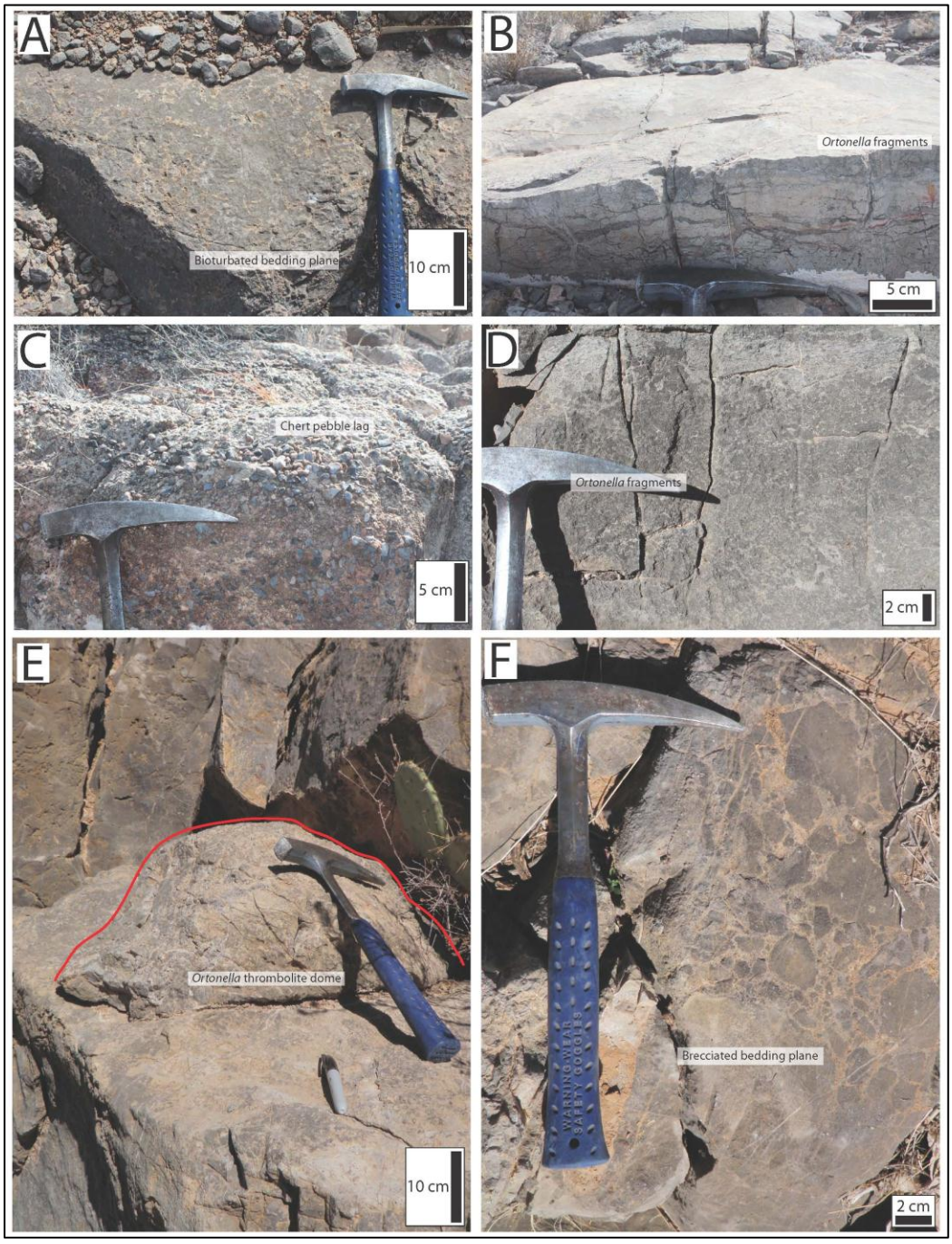

Figure 15: Outcrop Photographs of Green-algal Packstones and Grainstone.

A) *Ortonella* fragments (dark gray), Limonite Mine Section. B) Brecciated upper part of previous the previous outcrop. C) Angular chert pebble lag, Limonite Mine Section. D) *Ortonella* grainstone, Franklin Mountains. E) Thrombolitic *Ortonella* dome, Lower Waterfall Canyon Section. F) Brecciated upper bedding plane, Lower Waterfall Canyon Section.

contains small Thrombolitic domes composed almost entirely of *Ortonella* fragments with intraclasts and fine-grained quartz sand filling low relief areas (Figure 15E). Patchy small-scale brecciation occurs on the upper bedding planes between these mounds. Occasionally root structures filled with calcite spar occur on this plane (Figure 15F). In the Limonite Mine Section, this bed is capping a thin dense lag of very angular chert fragments and pebbles, which does not occur in the other two sections (Figure 15C). It is important to note that based on the various stratigraphic position of these beds, they are not correlative based lithologic characteristics and probably occurred as a very small isolated environments, implying that rapid facies changes occur over fairly small distances.

In thin section, beds appear entirely composed of large radiating clusters of calcified tubes of the green algae *Ortonella,* and are bound together with calcite microspar and spar (Figure 16A-D). All five thin sections made from these beds contain heavily micritized *Ortonella* fragments, sometimes encrusted with microbial growth, probably related to endolithic algae (Figure 16A - D). Non-skeletal grains, such as intraclasts and peloids, are abundant between *Ortonella* fragments and are usually cemented together with sparry calcite. (Figure 16B and 16D). Ooids are rare in these beds. Skeletal grains are much less common but disarticulated and abraded bivalves and brachiopods are present in the Limonite Mine beds. These coarser-grained elements comprise the grainy matrix in the middle parts of the beds in the Limonite Mine Section. Fine- to very-fine, well rounded quartz sand grains are present in the Limonite Mine beds and represent eolian sand based on their low abundance and well-rounded appearance. Some silica cement occurs in the Lower Waterfall Canyon exposures but overall these beds are cemented with calcite and contain very little micrite as mud.

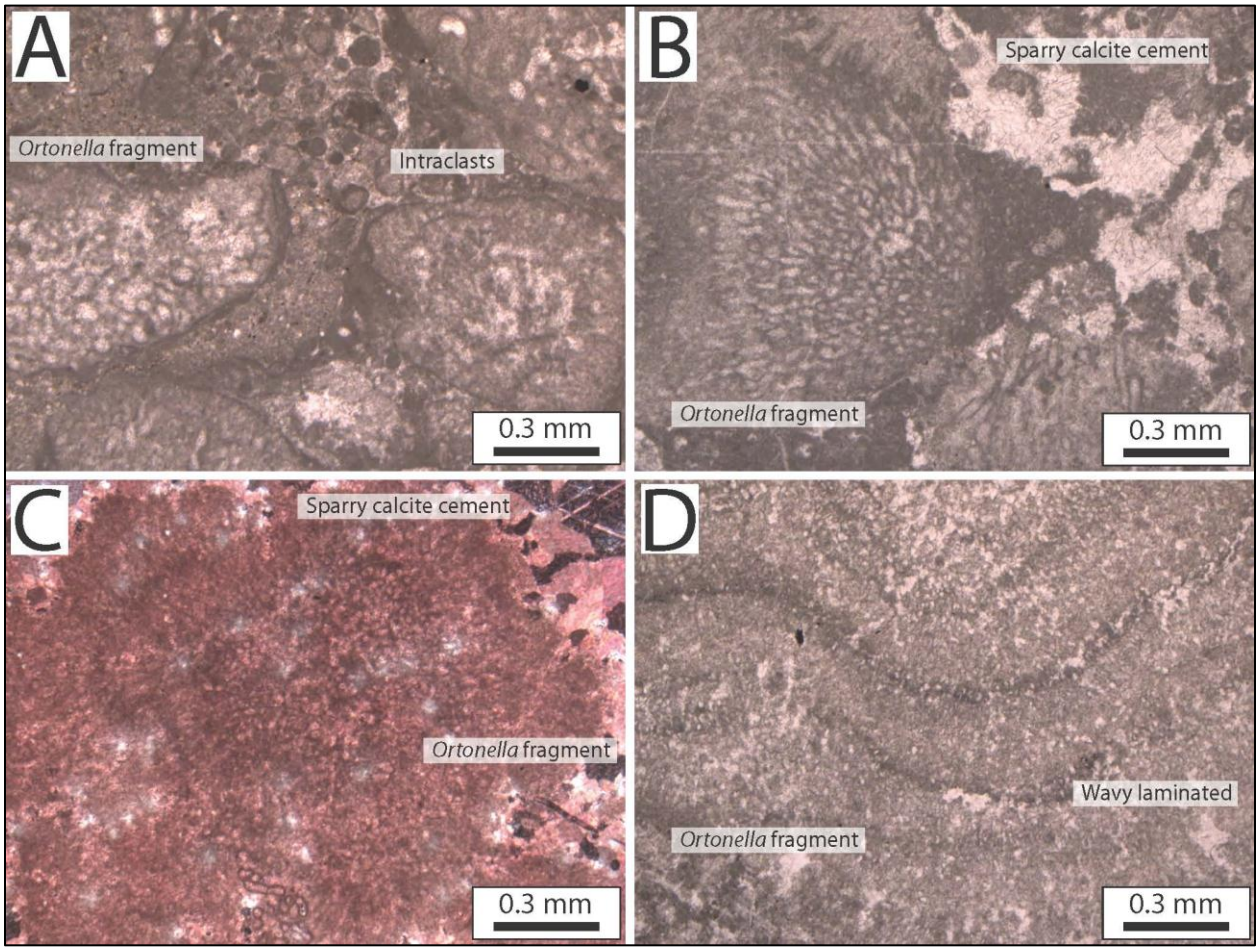

Figure 16: Photomicrographs of Green-algal Packstone and Grainstone.

A) *Ortonella* fragments and peloids, unstained, plane light. Sample LH-70. B) *Ortonella* fragment composed of radiating calcified tubules, unstained, plane light. Sample LH-71. C) *Ortonella* in sparry calcite cement, stained, cross polarized light. Sample LH-95. D) Oblique cross-section through an *Ortonella* fragment, unstained, plane light. Sample TM-7.

Depositional Environment Interpretation

Both outcrop and petrographic observations provided important evidence that isolate these samples as their own lithofacies despite their rare occurrence within the stratigraphic sections. The large angular chert pebbles present suggest a very different environmental interpretation

than would be found within the fossiliferous packstones and grainstones. These pebbles should represent a much higher energy environment in order to transport such large grains. Additionally, skeletal grains are always fragmented and abraded implying a moderate

amount of wave energy local to deposition. Finally, each thin section appears winnowed because it lacks abundant micrite mud and is almost entirely held together by coarsely crystalline sparry calcite cement. All of these characteristics describe a higher energy environment that fragmented green algal mats or domes, with some local source for chert pebbles. Despite these characteristics, this lithofacies always occurs stratigraphically between supratidal and intertidal facies. Consequently. this environment likely occurred near the low intertidal to high subtidal transition and represents a coastline that is subjected to a moderate amount of wave energy and is usually subaqueous to promote algal growth.

In Southwestern England, Kirkham (2005) describes a similar facies in the Visean Clifton Down Limestone. This limestone contains thrombolites composed almost entirely of *Ortonella* algae along with microbial encrusted brachiopod fragments and abundant peloids and ooids. Burrows are common and these beds occur interbedded with stromatolitic intervals. This is similar to what is observed in thin section for the beds in the Robledo and Franklin mountains that contain *Ortonella*. Additionally, beds in the Robledo Mountains directly overlie stromatolitic intervals. Based on these characteristics and Kirkham (2005) suggests these *Ortonella* thrombolites formed in shallow-water settings that could winnow the muddy sediment away, leaving space for early marine cements to develop. Consequently, green-algal packstone and grainstone beds in the lower interval of the lower Hueco member formed in shallow marine waters where *Ortonella* formed discrete thrombolites in the intertidal environment.

Ostracode Foram Wackestones to Packstone

Outcrop and Petrographic Characteristics

Ostracodes are abundant in many different lithofacies across the Robledo shelf and Orogrande Basin but this lithofacies is intended to describe a very restricted environment in which ostracodes comprise over 75% of the rock-forming grains. Outcrop exposures range in color from light to medium gray on weathered surfaces and tan to yellow where non-fabric selective dolomitization has diagenetically altered the rock (Figure 17A-F). On fresh surfaces, these outcrops are always very dark gray, appearing to be made completely of microcrystalline calcite. Sometimes fresh surfaces have a fetid odor, related to a higher organic content. Bed

thickness is highly variable and ranges from 1.0 - 20 m. Outcrops form both massive, cherty, laterally continuous ledges and large cliffs to poorly exposed, chert-covered slopes with irregular, low relief, lumpy exposures (Figure 17B and 17 F). Many of these beds have a mottled texture within the micrite matrix, related to either bioturbation or diagenetic alterations throughout the rock. Some locations that exhibit a heavily mottled texture on outcrop show no evidence in thin section that suggests significant diagenetic alterations or burrows. Consequently, this alteration is purely surficial and occurs infrequently. The only similarity between the beds where this mottled texture occurs is their relative position to local faults, suggesting some type of fluid alteration related to faulting. Massive, cliff forming units have a grainy matrix with abundant disarticulated ostracodes and with few forams, bivalve, and crinoid fragments (Figure 17B). Thinner beds typically appear laminated and have intraclasts and thin (1.0 -2.0 mm) root structures filled with coarse sparry calcite on their upper bedding plane (Figure 17A, 17C, and 17D). Large (10-20 cm) elongate to round, brown, white, black, and gray chert nodules are abundant and occur evenly spread throughout the matrix (Figure 17E and 17F).

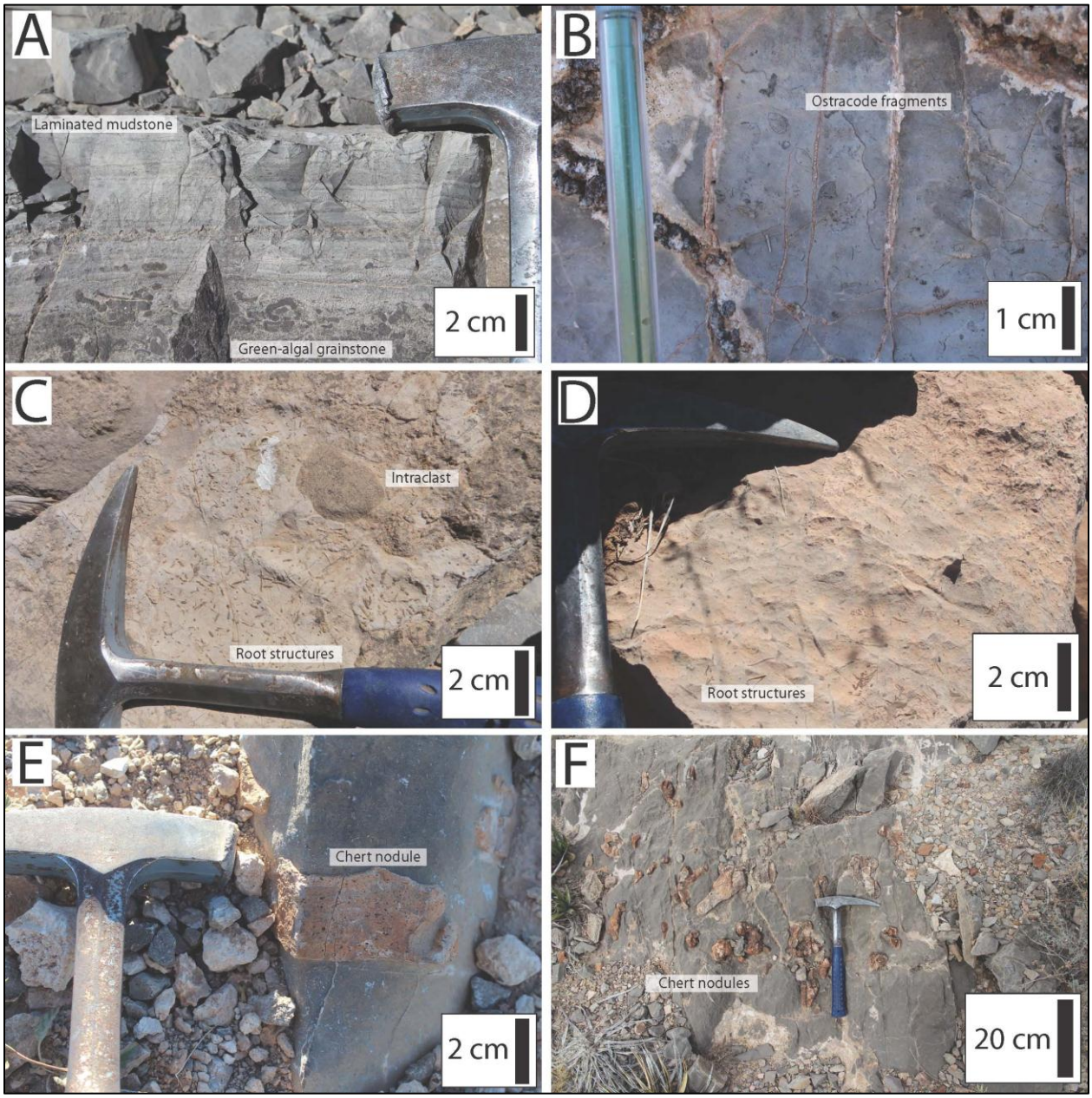

Figure 17: Outcrop Photographs of Ostracode Foram Wackestone.

A) Laminated ostracode wackestone overlying a green-algal packstone, Tom Mays Park Section. B) Articulated and disarticulated ostracodes, Reef Ridge Section. C) Root structures on upper bedding plane filled, Lower Waterfall Canyon Section. D) Root structures on upper bedding plane, Lower Waterfall Canyon Section. E) Chert nodule in muddy wackestone, Anthony Syncline Section. F) Chert nodules in a wackestone, Vinton Canyon Section.

Disarticulated and articulated ostracodes are the most abundant rock-forming grain in this lithofacies and exhibit either a prismatic and homogenous internal wall structure (Figure 18A C). Both encrusting and uniserial forams are the next most abundant skeletal grain, but their role as a rock forming grain is minimal. Locally, crinoids, echinoids, bryozoans, brachiopods, and trilobites are present as rare fragments. Peloids are common but ooids, oncoids, and intraclasts occur rarely (Plate 3). Very fine- to fine-grained, sub rounded, well-sorted quartz sand grains are also common and represent influx of eolian dust (Figure 18D). The matrix is primarily composed of dense microcrystalline calcite, which gives hand samples and thin sections a dark gray appearance. Calcite microspar cement is common and usually forms equant blocky crystals filling voids or small fractures but most commonly occurs filling intraparticle porosity (Figure 18A and 18B). However, in the Lower Waterfall Canyon Section, bladed isopachous calcite cements are observed in two different beds filling this intraparticle porosity. Dolomite and silica cements are rare and only fill vugs within the micrite matrix (Figure 18E). Local geopetal structures are common and based on the dark, dense, non-microbial micrite matrix, most beds appear laminated and compacted in thin section (Figure 18F). Additionally, microstylolites are common near ostracode tests that are fractured and compressed, appearing to have been over compacted.

Depositional Environment Interpretation

Two key criteria listed above suggest that deposition of this lithofacies occurred in a low energy restricted lagoon or bay, where some type of barrier dissipated wave energy before it could enter the lagoon. However, this lagoon would be much less restricted than the environment that produced the dolomudstone lithofacies. Work by Enos (1983) and Wilson and Jordan (1983) suggested that a fossil assemblage of only invertebrate filter feeders could represent a restricted

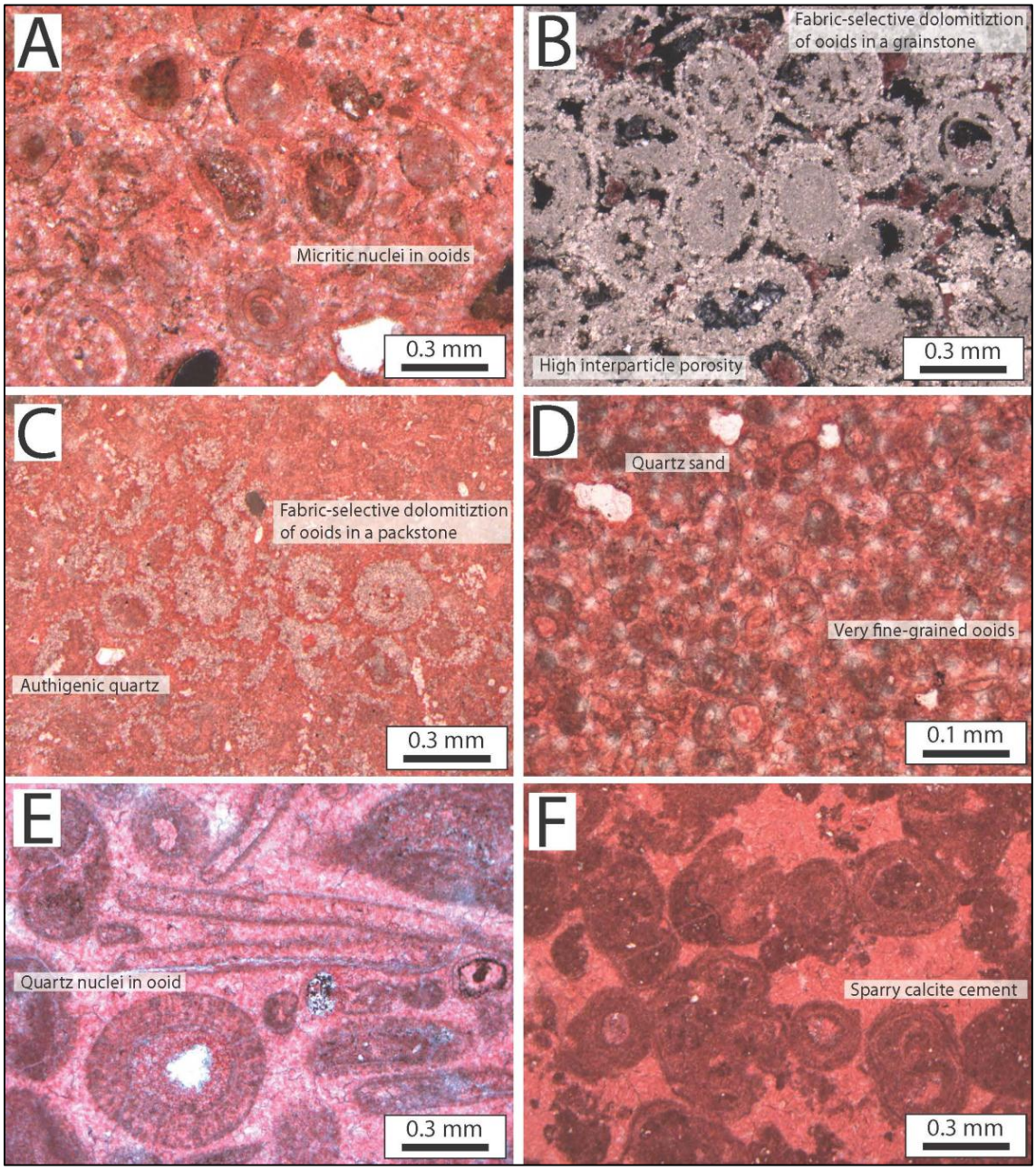

Figure 18: Photomicrographs of Ostracode Foram Wackestone.

A) Articulated ostracodes filled with calcite microspar, stained, plane light. Sample LH-52. B) Atriculated ostracode filled with calcite microspar at 10X, unstained, cross polarized light. Sample LH-125. C) Laminated ostracode tests, unstained, plane light. Sample TM-8. D) Very fine- to fine-grained quartz sand in a dense micrite matrix, stained, plane light. Sample LH-60. E) Dolomite cement filling vuggy porosity, stained, plane light. Sample LH-57. F) Laminated ostracode wackestone, stained, plane light. Sample LH-52.

marine environment, as the majority of invertebrate filter feeders can tolerate a wide variety of environmental conditions. However, these beds rarely contain an abundance of filter feeders but rather only contain ostracodes and forams. Enos (1983) also states that slow water circulation would result in depleted nutrients or abnormal salinities that would also inhibit faunal diversity. This suggests an even more restricted environment because of the low faunal diversity.

Enos (1983) describes semi-restricted, compartmentalized lagoons along the coast of Florida and along the northern coast of Cuba that contain rapid lateral and vertical facies transitions creating facies mosaics. Kjerfve (1986) classified coastal lagoons into three different types based on the access to water circulation, river input, wind stress, tides, and precipitation of evaporates. These three types of lagoons are choked, restricted, and leaky and are mainly defined based on their availability to water circulation from the ocean. Regardless, lagoons tend to be shallow water, low energy environments that can have variable water chemistries based on available circulation. In the lower Hueco strata, ostracode foram wackestones contain an abundance of microcrystalline calcite mud suggesting lower wave and tidal energy, allowing for deposition of fine-grained carbonate mud. Higher wave and tidal energy would have winnowed the mud out off of the sediment water interface, leaving only the coarser skeletal debris. Enos (1983) and Kjerfve (1994) both describe wind influences in modern day coastal lagoons in the Bahamas and on the Pacific coast of Mexico. In most ostracode foram wackestones, moderate amounts of fine-grained, well rounded, well sorted quartz sand grains are observed throughout these thin sections. It is likely that these sand grains represent eolian dust blown into the lagoon. As stated in the fenestral dolomudstone section, Shinn (1983) suggested this as a likely mechanism for incorporating sand into algal mats on the supratidal flat. Winds that would blow sand onto a supratidal flat would certainly have the potential to deposit eolian dust into the

adjacent restricted lagoon. Again, this demonstrates that all of these lithofacies in the supratidal and intertidal associations form within close proximity to each other and are all affected by local climatic conditions. These relationships suggest that ostracode foram wackestone represent a transitional environment between the supratidal and subtidal depositional environments.

2.1.3 Subtidal Carbonate Depositional Facies Association

This lithofacies association is composed of oolitic packstone and grainstone, fossiliferous packstone and grainstone, fusulinid packstone and grainstone, and phylloid algal bafflestone with different depositional patterns. Subtidal deposits form basinward of the paleoshoreline both above and below fair-weather wave base. Additionally these facies are rarely sub aerially exposed unless there is a significant change in sea-level related to major tectonic or eustatic events. Higher energy environments occur in the shallower locations and are concentrated around fair-weather wave base. Consequently, environments that are more basinward from fair-weather wave base are exposed to progressively less wave and tidal influences as the depositional profile deepens into the basin.

Oolitic Packstone and Grainstone

Outcrop and Petrographic Characteristics

In thin section, this lithofacies was defined by having greater than 50% ooids as the dominant rock forming grain. On outcrop, beds range in color from light to medium gray on both weather and fresh surfaces. In some locations in the Robledo Mountains however, non-fabric selective dolomitization has altered the weathered color to a tan-yellow (Figure 19A). Fresh surfaces of the dolomitized ooids appear slightly red, related to the iron content within the replacement dolomite. Bed thickness ranges from medium to thick bedded (0.5 - 2.5 m) and beds

typically occur as laterally continuous ledges with sharp basal contacts. Oolitic packstone beds form thin beds with no visible bedforms and are composed of small ooids (<0.5mm). Conversely, oolitic grainstone beds are thicker intervals that contain larger ooids (0.5-1 mm) and are usually laminated, planar cross-bedded, or contain hummocky cross-stratification (Figure 19B - D).

Besides ooids, there are also abundant skeletal and non-skeletal grains within this lithofacies, but typically account for less than 20% of the rock forming grains in both the packstone and grainstone (Figure 20A-F). Fragmented and abraded crinoids, echinoids, bryozoans, brachiopods, bivalves, gastropods, forams, and ostracodes are all observed in both thin section and on outcrop. Microbial encrustations and encrusting forams are rare but can be found in a few of the packstone lithofacies. Most of these skeletal grains are heavily abraded from the high energy environment in which ooids form. Pellets, peloids, angular chert pebbles, and intraclasts are also common but mainly restricted to the packstones. Moderate amounts of fine-grained, well-rounded quartz sand grains suggest that eolian sand was transported into the basin (Figure 20D and 20F).

Ooid morphology is similar between all stratigraphic sections. Most of the larger ooids that are not recrystallized with dolomite exhibit multiple radial growth layers (Figure 20A, 20D, and 20E). Where nuclei have not been removed through dissolution, their composition is either abraded skeletal grains or rounded quartz grains (Figure 20A and 20E). Smaller ooids occasionally have nuclei composed of microcrystalline calcite cement but in most places nuclei are filled with calcite microspar and spar cements (Figure 20A, 20D, and 20F). Most oolitic packstone beds contain ooids suspended in a microcrystalline matrix. Fabric selective dolomitization is common and completely recrystallizes ooids where it occurs (Figure 20B).

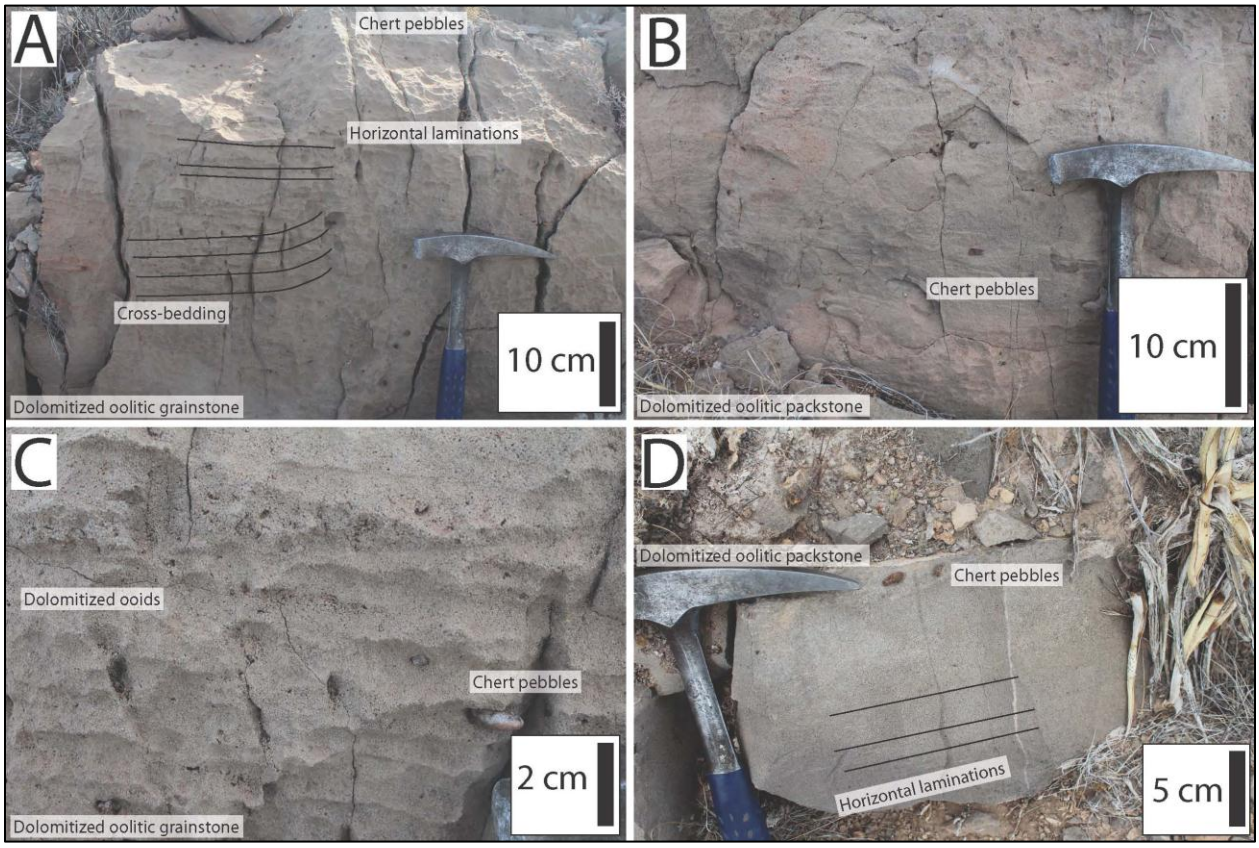

Figure 19: Outcrop Photographs of Oolitic Packstone and Grainstone.

A) Low angle planar ross-bedding in a dolomitized oolitic grainstone, Limonite Mine Section. B) Angular chert pebbles in a dolomitized oolitic packstone, Limonite Mine Section. C) Close up of oolitic grainstone with chert pebbles from B. D) Thin oolitic packstone, Tom Mays Park Section.

Oolitic grainstone beds in the Limonite Mine Section have been recrystallized through fabric selective dolomitization of ooids, leaving high interparticle porosity (Figure 20B).

Oolitic packstone and grainstone lithofacies are always found adjacent to supratidal and intertidal depositional facies. Thinner bedded packstones are commonly interbedded with dolomudstones while grainstone beds occurs between ostracode foram wackestone and

dolomudstone. The majority of oolitic packstone and all grainstone beds are confined to the Robledo Mountains. Few oolitic packstone lithofacies were found in lower Hueco strata from the Franklin Mountains.

Depositional Environment Interpretation

The presence of high energy sedimentary structures (cross bedding and hummocky cross-stratification), lack of micritic mud, and the high amount of ooids in these rocks suggests oolitic packstone and grainstone formed in high energy shallow marine environments, exposed to strong tidal and wave energy (Tucker and Wright, 1990). Wave energy would have been concentrated at these shoals/banks and acted as a barrier to the more landward restricted lagoons and intertidal flats. This lithofacies represents the highest energy environment on the depositional profile for the lower Hueco strata and marks an important transition between the supratidal and intertidal lithofacies to the more basinward subtidal lithofacies.

Different environmental conditions control the geomorphology of oolitic bars and shoals. In areas of strong wave or storm energy, shoals develop parallel to the shoreline and are typically cut through by tidal channels with spill over lobes on the lagoonal side (Hine, 1977; Tucker and Wright, 1990). Conversely, areas with strong tidal influence tend to have shoals that develop perpendicular to the shoreline as long linear bars separated by muddy troughs (Harris, 1979; Tucker and Wright, 1990). However, good exposures of oolitic packstone and grainstone in the Robledo Mountains exhibit characteristics of both shoreline parallel shoals and shoreline perpendicular bars. The geographic distribution in the Robledo Mountains appears to represent bars oriented perpendicular to the paleoshoreline but extensive faulting eliminates the possibility of determining this relationship. Additionally, extensive faulting creates a difficulty for determining the morphology of bars facies as their lateral extent is truncated by small scale

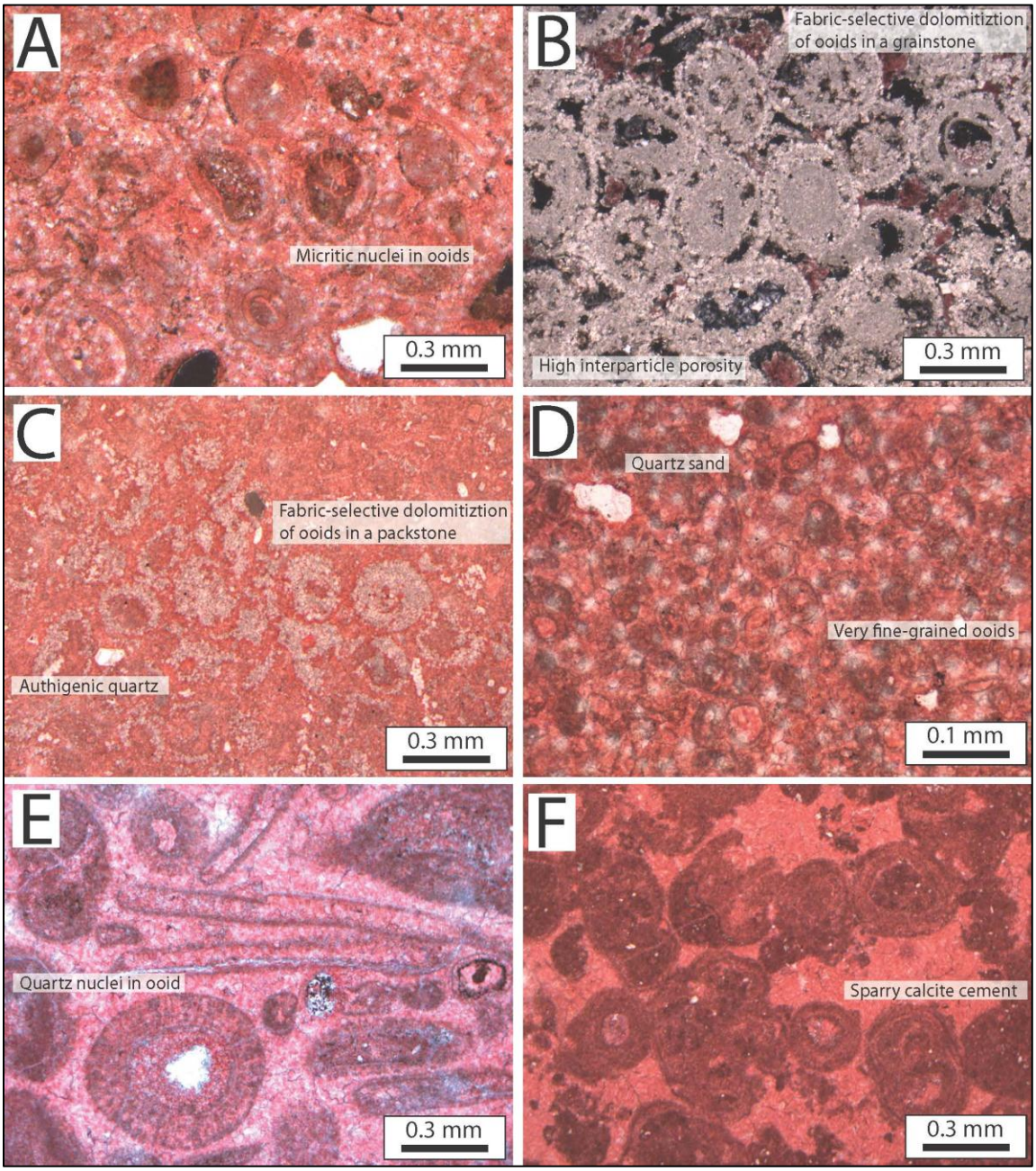

Figure 20: Photomicrographs of Oolitic Packstone and Grainstone.

A) Well-formed multi-layered ooids, stained, cross polarized light. Sample LH-80. B) Fabric-selective dolomitization of oolitic grainstone with open interparticle porosity, stained, cross polarized light. Sample LH-96. C) Fabric selective dolomitization of ooids, stained, plane light. Sample LH-48. D) Sandy oolitic packstone at 10X, stained, plane light. Sample LH-103. E) Quartz grain for nuclei in well formed, multi-layered ooid, stained, plane light. Sample LH-17. F) Micritized ooids in a sparry calcite cement, stained, plane light. Sample VC-5.

normal faults in the Robledo Mountains (Figure 6). Regardless, oolitic packstone and grainstone beds represent a distinctive location on the depositional profile.

Fossiliferous Packstone and Grainstone

Outcrop Characteristics

Fossiliferous packstone and grainstone is the most common lithofacies within the lower interval of the lower Hueco member in the Robledo and Franklin mountains. Though very similar, subtle differences between individual packstone and grainstone units are indicative of their relative location on the depositional profile. Consequently, for the purpose of parasequence identification and sequence stratigraphic correlation in areas where only fossiliferous packstones and grainstones are dominant, these lithologies have been subdivided based on faunal diversity and carbonate mud content. Grainstones are considered to represent winnowed deposits within fair-weather wave base while packstones are their down dip equivalent and form below fair-weather wave base. Four sub-lithofacies of the packstone and grainstone are identified: 1) fossiliferous grainstone, 2) bivalve, gastropod, packstone, 3) echinoid, brachiopod, packstone, and 4) *Tubiphytes*-red algal, bryozoan, packstone. All sub lithofacies were deposited on an open shelf with low to moderate slope. This lithofacies also occurs adjacent to, and interbedded with fusulinid packstone and grainstone and phylloid algal bafflestone lithofacies, which are described and interpreted in the following sections.

On outcrop, all 4 packstone and grainstone sub lithofacies appear very similar so their outcrop characteristics will be described as one lithofacies. The 4 sub lithofacies were defined based on petrographic characteristics, which will be discussed in the following section. Overall, this lithofacies forms very pronounced massive, thick (0.5 to 8 m), laterally continuous ledges

and cliffs with sharp, planar bounding surfaces (Figure 21A). Both packstone and grainstone weather light to dark gray and in some locations in the Robledo Mountains beds have a tan to yellow color, reflecting either higher quartz sand concentrations or non-fabric selective dolomitization. Fresh surfaces in packstone beds are always dark gray, while the same surface in grainstone beds range from light to dark gray (Figure 21B-F). Occasionally fresh surfaces in packstone and grainstone beds are tan to yellow. Chert nodules are common, but are much more abundant within the packstone units. Chert nodules range in color from white, brown, and dark gray and form rounded (< 20 cm in diameter) or elongate (between 10 to 30 cm on their long axis) nodules scattered throughout the matrix. In the Lower Waterfall Canyon Section of the Robledo Mountains, elongate brown chert nodules form parallel to meter-scale cross-stratification (Figure 21A). The dip direction on these cross-beds is to the east, dipping away from the paleoshoreline and into the basin. Locally in the Franklin Mountains, fusulinids and brachiopods are preferentially silicified and present within large chert nodules (Figure 21B-F).

Skeletal grains are common in both packstone and grainstone. However, more often in packstones, skeletal grains are articulated and well preserved as opposed to their grainstone counterparts, which are almost entirely composed of skeletal debris. Skeletal grains include articulated bivalves, brachiopods, fenestrate and ramose bryozoans, and crinoid columnals. Fusulinids are locally abundant as well as isolated patches of densely concentrated brachiopods and both solitary and colonial rugose corals (Figure 21B and 21F). Large (5 – 8 cm) articulated *Productid* brachiopods are commonly found associated with rugose coral colonies. Phylloid algae is common in most outcrops of this lithofacies, and is often occurs with *Tubiphytes* encrusting algae, dasycladacean algae, and laminar red algae. In summary, fossiliferous packstones and grainstones typically contain a diverse and heterogeneous mixture of many

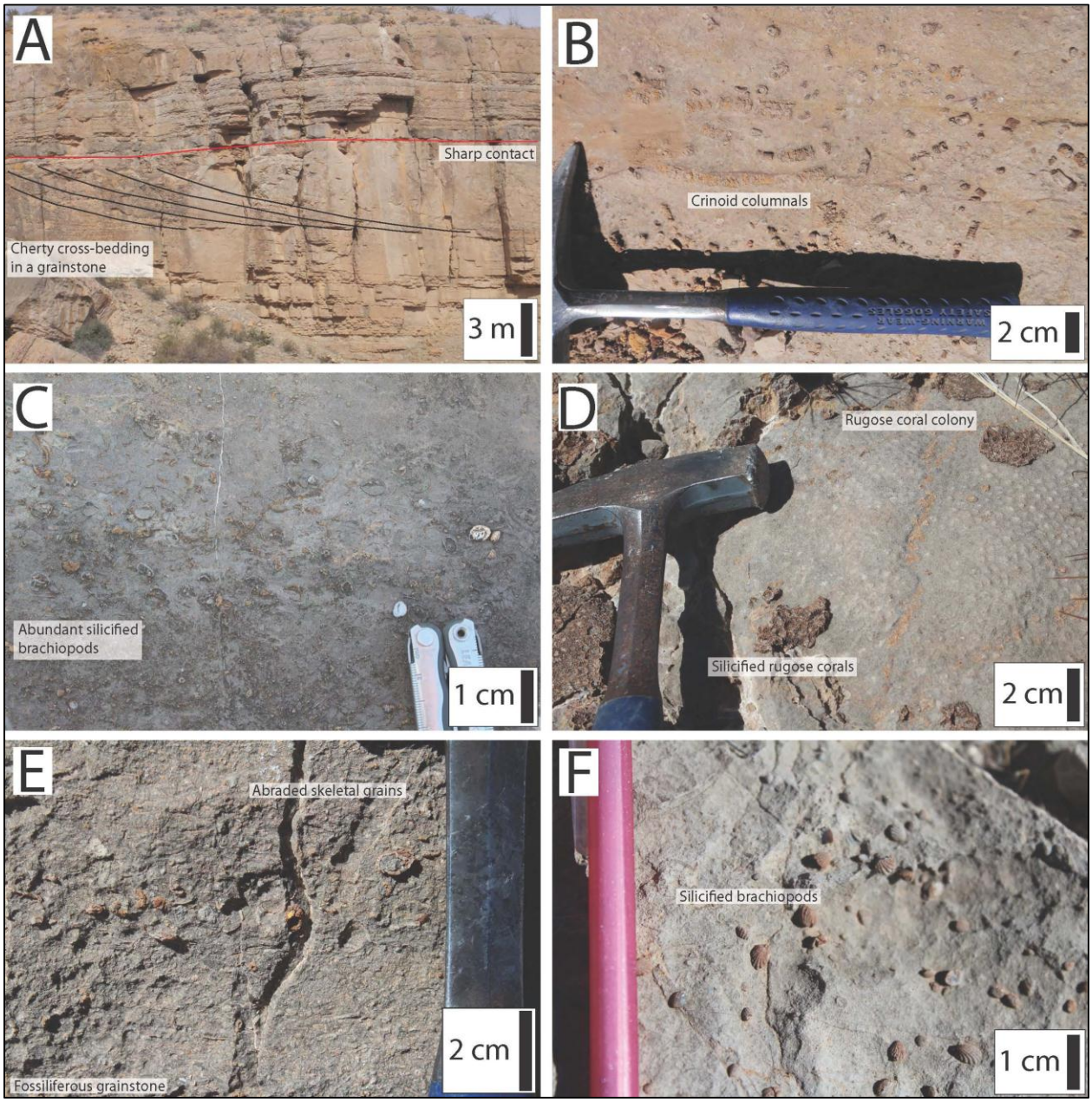

Figure 21: Outcrop Photographs of Fossiliferous Packstone and Grainstone.

A) Meter scale cross-bedding, Lower Waterfall Canyon Section. B) Crinoid columnals in a coarse-grained matrix, Lower Waterfall Canyon Section. C) High density of silicified brachiopods in medium gray muddy matrix, Anthony Syncline Section. D) Small rugose coral colony, Anthony Syncline Section. E) Close-up photograph of fossiliferous grainstone, Tom Mays Park Section. F) Silicified, articulated bivalves in a packstone, Tom Mays Park Section.

different open marine skeletal grains. However, some beds do contain higher concentrations of one fossil, showing that isolated communities of low diversity do occur across the shelf.

Sedimentary structures are rarely observed within these beds with most occurring within the grainstone. As previously mentioned, meter-scale cross-beds can be found in the large cherty cliff forming packstones of the Lower Waterfall Canyon Section but these are the only instance of large scale sedimentary structures in the lower interval of the Hueco member in both the Robledo and Franklin mountains (Figure 21A). Thin laminations and faint cross beds can be observed in a few of the dark grainstones but overall sedimentary structures are rare. This is likely because abundant burrows and bioturbation near the sediment-water interface disrupt and destroy all sedimentary structures before they are preserved (Wilson and Jordan, 1983).

Petrographic Characteristics

Petrographic analysis was important for identifying subtle differences in grain composition in both packstones and grainstones The 4 sub lithofacies of the packstone and grainstone lithofacies are described below in order from the more landward upper subtidal grainstones to the more distal algal-dominated packstones.

Fossiliferous Grainstone

Outcrop exposures of fossiliferous grainstone are very recognizable because of their dark gray color in the Franklin Mountains and their lighter tan color in the Robledo Mountains. However, in thin section these beds appear very similar because of the high diversity of abraded, disarticulated skeletal grains and lack of any mud in the matrix (Figure 22A and 22B). Crinoid columnals, echinoid plates, fenestrate bryozoans, brachiopods, bivalves, gastropods, forams, and ostracodes are very common but no trilobites or sponge spicules are observed in these beds. Non-

skeletal grains are rare, but peloids are more abundant in this sub lithofacies in the Franklin Mountains. No quartz sand is observed in this sub lithofacies.

Besides the abundance of skeletal grains, multiple different types of cements and diagenetic features are common within fossiliferous grainstone. The most common cement consists of equant or blocky crystals of calcite microspar and spar arranged in a drusy mosaic geometry that fills voids, vugs, intraparticle, and interparticle porosity (Figure 22A and 22B). Occasionally isopachous bladed cements are found lining larger vugs or intraparticle porosity. Localized dolomite cements are rare and only occur filling intraparticle porosity. Silica replacement of brachiopod, echinoid plates, and crinoid columnals is common and is probably associated with late-stage diagenesis related to burial (Figure 22A). Compaction features are also rare but microstylolites do occur in some of the beds from the Franklin Mountains.

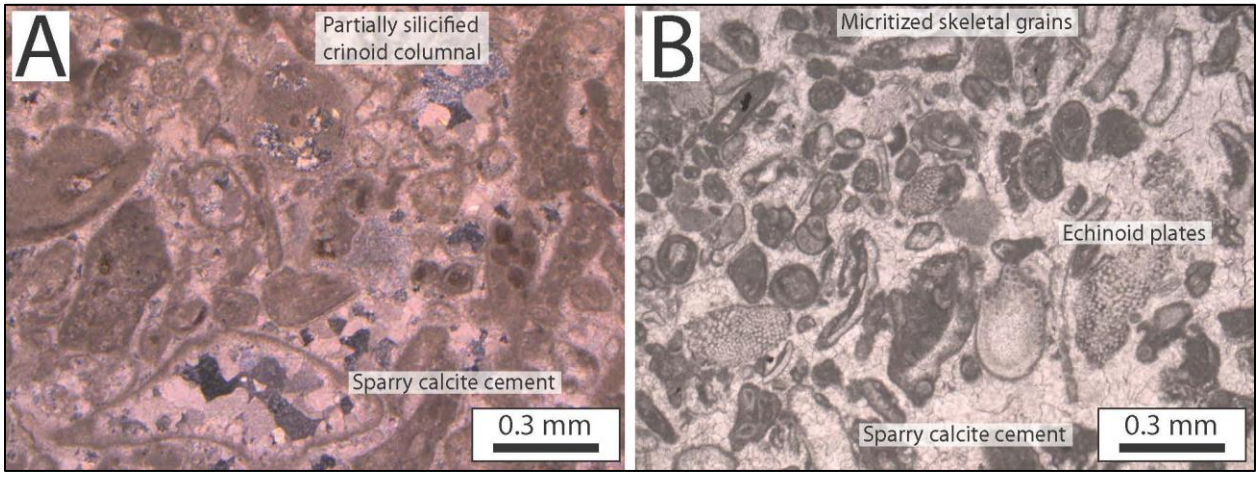

Figure 22: Photomicrographs of Fossiliferous Grainstone.

A) Fossiliferous grainstone, stained, cross polarized light. Sample AS-25. B) Fossiliferous grainstone with few ooids, unstained, plane light. Sample LH-106.

Bivalve, Gastropod Packstone

Bivalve, gastropod packstone sub lithofacies was separated out from the other packstones based on higher percentage (>50 % of all skeletal grains) of bivalves and gastropods. Other skeletal grains consist of small plates of phylloid algae, occasional *Tubiphytes*, crinoid columnals, echinoid plates, brachiopods, forams, fusulinids, and ostracodes (Figure 23A and 23B). Bryozoans, rugose corals, and sponge spicules are rare. Non-skeletal grains are also rare but consist of peloids, oncoids, authigenic quartz crystals, and very few well-rounded fine quartz grains.

The matrix of these packstones contains very dense micrite mud. Calcite microspar and spar is common filling moldic porosity in bivalve and gastropod shells, as well as in vugs and voids (23A). Occasionally, prismatic, foliated, and/or homogenous wall structures are preserved in bivalves with a multi-layer wall construction (Figure 23B). Rarely isopachous fibrous rim cements and dolomite cements occur within intraparticle porosity. Geopetal infill in gastropods is common and sometimes fragments of ostracodes are present within this fill. Compaction features are rare but some thin sections contain microstylolites and fragmented, compressed bivalve shells in a dark micritic matrix, suggesting over compaction. Overall, the main distinguishing features of this packstone are the abundant mollusk fragments within a dense detrital micrite matrix.

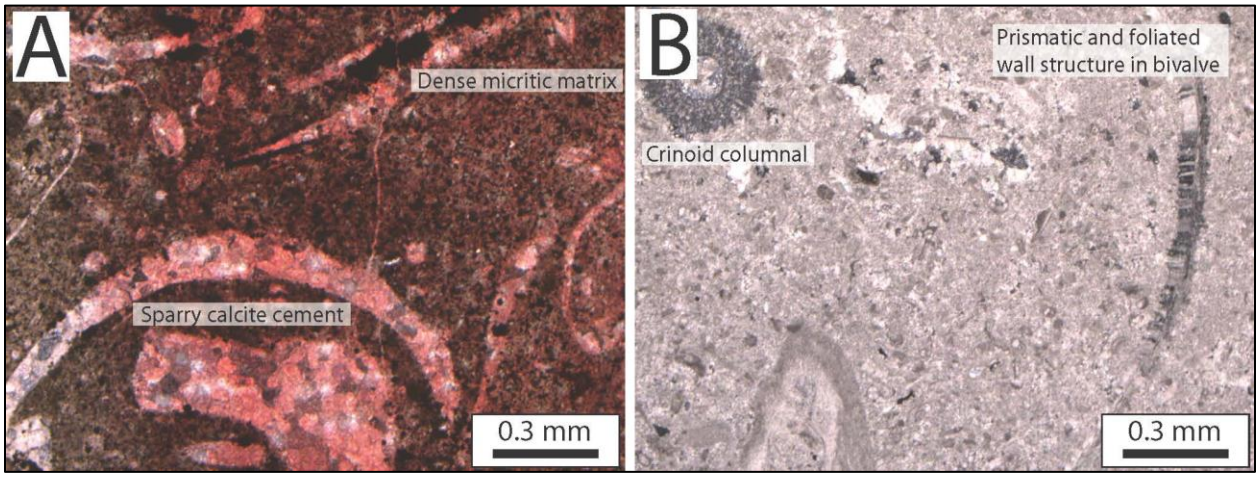

Figure 23: Photomicrographs of Bivalve, Gastropod Packstone.

A) Recrystallized bivalve fragments, stained, cross polarized light. Sample LH-65. B) Cross section of a multi-layered bivalve fragment with foliated outer layer and prismatic inner layer, unstained, cross polarized light. Sample LH-108.

Echinoid, Brachiopod Packstone

Echinoid, brachiopod packstone are identifiable by the abundance of crinoid columnals, echinoid plates, and brachiopods in both outcrop and thin section. Crinoid columnals are very abundant along with large echinoid plates that are often partially silicified (Figure 24A). Other skeletal grains are common such as bryozoans, brachiopods, rugose coral colonies, forams, and ostracodes while bivalves and gastropods are less common (Figure 24B). Also, trilobites and algae do not occur within these rocks. Additionally, only a few *Tubiphytes* are found encrusting on fenestrate bryozoan fragments. Peloids are the most common non-skeletal grain observed while ooids, oncoids, intraclasts, doubly-terminated authigenic quartz crystals, and quartz sand grains are rare.

The matrix in the packstone appears similar to the other packstones with abundant dense micrite mud forming the matrix (Figure 24A). However, blocky calcite microspar and spar cements are commonly found filling voids and intra particle porosity but do not typically exhibit any regular geometry. Silica and dolomite cements occur rarely within intraparticle and interparticle porosity (Figure 24B). Echinoid plates, crinoid columnals, rugose corals, and brachiopod shells are commonly recrystallized with silica.

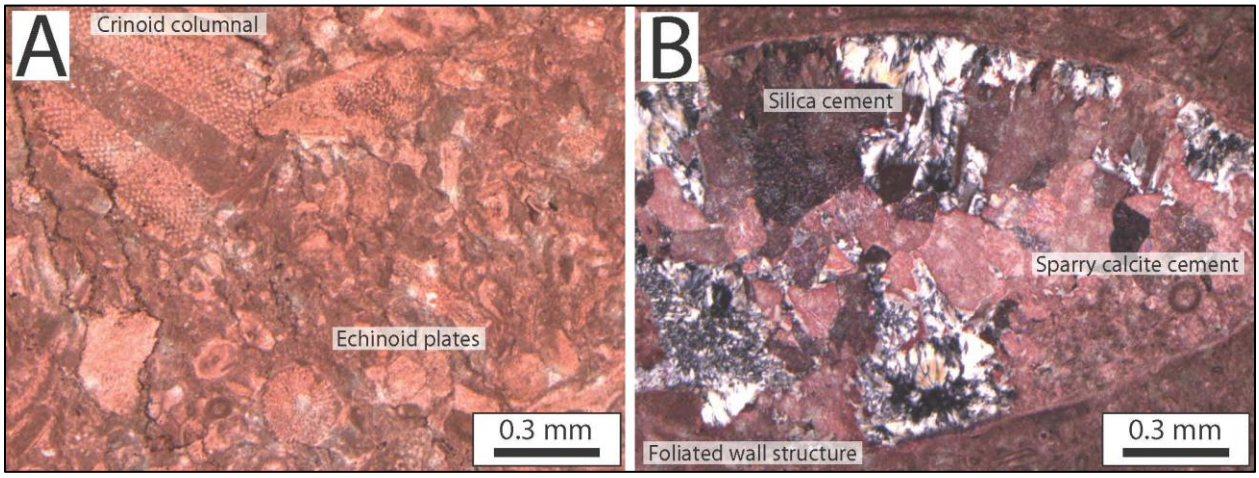

Figure 24: Photomicrographs of Echinoid, Brachiopod Packstone.

A) Crinoid columnals and echinoid plates, stained, plane light. Sample LH-46. B) Large brachiopod filled with calcite spar and silica cements, stained, crossed polarized light. Sample LH-22.

Tubiphytes-Red Algal Packstone

Tubiphytes-red algal packstone are recognizable only from petrographic identification of laminar red algae. *Tubiphytes* is commonly encrusted fenestrate bryozoans, and both trilobite fragments and siliceous sponge spicules occur frequently in this sub lithofacies (Figure 25A and 25B). Locally, there are abundant skeletal grains are crinoid columnals, echinoid plates, brachiopods, forams, fusulinids, and ostracodes. Bivalves, gastropods, and rugose corals are rare

along with non-skeletal grains, but few peloids are found in this sub lithofacies. These packstones were separated from the other skeletal packstones based on the unique occurrence of trilobites and laminar red algae. The other skeletal grains are common throughout all packstones and grainstones but these two skeletal grain types are not found in any other packstone or grainstone lithofacies.

Similar to the other packstone lithofacies, dense micrite mud forms the matrix (Figure 25A and 25B). Calcite microspar cement is much less common but sparry calcite cement is still present in partially recrystallized laminar red algae and also filling fractures and voids. Silica is commonly found recrystallizing crinoid columnals, echinoid plates, and bryozoan fragments. Chert nodules are still common in this sub lithofacies and microstylolites occur rarely in the dark micritic matrix.

The combination of laminar red algae, bryozoans encrusted with Tubiphytes, trilobite fragments, and abundant siliceous sponge spicules suggest deposition on deeper parts of the Robledo shelf (Figure 25A and 25B). In the Mississippian, *Tubiphytes*-fenestrate bryozoan buildups were found to be the primary constituents of Waulsortian mud mounds, which are considered as deeper water buildups compared to contemporaneous phylloid algal buildups (Lees et al., 1985; Lees and Miller, 1985; Monty et al., 1995). Additionally, Finks (1960) identified Permian siliceous sponge-bryozoan mounds in west Texas and suggested these formed in a slope to basinal facies. Beauchamp (1989) studied similar buildups but came to the conclusion that these buildups formed in cooler water climates on more distal parts of a ramp. Regardless, this fossil assemblage appears to represent deeper, possibly cooler water systems and consequently represent the deepest lithofacies in the study area.

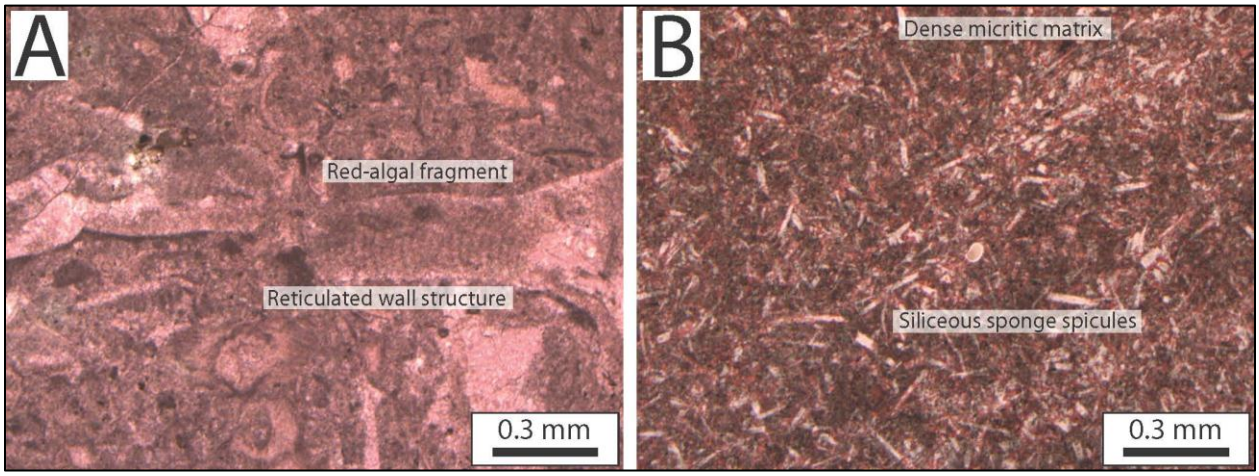

Figure 25: Photomicrographs for Tubiphytes-Red Algal Packstone.

A) Laminar red algae in skeletal packstone, stained, plane light. Sample AS-7. B) Sponge spicule packstone, stained, plane light. Sample LH-67.

Depositional Environment Interpretation

Based on the criteria discussed above, all of these sediments appear to be deposited on a broad carbonate shelf with low to moderate slope within the subtidal zone. Wilson and Jordan (1983) described skeletal grainstones in a middle shelf environment to represent deposits that formed small shoals from focused wave and tidal energy. In the Hueco Mountains to the east, Stoklosa et al. (1998) described similar grainstones in Wolfcampian stratigraphy and interpreted them as shallow shelf deposits in higher energy parts of the shelf based on the lack of carbonate mud and well-sorted fossil debris. Consequently, fossiliferous grainstones appear to represent the shallowest of packstone and grainstone facies and are confined to within fair-weather wave base where wave and current energy kept carbonate mud suspended in the water column and could fragment skeletal grains. Higher wave energy would have winnowed or washed the mud out of the grainstones while simultaneously fragmenting and abrading the skeletal grains (Figure 22A

and 22B). Both the abundance of mud and articulated skeletal grains indicate that packstones were deposited in a lower energy shelf environment compared to the grainstones.

Fossiliferous packstones and occasional wackestones are slightly more difficult to accurately place on the depositional profile for this region. However, the higher carbonate mud contents suggest that these sediments were deposited basinward of the grainstones, in regions of lower wave and current energy. Wilson and Jordan (1983) also suggest that finer -grained sediments are deposited on lower parts of a carbonate shelf where micrite mud can accumulate. Stoklosa et al. (1998) interprets similar packstones from the Hueco Mountains as deposition on the outer shelf below wave base based on high-faunal diversity and increased mud content. However, deposition was still considered to occur in fairly shallow water with low turbidity because of the presence of benthic fauna like rugose corals, dasycladacean green algae, and fusulinids.

Fusulinid Packstone and Grainstone

Outcrop and Petrographic Characteristics

Fusulinid packstone and grainstone can be found in both the Robledo and Franklin mountains but is not present in every measured stratigraphic section. Though fusulinids are commonly found in fossiliferous packstone and grainstone, classification as a fusulinid packstone or grainstone occurs when there is greater than 50% fusulinids as the dominant allochem (both skeletal and non-skeletal). Beds range in color from light to medium gray with abundant dark gray fusulinids but no other skeletal grains are typically observed on outcrop (Figure 26A-D). Occasionally, grainstone beds have a tan to light brown matrix and form very pronounced ledges. Fusulinid packstone and grainstone beds are usually thin to medium bedded

(0.2 - 1.0 m) and form poorly exposed slopes with lumpy, low relief exposures. In the Franklin Mountains, fusulinid beds tend to be thicker and contain a larger amount of fusulinids. These beds are interbedded with fossiliferous packstones and grainstones and often cap thin phylloid algal biostrome beds. Occasionally, dense lenses of fusulinid grainstone are found within fossiliferous grainstone beds, like in the Anthony Syncline and Tom Mays Park sections (Figure 26C). No sedimentary structures are observed in fusulinid packstone and grainstone beds.

Crinoid columnals, echinoid plates, bryozoans, brachiopods, bivalves, gastropods, rugose coral fragments, forams, and ostracodes occur within fusulinid packstones. However, skeletal grain diversity dramatically decreases within the grainstone, which are predominately composed of fusulinids, with rare echinoids and brachiopods. In both the packstone and grainstone, skeletal grains are abraded and disarticulated while the fusulinids are almost always well preserved. Non-skeletal grains are rare but ooids, oncoids, and fine-grained detrital quartz sand occur infrequently in these beds.

The matrix of fusulinid packstone is chiefly composed of micrite mud but blocky, equant calcite microspar and spar cement fills vugs, voids, and intraparticle porosity (27A-D). Isopachous calcite rim cements are rarely observed within intraparticle porosity of fusulinid chambers. Dolomite cement is also common in this porosity (Figure 27D). Grainstones are almost entirely composed of blocky, equant calcite microspar and spar cements. In some packstone beds, fabric selective dolomitization has recrystallized large parts of the matrix while fusulinid tests are left unaltered. (Figure 27A and 27B). The micrite matrix is preferentially dolomitized into finely crystalline dolomite rhombs less than 500 microns in diameter (Figure

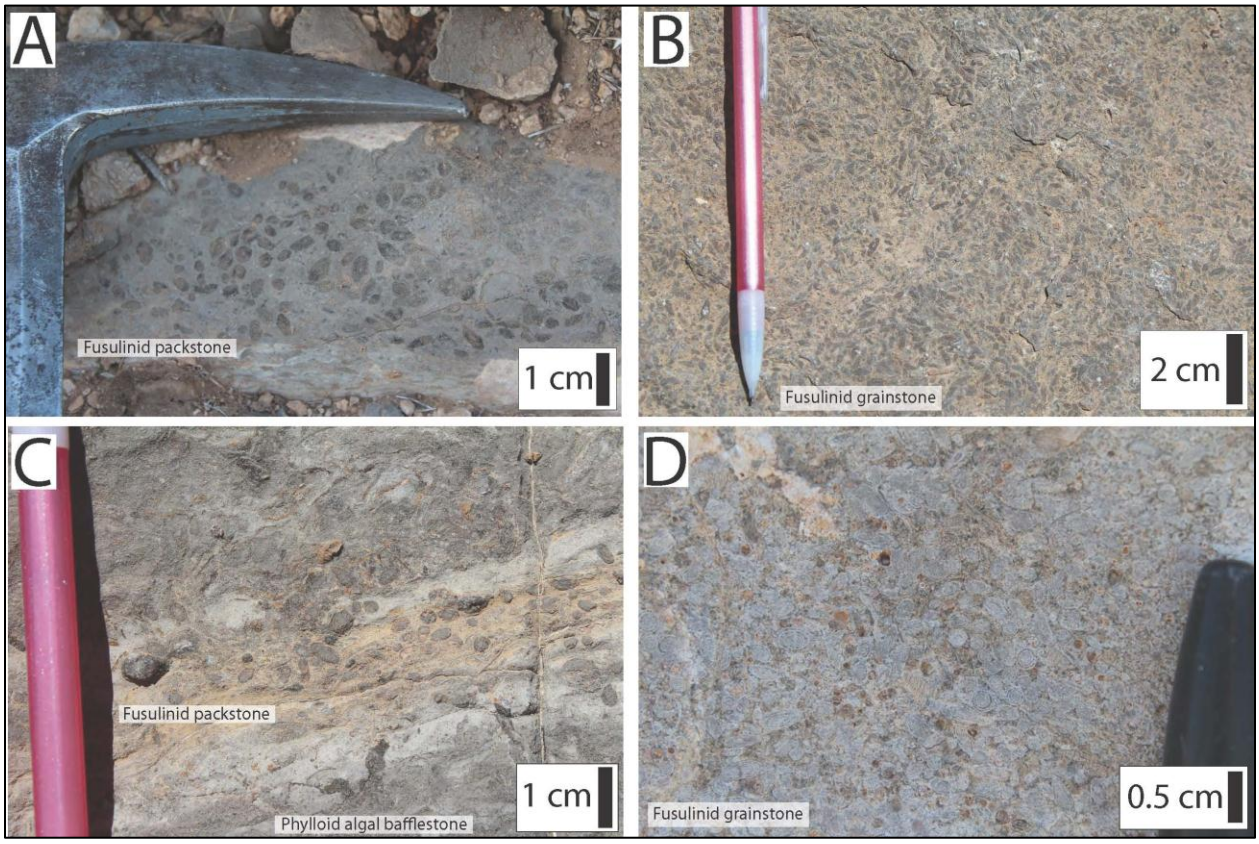

Figure 26: Outcrop Photographs of Fusulinid Packstone and Grainstone.

A) Fusulinid packstone, Lower Waterfall Section. B) Fusulinid grainstone, Tom Mays Park Section. C) Fusulinid packstone lens within a fossiliferous grainstone, Vinton Canyon Section. D) Fusulinid grainstone, Anthony Syncline Section.

27A and 27B). Silica recrystallization of crinoid columnals, echinoid plates, and brachiopods is common. Additionally, packstones appear compacted as they contain abundant stylolites and fractured, compressed fusulinid tests that indicate over compaction.

Fusulinid packstone and grainstone are always found interbedded with fossiliferous packstone, grainstone, and phylloid algal bafflestone. In the Robledo Mountains, they are found

within thin shoaling upward sequences of fossiliferous packstone and do not occur adjacent to phylloid algal bafflestone. However, in the Franklin Mountains, these beds are usually found capping phylloid algal bafflestone and are overlain by fossiliferous packstone and grainstone in a separate shoaling upward package. Despite this, fusulinid packstone represent a deeper part of the depositional profile compared to fusulinid grainstones that have been winnowed by higher wave or tidal energy in shallower water.

Depositional Environment Interpretation

Fusulinids of the late Paleozoic were a rapidly evolving group of normal marine foraminifera that are found in subsequent marine strata globally as isolated beds with low diversity or beds with a diverse fossil assemblage (Thompson, 1954; Ross, 1963; Scholle and Ulmer-Scholle, 2006). Consequently, they are an important tool for both regional and global biostratigraphic correlation along with depositional environment interpretations Work completed by Ross (1963) on the Standard Wolfcampian Series suggested that Permian fusulinids formed in shallow marine environments, proximal to bioherms and that thick walled fusulinids were specialized for higher energy conditions with more wave agitation. This is similar to their occurrence in the Franklin Mountains capping phylloid algal bistromal bafflestones. However, their occurrence in the Robledo Mountains is interbedded with fossiliferous packstones. Stoklosa et al. (1998) observed similar relationships in the Hueco Mountains and interpreted these fusulinid-rich beds to be deposited on the outer shelf. Regardless, fusulinid grainstones in the lower interval of the lower Hueco member are considered to be deposited within fair-weather wave base, in similar conditions to the fossiliferous grainstones, while packstones formed in a deeper, calmer water environment.

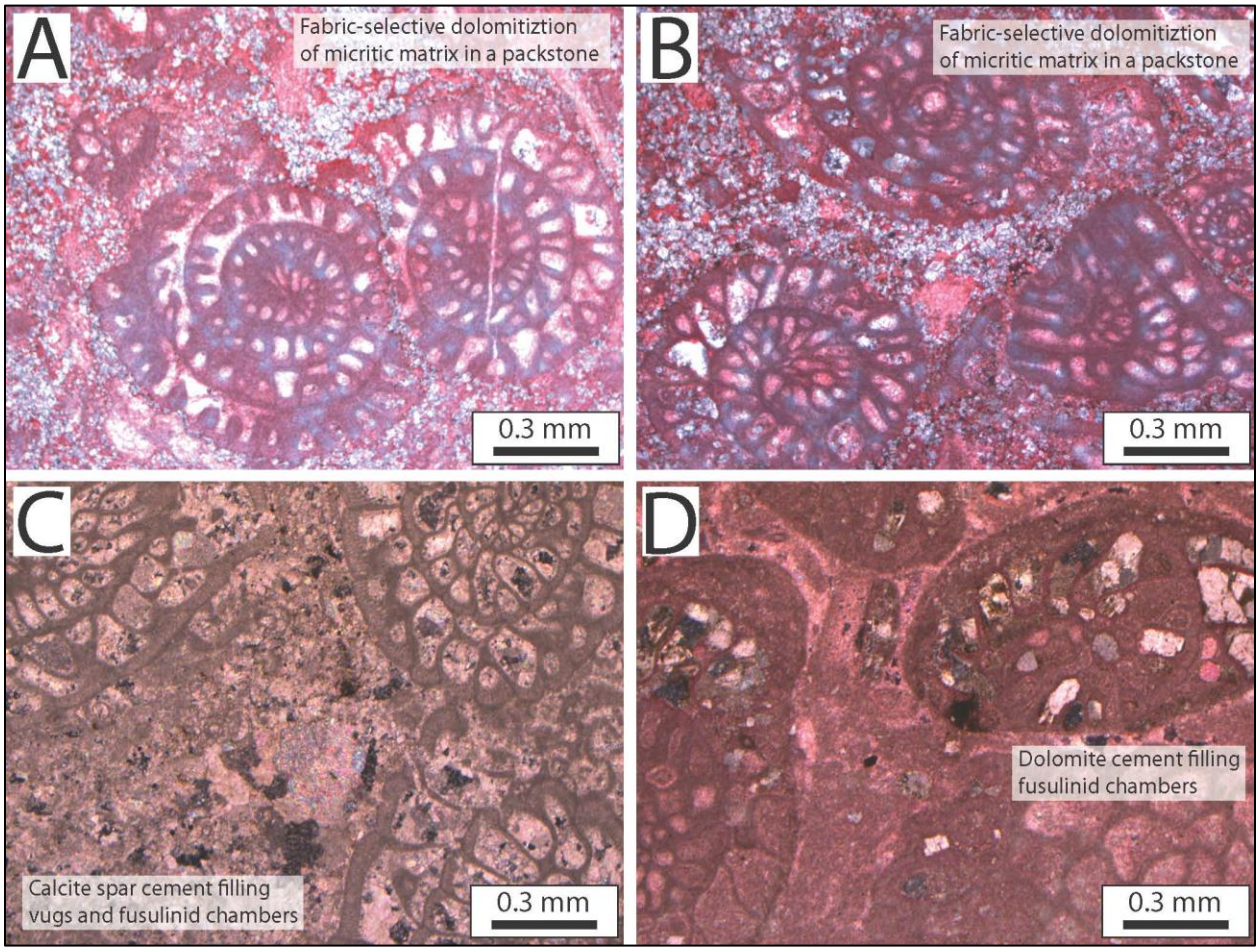

Figure 27: Photomicrographs of Fusulinid Packstone and Grainstone.

A) Sagittal sections through fusulinids with non-fabric selective dolomitization, stained, cross polarized light. Sample LH-30. B) Sagittal sections and fragmented fusulinids with non-fabric selective dolomitization, stained, cross polarized light. Sample LH-41. C) Fusulinid grainstone with pseudo-sagittal and fragmented tangential sections, stained, cross polarized light. Sample AS-16. D) Dolomite cement filling fusulinid chambers, stained, cross polarized light. Sample AS-19.

Phylloid Algal Bafflestone

Phylloid algae is commonly found in both of the Robledo and Franklin mountains where they form both mound-shaped bioherms and thinner, bistromal beds. The mound shaped bioherms are more abundant in the Robledo Mountains, in particular in the Quarry, Reef Ridge, and Lower Waterfall Canyon sections (Appendix A). Conversely, biostromes are more abundant within the Franklin Mountain sections. Despite these physical characteristics, phylloid algal biohermal and biostromal bafflestones exhibit similar outcrop and petrographic characteristics, the main difference being morphology of the bed itself.

Outcrop Characteristics

Biohermal Bafflestones

Biohermal bafflestones form mound-shaped bioherms that range in thickness between 1.0 and 6.0 m at their cores and have a lateral extent between 50 - 75 m (Figure 28A - C). Mounds or bioherms have a convex upward morphology and taper towards their flanks with a sharp basal contact with the underlying strata (Figure 28A). Bioherms typically weather tan to dark gray with individual plates of algae weathering light gray. In the Quarry Section, bioherms exhibit a much lighter color compared to bioherms in other areas and fresh surfaces appear yellow or even have a pink hue (Figure 28D and 28E). However, most fresh surfaces appear tan to dark gray depending on the amount of carbonate mud present and chert does not occur in any bioherm. Sedimentary structures are not present within the bioherms but outcrops that have lateral extent over 100 m exhibit a distinct thickening and thinning, suggesting mounds are complexes rather than an isolated single buildup. Despite this, all mounds in the lower interval of the lower Hueco member show dominant lateral and not vertical growth. Additionally, mound shaped bioherms are confined to a single stratigraphic interval and only occur in the Robledo Mountains.

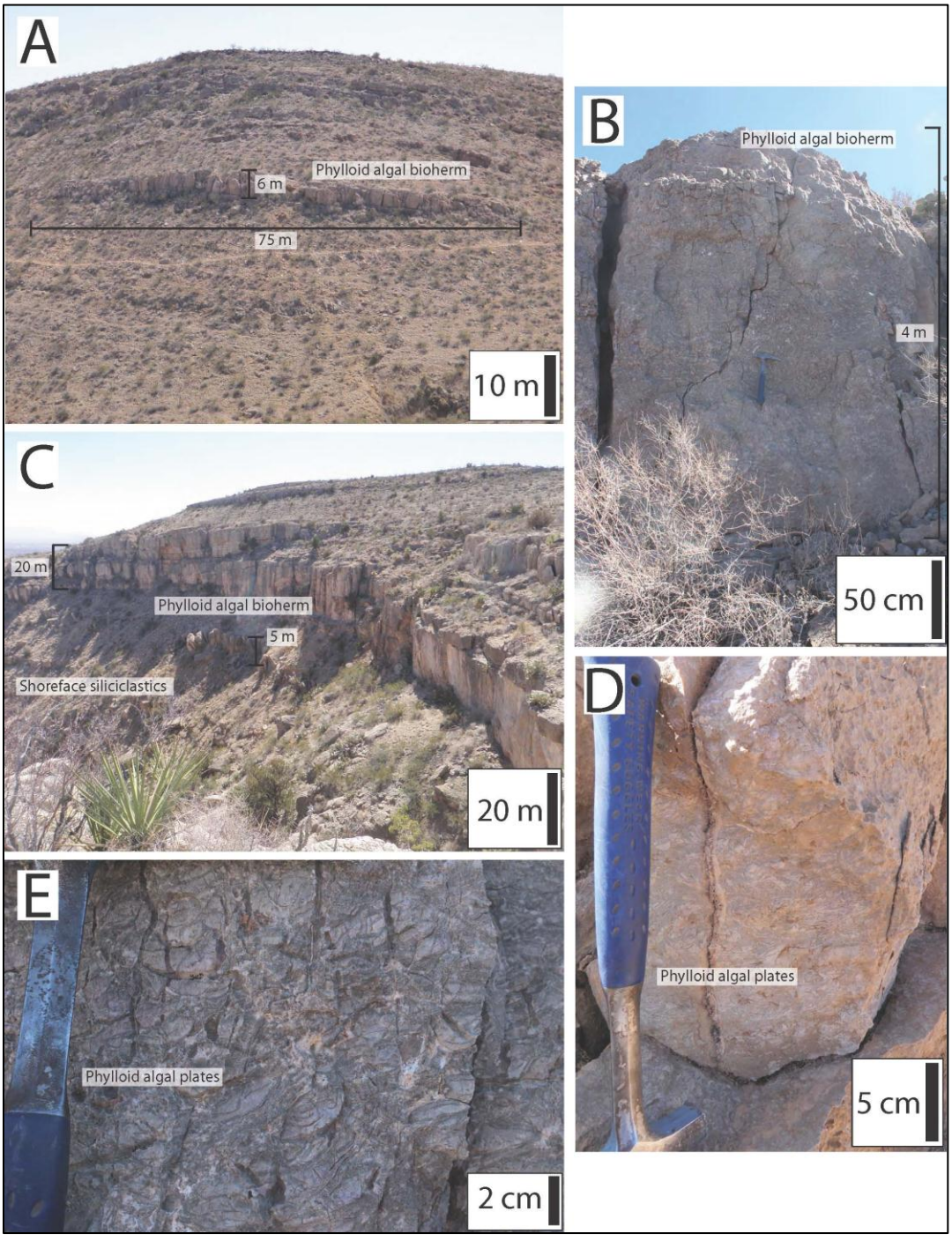

Figure 28: Outcrop Photographs of Phylloid Algal Biohermal Bafflestone.

A) Phylloid algal mound, Quarry Section. B) Poorly exposed phylloid algal mound, Lower Waterfall Canyon Section. C) Phylloid algal mound core, Reef Ridge Section. D) Close up of phylloid algal mound from B. E) Close up of weathered phylloid algal plates from C.

Biostromal Bafflestone

Phylloid algae can also form thin, laterally continuous beds called biostromes. Biostromes exhibit a tabular morphology that form laterally continuous ledges that do not thicken and thin like the bioherms. Beds thickness ranges from 0.3 - 1.0 m and are typically capped by fusulinid packstone or fossiliferous grainstone (Figure 29A and 29B). Most beds are dark gray based on the abundance of phylloid algae while some beds appear lighter gray because of higher mud content. Plates of phylloid algae appear dark gray on outcrop and biostromes appear to have a lower density of phylloid algal plates (Figure 29B and 29D). No sedimentary structures are observed within the biostromes themselves, but low angle, planar cross-beds and laminations are occasionally found within fossiliferous grainstones that directly overly them. Chert nodules are rare in biostromal beds. Few biostromal beds are observed in the lower interval of the lower Hueco member in the Robledo Mountains while biostromes beds are common in the Franklin Mountains.

Petrographic Characteristics

Biohermal and Biostromal bafflestones

After petrographic analysis, mound-shaped phylloid algal bioherms and tabular biostromes appear very similar based on grain types and diagenetic features. Broad, tabular plates of phylloid algae are the dominant rock-forming grains (Figure 30A-D). Other skeletal grains include crinoid columnals, echinoid plates, fenestrate and ramose bryozoans, brachiopods, bivalves, rugose corals, forams, ostracodes, and dasycladacean algae (Figure 30E). *Tubiphytes* is commonly found encrusting phylloid algal plates and brachiopods but also occurs independently within the matrix (Figure 30F). Brachiopods, bivalves, gastropods, trilobites, and fusulinids are much less common in biostromes and trilobites and gastropods are not observed in bioherms.

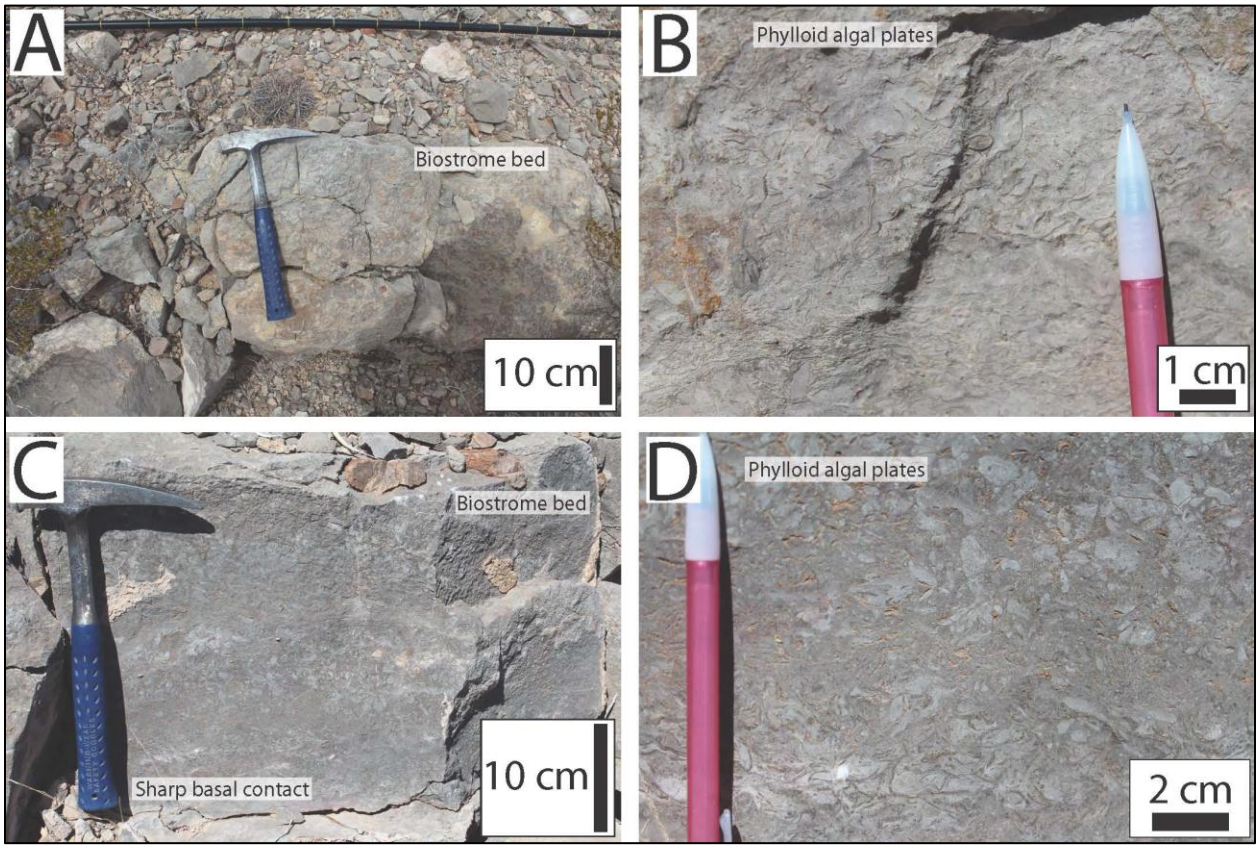

Figure 29: Outcrop photographs of Phylloid Algal Bistromal Bafflestone.

A) Thin phylloid algal bistrome, Vinton Canyon Section. B) Close-up of phylloid algal plates from A. C) Thin phylloid algal biostrome, Tom Mays Park Section. D) Close-up of phylloid algal plates from C.

Rarely oncoids and peloids are observed in biostromes and represent the only non-skeletal grains present in this lithofacies. The matrix of both biohermal and biostromal bafflestones is mainly composed of detrital micrite mud (Figure 30A, 30B, and 30E). Calcite microspar and spar cement is common filling small voids or vugs within the mud. This is related to the nature in which phylloid and green algae would have baffled fine-grained carbonate mud out of the water in the zone between fair-weather wave base and storm wave base. By doing this, small vugs could be created allowing early marine cements to form (Wahlman, 2002). Elongate,

tabular plates of phylloid algae have been dissolved and their molds filled with sparry calcite cement arranged in a drusy mosaic geometry (Figure 30A-F). Occasionally isopachous bladed cements are found filling phylloid algal plates but both cements never occur together. Additionally, bivalve and gastropods shells have been exposed to the same diagenetic effects and their molds are filled with the same type and style of cement. Dolomite cements are rare but are observed filling vugs in biostromes with large (> 0.5 mm) crystals, while baroque dolomites are more commonly associated with biohermal mounds. Pervasive dolomitization of bioherms and biostromes is not observed in the lower Hueco member in the Robledo or Franklin mountains. Silica replacement is common in crinoid columnals, brachiopods, bivalves, and gastropods. Diagenetic features in bafflestone are similar to what is observed in fossiliferous packstone as they form in adjacent environments.

Depositional Environment Interpretation

Wahlman (2002) states that phylloid algal buildups were dominant reef formers of the late Paleozoic in subtropical shelf and shelf-margin environments. In central and south-central New Mexico and west Texas, numerous exposures of phylloid algal mounds have been described (Candelaria, 1988; Jordan, 1971; Jordan, 1975; Kues and Giles, 2004; Soreghan and Giles, 1999; Toomey, 1991; Stoklosa et al., 1998; Wahlman, 1988; Wilson, 1967, and others). In all of these studies, phylloid algal mounds have been found to develop at or near the shelf margin of a carbonate platform with a distinct shelf-slope break. The shelf margin is ideal for these bioherms because there is a constant supply of normal marine seawater within a low turbidity, shallow environment (Wahlman 2002). Additionally, phylloid algae is understood to develop in shallow water, usually less than 20 m (Wray, 1968; Toomey, 1980; Wilson, 1975). Consequently

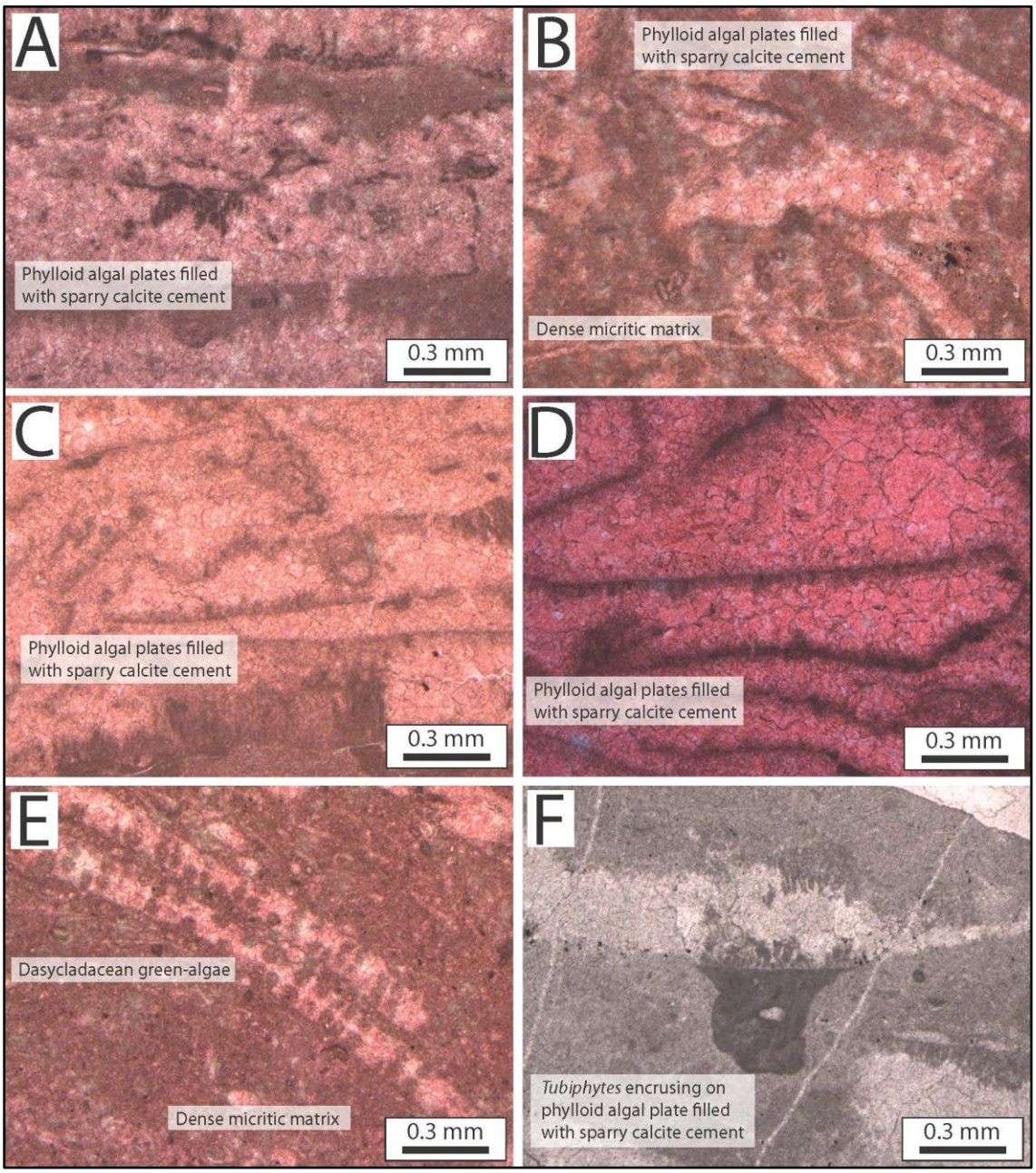

Figure 30: Photomicrographs of Phylloid Algal Bafflestone.

A) Large plates of phylloid algae with endolithic borings, stained, plane light. Sample LH-3. B) Thin plates of phylloid algae, stained, plane light. Sample LH-66-B. C) Stacked plates of phylloid algae, stained, plane light. Sample LH-2. D) Stacked plates of phylloid algae, stained, plane light. Sample LH-125. E). Thin plates of dasycladacean green-algae, stained, plane light.

phylloid algal mounds found in the lower Hueco on the Robledo shelf are interpreted to have developed under similar conditions but on a ramp depositional profile geometry based on the lack of dramatic thickness changes and lack of carbonate debris flows that are typical of a shelf margin.

Phylloid algal biostromes, however, form in a slightly different location than mounds under different environmental conditions. Wahlman (2002) described banks or biostromes as much larger than mounds and have a tabular shape that could not form mound-shaped features due to limitations on available accommodation space and the influence of constant wave and tidal energy. Ball et al. (1977) described banks of north-central Texas as low relief structures and that phylloid algae was the primary sediment contributor in these settings. Additionally, Toomey (1976) found that these banks were usually wackestones to packstones with low-diversity fauna that formed in very shallow water that would have been affected by significant wave energy. Consequently, banks found in the Franklin Mountains are interpreted to form in adjacent shallower parts of a shallow carbonate shelf. These would have developed more landward than the shelf-margin phylloid algal bioherms which is why they are commonly interbedded with fossiliferous and fusulinid packstones and grainstones.

2.1.4 Shoreface Siliciclastic Depositional Facies Association

Siliciclastic lithofacies in the lower interval of the lower Hueco member are rare and, where present, are less than 10 m in thickness and comprise less than 10% of any measured stratigraphic section (Figure 31). Siliciclastics range from dark gray shale to fine- to coarse-grained, brown, yellow, and tan weathering sandstone and are discussed below in order of most abundant to least abundant.

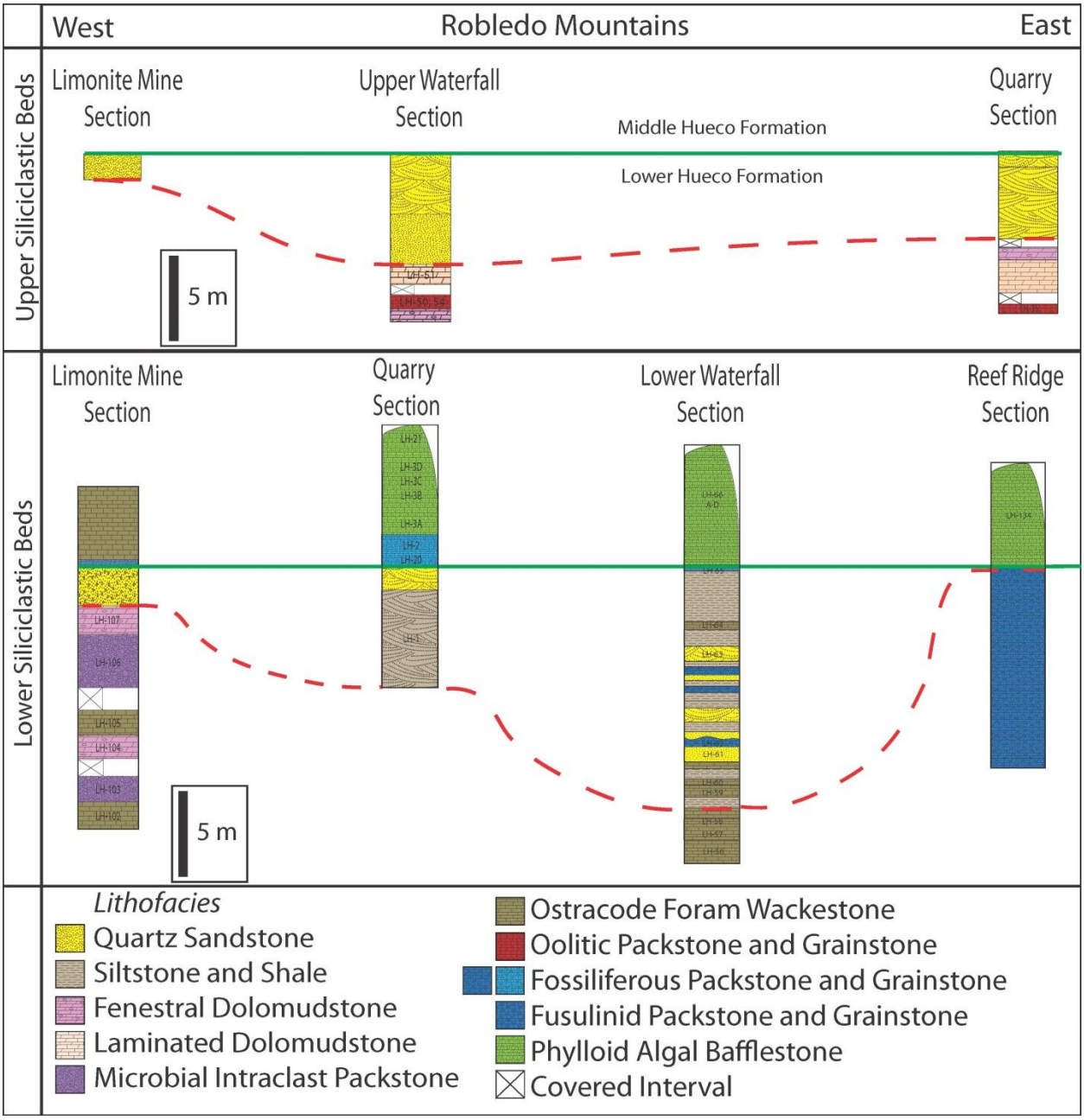

Figure 31: Shoreface Siliciclastic Correlation.

Shoreface siliciclastic correlations and thickness changes shown west to east across the Robledo Mountains. In the lower siliciclastic package, sands disappear before the Reef Ridge Section.

Marine Siliciclastics

Quartz Sandstone Lithofacies

In the Robledo Mountains, quartz sandstones crop out as medium to thick bedded, coarsening upward packages that weather tan to yellow and form laterally continuous ledges with sharp upper and lower bedding boundaries (Figure 32A and 32B). Coarse-grained sandstones contain localized planar cross-beds and granule sand lenses that weather slightly more resistant than the rest of the outcrop (Figure 32C and 32D). Angular chert pebbles are also common but typically are found as thin (0.2 - 0.5 m) lags at the top of these coarsening-upward packages (Figure 32D and 32E). Finer-grained sandstones are usually present below the coarse-grained intervals as medium to thick beds (0.5 – 2.0 m) and contain hummocky cross-stratification (Figure 32A). Outcrops of finer-grained intervals are slightly less resistant to weathering, are often highly fractured, and sometimes contain small round burrows filled with slightly darker, finer-grained sand and occasional oncoids (Figure 32F).

Quartz grains are the dominant rock-forming grains in these sandstones along with some lithic fragments and rare bioclasts. Quartz grains range in size from fine- to coarse-grained and are sub-angular to sub-rounded and moderately well-sorted (Figure 33A - D). Well-rounded feldspars are very rare in sandstone beds (Figure 33B). Lithic fragments are composed of small (0.1 mm – 0.5 mm) chert, sandstone, carbonate mudstone, or dolomudstone clasts and form of both flat and rounded pebbles, suggesting a variety of local sources provided clasts for this lithofacies (Figure 32E and 33C). Often, more angular lithic fragments are representative of the underlying beds. Skeletal bioclasts are rare in this lithofacies but consist of abraded brachiopod, bryozoan, ostracode, and bivalve fragments. Non-skeletal bioclasts are also rare but few ooids, oncoids, and rounded glauconite grains occur in the Robledo Mountains (Figure 32F, 33C, and

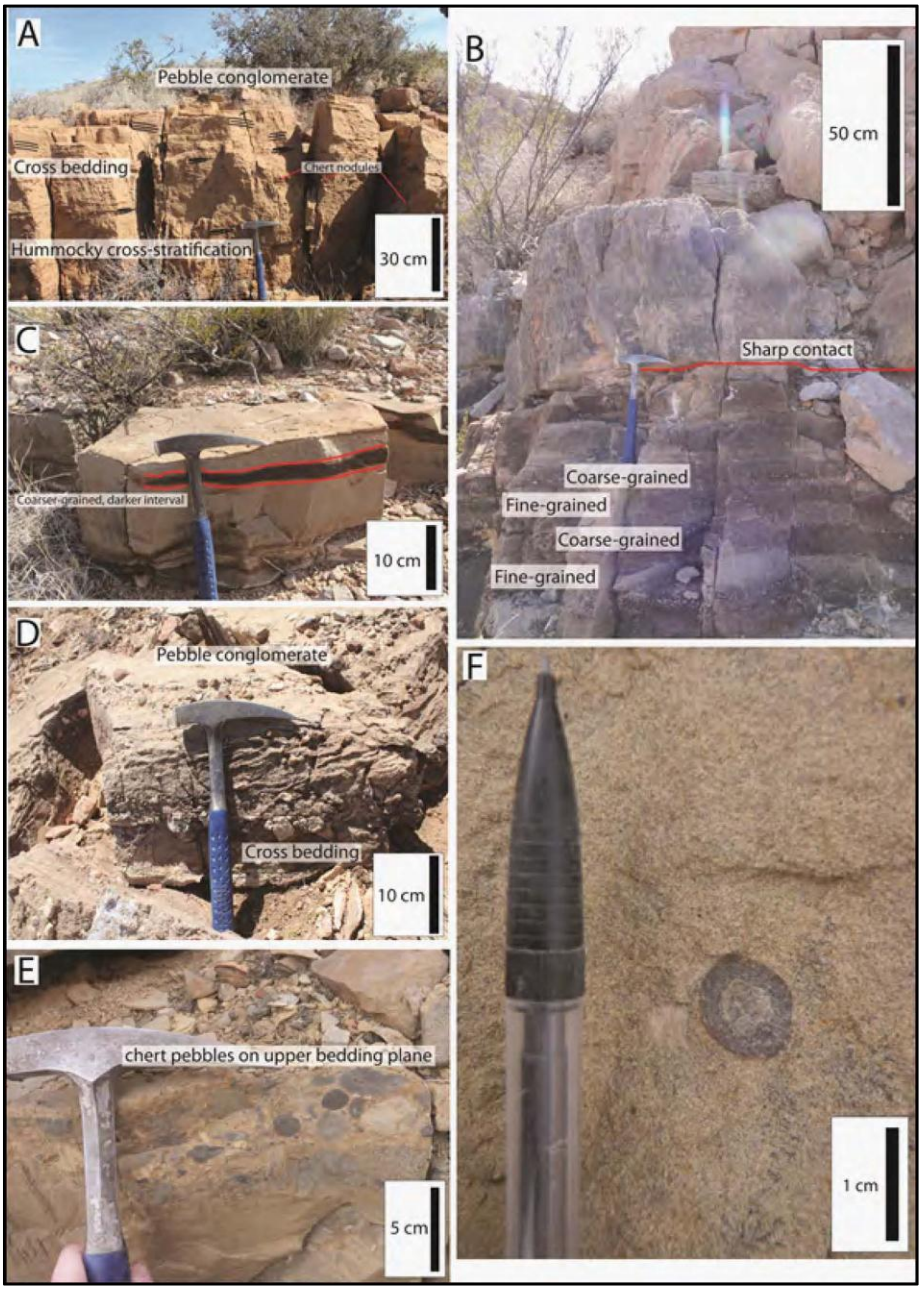

Figure 32: Outcrop Photographs of Quartz Sandstone.

A) Coarsening-upward quartz sandstones, Limonite Mine Section. B) Coarsening-upwards sands below a phylloid algal bioherm, Quarry Section. C) Dark coarse-grained sandstone lense, Limonite Mine Section. D) Planar cross-bedding, Lower Waterfall Canyon Section. E) Chert, mudstone (light gray), and dolomudstone (yellow) pebbles, Lower Waterfall Canyon Section. F) Lone oncoid, Lower Waterfall Canyon Section.

33D). Most sandstone beds are cemented with calcite microspar and spar but the more tan to brown-yellow sandstones are dolomite cemented. No thin sections were made from these dolomitic sandstone beds.

As previously discussed, sandstone beds form coarsening-upward packages of sediments but are confined to stratigraphic sections in the Robledo Mountains. Sandstones are only present in four stratigraphic sections in the Robledo Mountains and beds thickness increases from west to east across the range (Figure 31). However, in the northernmost stratigraphic section (Reef Ridge), no sandstones are present, suggesting these beds do not extend along strike to the north. Correlative strata in the Reef Ridge Section is represented by thin oolitic packstones, ostracode wackestones, and microbial intraclast packstones that contain moderate to high (30-50%) amounts of sub-rounded quartz sand grains.

Quartz sandstone lithofacies is also present at the top of the Limonite Mine and Quarry sections as a thin (<5m) bed, which marks the transition from the lower to the upper interval of the lower Hueco member, and marks the beginning of the lower-middle Hueco transition as defined by Mack et al. (2013) (Figure 2 and 31). Additionally, there are a few thin (<1m), discontinuous sandy beds that occur throughout the upper part of the stratigraphic sections in the Robledo Mountains. Siliciclastics are extremely rare in the lower Hueco strata in the Franklin Mountains compared to the Robledo Mountains. Only limited beds in the Franklin Mountains contain small amounts of quartz sand grains but there are no observed sandstone beds.

Siltstones and Shales

The remaining siliciclastic intervals crop out as poorly exposed, thin bedded (0.1 – 0.3 m) siltstones and shales that weather tan, dark gray, and less commonly green. These beds are

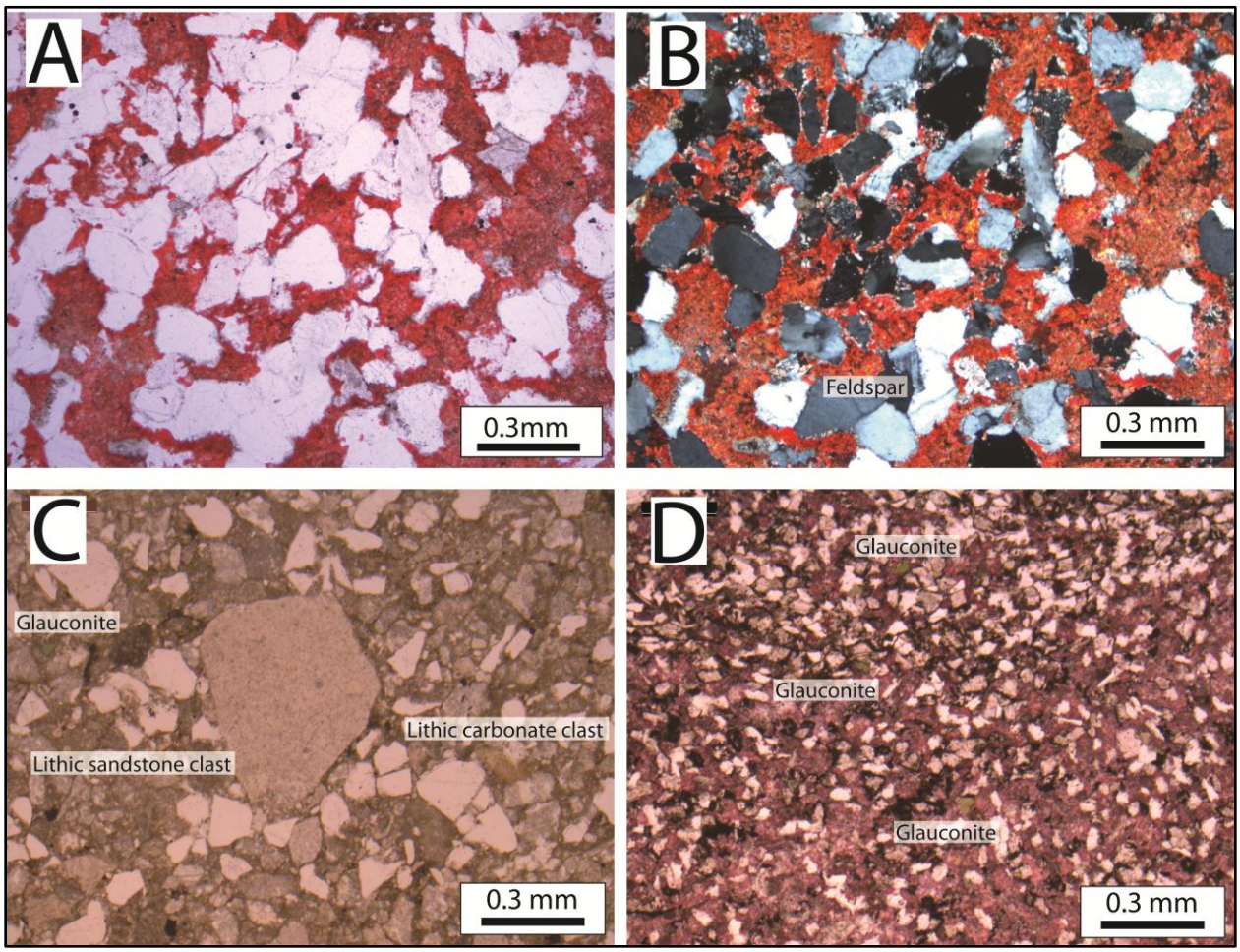

Figure 33: Photomicrographs of Quartz Sandstone.

A) Calcite cemented sandstone, stained, plane light. Sample LH-1. B) Calcite cemented sandstone, stained, cross polarized light. Sample LH-1. C) Calcite cemented sandstone with sandy lithic fragment, unstained, plane light. Sample LH-63. D) Calcite cemented sandstone with glauconite grains, stained, plane light. Sample LH-114.

commonly interbedded with each other and found beneath the previously described sandstones. Sedimentary structures are rare but wave oscillation ripples are present on the upper bedding plane of one thin bed in the Lower Waterfall Canyon Section. This was the only occurrence of sedimentary structures in the siltstone and shale intervals. In the Franklin Mountains, the Vinton

Canyon Section contains two intervals of poorly exposed, green shale. This is the only exposure of siliciclastics within the lower Hueco member in the Franklin Mountains and is possibly correlative to siliciclastic covered intervals within the Tom Mays Park and Anthony Syncline Sections.

Grain types within these siltstones and shales are difficult to determine because of the very fine-grained nature of these rocks. No skeletal or non-skeletal bioclasts were observed at any of these outcrops. Beds are weakly calcite cemented and no diagenetic alterations were observed. The majority of beds are located at the base of the Lower Waterfall Canyon Section interbedded with thin ostracode wackestone, fossiliferous packstone, and microbial intraclast packstone beds (Appendix A.4). Siltstones and shales are not present in any other stratigraphic section from the Robledo Mountains used in this study.

Depositional Environment Interpretation

Siliciclastics in the middle part of the Robledo Mountain stratigraphic sections contain both hummocky cross-stratification and planar cross-bedding in a coarsening upward sequence (Figure 34). Hummocky cross-stratification was originally identified by Campbell (1971), Harms et al. (1975), and Hamblin and Walker (1979) to describe a sedimentary structure created by oscillatory currents superimposed with unidirectional flow. These characteristics lead to their interpretation that this particular type of sedimentary structure would form because of storm influence, as sediments would be exposed to a variety of high energy environments within a relatively short period of time. Their interpretations also stated that in order to preserve these structures, deposition must have occurred below fair-weather wave base. DeCelles (1987) observed similar characteristics within middle Tertiary outer-shelf storm deposits in southern California, representing deposition during the waning stages of storms that would have affected

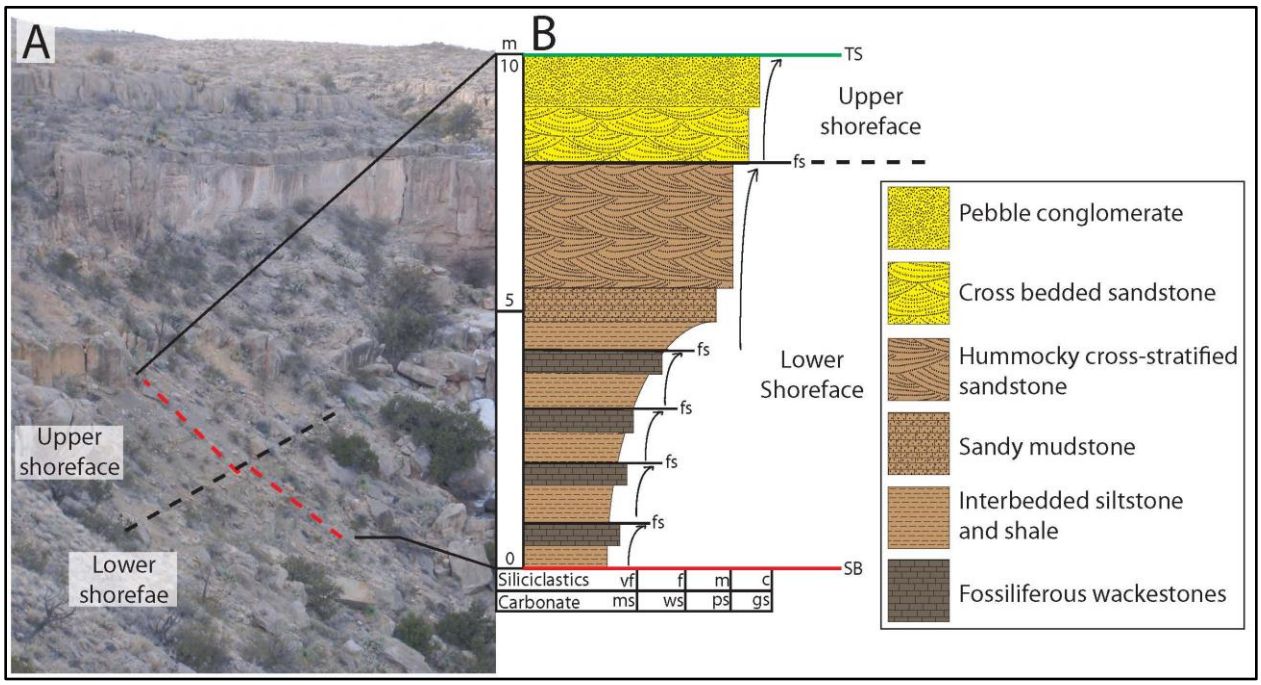

Figure 34: Marine Siliciclastics Stacking Patterns.

A) Outcrop photograph of the shoreface siliciclastic interval from the Lower Waterfall Canyon Section. Siliciclastics typically crop out as poorly exposed slopes compared to the massive, cliff forming carbonate above. B) Typical progradational stacking patterns of lower Hueco shoreface siliciclastic from the Robledo Mountains. Lower shoreface shales are cyclically interbedded with thin carbonate mudstones that contain rare skeletal fragments. Carbonate mudstones become progressively sandier up section and shale beds occasionally have wave oscillation ripples in this interval. Above these shales and mudstones are calcite cemented sandstones with hummocky and planar cross-stratification, indicating an upper shoreface, higher energy regime. A thin pebble conglomerate composed of angular chert pebbles and lithic fragments caps these cycles.

the sediment water interface below fair-weather wave base. Consequently, hummocky cross-stratified sandstones within the lower interval of the lower Hueco member are associated with lower shoreface and inner-shelf storm deposits.

Each occurrence of hummocky cross-stratification is overlain by coarser-grained sandstones with low-angle, centimeter-scale planar cross-beds. This sedimentary structure is

commonly interpreted as upper shoreface to foreshore deposits that are reworked by constant wave energy (Clifton et al. 1971; DeCelles, 1987). Howard and Scott (1983) observed abundant low angle cross-beds in Pleistocene to Holocene sequences along the Georgia coast and interpreted them to describe a foreshore environment. Within this environment, higher inclined cross-beds represented the migrating edge of small sand ridges or bar forms. Wunderlich (1972) describes very similar structures on the Sapelo Island beach of Georgia but with higher angle cross-beds grading into lower angle ripple cross laminae. This gradational change is not observed within the coarsening upward sequence in the lower Hueco lower interval and possible reasons are discussed below.

Correlative siliciclastic intervals to coarsening-upward sequences in the Lower Waterfall Canyon Section (Appendix A.4) do not contain any of the previously listed sedimentary structures. Siliciclastics here consist of siltstone and shale with rare millimeter scale oscillation ripple cross-laminae interbedded with occasional ostracode wackestone and mudstone beds (Figure 31). Because these sediments occur on the same stratigraphic level of their higher energy counterparts, these interbedded siltstone and shale must represent a more basinal depositional environment.

Sandstones in the Robledo Mountains are concentrated at the west and center parts of the Robledo Mountains while the siltstone and shale are located only on the eastern flank. Relative thickness of these units changes across the Robledo Mountains, progressively thickening from west to east, with the thickest siliciclastic interval represented by the interbedded siltstones and shales (Figure 31). Additionally, these sandstone intervals represent shallowing upward sequences showing a transition from lower shoreface (hummocky cross-stratified sands) to upper

shoreface (coarse-grained cross-bedded sandstones) and capped with a chert pebble conglomerate.

Based on these field and petrographic observations, thickness variations, and facies changes, marine siliciclastics in the Robledo Mountains represent an estuarine environment (Figure 35). Allen and Posamentier (1993) documented the facies systems associated with sedimentary fill of the Gironde Estuary in France. Their observations showed coarsening upward sequences of hummocky cross-stratified and planar cross-bedded sands located at the estuary mouth, where tidal energy is concentrated when entering the estuary. These observations correlate with the coarsening upward sequences observed in the both sand intervals in the Quarry Section and the sand interval in the Limonite Mine Section (Figure 35). Additionally, Allen and Posamentier found scattered gravel and shell debris are observed within the estuary mouth sands which are interpreted to have been transported landward, into the estuary. Similarly bivalve and brachiopod fragments and intraclasts were observed through petrographic analysis within these siliciclastic intervals in the Robledo Mountains (Figure 33C). However, no gravel deposits are found as this is a carbonate dominated system and fluvial gravel may not have been transported to more distal parts of the shelf.

Both Allen and Posamentier (1993) and Dalrymple et al. (2006) place finer-grained sands in more landward parts of the estuary, similarly to what is observed in the Robledo Mountains with massive, fine sandstones located in the Limonite Mine Section to the west (Figure 31). Lastly, the Lower Waterfall Section contains interbedded siltstones and shales with subordinate wackestones and mudstones. This is interpreted to be deposition more basinal than the estuary mouth sands and bars (Figure 35). Wave oscillation ripples are observed in both their work representing more distal parts of the estuary mouth, similarly to what is observed in the Lower

Waterfall Canyon Section. However, neither Allen and Posamentier or Dalyrmple discuss the occurrence of carbonate mudstones and wackestones. This is probably because their work involves estuarine fill within siliciclastic-dominated systems, whereas the lower Hueco lower interval and associated estuary fill were deposited within a carbonate-dominated system.

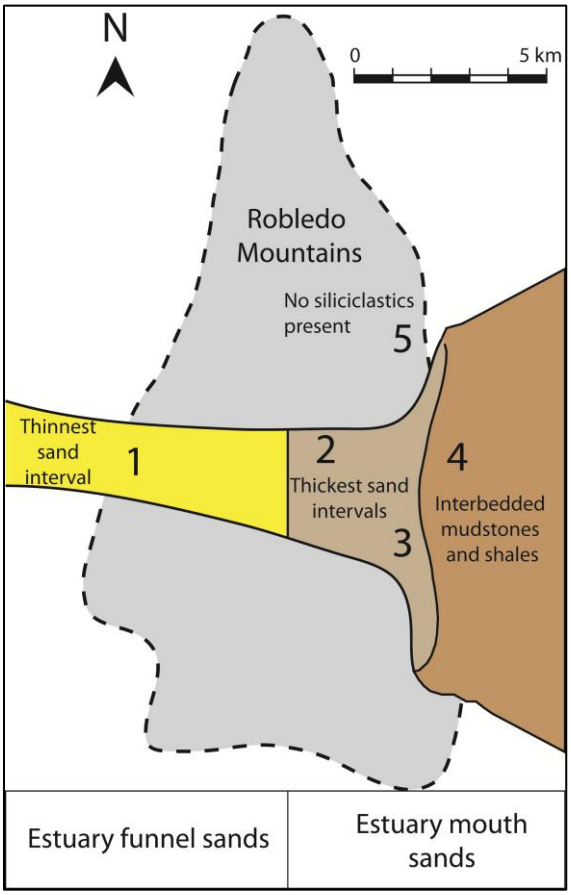

Figure 35: Distribution of Marine Siliciclastics in the Robledo Mountains.

Schematic map showing the location of stratigraphic sections in the Robledo Mountains and the relative distribution of siliciclastics during lowstand and early transgression. The thinnest sandstone beds occur on the western scarp of the range while sands become progressively thicker and coarser-grained to the east. Sandstone beds thin considerably between the Quarry Section and the Limonite Mine Section and are not present in the Reef Ridge Section. 1) Limonite Mine Section. 2) Upper Waterfall Canyon Section. 3) Quarry Section. 4) Lower Waterfall Canyon Section. 5) Reef Ridge Section. Estuary modeled from Allen and Posamentier (1993) and Dalrymple et al. (2006).

2.2 Depositional Profile Geometry

The type and distribution of the depositional facies from the lower interval of the lower Hueco were used to interpret the geometry of the depositional profile of the Robledo shelf on the western margin of the Orogrande Basin (Plate 1). Each environment's position on the profile was defined based on the lithofacies characteristics described and interpreted in the previous section, along with stratigraphic position within the lower Hueco member. This depositional profile summarizes the typical Waltherian facies used to construct the sequence stratigraphic framework for the lower Hueco member. Depositional environments, and their associated modern analogues, as described in the previous section were used to understand the paleogeography for this region.

The most landward environments are represented by supratidal flats and estuary channels (Plate 1). Basinward of these environments are the intertidal flats and channels (Plate 1). These environments are cyclically flooded and sub aerially exposed as tidal energy influences the coastline on a regular basis. Additionally, depositional environments in this lithofacies association appear to form in a facies pattern that can change both perpendicular and parallel to the shoreline, thus do not appear to follow laterally consistent facies belts which is typical of low relief carbonate ramps (Ahr, 1973; Tucker and Wright, 1990). Intertidal lagoons formed two different types of lithofacies depending on paleogeographic position and climate. Ostracode foram wackestone and packstone represent a restricted lagoon environment, allowing ostracodes and forams to flourish while dramatically reducing diversity in the fossil assemblage. Dolomudstones appear to occupy roughly the same paleogeographic position on the depositional profile but represent more hypersaline conditions in which no invertebrate faunal assemblages are found. Consequently, these local changes in lithofacies are representative of a delicate

balance between increasing aridity coupled with a decrease in water circulation into the lagoon, rather than significant change in relative sea-level. However, adjacent to these lagoons are green-algal packstones that would form in shallow, normal marine, low turbidity environments where green algae could flourish. Green-algal packstones represent an increase in water circulation and a change to more normal salinities. Further basinward of these environments were oolitic shoals composed of oolitic packstone and grainstone, with packstones being the deeper of the two lithofacies. Ooid shoals form on topographic highs that acted as barriers to landward shallow ostracode foram lagoons and green-algal environments.

Down-dip from intertidal environments, subtidal fossiliferous packstone and grainstone formed in open marine environments with normal salinities and low turbidity. Grainstones formed above fair-weather wave base, adjacent to the oolitic grainstone, where constant wave energy could simultaneously disarticulate, fragment, abrade, and winnow these sediments. Fossil assemblages in the more basinward fossiliferous packstones were transported landward through storm, wave, and possibly tidal currents and deposited in grainstone shoals adjacent to or surrounding the oolitic packstone and grainstone. However, based on the broad geographic extent of fossiliferous grainstones compared to oolitic grainstones, ooid production was spatially and temporally localized, and restricted to times of higher relative sea-level and more arid environments (Shinn, 1983).

Fossiliferous packstones cover the majority of the carbonate ramp and would have spanned a large paleogeographic area of the Robledo shelf. Packstones formed in environments that were below fair-weather wave base and extend out to near the shelf margin. Storms would have periodically winnowed these sediments or even transported them landward towards the shoals.

Near the shelf margin, phylloid algae formed low relief mound-shaped bioherms responding to favorable photic zone water depths, open, normal marine circulation with a high nutrient supply, and low turbidity conditions. Basinward of the phylloid algal bioherms are the deeper water, *Tubiphytes*-red algal, trilobite packstones (Plate 1). Red algae and trilobites are more tolerant of deeper water, lower light, and temperature conditions. In the Permian Basin, late Pennsylvanian trilobites were distributed in shallow marine environments while the middle Permian trilobite species were confined to deeper areas of the Delaware and Marfa basins (Brezinski, 1992). Based on this relationship, trilobites could have existed in deeper parts of the Robledo shelf in the early Permian. Consequently, this depofacies represents the deepest environment observed in the lower Hueco member on the Robledo shelf.

Thick sequences of shallow water carbonate strata are deposited in shallow marine settings with 3 different profile geometries: 1) a carbonate platform with a pronounced break in slope into deep water (shelf margin), 2) a gently sloping surface that grades into the basin (ramp), or 3) a shallow water platform completely surrounded deep water (isolated platform) (e.g. Ahr, 1973; Ginsburg and James, 1974; Wilson, 1975; Kendall and Schlager, 1981; Read, 1982, 1985; Tucker, 1985; Tucker and Wright, 1990). Based on the interpreted distribution of depositional facies across the shoreline to basin depositional profile, conditions remained fairly shallow across the 70 km extend of the western Robledo shelf in the Orogrande Basin. Consequently, the shallow water carbonates of the lower Hueco member appear to represent a carbonate ramp style geometry.

In other areas, the presence of phylloid algal bioherms is used to mark a distinct shelf margin with a steep break in slope (Wilson, 1975; Toomey, 1991; Simo, et al., 2001; Wahlman, 2002; Grammer and Ritter, 2009, and others). Phylloid algal bioherms in these studies display

significant vertical growth compared to their lateral extent and typically have adjacent facies with abundant carbonate detritus, suggesting slope failures at the shelf margin. Neither characteristic are observed in and adjacent to the phylloid algal buildups in the Robledo and Franklin mountains. Additionally, no carbonate debris, calciturbidites, or deep basinal shales are observed in any stratigraphic section used in this study, suggesting no high relief slope formed in this region, confirming the interpretation of this region as a carbonate ramp.

2.3 Depositional Sequence Stratigraphy

Carbonate sequence stratigraphy is different from siliciclastic sequence stratigraphy based on the sediment source and depositional profile geometry where carbonate deposits occur (Catuneanu, 2006). Many workers have defined how depositional profile geometry can alter the sequence stratigraphic framework for a region (Vail et al, 1977; Van Wagoner et al., 1988; Sarg, 1988). However, tectonic subsidence, eustatic sea-level change, sediment volume, and climate are the main controls on facies distribution and stratal stacking patterns in carbonate dominated environments (Vail and Todd, 1981; Sarg, 1988). This study utilized the spatial and temporal distribution of depositional environments to understand how these controls affect the sequence stratigraphic framework. Techniques outline by Posamentier and Vail (1988), Van Wagoner et al., (1988) Sarg (1988), Catuneanu (2006) were used to construct the sequence stratigraphic framework in this study.

During the late Paleozoic, carbonate sequences formed thick aggrading and prograding packages deposited on depositional profiles ranging from low angle ramps to high relief carbonate platforms with a pronounced shelf-slope break (Vail, 1987; Posamentier and Vail, 1988). The Permian Basin Complex of west Texas and southern New Mexico is described largely as a high-relief carbonate platform surrounded by deep-water siliciclastic basins (Cys and

Gibson, 1988). However, as illustrated by the lithofacies observed on the Robledo Shelf, the western margin of the Orogrande Basin represents a ramp style depositional geometry that does not have a deep-water siliciclastic basin adjacent to carbonate deposition.

Depositional facies analysis of 8 stratigraphic sections from the western margin of the Orogrande Basin was used as the basis to interpret the sequence stratigraphic framework for this margin. In order to do this correctly, depofacies were grouped into shallowing-upward cycles based on the Waltherian relationships of adjacent lithofacies described by the depositional profile (Plate 1). Shallowing-upward cycles bounded by flooding surfaces, known as parasequences, were then grouped into parasequence sets based on upward stacking patterns. The style of parasequence sets were then used to interpret placement of systems tracts and significant sequence stratigraphic surfaces.

2.3.1 Cycle Types

Depofacies analysis was used to define shallowing-upward cycle types in the lower Hueco member on the western margin of the Orogrande Basin. Four different cycle types are recognized: 1) shoreface siliciclastic, 2) peritidal carbonate, 3) subtidal carbonate, and 4) subtidal carbonate buildup (Figure 36). Each cycle consists of two to six different depofacies, which is dependent on position on the depositional profile, eustatic sea-level, and local subsidence.

Shoreface siliciclastic cycles

Shoreface siliciclastic cycles are 5 to 10 m thick and are composed entirely of quartz sandstone and interbedded siltstone and shale. These cycles consist of lower shoreface interbedded siltstone and shales overlain by fine- to medium-grained hummocky cross-stratified quartz sandstone. Lower shoreface beds are overlain by upper shoreface medium- to coarse-

grained planar cross-bedded sandstone capped by a pebble conglomerate (Figure 36). The entire cycle forms both upward coarsening and upward shallowing sequences, suggesting shoreface progradation. Additionally, shoreface siliciclastic cycles only occur at two stratigraphic intervals within the lower Hueco member and each interval only contains one cycle of shoreface siliciclastics. The base of each cycle is represented by an erosional unconformity while the top forms a sharp, well-define contact between siliciclastic and overlying carbonate beds.

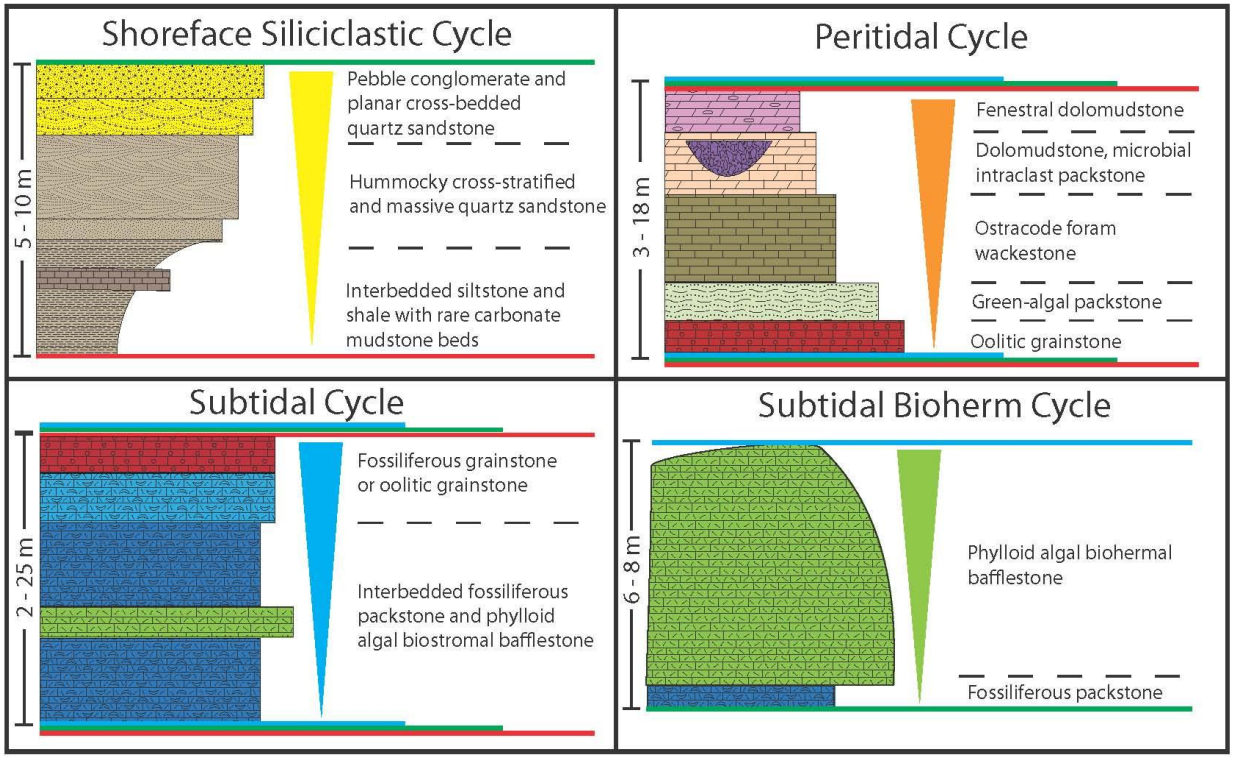

Figure 36: Cycle Types.

Four shallowing upward depositional cycle types are observed in the Lower Hueco strata from the Robledo Shelf. 1) shoreface siliciclastic, 2) peritidal carbonate, 3) subtidal carbonate, and 4) subtidal bioherm.

Peritidal carbonate cycles

Peritidal carbonate cycles are common in the lower Hueco strata and are typically 3 to 18 m thick. The basal bed is typically shallow subtidal oolitic packstone or grainstone that is overlain by intertidal ostracode foram wackestone and dolomudstone. Dolomudstone beds have channelized microbial intraclast packstone beds and the entire cycle is capped with supratidal fenestral dolomudstone (Figure 36). Peritidal carbonate cycles are often bounded above and below by other peritidal cycles suggesting an overall aggradational trend in stacking patterns. Consequently, peritidal cycles commonly extend between all measured stratigraphic sections in this study. The base of peritidal carbonate cycles can be either a transgressive surface, maximum flooding surface, or both depending on stacking patterns and position on the depositional profile. Cycle tops are either defined by transgressive surfaces or erosional sequence boundaries overlain by shoreface siliciclastic cycles.

Subtidal carbonate cycles

Most subtidal carbonate cycles are thicker on average compared to both shoreface siliciclastic and peritidal carbonate cycles, but range in thickness from 2 to 25 m depending on the position on the depositional profile. These cycles consist of interbedded fossiliferous packstone and phylloid algal biostromal bafflestone (Figure 36). Shallow subtidal fossiliferous grainstone caps subtidal carbonate cycles, suggesting the entire cycle was deposited at or below fair-weather wave base. Subtidal carbonate cycles are bounded above and below with sequence boundaries, transgressive surfaces, maximum flooding surfaces, or all three superimposed on each other depending on stacking patterns and the position on the depositional profile. Subtidal carbonate cycles that are wedged between peritidal carbonate cycles are bounded at their base by a transgressive surface that typically contains a coarse-grained lag deposit. The upper surface in

this case is a maximum flooding surface. However, subtidal carbonate cycles that are wedged between other subtidal carbonate cycles are bounded above and below by a transgressive surface, maximum flooding surface, sequence boundary, or all three superimposed on each other. This relationship suggests an overall progradational stacking pattern. Consequently, subtidal carbonate cycles are important for tracking the position of fair-weather wave base and the relative position of the shoreline across the Robledo Shelf.

Subtidal carbonate bioherm cycles

Subtidal carbonate buildup cycles are important stratigraphic intervals because they contain both phylloid algal biohermal and biostromal bafflestones. These cycles range in thickness from 6 to 8 m and are composed of interbedded subtidal carbonate fossiliferous packstone and phylloid algal bafflestone (Figure 36). However, depositional controls such as eustatic sea-level or local subsidence control the morphology of phylloid algal beds (bioherm or biostrome) in each cycle. Phylloid algal bioherms are present in subtidal carbonate buildup cycles that are consistent with higher magnitude increases in relative sea-level while biostromes are found in smaller transgressive systems tract deposits. Despite these different characteristics, the base of subtidal carbonate buildup cycles are always transgressive surfaces, while the tops are always maximum flooding surfaces. Cycles with biohermal or biostromal bafflestone always exhibit an overall retrogradational stacking pattern. Additionally, these cycles are either found between peritidal cycles or between shoreface siliciclastic and subtidal cycles. This relationship suggests a significant connection between depositional morphology and either significant sea-level rise or increased local subsidence.

2.3.2 Sequences and Systems Tracts

Based on parasequence stacking patterns and location of significant unconformity and flooding surfaces, the lower Hueco member on the Robledo Shelf forms two third-order depositional sequences that are divided into multiple fourth-order sequences (Plate 2). Both the third– and fourth-order sequences contain systems tracts composed of the cycle types described above. The third-order sequences have been titled Sequence 1 and Sequence 2, respectively and fourth-order sequences within Sequence 1 and 2 are labeled with letters (A,B, C, and D respectively) (Plate 2).

2.3.3 Depositional Sequence 1

Lowstand systems tract

In the third-order Sequence 1 of the lower Hueco member of the Hueco Limestone, the lowstand systems tract is represented by the Pennsylvanian-Permian boundary that makes a regional subaerial unconformity across the both shelves of the Orogrande Basin. Lowstand deposits are not preserved at this boundary in either the Robledo or Franklin mountains and evidence of subaerial exposure is poor because of a lack of exposure of this horizon. Because of the extent of subaerial exposure, this sequence boundary can be classified as a Type 1 sequence boundary in which lowering of relative sea-level dramatically outpaces local subsidence.

Transgressive Systems Tract

The transgressive systems tract in Sequence 1 is represented by the fourth-order Sequence 1A, which directly overlies the Pennsylvanian-Permian boundary. It is bounded at its base by a sequence boundary and its top by a maximum flooding surface (Plate 2). Sequence 1A contains part of 2 fourth-order sequences. The lower fourth-order sequence is dominated by retrograding peritidal carbonate cycles culminating at transgression by deposition across the deep

subtidal cycle (Sequence 1A: Plate 2). At maximum transgression, subtidal cycles are distributed across the majority of the Robledo shelf during these transgressions and shallow subtidal shoals are restricted to exposures in the Robledo Mountains.

Highstand Systems Tract

The upper part of Sequence 1 is represented by a third-order highstand systems tract composed of the fourth-order sequences 1B and 1C and bounded by a maximum flooding surface below and sequence boundary above. The transgressive systems tracts in fourth-order sequences 1B and 1C are composed of 1 cycle of subtidal carbonates that have a pronounced chert pebble lag at the sequence boundary and subsequent transgressive surface (Figure 15C). Highstand systems tracts in sequences 1B and 1C consist of 2 or 3 cycles of peritidal carbonates that form an overall aggradational to slightly retrogradational stacking pattern within the third-order Sequence 1 highstand. At times of fourth-order sea-level highstand, peritidal carbonates span the entire Robledo shelf and shallow subtidal shoals are concentrated in the Franklin Mountains.

Overall, Sequence 1 is dominated by thick fourth-order highstand peritidal cycles interlayered with thin transgressive subtidal cycles wedged between them. Highstand fourth-order peritidal carbonate cycles are dominated by progressively shallower water peritidal facies upward through Sequence 1 as supratidal fenestral dolomudstones become more abundant in the upper part of this Sequence. However, the supratidal and intertidal environments do not extend as far basinward across the shelf and form an overall retrogradational stacking pattern. The upper sequence boundary of Sequence 1 is an erosional unconformity formed by lowstand fluvial incision into the underlying highstand Sequence 1 peritidal carbonate cycles. Fluvial incision here is in response to significant lowering in base-level that corresponds with a pronounced

basinward shift in depositional facies and thus another Type 1 sequence boundary between Sequence 1 and 2.

2.3.4 Depositional Sequence 2

Lowstand systems tract

The significant lowering in relative sea level preceding the deposition of Sequence 2 produced another Type 1 sequence boundary and caused fluvial incision at the base of Sequence 2 into the underlying peritidal carbonates of Sequence 1. In Sequence 2, the lowstand systems tract is composed of one cycle of shoreface siliciclastics bounded below by a Type 1 sequence boundary and above by a transgressive surface. The occurrence of shoreface siliciclastics mark an abrupt basinward shift from aggrading-retrograding peritidal carbonates facies to progradational shoreface siliciclastics (Plate 2). This abrupt basinward shift and rapid transition to siliciclastic dominated environments is associated with lower-order, higher magnitude lowering of relative sea-level and a regional unconformity. Consequently, lowstand systems tracts are only found in two stratigraphic intervals in the lower Hueco member (Plate 2). These shoreface siliciclastic cycles are confined to the incised valley system and are not present in more distal parts of the ramp. As relative sea-level begins to rise during the late lowstand, the incised valley system becomes flooded and drowned and shoreface siliciclastic cycles fill the available accommodation space forming an estuary. Wave, tidal current, and storm energy are concentrated at the estuary mouth, forming hummocky-cross stratified sandstones and estuary mouth bars with planar cross-bedding (Figure 31, 32A, 32D, and 35). Coarser-grained pebble conglomerate beds are confined to the estuary funnel, landward of the estuary mouth (Figure 35). The remaining siliciclastics form interbedded siltstone and shales seaward of the estuary mouth, below both fair-weather and storm wave base.

Lowstand incised valley systems are typically represented by amalgamated fluvial channel fills overlying subaerial unconformities (Catuneanu, 2006). However, there are cases where lowstand deposits are missing from the stratigraphic framework either because of non-deposition from sediment bypass or subsequent erosion during transgression (Dalyrmple, 1992; Ainsworth and Walker, 1994). This would explain the lack of evidence of a large regional sub-aerial unconformity and lack of amalgamated fluvial channels in the stratigraphic sections from the Robledo Mountains.

Transgressive Systems Tract

Higher magnitude transgression following the significant lowering in relative sea level at the lower boundary of Sequence 2 provided the necessary conditions to develop a retrograding subtidal bioherm cycle. The transgressive systems tract of Sequence 2 contains the fourth-order Sequence 2A which is bounded below by a transgressive surface and above by a sequence boundary (Plate 2). Sequence 2A consist of retrograding packages of subtidal and subtidal bioherm cycles that range in thickness from 2-10 m and are on average much thicker than the transgressive systems tracts of Sequence 1. This stratigraphic interval is also the only stratigraphic interval in the lower Hueco member on the Robledo Shelf that contains mound-shaped phylloid algal bioherms. Additionally, the phylloid algal bioherms sit directly above the lowstand incised-valley shoreface siliciclastics and are overlain by the deeper-water, *Tubiphytes*-red algal packstone that forms the base of the overlying highstand systems tract. The highstand systems tract in Sequence 2A consists of a single thick (~20 m) cycle of subtidal carbonates that form a progradational stacking pattern that spans the entire Robledo Shelf. A thin peritidal carbonate cycle forms the uppermost part of this fourth-order highstand systems tract. Overall,

the transgressive systems tract in Sequence 2 is dominated by subtidal carbonate cycles that locally contain phylloid algal bioherms and from an overall retrogradational stacking pattern.

Highstand Systems Tract

The highstand systems tract of Sequence 2 contains the fourth-order sequences 2B, 2C, and 2D. Sequence 2B is the only fourth-order sequence in this interval that contains any lowstand deposits. Lowstand deposits in this sequence are represented by a thin (2.5 m) marine sandstone with no sedimentary structures and is only present in 1 stratigraphic section (Plate 2). The transgressive systems tracts of sequences 2B, 2C, and 2D are composed 2 or 3 subtidal carbonate cycles that thicken basinward and contain phylloid algal biostromes. These cycles thicken basinward in all fourth-order sequences in Sequence 2. Highstand systems tracts in sequences 2B, 2C, and 2D consist of 2 to 3 thin peritidal carbonate cycles that form an overall progradational stacking pattern (Plate 2). However, unlike Sequence 1, peritidal carbonate cycles are confined to exposures in the Robledo Mountains and subtidal carbonate cycles span the majority of the Robledo Shelf. Consequently, highstand systems tracts in Sequence 2 are dominated by subtidal carbonate cycles with shallow subtidal shoals concentrated further landward (Plate 2, Sequences 1 and 2). This relationship between the relative location of the shoreline based on the position of wave-dominated shoals and the different composition of highstand systems tracts suggests that deposition during the latter half of lower Hueco member deposition was due to an overall higher relative sea level as compared to Sequence 1. Additionally, highstand systems tracts are the most abundant and thickest systems tracts preserved in the lower Hueco member on the Robledo Shelf.

The upper boundary of Sequence 2 is also marked by a Type 1 sequence boundary and fluvial incision into underlying peritidal cycles forming an incised valley. This incised valley is

filled by a single shoreface siliciclastic cycle whose base forms the contact between the lower and upper intervals of the lower Hueco member and marks the base of the lower-middle Hueco transition interval as defined by Mack et al. (2013).

2.4 Fusulinid Biostratigraphy

To enhance the accuracy of stratigraphic correlations in this study, lithographic and sequence stratigraphic correlation was augmented by fusulinid biostratigraphy. Fusulinid samples were collected from 17 beds within the Robledo and Franklin mountains. Hand samples were made into oriented thin sections for proper taxonomic identification by Dr. Greg Wahlman of Wahlman Geological Services, LLC. Fusulinid species will be discussed in order of oldest to youngest as found in the strata.

The basal part of the Reef Ridge Section in Sequence 1A contains the earliest occurrence of fusulinid species in the stratigraphic sections from the Robledo Mountains (Plate 2). However, non-oriented thin sections were made from these beds and thin sections only contain fragmented fusulinids with oblique cuts (LH-121, LH-124, and LH-126). Despite this, fusulinids could be distinctly identified as *Schwagerina sp*. with large proloculi, a known Wolfcampian species. The next occurrence of fusulinids is in the Anthony Syncline Section in the Franklin Mountains in Sequence 1A and 1B (Plate 2). Four distinctive intervals from the lower 50 m of this section were used for identification (Samples: AS-8, AS-12, AS-13, and AS-16B) (Appendix A.6). These intervals contain mainly Wolfcampian *Schwagerina* species; *Schwagerina. grandensis*, and questionable *Schwagerina andresensis* as well as one well oriented sample of *Schwagerina vervillei.* Specimens of *Pseudofusulina robleda* are also present in these beds which represents a transitional species that spans the latest Virgilian into the early Wolfcampian (Figure 37)

(Wahlman and King, 2002). This interval of fusulinid-rich beds was the only one used for identification of species in the Anthony Syncline Section.

Moving up section and into younger strata, the next interval that contains fusulinids is located in the Lower Waterfall Canyon Section in Sequence 2B. Two beds in this stratigraphic section contained abundant fusulinids that could be used to identify species (LH-62 and LH-82) (Appendix A.4). Fusulinid thin sections from sample LH-62 only had oblique cuts that were poorly oriented. Species could only be identified as *Schwagerina* sp., which could be either latest Pennsylvanian or early Wolfcampian. However, polished hand samples of LH-82 contained *Pseudoschwagerina* cf. *morsei*, which indicates an early Wolfcampian age (Figure 37).

Fusulinid beds in both the Quarry and Upper Waterfall Canyon sections occur on roughly the same stratigraphic interval as the fusulinid bearing beds in the Lower Waterfall Canyon Section in Sequence 2B. Fusulinid species from the Upper Waterfall Canyon Section (LH-41 and LH-42) were tentatively identified to be *Schwagerina* cf. *andresensis* and *S.* cf. *grandensis*, but samples were not well oriented enough for confident identification (Figure 37). In the Quarry Section, multiple beds contained abundant fusulinids in both packstones and grainstones (LH-17, LH-29, LH-30, LH-37, and LH-38) (Appendix A.3). Sample LH-29 contained the best oriented fusulinids that were confidently identified as the early Wolfcampian species *Pseudoschwagerina rhodesi.* The other thin sections only contained poorly oriented samples of juvenile *Pseudoschwagerina* sp. and the transitional *Schwagerina* aff. *grandensis* (Figure 37).

Samples from Tortugas Mountain were very difficult to identify based on the pervasive non-fabric selective dolomitization and silicification of the fusulinid tests. However, hand samples contained very large inflated fusulinids (> 1 cm in diameter) that are representative of

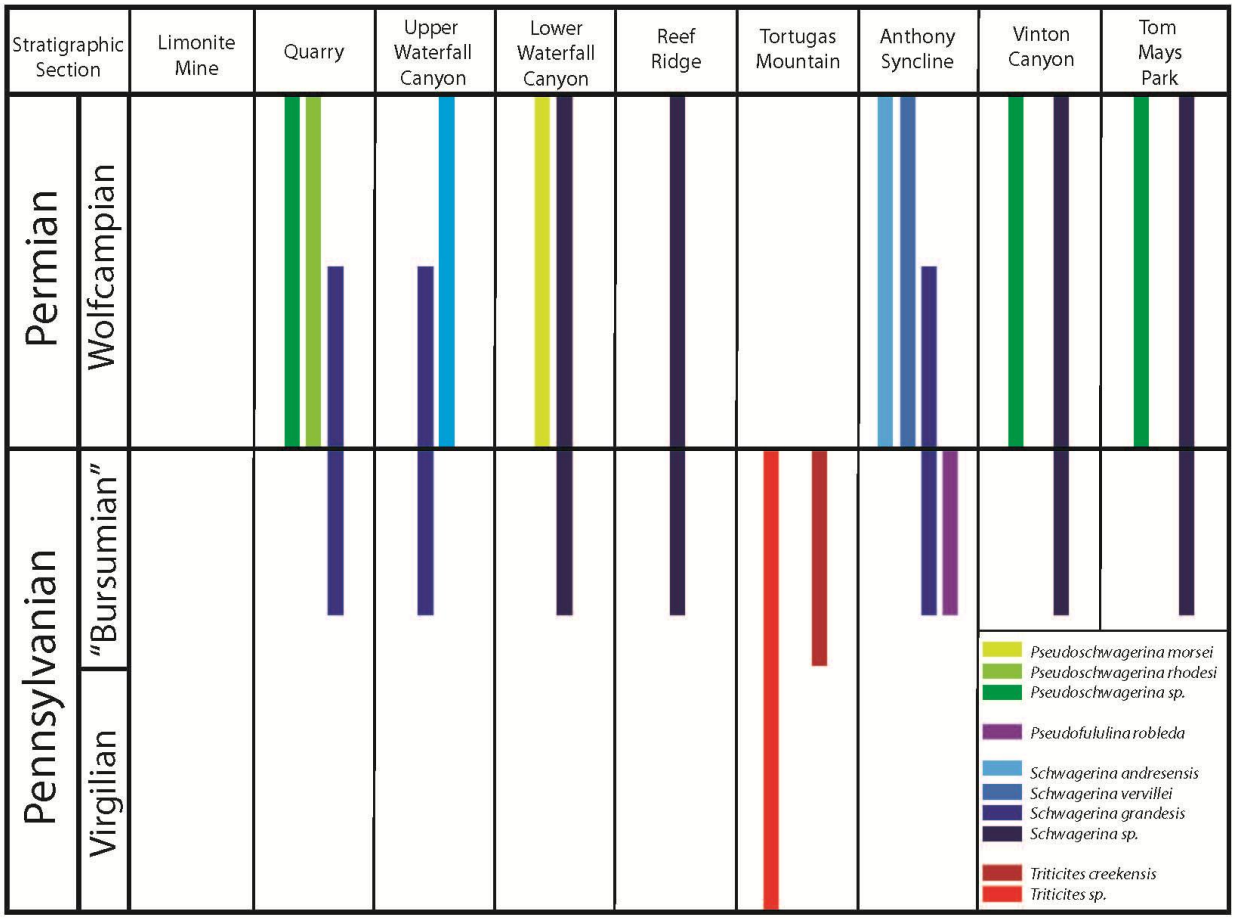

Figure 37: Fusulinid Biostratigraphy.

Fusulinid species with relative ages from each stratigraphic section used in this study. The Limonite Mine Section was the only measured stratigraphic section that did not contain any fusulinids. Fusulinid identification was done by Dr. Greg Wahlman (Wahlman Geological Services, LLC).

the late Pennsylvanian in the Orogrande Basin. Both hand samples and thin sections were used to identify these species as *Triticities creekensis* as well as other *Triticities* sp. that were too diagenetically altered to make accurate identification (Figure 37). Because these were the only fusulinids found in the Tortugas Mountain Section, this section was considered latest Virgillian

and probably part of the Bursum Formation. Consequently, this section was not used for lithofacies and depositional environment interpretations or sequence stratigraphic correlations. Details and descriptions of this stratigraphic section are located in Appendix B.

Overall, most fusulinid species identified in this study were affiliated with the early Wolfcampian with few samples showing latest Pennsylvanian fusulinid assemblages. These latest Pennsylvanian fusulinids can also be representative of the Bursum Formation and the proposed "Bursumian" stage for the late Pennsylvanian by Wahlman and King (2002). Despite this, all units used in this study are Wolfcampian in age however, more work needs to be done to isolate the exact biostratigraphic horizon that represents the Pennsylvanian-Permian boundary in each area.

Chapter 3

DISCUSSION

3.1 Controls on Lithofacies Variations and Distribution

The spatial and temporal distribution of early Wolfcampian strata in the Orogrande Basin was primarily influenced by glacio-eustatic sea-level changes superimposed upon an erosionally modified ramp depositional profile. Lithofacies on the Robledo shelf represent a facies mosaic of peritidal and intertidal depositional facies defining the Wolfcampian paleoshoreline. For these environments, relative sea-level changes had the most dramatic effect on their spatial and temporal distribution.

3.1.1 Siliciclastics

Early Wolfcampian siliciclastics on the Robledo shelf occur infrequently but represent very important horizons within the stratigraphic framework of the lower interval of the lower Hueco member. The spatial distribution of lowstand siliciclastics is primarily controlled by the depositional profile geometry and topography of the region. Incised valley systems on the shelf are the basinward equivalent of fluvial systems and their occurrence is dependent on the presence of local fluvial systems. The absence of marine siliciclastics in the Franklin Mountains is likely due to sediment bypass of the shelf during times of lowstand and lack of a local fluvial drainage system across this area (Figure 38A and D).

Incised valley systems and the associated lowstand shoreface siliciclastics are the depofacies and environments that were most affected by fluctuations in sea-level. Siliciclastics only occur at lower-order, higher magnitude lowering in relative sea-level making their temporal distribution on the Robledo Shelf entirely dependent on periods of time of major sea-level

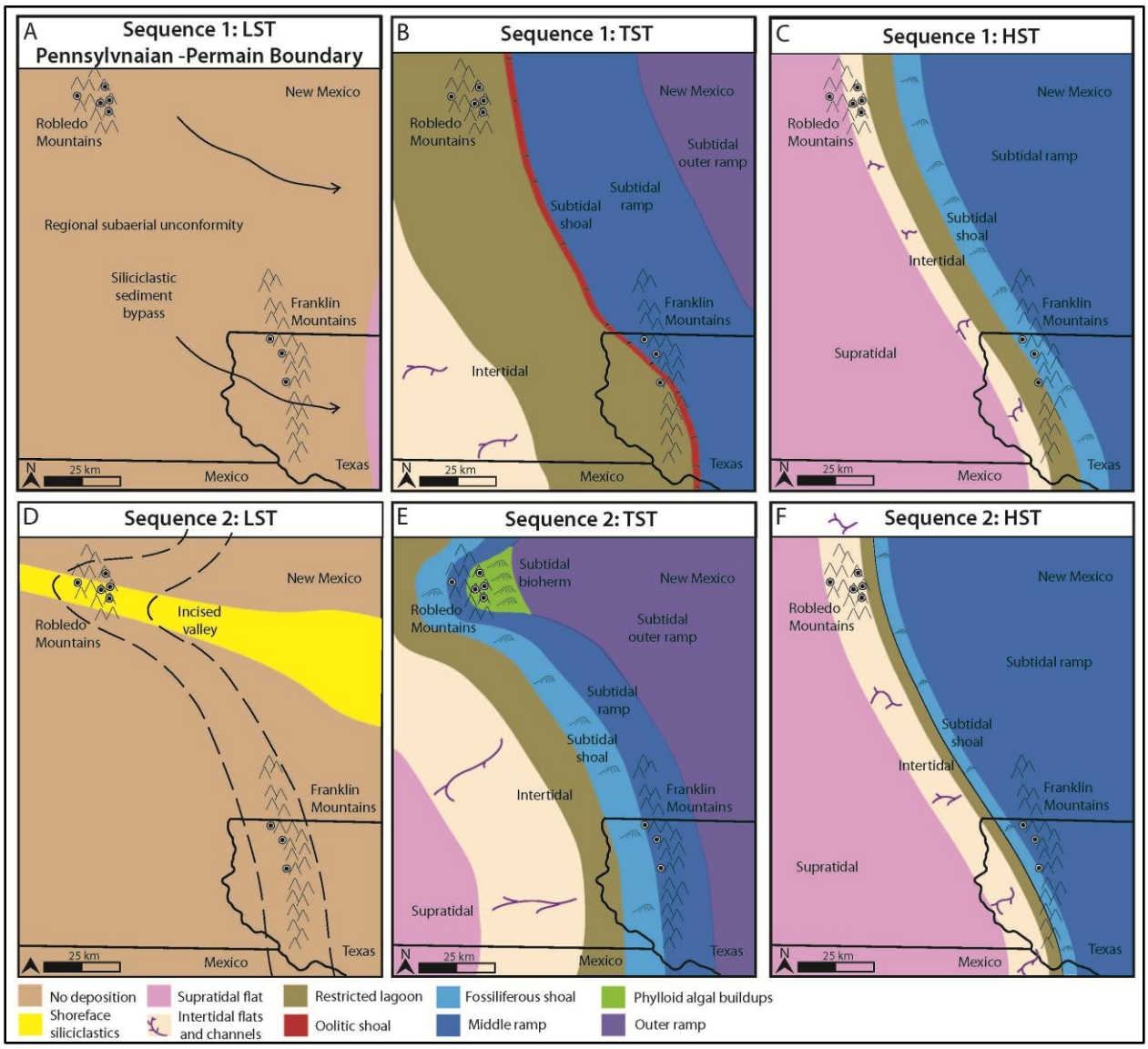

Figure 38: Early Wolfcampian Paleogeography.

Based on the depositional facies distribution and sequence stratigraphic correlation, the paleocoastline of the western margin of the Orogrande Basin appears to have large embayments that cause the distribution of depofacies to follow a radial pattern and not parallel a straight shoreline. This is consistent with a facies deepening trend from west to east in the Robledo Mountains and south to north in the Franklin Mountains. Additionally, lowstand erosion in the Robledo Mountains in the form of an incised valley may have helped form this curved embayment on this margin.

lowstands. Consequently, marine siliciclastics were only preserved in backing-filling estuaries within incised valleys as relative sea-level began to rise during the late lowstand above Type 1 sequence boundaries. Within these incised valley systems, marine siliciclastics follow similar distribution and stacking patterns to what has been defined by both Allen and Posamentier (1993) and Dalrymple et al. (2006) in regards to sedimentation in estuary deposits. This would suggest that a large percentage of the current Robledo Mountains existed as a broad estuary during times of lowstand in the early Wolfcampian (Figure 35). However, marine siliciclastics are not observed in the early Wolfcampian strata of the Franklin Mountains. Siliciclastics appear to have completely bypassed the Orogrande Basin and moved southward and were likely deposited somewhere in present day Mexico (Figure 39), but no stratigraphic studies of age equivalent strata have been completed in that region. Additionally, their distribution may have also been a controlling factor on the distribution of phylloid algal biohermal bafflestones, providing topographic highs related to differential compaction.

This scenario is different than what is observed for Wolfcampian siliciclastics in the adjacent Delaware basin. Cys and Gibson (1988) summarize deposition in the Delaware basin by deep water shales with occasional thin limestone or sandstones that were deposited in deep-marine waters in a rapidly subsiding basin. Additionally, Silver and Todd (1969) recognized at times of lower sea-level, submarine fans composed of siliciclastics and carbonate detritus built into the more distal parts of the basin. However, in the Orogrande Basin, no submarine fans or calciturbidites are found in any of the lower Hueco strata. The complete lack of siliciclastics during this time period in the Orogrande suggests that this basin was much shallower than the surrounding basins. It was more likely that the Orogrande Basin deepened considerably from north to south towards present day Mexico rather than developing a distinctively deep

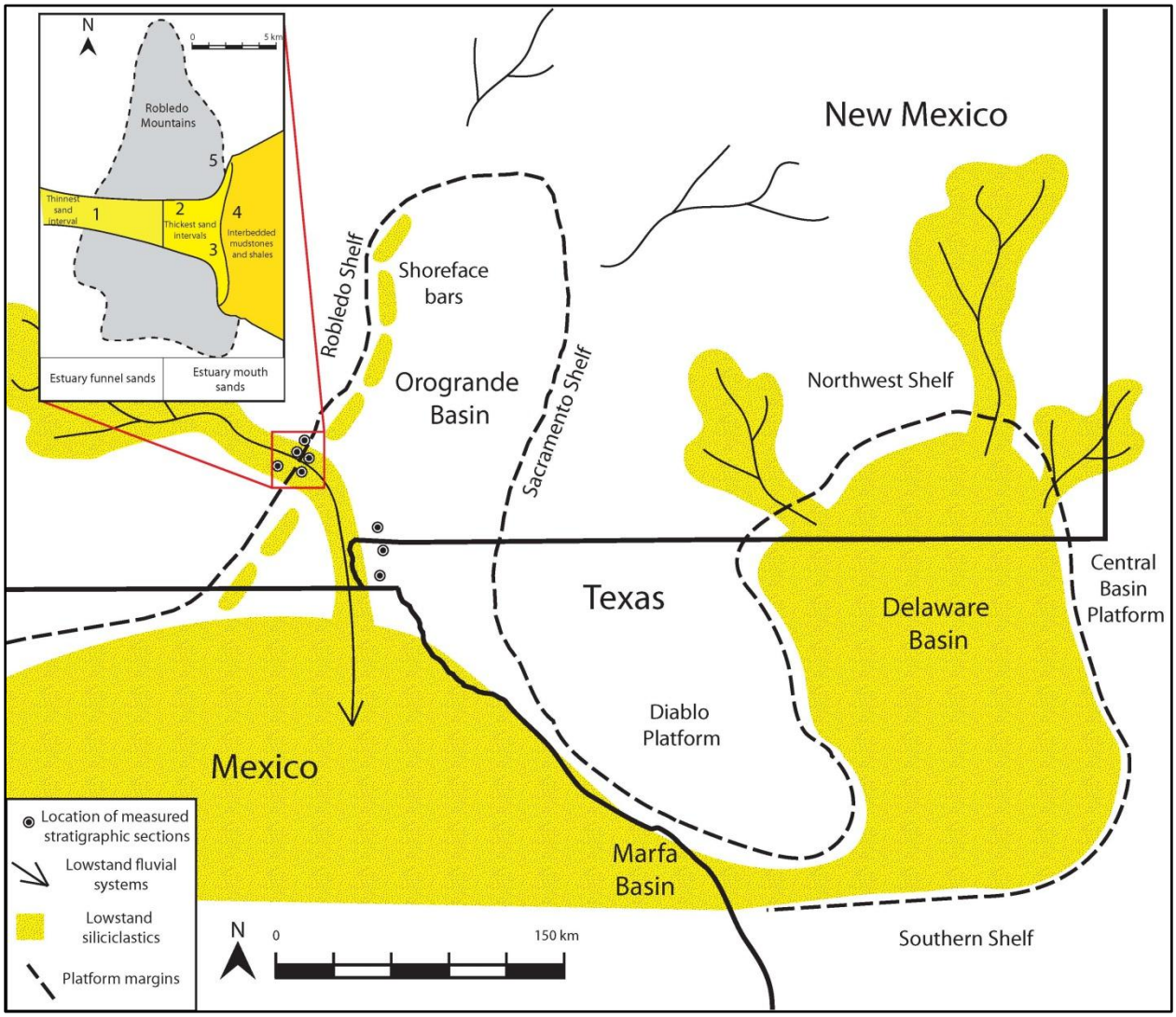

Figure 39: Distribution of Lowstand Siliciclastics.

Lowstand siliciclastics occur infrequently but cyclically in the lower Hueco strata on the Robledo shelf. Their only occurrence is in the Robledo Mountains as a backfilling estuary during late stages of lowstand and early stages of transgression. Consequently, the majority of siliciclastics must have bypassed the shelf during lowstand and were deposited further to the south, similar to the Delaware Basin to the east.

depocenter at its geographic center between the eastern and western margins (Figure 38). More work on lower Hueco member strata in the geographic center of the Orogrande Basin would help to determine if siliciclastics were being transported to the basin center or completely bypassing the Orogrande Basin for a more southern depocenter.

3.1.2 Carbonates

The distribution of carbonate deposition in the Orogrande Basin during the early Wolfcampian was also controlled by changes in relative sea-level but not to the extent that siliciclastics were. Instead, carbonate production and deposition was fairly uniform throughout the early Wolfcampian and only temporally ceased at times of sea-level lowstand and subaerial exposure (Figure 38A-F).

Phylloid algal mounds appear to have been most affected by a variety of depositional controls in this region. Consequently, this depofacies is only found in later stages of large scale transgressions that directly overly shoreface siliciclastic cycles. Their spatial distribution is controlled by the presence of underlying shoreface siliciclastics that provided topographic highs that would help initiate phylloid algal growth because of differential compaction over early-cemented sandstones. Phylloid algal mound development would have followed the depositional trend of the incised valley system and not necessarily parallel to the paleoshoreline as a broad facies belt (Figure 38B). The temporal distribution of phylloid algal mounds was primarily controlled by relatively rapid rising sea level above stratigraphic intervals that contain lowstand shoreface siliciclastics (Sequence 2A: Plate 2). This rapid increase in sea level provided the necessary accommodation space for vertical mound growth. Both the availability of topographic highs related to lowstand siliciclastics and a rapid rise in sea level were two factors that favored

bioherm development, which is why these buildups are absent in most of the lower Hueco strata on the Robledo Shelf.

On the eastern margin, the Pedernal Uplift allowed for more structural controls on the stratigraphic distribution of lithofacies, in particular phylloid algal bioherms. Soreghan and Giles (1999b) determined active tectonism to be a strong influence on the distribution and size of slightly older Pennsylvanian phylloid algal bioherms from the Holder Formation of the Sacramento Mountains. Active faulting on the Sacramento Shelf provided topographic highs for these bioherms to develop despite rapid subsidence related to the crustal loading from the adjacent Pedernal uplift, coupled with dramatic glacio-eustatic sea-level fluctuations. Rapid subsidence of the shelf with uplift of topographic highs during marine transgression provided long periods of high accommodation space resulting in very thick phylloid algal mounds. This type of structural influence is not an apparent factor in mound distribution on the Robledo shelf as no growth strata are observed and these phylloid algal bioherms are much smaller than bioherms developed on the Sacramento Shelf (~5 m on the Robledo shelf compared to > 30 m on the Sacramento shelf). Consequently, waning tectonism and the stability of the Robledo Shelf did not provide these active topographic highs on this margin so phylloid algae utilized the availability of small topographic highs, such as those created by differential compaction of incised valley sandstone complexes. With no active uplift and consistent increasing sea-level through Sequence 2, mounds on this margin were drowned as they could not “keep up” with rising sea level.

The spatial and temporal distribution of most deopofacies was not as restricted as phylloid algal biohermal bafflestones and shoreface siliciclastics. During Sequence 1 (Plate 2), supratidal and intertidal environments covered large parts of the Robledo shelf and their

distribution was only controlled by changes in relative sea-level. Changes in sea-level would have moved the broad facies belts landward or basinward because relatively low subsidence rates on a low angle ramp caused carbonate sediments to prograde far into the Orogrande Basin (Figure 38). This low ramp profile allowed the entire Robledo Shelf to flood during the sea-level rise observed in Sequence 2 (Figure 38) and dramatically reduce the size of intertidal and peritidal carbonate environments.

During Sequence 2 (Figure 38), major transgression and overall higher sea-level and deposition of dominantly subtidal facies across the Robledo Shelf meant that environments were less affected by higher-order lower, lower-magnitude sea-level changes. These environments were constantly submerged, with most occurring below fair-weather wave base. Because of this, depositional environments that produced fossiliferous packstone and grainstone could migrate both parallel and perpendicular to the paleoshoreline, creating cyclic Waltherian facies shifts. Fossiliferous grainstones would have tracked the position of highest wave energy, between fair-weather wave base and sea-level, and are present during both transgressive and highstand systems tracts.

No significant thickness changes are present in this stratigraphy that would suggest changes in depositional profile geometry or increased rates of subsidence. Based on these observations ascertained from this detailed study on early Wolfcampian stratigraphy, sea-level fluctuations strongly influenced the distribution of lithofacies and depositional environments on the Robledo shelf. The Powwow Conglomerate that represents the regional erosional unconformity at the base of the Permian strata in the Sacramento and Hueco mountains (King et al., 1945; Williams, 1963; and others) is absent at the stratigraphic sections used in this study. This corresponds well with the conclusions made by Kottlowski (1960) and Kottlowski and

Seager (1988) who suggested the Robledo shelf was much more stable compared to the eastern margin, experiencing relatively low rates of subsidence during the early Permian.

Depositional trends in on the Robledo shelf were also influenced by the local paleogeography. Based on the facies distribution and sequence stratigraphic analysis, this margin of the Orogrande basin appears to represent a large embayment rather than a simple linear, northwest to southeast-trending shoreline as previously depicted by Kues and Giles (2004) (Figure 38E and 39F). Depofacies in the Robledo Mountains deepen from west to east while deepening from south to north in the Franklin Mountains. This explains the distribution of intertidal restricted lagoonal facies in the Robledo Mountains while the more landward dolomudstone lithofacies are consistently in a more basinward position, down dip of the restricted lagoonal facies in the Franklin Mountains (Plate 2, Sequence 1). Also, erosive lowstand fluvial systems may have helped to form this embayment centered around the Robledo Mountains by creating a topographic low that would provide more accommodation space during times of transgression than other regions of the ramp (Figure 38D and 39E).

3.2 Early Wolfcampian Transgression

Sequence stratigraphic analysis of the lower Hueco member revealed that sea-level was on average much lower at the start of lower Hueco time, which corresponds well with previous studies (King, et al. 1945; Kottlowski et al., 1956; Kottlowski and LeMone, 1994; Kues and Giles, 2004). This also coincides well with the regional unconformity originally defined by King et al. (1945) at the Pennsylvanian-Permian boundary and deposition of the Powwow conglomerate basinward. Additionally, a compilation of studies comparing oxygen and carbon isotopes from late Paleozoic strata in Gondwana suggests that the maximum extent of glacial ice occurred during the early Permian (Isbell et al., 2003; Fielding et al., 2008). Greater global ice

volumes would dramatically reduce eustatic sea-level and would explain the large scale unconformity observed at the transition into the early Permian.

During the early early Permian, intertidal and peritidal environments still dominate the lower Hueco depositional profile of the Robledo shelf, with few subtidal environments deposited further into the basin (Sequence 1, Plate 2). However, the upper half of the lower Hueco (Sequence 2, Plate 2) is almost completely dominated by subtidal facies even in the stratigraphic sections most proximal to the basin margin. This relationship suggests a significant increase in sea-level throughout lower Hueco time, specifically in Sequence 2. Recent oxygen and carbonate isotope data (Koch, 2010) from both the Pennsylvanian Holder Formation and the entire early Permian Hueco Group in the Orogrande Basin, suggests relatively lower sea level at the base of the Permian, possibly related to expansion of global ice volumes based on an increase in $\delta^{18}O$ and $\delta^{13}C$ values. In summary, the sequence stratigraphic analysis completed here appears to describe a progressive rise in sea-level within thick cycles of carbonate rocks deposited on the Robledo shelf throughout the early Wolfcampian.

Chapter 4

CONCLUSIONS

The lower Hueco member of the Hueco Limestone on the western margin of the Orogrande Basin consists of 11 depositional lithofacies that are located in the Robledo and Franklin mountains of southern New Mexico and west Texas respectively. From shoreline to basin these are: 1) quartz sandstone, 2) quartz siltstone and shale, 3) fenestral dolomudstone, 4) dolomudstone, 5) green-algal packstone to grainstone, 6) microbial intraclast packstone, 7) ostracode foram wackestone, 8) oolitic packstone and grainstone, 9)fossiliferous packstone and grainstone, 10) fusulinid packstone and grainstone, and 11) phylloid algal bafflestone. Based on the spatial and temporal distribution of these lithofacies, four depofacies associations were developed to describe their relative position on the Wolfcampian depositional profile: 1) shoreface siliciclastics, 2) supratidal carbonate, 3) intertidal carbonate, and 4) subtidal carbonate. Waltherian transitions between these lithofacies and subsequent lithofacies associations suggests this margin of the Orogrande Basin existed as a shallow marine carbonate ramp, deepening from west to east during the early Wolfcampian. Phylloid algal bioherms form thin, isolated buildups locally concentrated in the Robledo Mountains while the remaining depositional ramp is dominated by wide facies belts of intertidal and supratidal carbonate environments.

Sequence stratigraphic analysis of this region shows two distinctive third-order sequences (Sequence 1 and Sequence 2) within the lower Hueco member. Sequence 1 is bounded at its base by a regionally extensive Type 1 sequence boundary that represents a regional unconformity at the Pennsylvanian-Permian boundary across the Orogrande Basin. Highstand systems tract deposition during Sequence 1 are characterized by thick fourth-order highstand systems tracts

composed of aggradational and progradational peritidal carbonate cycles with very thin to absent transgressive systems tracts composed of 1 or 2 subtidal carbonate cycles. The upper boundary surface of Sequence 1 is also a Type 1 sequence boundary that forms a distinctive erosive unconformity with an incised valley filled with estuarine marine siliciclastic in the Robledo Mountains.

Sequence 2 in the lower Hueco member begins with fluvial incision forming an incised valley on the shelf and early transgressive estuarine shoreface siliciclastics backfilling the incised valley during the late stage of sea-level lowstand. Phylloid algal bioherms are only present in one stratigraphic interval in Sequence 2 and represent transgressive deposits related to increased rates of sea-level rise and initial development on topographic highs created by differential compaction of lowstand shoreface siliciclastics. Sequence 2 is characterized by transgressive and highstand subtidal carbonate and subtidal carbonate bioherm cycles, suggesting higher average sea level compared to Sequence 1. Peritidal cycles are still present but are confined to exposures in the Robledo Mountains. Sequence 2 is also capped with another Type 1 sequence boundary with fluvial incision from the overlying upper interval of the lower Hueco member. The fluvial incision is consistent with another incised valley filled with late lowstand estuarine shoreface siliciclastics. These shoreface siliciclastics represent the contact with the overlying upper interval of the lower Hueco member as described by Mack et al. (2013).

Phylloid algal mounds are confined to 1 stratigraphic interval within a higher magnitude transgressive systems tract. Additionally, this transgressive systems tract directly overlies a distinctive incised valley filled with estuarine marine siliciclastics. Because of these two relationships, the spatial distribution of phylloid algal mounds are confined to locations where marine siliciclastics can provide antecedent topographic highs that initiate phylloid algal mound

development because of differential compaction and early cementation of sandstones. The temporal distribution of phylloid algal mounds is subsequently limited to times of a relatively rapid rise in sea-level, providing maximum accommodation space above these antecedent topographic highs. In times of higher magnitude transgression proceeding lowstand systems tracts characterized by incised valley systems, phylloid algal bioherms will develop on a similar paleogeographic trend as the underlying lowstand incised valley and not follow shoreline parallel facies belts. This has important implications for hydrocarbon exploration in regions where low-angle carbonate ramps represent the depositional geometry and phylloid algal bioherms targeted stratigraphic horizons. Additionally, this relationship would provide two stratigraphic intervals with good reservoir qualities: a lower marine siliciclastic reservoir with coarse-grained, well-sorted sands providing high primary porosity and an upper phylloid algal reservoir with high secondary porosity related to dissolution of phylloid algal plates.

Fusulinid biostratigraphy from the Robledo and Franklin mountains confirmed that all of these intervals contained early Wolfcampian (Nealian) fusulinid assemblages. In the Robledo Mountains the presence of *Pseudoschwagerina rhodesi, Pseudoschwagerina* cf. *morsei* and juvenile *Pseudoschwagerina* sp., along with *Schwagerina* cf. *andresensis* and the Pennsylvanian-Permian *Schwagerina* aff. *grandensis* all confirm that this strata is early Wolfcampian in age. Fusulinid assemblages in the Franklin Mountains consist of *Pseudofusulina robleda, Schwagerina grandensis,* along with questionable specimens of *Schwagerina andresensis* and *Schwagerina vervillei.* At Tortugas Mountain in southern New Mexico, only one species of fusulinid was identified, *Triticities creekensis,* which places this stratigraphy in the late Pennsylvanian Virgilian stage and possibly in the Bursum Formation. Fusulinids from the eight stratigraphic sections used in this study represent common early Wolfcampian fusulinid species.

During the early Wolfcampian, the lower Hueco member on the Robledo shelf records a consistent increase in relative sea-level throughout its deposition. This is very evident by the differences in lithofacies observed between Sequence 1 and Sequence 2 in the sequence stratigraphic analysis for this region. Sequence 2 is dominated by the deeper subtidal environments in both the Robledo and Franklin mountains while Sequence 1 is mainly composed of shallower supratidal and intertidal lithofacies in both ranges. Deposition of these lithofacies was mainly controlled by changes in relative sea level with little effect from local subsidence as compared to the eastern margin of this basin. Uplift on the eastern side of this basin had little to no effect on the western margin while it had dramatic effects on the thicknesses and distribution of sediments local to it. Additionally, the local paleogeography of the western margin contained irregular embayments rather than a linear simple, northwest to southeast trending coastline as previously thought.

Compared to the older latest Virgilian and strata (Panther Seep Formation) and the slightly younger middle Hueco member, the lower Hueco lower interval represents very different depositional sequences and lithofacies. The late Pennsylvanian glacial-eustasy that controlled cyclic mixed carbonate and siliciclastics Virgilian deposition disappears into the early Wolfcampian as seen by the thick sequences of relatively clean carbonates that form the lower Hueco member on the Robledo shelf. Deposition of the lower Hueco upper interval (Mack et al. 2013) marks the start of more cyclic mixed carbonate and siliciclastic intervals which transitions into the middle Hueco member. Consequently, this study has focused on illuminating these depositional and sequence stratigraphic differences observed in the lower Hueco member to compare with the older and younger strata in the Orogrande Basin and in other regions that have a similar stratigraphic architecture. It is very evident that more work on the Hueco Limestone

would help to understand the regional stratigraphic architecture that is more complex than once perceived. Additionally, these late Paleozoic carbonate dominated systems require very detailed outcrop, petrographic, and geochemical work to properly understand the stratigraphic architecture and depositional controls of the region.

REFERENCES

Ahr, W.M., 1973, Carbonate Ramp: alternative to Shelf Model: The American Association of Petroleum Geologists, Bulletin 57 (9), p. 1826.

Ainsworth, R.B. and Walker, R.G., 1994, Control of estuarine valley-fill deposition by fluctuations of relative sea-level, Cretaceous Bearpaw-Horsehoe Canyon transition, Drumheller, Alberta, Canada, *in* Dalrymple, R.G., Boyd, R., and Zaitlin, B.A., eds., Incised-valley systems: Origin and Sedimentary Sequences, Society of Environmental Paleontologists and Mineralogists, Special Publication no. 51, p. 159-174.

Algeo, T.J., Wilson, J.L., and Lohmann, K.C, 1991, Eustatic and tectonic controls on cyclic sediment accumulation patterns in lower-middle Pennsylvanian strata of the Orogrande basin: New Mexico: New Mexico Geological Society 42nd Field Conference Guidebook, p. 203-212.

Algeo, T.J., 1992, Continental-scale wrenching of southwestern Laurussia during the Ouachita-Marathon orogeny and tectonic escape of the Llano block, *in* Lindsay, R.F. and Reed, C.L., eds., Sequence stratigraphy applied to Permian Basin reservoirs: Outcrop analogs in the Caballo and Sacramento Mountains of New Mexico, West Texas Geological Society, Publication no. 92-92, p. 115-131.

Allen, G.P., and Posamentier, H.W., 1993, Sequence stratigraphy and facies model of an incised valley fill: The Gironde estuary, France: Journal of Sedimentary Petrology, Vol. 63, no. 3, p. 378-391.

Baars, D.L. and Torres, A.M., 1991, Late Paleozoic Phylloid Algae – A Pragmatic Review: Palaios, Vol.6, p. 513-515.

Ball, S.M., Pollard, W.D., and Roberts, J.W., 1977, Importance of phylloid algae in development of depositional topography – reality or myth, *in* Frost, S.H., Weiss, M.P., and Saunders, J.B., eds., Reefs and Related Carbonates – Ecology and Sedimentology: American Association of Petroleum Geologists Studies in Geology, no. 4, p. 239-259.

Bathurst, R.C.G, 1975, Developments in Sedimentology, Carbonate Sediments and their Diagenesis: Amsterdam, Elsevier, 658 p.

Beauchamp, B., 1989, Lower Permian (Sakmarian) *Tubiphytes*-bryozoan buildups, southwestern Ellesmere Island, Canadian Arctic Archipelago, *in* Geldsetzer, H.H.J., James, N.P., and Tebutt, G.E., eds., Reefs, Canada and Adjacent Areas: Canadian Society of Petroleum Geologists, Memoir 13, p. 585-589.

Beede, J.W., 1920, Notes on the geology and oil possibilities of the northern Diablo Plateau in Texas: Texas University Bulletin 2433.

Campbell, C.V., 1971, Depositional model-Upper Cretaceous Gallup beach shoreline, Shiprock area, northwestern New Mexico: Journal of Sedimentary Petrology, Society of Environmental Paleontologists and Mineralogists, Vo. 41, p. 395-409.

Candelaria, M.P., 1988. Synopsis of the Late Paleozoic depositional history of the Orogrande Basin, New Mexico and Texas, *in* Robichaud, S.R. and Gallick, C.M., eds., Basin to Shelf Transition of the Wolfcampian Stratigraphy of the Orogrande Basin: Society of Environmental Paleontologists and Mineralogists, Permian Basin Section, Publication 88-28, p. 1-5.

Catuneanu, O., 2006, Principles of Sequence Stratigraphy: Oxford, Elsevier, 375 p.

Choquette, P.W., 1983, Platy Algal Reef Mounds, Paradox Basin, *in* Scholle, P.A., Debout, D.G., and More, C.H., eds., Carbonate Depositional Environments: American Association of Petroleum Geologists, Memoir 33, p. 454-462.

Clifton, H.E, Hunter, R.E., and Phillips, R.L., 1971, Depositional structures and processes in the non-barred high-energy nearshore: Journal of Sedimentary Petrology, Vol. 41, no. 3, p. 651-670.

Connally, W.M. and Stanton, R.J.Jr., 1983, Sedimentation and paleoenvironment of Morrowan strata in the Hueco Mountains, west Texas, *in* Geology of the Sierra Diablo and southern Hueco Mountains, west Texas: Field Conference Guidebook, Society of Economic Paleontologists and Mineralogists, Permian Basin Section, Publication 83-22, p. 36-64.

Craft, J.H. and Bridge, J.S., 1987, Shallow-marine sedimentary processes in the Late Devonian Catskill Sea, New Your State: Geological Society of American Bulletin, Vol. 98, p. 663-680.

Cressman, E.R. and Noger, M.C., 1976, Tidal-flat carbonate environments in the High Bridge Group (Middle Orodovician) of central Kentucky, Lexington, University of Kentucky Geological Survey, Series X, Report of Investments 18, p. 1-15.

Crowell, J.C., 1999, Pre-Mesozoic ice ages; their bearing on understanding the climate system: Geological Society of America Memoir, Vol. 192, p. 106.

Cys, J.M. and Gibson, W.R., 1988, Pennsylvanian and Permian geology of the Permian Basin region, *in* Sedimentary Cover – North American craton, U.S.: The geology of North

America, Vol. D-2, Decade of North American Geology, Geological Society of America, p. 277-289.

Dalrymple, R.W., 2006, Incised valleys in time and space: an introduction to the volume and an examination of the controls on valley formation and filling, *in* Dalrymple, R.W., Leckie, D.A., and Tillman, R.W., eds., Incised Valleys in Time and Space: Society of Economic Paleontologists and Mineralogists Special Publication 85, p. 5-12.

Dalrymple, R.W., Zaitlin, B.A., and Boyd, R., 1992, Estuarine facies models: Conceptual basis and stratigraphic implications: Journal of Sedimentary Petrology, Vol. 62, p. 1130-1146.

DeCelles , P.G., 1987, Variable preservation of middle Tertiary, coarse-grained nearshore to outer-shelf storm deposits in southern California: Journal of Sedimentary Petrology, Vol. 57, no. 2, p. 250-264.

Deffeyes, K.S., Lucia, F.J., and Weyl, P.K., 1965, Dolomitization of recent and Plio-Pleistocene sediments by marine evaporate waters on Bonaire, Netherlands Antilles, *in* Dolomitization and limestone diagenesis: Society of Environmental Paleontologists and Mineralogists Special Publication 13, p. 71-88.

Dott, R.H.Jr., 1982, Episodic sedimentation – How normal is average? How rare is rare? Does it matter?: Journal of Sedimentary Petrology, Society of Environmental Paleontologists and Mineralogists Presidential Address, Vol. 53, no. 1, p. 5-23.

Durr, C.W., 2010, Early Permian sedimentation form the Robledo Shelf to the western Orogrande basin, Robledo and Doña Ana Mountains, south-central New Mexico: unpub. M.S. thesis, New Mexico State University, Las Cruces, 62 p.

Enos, P., 1983, Shelf Environment, *in* Scholle, P.A., Debout, D.G., and More, C.H., eds., Carbonate Depositional Environments: American Association of Petroleum Geologists, Memoir 33, p. 267-295.

Erxleben, A.W., 1975, Depositional systems in Canyon Group (Pennsylvanian Systems), north-central Texas: Texas Bureau of Economic Geology Report of Investigations, No. 82, p. 1-75.

Evans, G., Schmidt, V., Bush, P.R., and Nelson, H., 1969, Stratigraphy and geologic history of the sabkha, Abu Dhabi, Persian Gulf: Sedimentology, Vol. 12, p. 145-159.

Fielding, C.R., Frank, T.D., Birgenheier, L.P., Rygel, M.C., Jones, A.T., and Roberts, J., 2008, Alternating glacial and non-glacial intervals characterize the late Paleozoic Ice Age: stratigraphic evidence from eastern Australia: Journal of the Geological Society of London, Vol. 165, p. 129-140.

Finks, R.M., 1960, Late Paleozoic sponge faunas of the Texas region, the siliceous sponges: American Museum of Natural History Bulletin, Vol. 120, p. 1-160.

Fischer, A.G., 1964, The Lofer cyclotherms of the Alpine Triassic, *in* D.F. Merriam, ed., Symposium on cyclic sedimentation: State Geological Survey Kansas Bulletin 169, Vol. 1, p. 107-149.

Giles, K.A. and Soreghan, G.S., 1999, Attributes of two different types of phylloid algal mounds, Orogrande basin, NM, AAPG abstracts, Vol. 8, A47.

Ginsburg, R.N. and James, N.P., 1974, Holocene carbonate sediments of continental margins, *in* Burke, C.A. and Drake, C.L., eds., The Geology of Continental Margins: Springer-Verlag, New York, p. 137-155.

Google earth V 7.1.1.1888 (November 5, 2012). Franklin Mountains, Texas. Eye alt 1.50km, Google 2013, INEGI 2013, http://www.earth.google.com [July 12, 2013].

Google earth V 7.1.1.1888 (April 15, 2013). Robledo Mountains, New Mexico. Eye alt 1.56km, Google 2013, INEGI 2013, http://www.earth.google.com [July 12, 2013].

Graham, S.A., Dickinson, W.R., and Ingersoll, R.V., 1975, Himalayan-Bengal model for flysch dispersal in the Appalachian-Ouachita system: Geological Society of America Bulletin, Vol. 86, p. 273-286.

Grammer, G.M. and Ritter, A.L., 2009, Phylloid algae mounds in the Paradox Basin, southwestern USA: an alternative to the in situ constructional growth model: International Association for Sedimentology Special Publication 41, p. 239-254.

Hamblin, A.P. and Walker, R.G., 1979, Storm dominated shallow marine deposits: the Fernie-Kootenay (Jurassic) transition, southern Rocky Mountains, Canada: Journal of Earth Science, Vol. 16, p. 1637-1690.

Harbour, R.L., 1972, Geology of the Northern Franklin Mountains, Texas and New Mexico: U.S. Geological Survey Bulletin 1298, 129 p.

Harms, J.C., Southard, J.B., Spearing, D.R., and Walker, R.G., 1975, Depositional environments as interpreted from primary sedimentary structures and stratification sequences: Society of Environmental Paleontologists and Mineralogists Short Course no. 2, 161 p.

Harris, P.M., 1979, Facies anatomy and diagenesis of a Bahamian ooid shoal: Sedimenta 7, Comparative Sed. Lab, Miami, 163 p.

Heckel, P.H., 1994, Evaluation of evidence for glacio-eustatic control over marine Pennsylvanian cyclotherms in North America and consideration of possible tectonic effects, *in* Dennison, J.M., and Ettensohn, F.R., eds., Tectonic and Eustatic Controls on Sedimentary Cycles: Society of Environmental Paleontologists and Mineralogists Concepts in Sedimentology and Paleontology, Vol. 4, p. 65-87.

Heckel, P.H., and Cocke, J.M., 1969, Phylloid algal-mound complexes in outcropping Upper Pennsylvanian rocks of the Midcontinent: American Association of Petroleum Geologists Bulletin, Vol. 53, p. 1058-1074.

Heckel, P.H., 1972, Pennsylvanian stratigraphic reefs in Kansas, some modern comparisons and implications: Geologische Rundschau, Vol. 61, p. 584-598.

Heckel, P.H., 1977; Origin of physphatic black shale facies in Pennsylvanian cyclotherms of Mid-Continent North America: American Association of Petroleum Geologists Bulletin, Vol. 61, p. 1045-1068.

Heckel, P.H., 1986, Sea-level curve for Pennsylvanian eustatic marine transgressive-regressive depositional cycles along midcontinent outcrop belt, North America: Geology, Vol. 14, p. 330-334.

Hine, A.C., 1977, Lily Bank, Bahamas: history of an active oolite sand shoal: Journal of Sedimentary Petrology, Society of Environmental Paleontologists and Mineralogists, Vol. 47, p. 1554-1581.

Howard, J.D., and Scott, R.M., 1983, Comparison of Pleistocene and Holocene barrier island beach-to-offshore sequences, Georgia and northeast Florida coasts, U.S.A.: Sedimentary Geology, Vol. 34, p. 167-183.

Illing, L.V., Wells, A.J., and Taylor, J.C.M., 1965, Penecontemporary dolomite in the Persian Gulf, *in* Pray, L.C., and Murray, R.C. eds., Dolomitization and Limestone Diagenesis: Society of Environmental Paleontologists and Mineralogists Special Publication 13, p. 89-111.

International Chronostratigraphic Chart, 2012: International Commission on Stratigraphy, www.stratigraphy.org.

Isbell, J.L., Lenaker, P.A., Askin, R.A., Miller, M.F., and Babcock, L.E., 2002, Reevaluation of the timing and extent of late Paleozoic glaciations in Gondwana: role of the Transantartic Mountains: Geology, Vol. 31, p. 977-980.

Johnson, J.H., 1956, Archaeolithophyllum, a new genus of Paleozoic coralline algae: Journal of Paleontology, Vol. 30, p. 53-55.

Johnson, J.H., 1946, Lime-secreting algae from the Pennsylvanian and Permian of Kansas: Geological Society of America Bulletin, Vol. 57, p. 1087-1120.

Jordan, C.F. and Wilson, J.L.,1971, The late Paleozoic section of the Franklin Mountains: Robledo Mountains, New Mexico and Franklin Mountains, Texas: Permian Basin Section, Society of Economic Paleontologists and Mineralogists, Field Conference Guidebook, p. 77-87.

Jordan, C.F., 1975, Lower Permian (Wolfcampian) sedimentation in the Orogrande basin, New Mexico: New Mexico Geological Society Guidebook, 26th Field Conference, Las Cruces County. p. 109-117.

Kendall, C.G.St.C. and Schlager, W., 1981, Carbonates and relative changes in sea-level: Marine Geology, Vol. 44, p. 181-212.

Kendall, C.G.St.C. and Skipwith, P.A.d'E, 1969, Holocene shallow-water carbonate and evaporate sediments of Khor al Bazam, Abu Dhabi, southwest Persian Gulf: American Association of Petroleum Geologists Bulletin, Vol. 53, 841-869.

Kenter, J.A.M., Gartner, G.L.B., DeCoo, C.M., and Bahamonde, J.R., 1997, Outcrops of intact Lower Carboniferous carbonate platforms in Asturias (northern Spain) as analogues of coeval reservoirs in the subsurface of the Precaspian Basin (Kazakhstan, Russia) (abstract): American Association of Petroleum Geologists, Annual Meeting, Abstracts with Program, p. A59.

King, P.B., 1934, Permian stratigraphy of trans-Pecos Texas: Geological Society of America Bulletin, Vol. 45, p. 697-798.

King, P.B, and King, R.E., 1929, Stratigraphy of outcropping Carboniferous and Permian rocks of trans-Pecos Texas: American Association of Petroleum Geologists Bulletin, Vol. 13, p. 907-926.

King, P.B., King, R.E., and Knight, J.B., 1945, Geology of the Hueco Mountains, El Paso and Hudspeth Counties, Texas: U.S. Geological Survey Oil and Gas Investigations, Preliminary Map No. 36, 2 sheets.

King, W.E., and Kelley, R.E., 1980, Geology and paleontology of Tortugas Mountain, Doña Ana County, New Mexico: New Mexico Geology, Vol. 2, Number 3, p. 33-35.

Kjerfve, B., 1994, Coastal Lagoon Processes: Elsevier Oceanography Series, Vol. 60, 577 p.

Kluth, C.F. and Coney, P.J., 1981, Plate tectonics of the Ancestral Rocky Mountains: Geology, v.9, p. 10-15.

Koch, J.T., 2010, A sequence stratigraphic and isotopic study of the uppermost Pennsylvanian-Lower Permian carbonate strata, Orogrande Basin, New Mexico, Dissertation, University of Nebraska, Lincoln, 236 p.

Kottlowski, F.E., 1963, Paleozoic and Mesozoic strata of southwestern and south-central New Mexico: New Mexico State Bureau of Mines and Mineral Resources Bulletin 79, p. 100.

Kottlowski, F.E. and LeMone, D.V., 1994, San Andres Mountains stratigraphy revisited: Field Guide to the Paleozoic section of the San Andres Mountains: 1994 Annual Field Trip Guidebook, Permian Basin Section, Society of Economic Paleontologists and Mineralogists, Publication 9435, p. 31-45.

Kottlowski, F.E. and Seager, W.R., 1988, Robledo Mountains, key outcrops in south-central New Mexico: New Mexico Geological Society, 49th Field Conference Guidebook, p. 3-4.

Kottlowski, F.E., Thompson, S., King, W.E., and Seager, W.R., 1988, Pedregosa and Orogrande Basin, *in* Sedimentary Cover – North American craton, U.S.: The geology of North America, Vol. D-2, Decade of North American Geology, Geological Society of America, p. 299-306.

Kottlowski, F.E., Flower, R.H., Thompson, M.L., and Foster, R.W., 1956, Stratigraphic studies of the San Andres Mountains, New Mexico: New Mexico Bureau of Mines and Mineral Resources, Memoir 1, p. 132.

Kottlowski, F.E., 1960, Summary of Pennsylvanian sections in southwestern New Mexico and southeastern Arizona: New Mexico State Bureau of Mines and Mineral Resources Bulletin 66, p. 187.

Kreisa, R.D., 1981, Storm-generated sedimentary structures in subtidal marine facies with examples from the Middle and Upper Ordovician of southwestern Virginia: Journal of Sedimentary Research, Vol. 51, no. 3, p. 823-848.

Kues, B.S. and Giles, K.A., 2004. The late Paleozoic ancestral Rocky Mountains system in New Mexico, *in* Mack, G.H. and Giles, K.A., eds., The Geology of New Mexico, A geologic History: New Mexico Geological Society, p. 95-136.

Laporte, L.F., 1967, Carbonate deposition near mean sea level and resultant facies mosaic, Manlius formation (Lower Devonian) of New Your State: American Association of Petroleum Geologists Bulletin, Vol. 51, p. 73-101.

Leckie, D.A. and Walker, R.G., 1982, Storm- and tide-dominated shorelines in Cretaceous Moosebar-Lower Gates interval0outcrop equivalents of deep basin gas traps in western Canada: American Association of Petroleum Geologists Bulletin, Vol. 66, p. 138-157.

Lees, A.V., Hallet, V., and Hibo, D., 1985, Facies variation in Waulsortian buildups, Part 1 – a model from Belgium: Geological Journal, Vol. 20, p. 133-158.

Lees, A.V., and Miller, J., 1985, Facies variations in Waulsortian buildups, Part 2 – Mid-Dinantian buildups from Europe and North American: Geological Journal, Vol. 20, p. 159-180.

LeMone, D.V., Simpson, R.D., and Klement, K.W., 1975, Wolfcampian upper Hueco Formation of the Robledo Mountains, Doña Ana County, New Mexico: New Mexico Geological Society Guidebook, 26th Field Conference, p. 119-121.

LeMone, D.V., 1982, Stratigraphy of the Franklin Mountains, El Paso County, Texas and Doña Ana County, New Mexico, *in* Delaware Basin Field Trip: West Texas Geological Society Guidebook, No. 82-76, p. 42-72.

Logan, B.W., Rezak, R., and Ginsburg, R.N., 1964, Classification and environmental significance of algal stromatolites: Journal of Geology, Vol. 72, no. 1, p. 68-83.

Lucas, S.G., Heckert, A.B., Estep, J.W., and Cook, C.W., 1998, Stratigraphy of the Lower Permian Hueco in the Robledo Mountains, Doña Ana County, New Mexico: New Mexico Museum of Natural History and Science Bulletin No. 12, p. 43-55.

Mack, G.H., 2003, Lower Permian terrestrial paleoclimate indicators in New Mexico and their comparison to paleoclimate models, New Mexico Geological Society Guidebook, 54th Field Conference, Geology of the Zuni Plateau, p. 231-240.

Mack, G.H., 2004, Middle to Late Cenozoic crustal extension, sedimentation, and volcanism in the southern Rio Grande Rift, Basin and Range, and southern Transition Zone of southwest New Mexico, *in* Mack, G.H. and Giles, K.A., eds., The Geology of New

Mexico – A Geologic History, New Mexico Geological Society, Special Publication 11, p. 389-406.

Mack, G.H., Giles, K.A., and Durr, C.W., 2013, Sequence stratigraphy of the lower-middle Hueco transition interval (lower Permian, Wolfcampian), Robledo Mountains, New Mexico, New Mexico Geology, Vol. 35, No. 2.

Mack, G.H. and James, W.C., 1986, Cyclic sedimentation in the mixed siliciclastic-carbonate Abo-Hueco transitional zone (Lower Permian), southwestern New Mexico: Journal of Sedimentary Petrology, Vol. 56, p.635-647.

Mack, G.H., James, W.C., and Seager, W.R., 1988, Wolfcampian (Early Permian) stratigraphy and depositional environments in the Doña Ana and Robledo Mountains, south-central New Mexico, *in* Robichaud, S.R., and Gallick, C.M., eds., Basin to shelf facies transition of the Wolfcampian stratigraphy of the Orogrande Basin: Society of Environmental Paleontologists and Mineralogists, 1988 Permian Basin Section Annual Field Seminar, Publication no. 88-28, p. 97-106.

Mazzullo, S.J. and Reid, A.M., 1987. Basinal Lower Permian facies, Permian Basin, part II – depositional setting and reservoir facies of Wolfcampian-lower Leonardian basinal carbonates: West Texas Geological Society Bulletin, v. 26, p. 5-10.

Mazzullo, S.J., 1995. Permian stratigraphy and facies, Permian Basin (Texas-New Mexico) and adjoining areas of the Midcontinent United States, *in* Scholle, P.A, Peryt, T.M., and Ulmer-Scholle, D.S., eds., The Permian of Northern Pangaea: Springer-Verlag, Berlin, V.2, p. 41-60.

Mohseni, H. and Al-Aasm, I.S., 2004, Tempestite deposits on a storm-influenced carbonate ramp: an example from the Pabdeh Formation (Paleogene), Zagros Basin, Southwest Iran, Journal of Petroleum Geology, Vol. 27, no. 2, p. 163-178.

Monty, C.L.V., Bosence, D.W.J., Bridges, P.H., and Pratt, B.R., eds., 1995, Carbonate Mud-Mounds – Their Origin and Evolution: International Association of Sedimentologists, Special Publication 23, 537 p.

Myrow, P.M and Southard, J.B., 1996, Tempestite deposition: Journal of Sedimentary Research, Vol. 66, no. 5, p. 875-887.

Posamentier, H.W., and Vail, P.R., 1988, Eustatic controls on clastic deposition II-sequence and systems tract models, *in* C.K. Wilgus, B.S. Hastings, C.G.St.C. Kendall, H.W. Posamentier, C.A. Ross and J.C. Van Wagoner, eds., Sea Level Changes: An Integrated Approach: Society of Environmental Paleontologists and Mineralogists Special Publication 42, p. 125-154.

Pray, L.C. and Wray, J.L., 1963, Porous algal facies (Pennsylvanian) Honaker Trail, San Juan Canyon, Utah: Shelf Carbonates of the Paradox Basin. Four Corners Geological Society 4th Field Conference Guidebook, p. 204-234.

Pray, L.C., 1961, Geology of the Sacramento Mountains escarpment, Otero County, New Mexico: New Mexico Bureau of Mines and Mineral Resources Bulletin 35, p. 144.

Read, J.F., 1985, Carbonate Platform Facies Models: American Association of Petroleum Geologists Bulletin, Vol. 69, no. 1, p. 1-21.

Read, J.F., 1982, Carbonate platforms of passive (extensional) continental margins: Types, characteristics and evolution: Tectonophysics, Vol. 81, p. 195-212.

Richardson, G.B., 1904, Report of reconnaissance in Trans-Pecos Texas north of the Texas and Pacific Railway: University of Texas Bulletin No. 23, 119 p.

Ross, C.A., 1963, Standard Wolfcampian Series (Permian), Glass Mountains, Texas: Geological Society of America, Memoir 88, 205 p.

Ross C.A. and Ross, J.R.P, 1985, Paleozoic tectonics and sedimentation in west Texas, southern New Mexico and southern Arizona, *in* Structure and tectonics of Trans-Pecos Texas: West Texas Geological Society, Field trip Guidebook, p. 221-230.

Ross, C.A., and Ross, J.R.P., 1988, Late Paleozoic transgressive-regressive deposition, *in* C.K. Wilgus, B.S. Hastings, C.G.St.C. Kendall, H.W. Posamentier, C.A. Ross and J.C. Van Wagoner, eds., Sea-Level Changes: An Integrated Approach: Society of Environmental Paleontologists and Mineralogists Special Publication 42, p. 227-247.

Ross, J.R.P. and Ross, C.A., 1990, Late Paleozoic bryozoan biogeography, *in* McKerrow, W.S., and Scotese, C.R., eds., Paleozoic Paleography and biogeography: Geological Society of London, Memoir 12, p. 353-361.

Ross, C.A., and Ross, J.R.P., 1986, Paleozoic paleotectonics and sedimentation in Arizona and New Mexico, *in* Paleotectonics and sedimentation in the Rocky Mountain region, United States: American Association of Petroleum Geologists, Memoir 41, p. 653-668.

Sarg, J.F., 1988, Carbonate sequence stratigraphy, *in* C.K. Wilgus, B.S. Hastings, C.G.St.C. Kendall, H.W. Posamentier, Ross, C.A. and Van Wagoner, J.C., eds., Sea Level Changes:

An Integrated Approach: Society of Environmental Paleontologists and Mineralogists Special Publication 42, p. 155-182.

Schatzinger, R.A., 1983, Phylloid algal and sponge-bryozoan mound-to-basin transition – a late Paleozoic facies tract from Kelly-Snyder Field, west Texas, *in* Harris, P.M. eds., Carbonate Buildups – A Core Workshop: Society of Economic Paleontologists and Mineralogists, Core Workshop 4, p. 244-303.

Scholle, P.A. and Ulmer-Scholle, D.S., 2003, A Color Guide to the Petrography of Carbonate Rocks: Grains, Textures, Porosity, Diagenesis: American Association of Petroleum Geologists, Memoir 77, p. 28-31.

Seager, W.R., 1981, Geology of Organ Mountains and southern San Andres Mountains, New Mexico: New Mexico Bureau of Mines and Mineral Resources, Memoir 36, p. 97.

Seager, W.R., 2004, Laramide (Late Cretaceous – Eocene) tectonics of southwestern New Mexico: *in* Mack, G.H. and Giles, K.A., Eds., The Geology of New Mexico – A geologic history, New Mexico Geological Society, Special Publication 11, p. 183-202.

Seager, W.R., Kottlowski, F.E., and Hawley, J.W., 1976, Geology of Doña Ana Mountains, New Mexico: New Mexico Bureau of Mines and Mineral Resources, Circular 147, p. 36.

Seager, W.R., Kottlowski, F.E. and Hawley, J.W., 2008, Geologic Map of the Robledo Mountains and vicinity, Doña Ana County, New Mexico: New Mexico Bureau of Geology Mineral Resources, Open-file Report 509, 12 pp.

Seager, W.R., Kottlowski, F.E., and Hawley, J.W., 1976, Geology of Doña Ana Mountains, New Mexico: New Mexico Bureau of Mines and Mineral Resources, Circular 147, p.36.

Seager, W.R. and Mack, G.H., 1991, Geology of Garfield quadrangle, Sierra and Doña Ana Counties, New Mexico: New Mexico Bureau of Mines and Mineral Resources Bulletin 128, p. 24.

Seager, W.R. and Mack, G.H, 1986, Laramide basement-cored uplift and basins in south-central New Mexico: New Mexico Geological Society Guidebook, 37th Field Conference, p. 123-131.

Seager, W.R. and Mack, G.H., 1998, Geology of McLeod Tank quadrangle, Sierra and Doña Ana Counties, New Mexico: New Mexico Bureau of Mines and Mineral Resources, Geologic Map 77, scale 1:24,000.

Seguret, M., Moussine-Pouchkine, A., Gabaglia, G.R., and Bouchette, F., 2001, Storm deposits and storm-generaged coarse carbonate breccias on a pelagic outer shelf (South-East Basin, Fance): Sedimentology, Vol. 48, 231-254.

Shinn, E.A., Ginsburg, R.N., and Lloyd, R.M, 1965, Recent supratidal dolomite from Andros Island, Bahamas, *in* Pray, L.C. and Murray, R.C., eds., Dolomitization and Limestone Diagenesis: Society of Environmental Paleontologists and Mineralogists, Special Publication 13, p. 112-123.

Shinn, E.A., 1983, Tidal Flat Environment, *in* Scholle, P.A., Bebout, D.G, and More, C.H., eds., Carbonate Depositional Environments: American Association of Petroleum Geologists, Memoir 33, p. 171-210.

Silver, B.A. and Todd, R.G., 1969, Permian cyclic strata, northern Midland and Delaware basins, west Texas-New Mexico: American Association of Petroleum Geologists Bulletin, Vol. 53, p. 2223-2251.

Simo, J.A., Wahlman, G.P., Beall, J.L., Stoklosa, M.L., and Piccoli, L., 2001, Wolfcampian shelf margins, Hueco Mountains, west Texas, *in* Stoudt, E.L. and Sivis, D.J., eds., Wolfcampian of west Texas (Permian Basin, Sierra Diablo and Hueco Mountains) Shelfal and Periplatform carbonate Reservoirs and Outcrop Analog: Permian Basin Section, Society of Environmental Paleontologist and Mineralogists, Core Workshop and Field Trip Guidebook, Publication 2001-41, p. 8-1 – 8-26.

Sloss, L.L., 1963, Sequences in the cratonic interior of North America: Geological Society of America Bulletin, Vol. 74, p. 93-114.

Smith, G.A., 2004, Middle to late Cenozoic development of the Rio Grande Rift and adjacent regions in northern New Mexico: *in* Mack, G.H and Giles, K.A., Eds., The Geology of New Mexico – A geologic history: New Mexico Geological Society, Special Publication 11, p. 331-358.

Soreghan, G.S. and Giles, K.A., 1999a, Amplitudes of Late Pennsylvanian glacioeustasy: Geology, v.27, p. 25-258.

Soreghan, G.S. ad Giles, K.A., 1999b, Facies character and stratal responses to accommodation in Pennsylvanian bioherms, western Orogrande basin, New Mexico: Journal of Sedimentary Petrology, Vol. 69, p. 893-908.

Stoklosa, M.L., Simo, J.A., and Wahlman, G.P., 1998, Facies description and evolution of a Wolfcampian (early Permian) shelf margin: Hueco Mountains, west Texas: New Mexico Geological Society Guidebook, 49th Field Conference, Las Cruces County II. p. 177-186.

Swift, D.J.P., Figueiredo, A.G.Jr., Freeland, G.L., and Oertel, G.F., 1983, Hummocky cross-stratification and megaripples: a geological double standard?: Journal of Sedimentary Petrology, Society of Environmental Paleontologists and Mineralogists, Vol. 53, p. 1295-1317.

Tebbutt, G.E., Conely, C.D., and Boyd, D.W., 1965, Lithogenesis of a distinctive carbonate rock fabric, *in* Parker, R.B., eds., Contributions to geology: Laramie, University of Wyoming, p. 1-13.

Thompson, M.L., 1954, American Wolfcampian fusulinids: University of Kansas Paleontological Contributions, Protozoa, Article 5, p. 226.

Toomey, D.F., 1981, Organic buildup constructional capability in Lowe Ordovician and late Paleozoic mounds, *in* Grey, J. et al., Eds., Communities of the Past: Stroudsberg, Pennsylvania, Hutchinsons and Ross, p. 35-68.

Toomey, D.F., 1976, Paleosynecology of a Permian plant dominated marine community: Neues Jahrbuch für Palaontologie, Abhandlung, Vol. 152, p. 1-18.

Toomey, D.F., 1980, History of a Late Carboniferous phylloid algal bank complex in northeastern New Mexico: Lethaia, Vol. 13, p. 249-267.

Toomey, D.F., 1991, Late Pennsylvanian phylloid-algal bioherms, Orogrande basin, south-central New Mexico and west Texas: New Mexico Geological Society Guidebook, 42nd Field Conference, p. 213-220.

Toomey, D.F., and Winland, H.D., 1973, Rock and biotic facies associated with a middle Pennsylvanian (Desmoinesian) algal buildup, Nena Lucia field, Nolan County, Texas: American Association of Petroleum Geologists Bulletin, Vol. 57, p. 1053-1074.

Tucker, M.E. and Wright, V.P., 1990, Carbonate Sedimentology, Malden, Blackwell, 482 p.

Tucker, M.E., 1985, Shallow-marine carbonate facies and facies models, *in* Brenchley, P.J., and Williams, B.P.J, eds., Sedimentology: Recent Developments and Applied Aspects, Geological Society of London, Special Publication 18, p. 139-161.

Vail, P.R. and Todd, R.G., 1981, Northern North Sea Jurassic unconformities, chronostratigraphy and sea-level changes from seismic stratigraphy, *in* Illing, L.V. and Hobson, G.D., eds., Petroleum Geology of the Continental Shelf of North-West Europe, Heyden and Son, London, p. 216-235.

Vail, P.R., Mitchum, R.M., and Thompson, S., 1977, Seismic stratigraphy and global changes of sea level, *in* Payton, C.E., eds., Seismic Stratigraphy – Applications to Hydrocarbon Exploration: American Association of Petroleum Geologists, Memoir 26, p. 63-97.

Vail, P.R., 1987, Seismic stratigraphy interpretation procedure, *in* Atlas of Seismic Stratigraphy: American Association of Petroleum Geologists, Studies in Geology 27, p. 1-10.

Van Wagoner, J.C., Posamentier, H.W., Mitchum, R.M.Jr., Vail, P.R., Sarg, J.F., Loutit, T.S., and Hardenbol, J., 1988, An overview of sequence stratigraphy and key definitions, *in*

Sea Level Changes: An Integrated Approach: Society of Environmental Paleontologists and Mineralogists, Special Publication 42, p. 39-45.

Veevers, J.J. and Powell, C.M., 1987, Late Paleozoic glacial episodes in Gondwanaland reflected in transgressive-regressive depositional episodes in Euramerica: Geological Society of America Bulletin, Vol. 98, p. 475-487.

Wahlman, G.P, 1988, Subsurface Wolfcampian (Lower Permian) shelf-margin reefs in the Permian Basin of west Texas and southeastern New Mexico: Midcontinent Society of Economic Paleontologists and Mineralogists, Special Publication No. 1, p. 177-204.

Wahlman, G.P., 2002, Upper Carboniferous-Lower Permian (Bashkirian-Kungurian) Mounds and Reefs, Phanerozoic Reef Patterns: Society of Economic Paleontologists and Mineralogists, Special Publication No. 72, p. 271-338.

Wahlman, G.P. and King, W.E., 2002, Latest Pennsylvanian and earliest Permian fusulinid biostratigraphy, Robledo Mountains and adjacent ranges, south-central New Mexico: New Mexico Bureau of Geology and Mineral Resources, Circular 208.

Wanless, H.R. and Cannon, J.R., 1966, Late Paleozoic Glaciation, Earth-Science Review, Vol. 1, no. 4, p. 247-286.

Wells, A., 1962, Primary dolomitization in Persian Gulf, Nature, Vol. 194, no. 4825, p. 274-275.

Wermund, E.G., 1975, Upper Pennsylvanian limestone banks, north-central Texas: Texas Bureau of Economic Geology, Geological Circular 75-3, p. 1-34.

Williams, T.E., 1963, Fusulinidae of the Hueco Group (Lower Permian), Hueco Mountains, Texas: Bulletin of the Peabody Museum Natural History 18, 123 p.

Williams, T.E., 1966, Permian Fusulinidae of the Franklin Mountains, New Mexico-Texas: Journal of Paleontology, Vol. 40, p. 1142-1156.

Wilson, J.L., and Jordan, C.F., 1983, Middle Shelf Environment *in* Scholle, P.A., Bebout, D.G., and Moore, C.H., eds., Carbonate Depositional Environments: American Association of Petroleum Geologists, Memoir 33, p. 297-343.

Wilson, J.L., 1977, Regional distribution of phylloid algal mounds in the late Pennsylvanian and Wolfcamp strata of southern New Mexico, *in* Pray, L.C., and others, eds., Geology of the Sacramento Mountains, Otero County, New Mexico: West Texas Geological Society, Sacramento Mountains field trip, p. 1-7.

Wilson, J.L. and Jordan, C.F., 1988, Late Paleozoic-Early Mesozoic rifting in southern New Mexico and northern Mexico: Controls on subsequent platform development, *in* Robichaud, S.R. and Gallick, C.M., eds., Basin to Shelf Facies Transition of the Wolfcampian Stratigraphy of the Orogrande Basin: Society of Environmental Paleontologists and Mineralogists, Permian Basin Section, Publication 88-28, p. 79-88.

Wray, J.L., 1977, Calcareous Algae: Amsterdam, Elsevier, Developments in Paleontology and Stratigraphy no. 4, p. 185.

Wunderlich, F., 1972, Georgia coastal region, Sapelo Island, U.S.A., *in* Sedimentology and Biology III, Beach dynamics and beach development: Senkcenbergiana, Mar., 4, p. 47-79.

APPENDIX A

Lower Hueco Member Measured Stratigraphic Sections from the Robledo and Franklin Mountains.

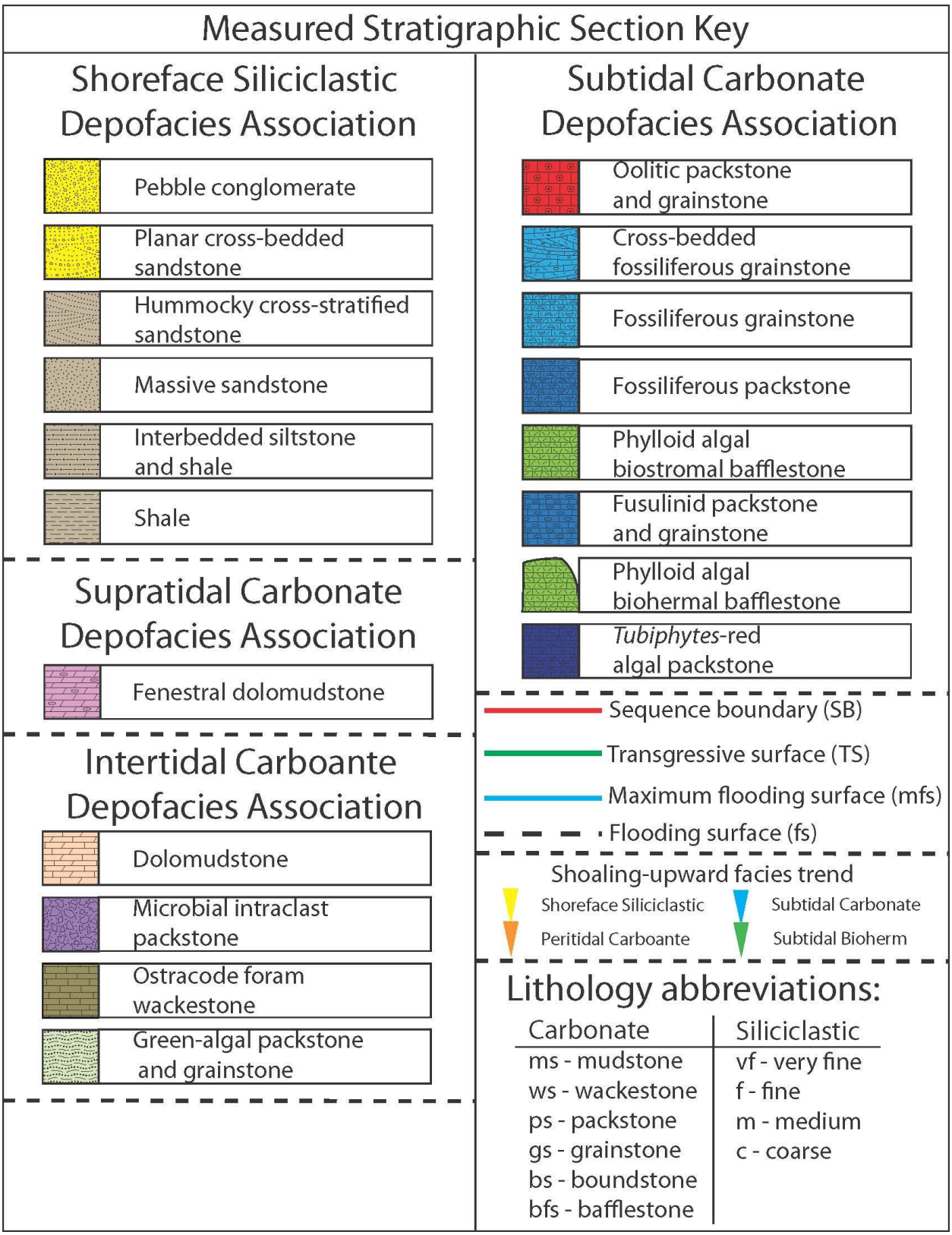
Measured Stratigraphic Section Key
Shoreface Siliciclastic Depofacies Association
Pebble conglomerate
Planar cross-bedded sandstone
Hummocky cross-stratified sandstone
Massive sandstone
Interbedded siltstone and shale
Shale
Supratidal Carbonate Depofacies Association
Fenestral dolomudstone
Intertidal Carboante Depofacies Association
Dolomudstone
Microbial intraclast packstone
Ostracode foram wackestone
Green-algal packstone and grainstone
Subtidal Carbonate Depofacies Association
Oolitic packstone and grainstone
Cross-bedded fossiliferous grainstone
Fossiliferous grainstone
Fossiliferous packstone
Phylloid algal biostromal bafflestone
Fusulinid packstone and grainstone
Phylloid algal biohermal bafflestone
Tubiphytes-red algal packstone
Sequence boundary (SB)
Transgressive surface (TS)
Maximum flooding surface (mfs)
Flooding surface (fs)
Shoaling-upward facies trend
Shoreface Siliciclastic
Peritidal Carboante
Subtidal Carbonate
Subtidal Bioherm
Lithology abbreviations:
Carbonate
ms - mudstone
ws - wackestone
ps - packstone
gs - grainstone
bs - boundstone
bfs - bafflestone
Siliciclastic
vf - very fine
f - fine
m - medium
c - coarse

A.1

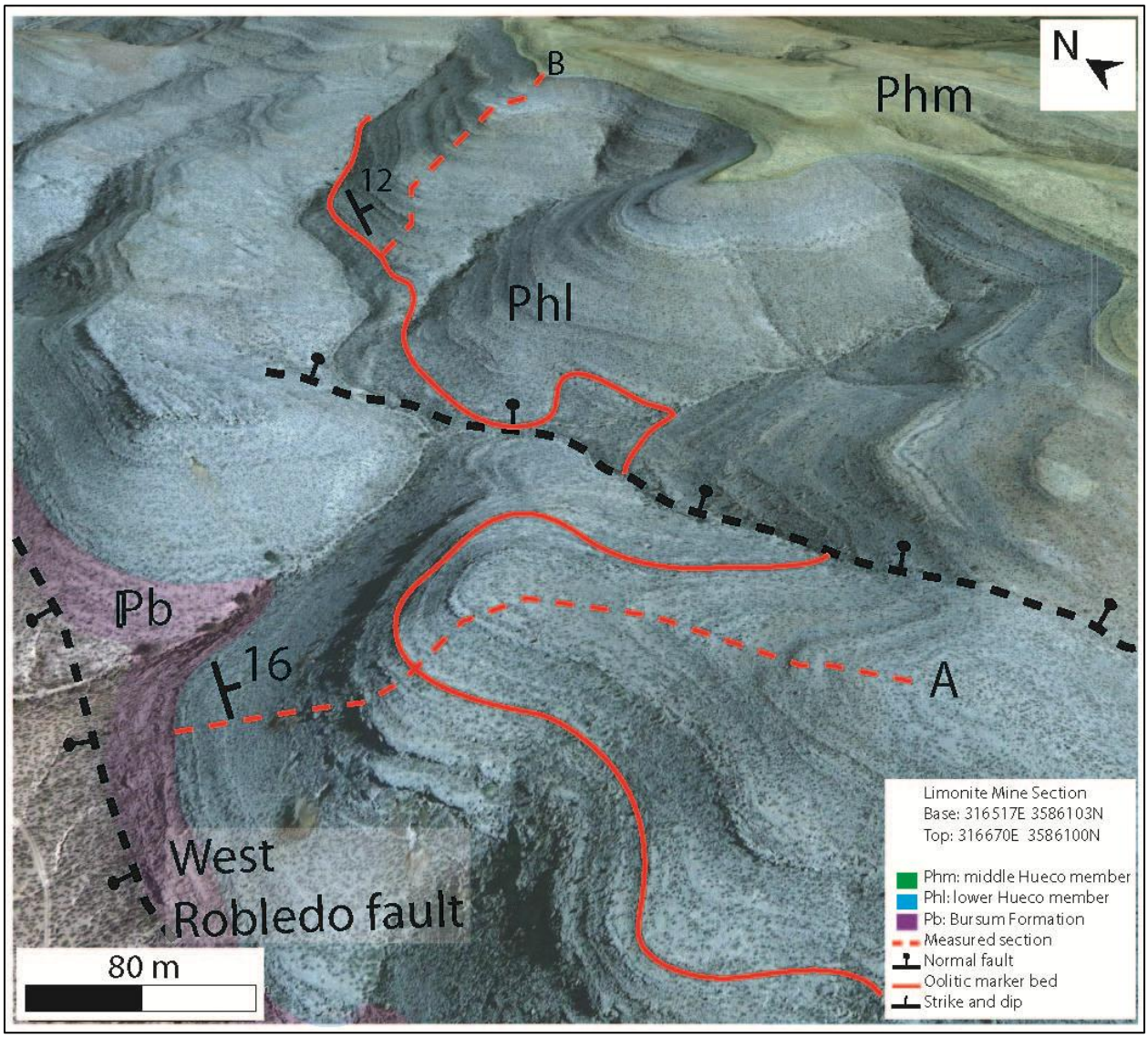

Oblique Aerial Photograph of the Limonite Mine Section Location.

Oblique aerial photograph overlain by the geologic units mapped by Seager et al. (2008), the transect of the measured stratigraphic section is shown by a red dashed line. Aerial photograph is courtesy of Google Earth.

Limonite Mine Measured Section, Robledo Mountains, New Mexico

UTM Base: 13S 316517 E 3586103 N,
UTM Top: 316670E 3586100N

Interval: 0-50 m
Base: Strike: 015, Dip: 16E

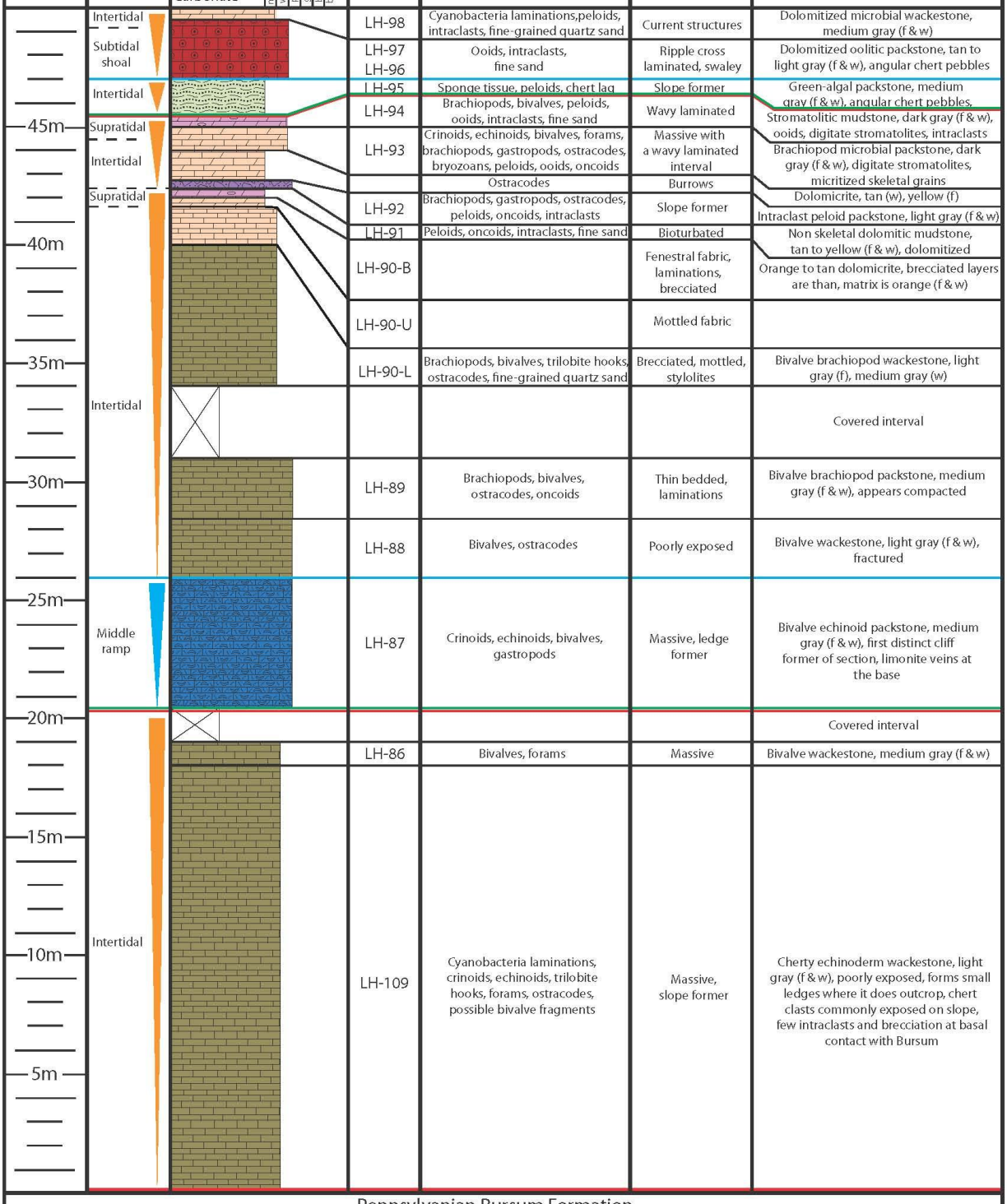

Sample	Grain types: skeletal and non skeletal	Sedimentary structures	Description
LH-98	Cyanobacteria laminations,peloids, intraclasts, fine-grained quartz sand	Current structures	Dolomitized microbial wackestone, medium gray (f & w)
LH-97 LH-96	Ooids, intraclasts, fine sand	Ripple cross laminated, swaley	Dolomitized oolitic packstone, tan to light gray (f & w), angular chert pebbles
LH-95	Sponge tissue, peloids, chert lag	Slope former	Green-algal packstone, medium gray (f & w), angular chert pebbles,
LH-94	Brachiopods, bivalves, peloids, ooids, intraclasts, fine sand	Wavy laminated	Stromatolitic mudstone, dark gray (f & w), ooids, digitate stromatolites, intraclasts
LH-93	Crinoids, echinoids, bivalves, forams, brachiopods, gastropods, ostracodes, bryozoans, peloids, ooids, oncoids	Massive with a wavy laminated interval	Brachiopod microbial packstone, dark gray (f & w), digitate stromatolites, micritized skeletal grains
	Ostracodes	Burrows	
LH-92	Brachiopods, gastropods, ostracodes, peloids, oncoids, intraclasts	Slope former	Dolomicrite, tan (w), yellow (f) Intraclast peloid packstone, light gray (f & w)
LH-91	Peloids, oncoids, intraclasts, fine sand	Bioturbated	Non skeletal dolomitic mudstone, tan to yellow (f & w), dolomitized
LH-90-B		Fenestral fabric, laminations, brecciated	Orange to tan dolomicrite, brecciated layers are than, matrix is orange (f & w)
LH-90-U		Mottled fabric	
LH-90-L	Brachiopods, bivalves, trilobite hooks, ostracodes, fine-grained quartz sand	Brecciated, mottled, stylolites	Bivalve brachiopod wackestone, light gray (f), medium gray (w)
			Covered interval
LH-89	Brachiopods, bivalves, ostracodes, oncoids	Thin bedded, laminations	Bivalve brachiopod packstone, medium gray (f & w), appears compacted
LH-88	Bivalves, ostracodes	Poorly exposed	Bivalve wackestone, light gray (f & w), fractured
LH-87	Crinoids, echinoids, bivalves, gastropods	Massive, ledge former	Bivalve echinoid packstone, medium gray (f & w), first distinct cliff former of section, limonite veins at the base
			Covered interval
LH-86	Bivalves, forams	Massive	Bivalve wackestone, medium gray (f & w)
LH-109	Cyanobacteria laminations, crinoids, echinoids, trilobite hooks, forams, ostracodes, possible bivalve fragments	Massive, slope former	Cherty echinoderm wackestone, light gray (f & w), poorly exposed, forms small ledges where it does outcrop, chert clasts commonly exposed on slope, few intraclasts and brecciation at basal contact with Bursum

Pennsylvanian Bursum Formation

Limonite Mine Measured Section, Robledo Mountains, New Mexico

UTM Base: 13S 316517 E 3586103 N,
UTM Top: 316670E 3586100N

Interval: 50-100 m

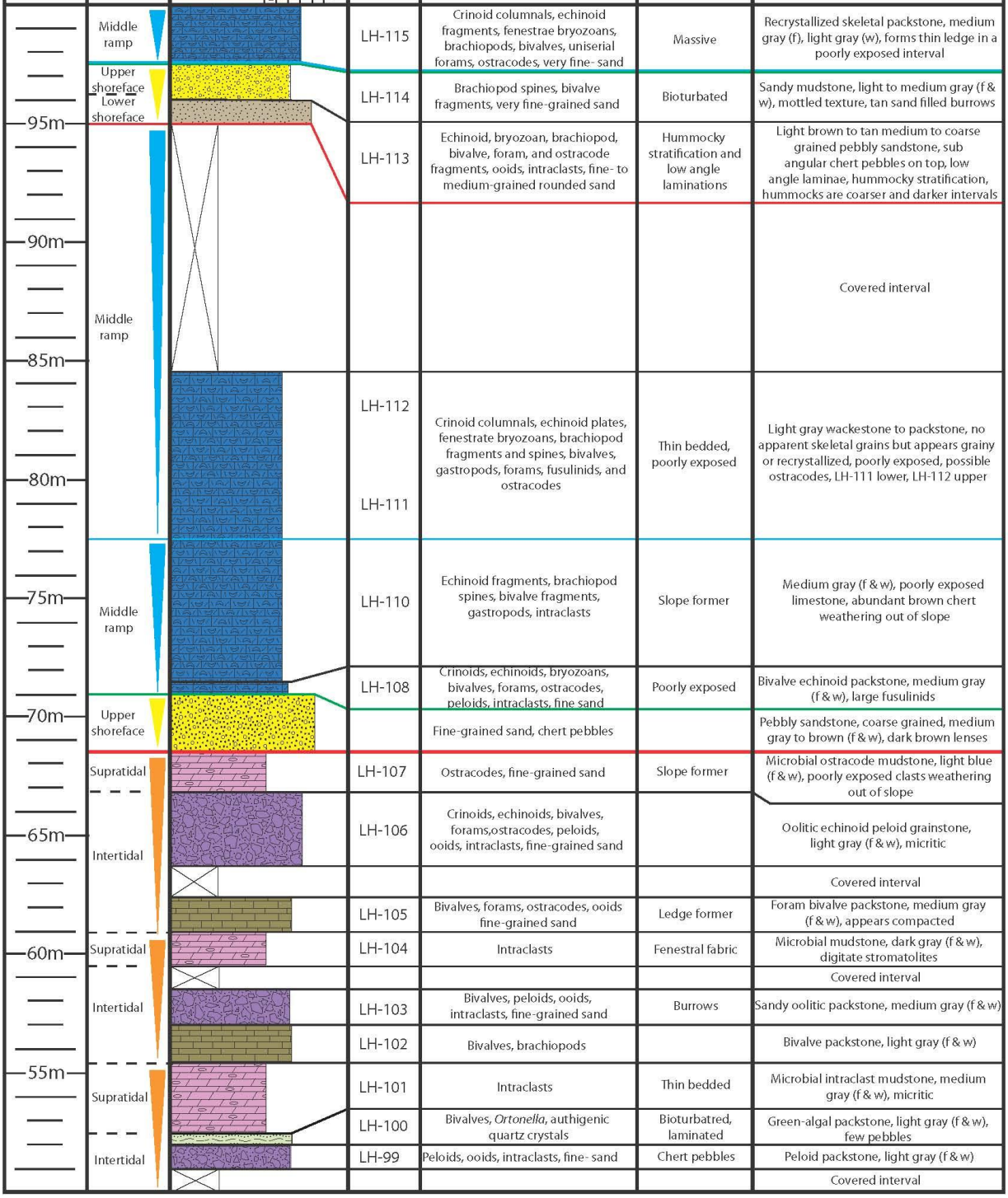

Limonite Mine Measured Section, Robledo Mountains, New Mexico

UTM Base: 13S 316517 E 3586103 N,
UTM Top: 316670E 3586100N

Interval: 100-143 m
Top: Strike: 019, Dip: 12E

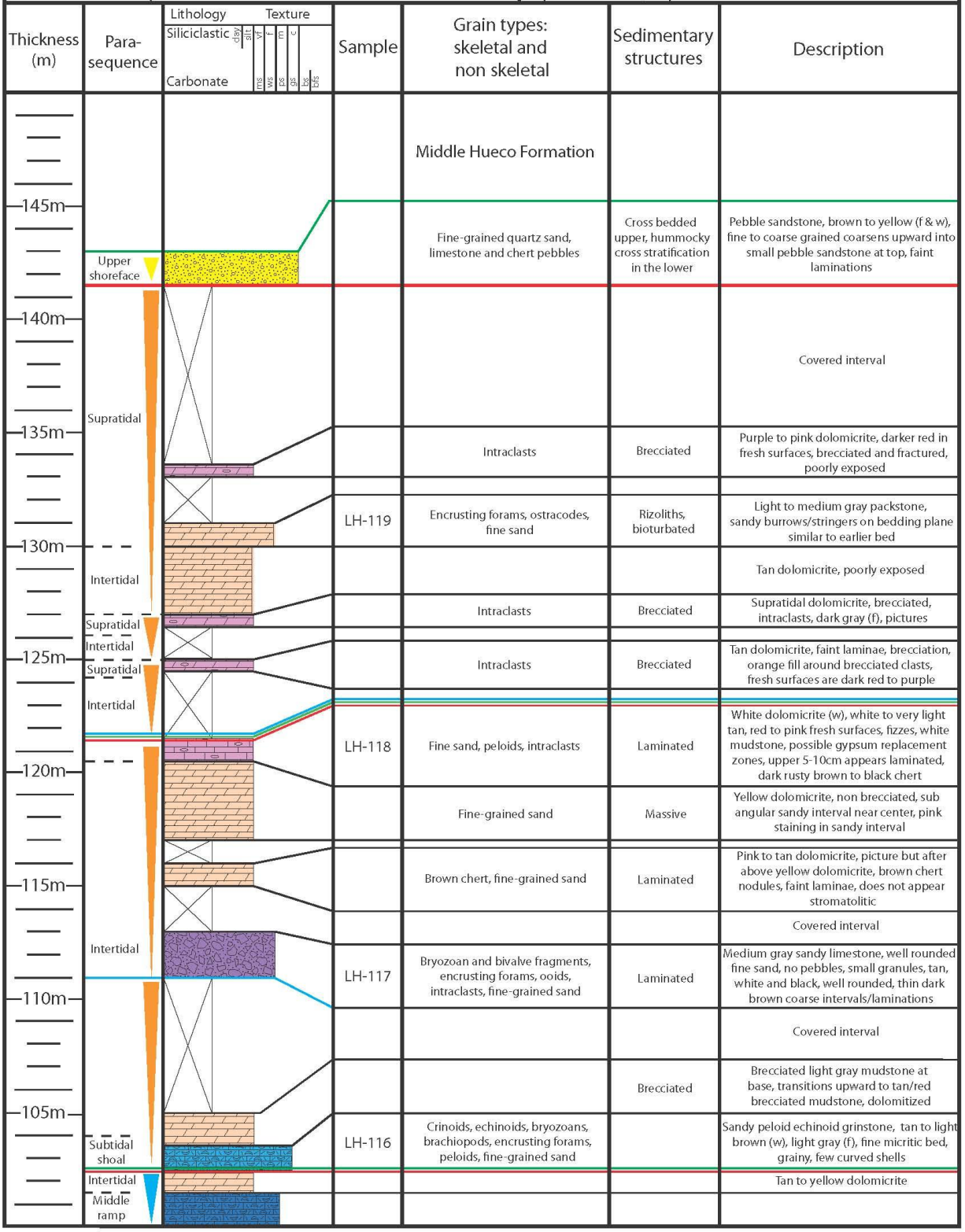

A.2

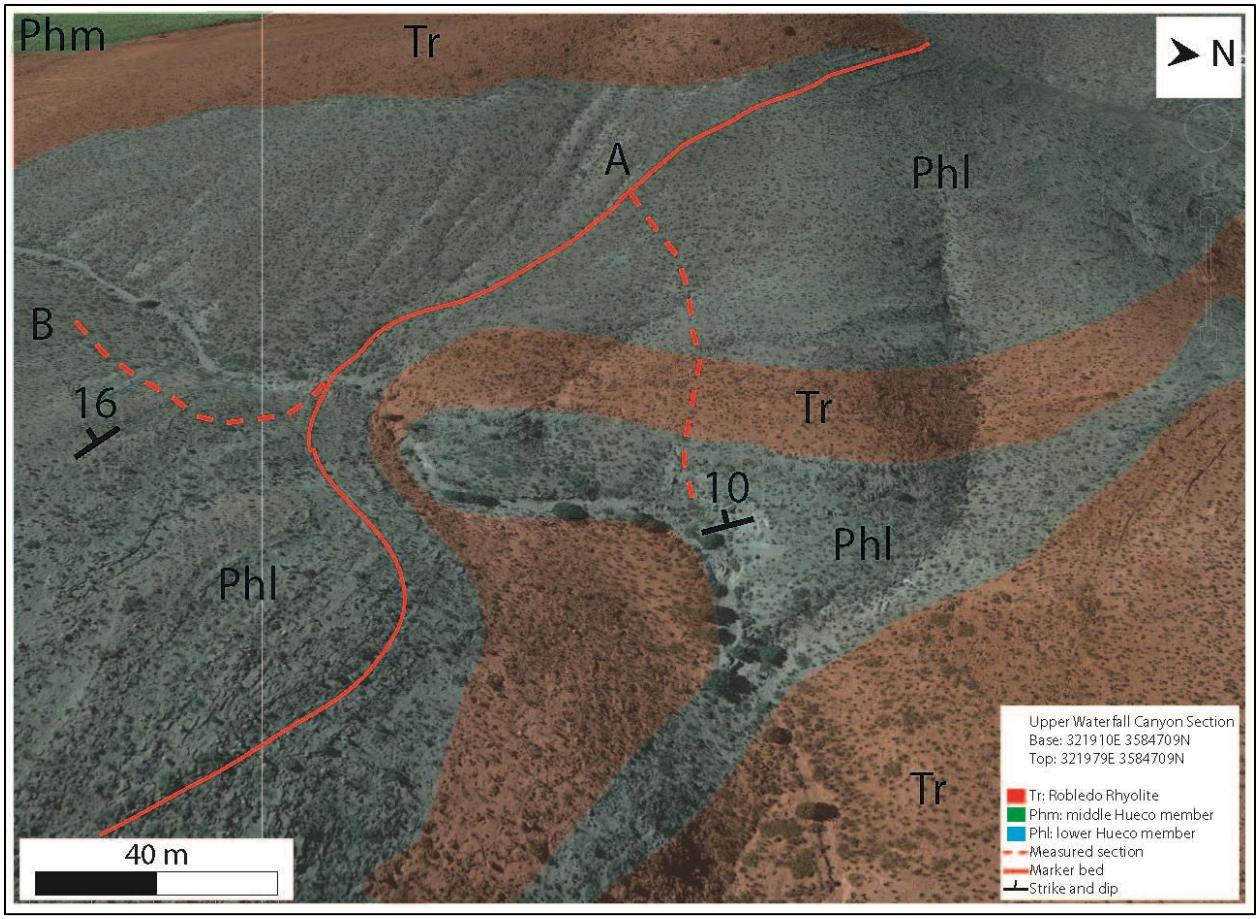

Oblique Aerial Photograph of the Upper Waterfall Canyon Section Location.

Oblique aerial photograph overlain by the geologic units mapped by Seager et al. (2008), the transect of the measured stratigraphic section is shown by a red dashed line. Aerial photograph is courtesy of Google Earth.

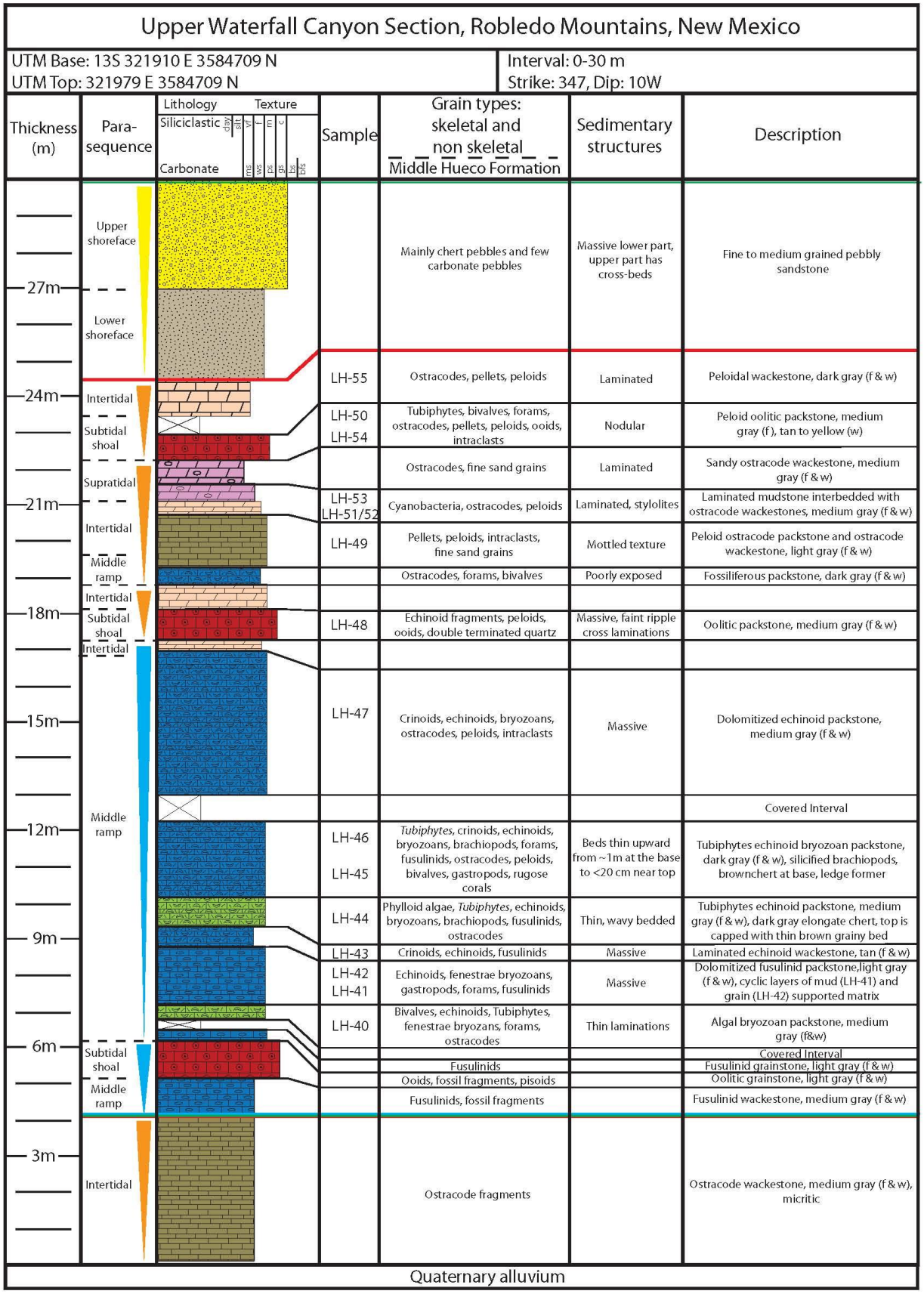
Upper Waterfall Canyon Section, Robledo Mountains, New Mexico
UTM Base: 13S 321910 E 3584709 N
UTM Top: 321979 E 3584709 N
Interval: 0-30 m
Strike: 347, Dip: 10W
Thickness (m)
Para-sequence
Lithology
Texture
Siliciclastic
Carbonate
clay
silt
vf
f
m
c
mds
wks
pks
gs
bs
bfs
Sample
Grain types: skeletal and non skeletal
Middle Hueco Formation
Sedimentary structures
Description
27m
24m
21m
18m
15m
12m
9m
6m
3m
Upper shoreface
Lower shoreface
Intertidal
Subtidal shoal
Supratidal
Intertidal
Middle ramp
Intertidal
Subtidal shoal
Intertidal
Middle ramp
Subtidal shoal
Middle ramp
Intertidal
LH-55
Mainly chert pebbles and few carbonate pebbles
Massive lower part, upper part has cross-beds
Fine to medium grained pebbly sandstone
Ostracodes, pellets, peloids
Laminated
Peloidal wackestone, dark gray (f & w)
LH-50
LH-54
Tubiphytes, bivalves, forams, ostracodes, pellets, peloids, ooids, intraclasts
Nodular
Peloid oolitic packstone, medium gray (f), tan to yellow (w)
Ostracodes, fine sand grains
Laminated
Sandy ostracode wackestone, medium gray (f & w)
LH-53
LH-51/52
Cyanobacteria, ostracodes, peloids
Laminated, stylolites
Laminated mudstone interbedded with ostracode wackestones, medium gray (f & w)
LH-49
Pellets, peloids, intraclasts, fine sand grains
Mottled texture
Peloid ostracode packstone and ostracode wackestone, light gray (f & w)
Ostracodes, forams, bivalves
Poorly exposed
Fossiliferous packstone, dark gray (f & w)
LH-48
Echinoid fragments, peloids, ooids, double terminated quartz
Massive, faint ripple cross laminations
Oolitic packstone, medium gray (f & w)
LH-47
Crinoids, echinoids, bryozoans, ostracodes, peloids, intraclasts
Massive
Dolomitized echinoid packstone, medium gray (f & w)
Covered Interval
LH-46
LH-45
Tubiphytes, crinoids, echinoids, bryozoans, brachiopods, forams, fusulinids, ostracodes, peloids, bivalves, gastropods, rugose corals
Beds thin upward from ~1m at the base to <20 cm near top
Tubiphytes echinoid bryozoan packstone, dark gray (f & w), silicified brachiopods, brownchert at base, ledge former
LH-44
Phylloid algae, Tubiphytes, echinoids, bryozoans, brachiopods, fusulinids, ostracodes
Thin, wavy bedded
Tubiphytes echinoid packstone, medium gray (f & w), dark gray elongate chert, top is capped with thin brown grainy bed
LH-43
Crinoids, echinoids, fusulinids
Massive
Laminated echinoid wackestone, tan (f & w)
LH-42
LH-41
Echinoids, fenestrae bryozoans, gastropods, forams, fusulinids
Massive
Dolomitized fusulinid packstone,light gray (f & w), cyclic layers of mud (LH-41) and grain (LH-42) supported matrix
LH-40
Bivalves, echinoids, Tubiphytes, fenestrae bryozans, forams, ostracodes
Thin laminations
Algal bryozoan packstone, medium gray (f&w)
Covered Interval
Fusulinids
Fusulinid grainstone, light gray (f & w)
Ooids, fossil fragments, pisoids
Oolitic grainstone, light gray (f & w)
Fusulinids, fossil fragments
Fusulinid wackestone, medium gray (f & w)
Ostracode fragments
Ostracode wackestone, medium gray (f & w), micritic
Quaternary alluvium

A.3

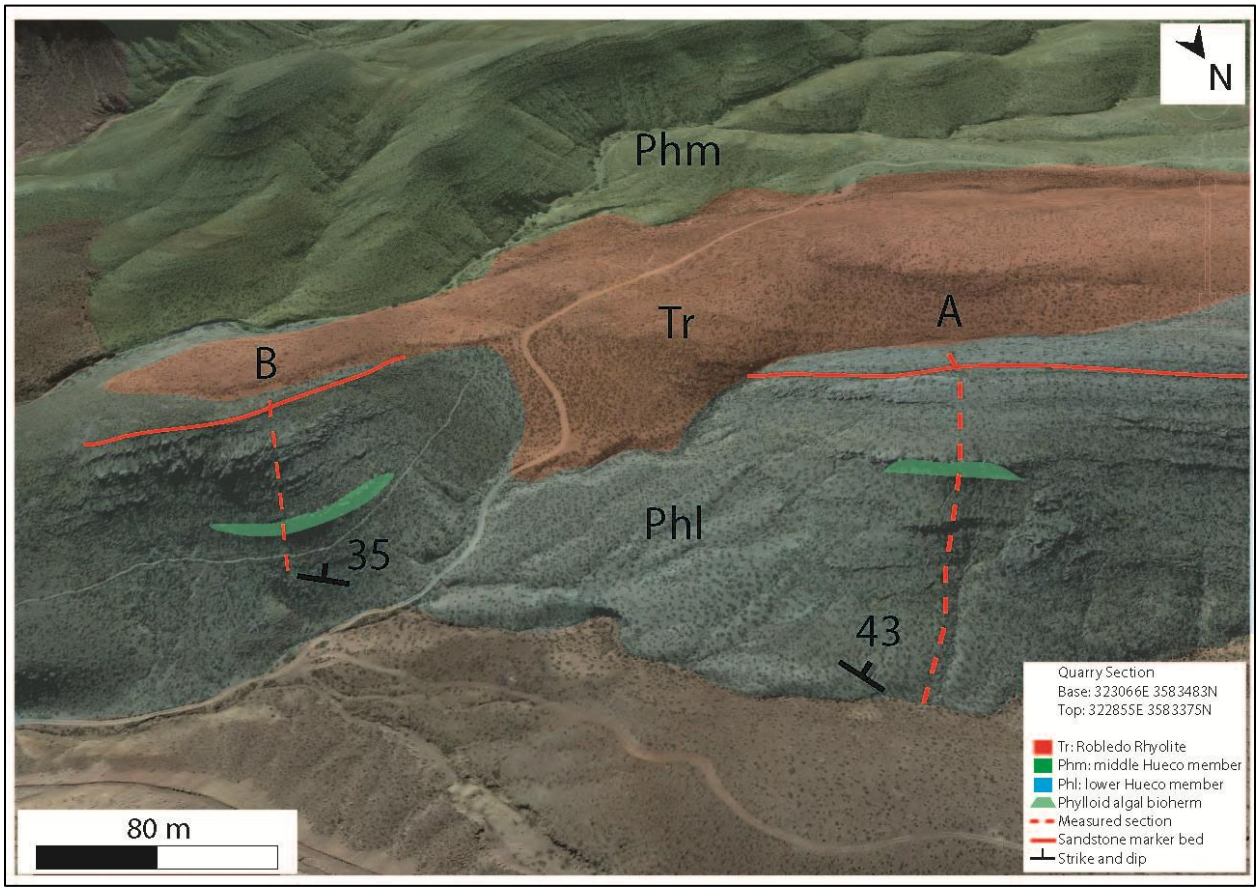

Oblique Aerial Photograph of the Quarry Section Location.

Oblique aerial photograph overlain by the geologic units mapped by Seager et al. (2008), the transect of the measured stratigraphic section is shown by a red dashed line. Aerial photograph is courtesy of Google Earth.

Quarry Section, Robledo Mountains, New Mexico

UTM Base: 13S 323066E 3583483N
UTM Top: 322855E 3583375N

Interval: 0-50 m
Base: Strike: 340, Dip: 43

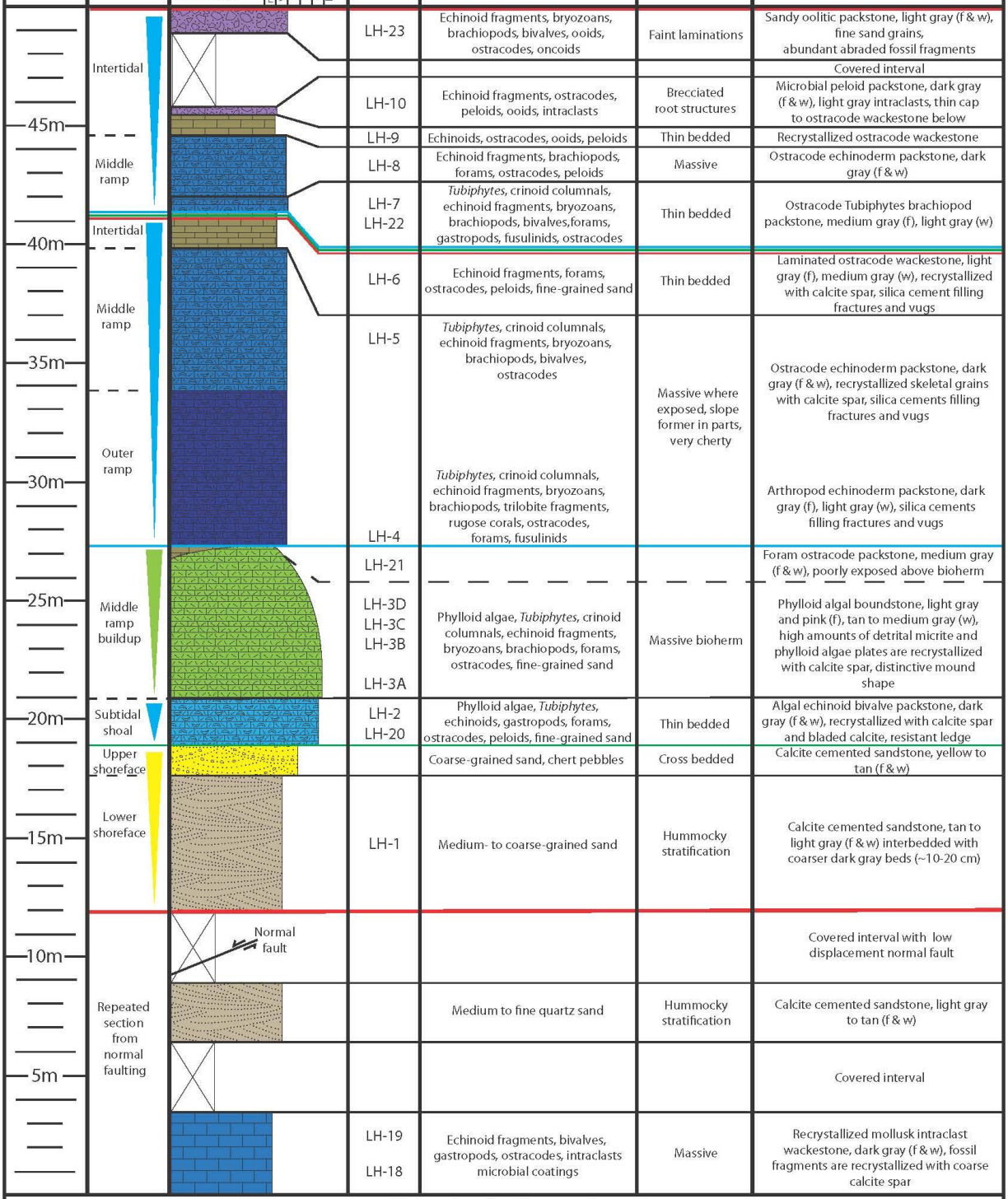

Pennsylvanian Bursum Formation

Quarry Section, Robledo Mountains, New Mexico

UTM Base: 13S 323066E 3583483N
UTM Top: 322855E 3583375N

Interval: 50-90 m
Top: Strike: 330, Dip: 35

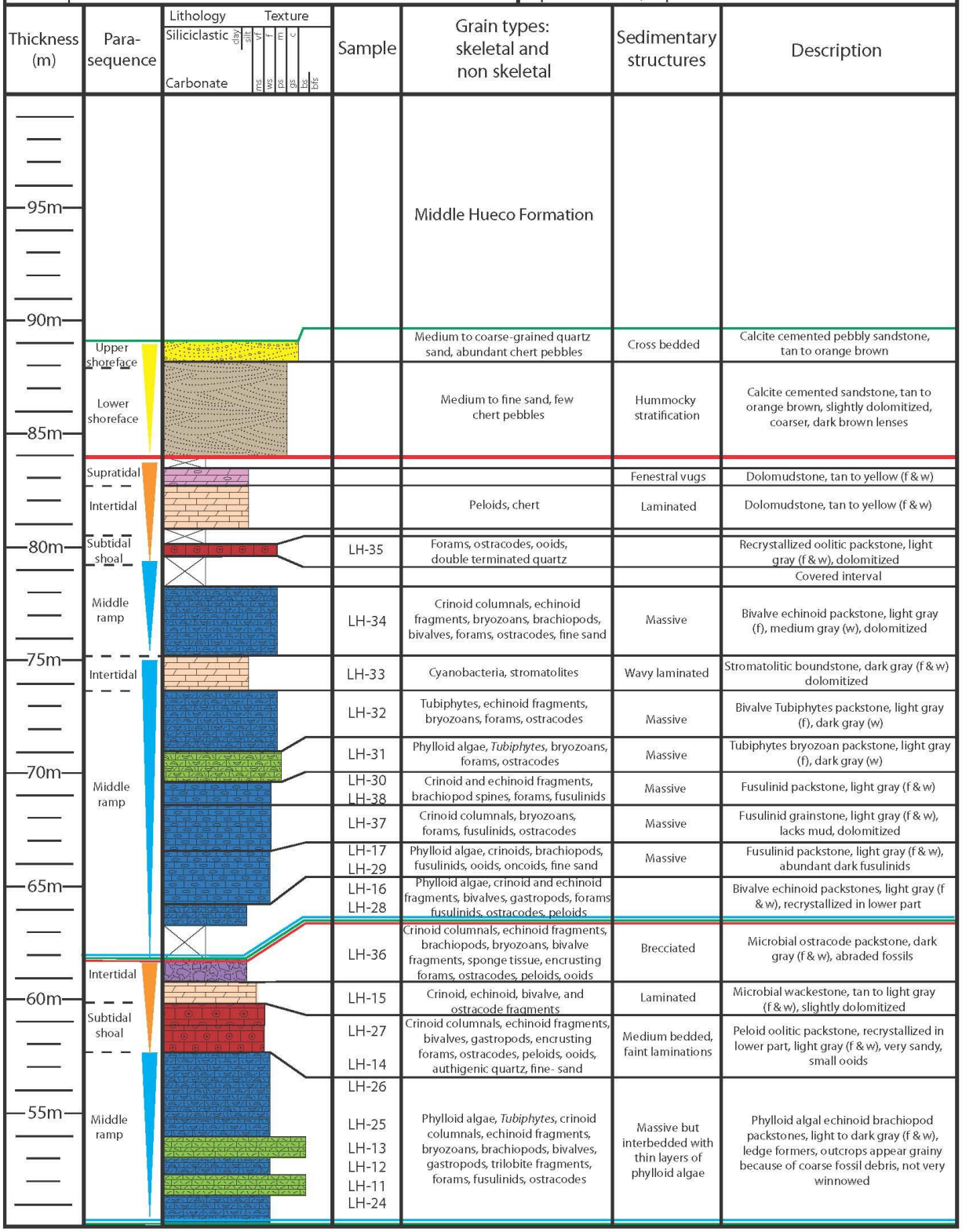

A.4

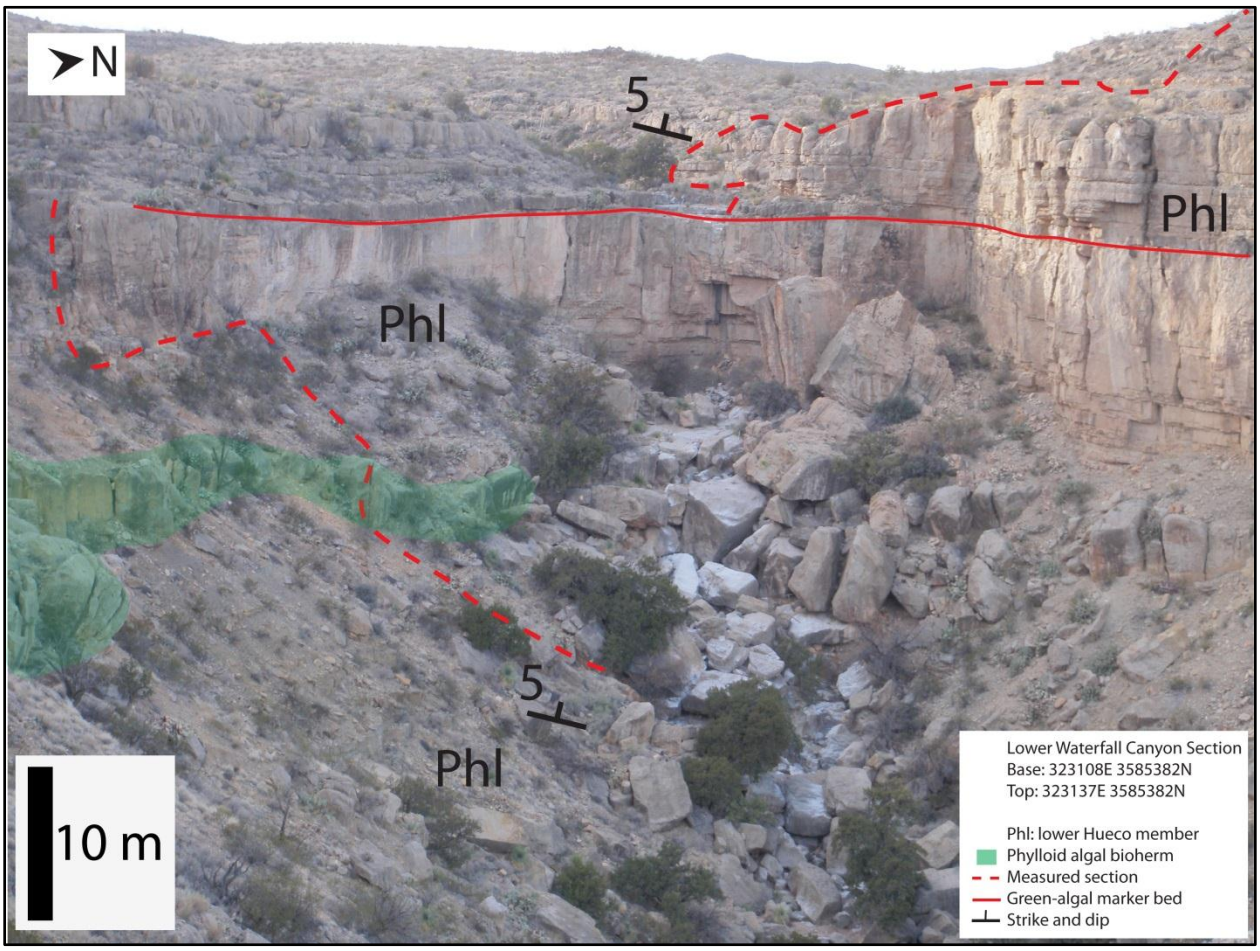

Outcrop Photograph of the Lower Waterfall Canyon Section Location.

Field photograph taken facing west into the Waterfall Canyon on the eastern flank of the Robledo Mountains. Intensive debris flows have covered the lower beds in this section and more than likely the basal contact with the underlying Pennsylvanian Bursum Formation.

Lower Waterfall Canyon Section, Robledo Mountains, New Mexico

UTM Base: 13S 323108E 3585382N
UTM Top: 323137 3585382

Interval: 0-30m
Base: Strike: 017, 5W

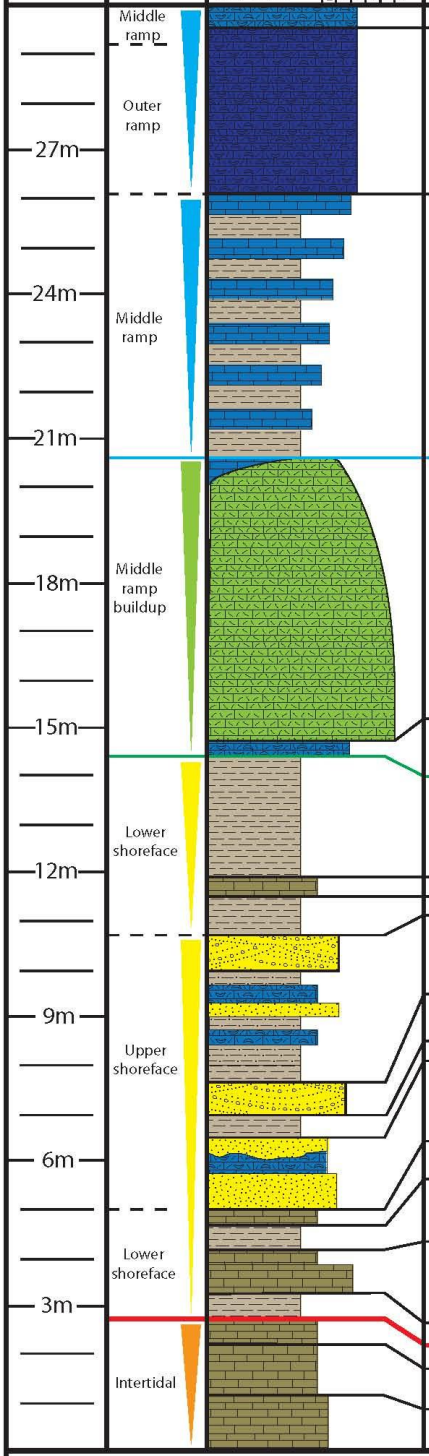

Thickness (m)	Para-sequence	Sample	Grain types: skeletal and non skeletal	Sedimentary structures	Description
27m	Middle ramp / Outer ramp	LH-67	Crinoid columnals, echinoid fragments, bryozoans, brachiopods, siliceous sponge spiclues, fusulinids, ostracodes, rugose corals	Thin bedded, thicken upwards to medium bedded at top	Siliceous sponge bryozoan packstone, tan to yellow (f & w), lower part of massive cliff
24m	Middle ramp		Fossil fragments, fine-grained sand	Thin wavy bedded limestone interbedded with shale	Interbedded shale and mudstone, poorly exposed
21m					
18m	Middle ramp buildup	LH-66 A-D	Phylloid algae, *Tubiphytes*, crinoid columnals, echinoid fragments, fenestrae and ramose bryozoans, brachiopods, bivalves, ostracodes	Large mounded structure	Phylloid algal boundstone, dark gray (f & w), some phylloid algae weathers light gray, highly recrystallized, chert filling fractures, outcrop is very fractured on shaley slope
15m		LH-65	Fenestrae and ramose bryozoans, bivalves, brachiopods, gastropods, ostracodes, fine-grained sand	Thin bedded	Brachiopod mollusk packstone, tan to yellow (f & w), very sandy
	Lower shoreface				Dark gray fissle shale
12m		LH-64	Ostracodes, fine-grained sand	Thin bedded	Ostracode mudstone, light gray (f & w)
					Dark gray fissle shale
		LH-63	Bryozoan fragments, bivalve fragments, oncoids, intraclasts, fine-grained sand	Thin bedded	Interbedded dark gray fissle shale, brown siltstone, dark gray micritic mudstone, and tan calcite cement sandstones with fossil fragments (LH-63)
9m			Fossil fragments, fine- to medium-grained sand, intraclasts, oncoids	Massive	Intraclast packstone, yellow to tan (f & w), angular clasts, sandy
	Upper shoreface				Dark gray fissle shale
		LH-62	Fusulinids, intraclasts	Oscillation ripples, scour marks	Fusulinid packstone at base (light gray f & w), coarsens upward into bioturbaded intraclast sandy limestone that is capped with ripples and scour marks
6m		LH-61	Ostracodes, fine-grained sand		Ostracode wackestone, dark gray (f & w), micritic
				Blocky	Interbedded mudstone and shale, gray (f), dark brown (w), fine to medium yellow and brown grains within shale
	Lower shoreface	LH-60 LH-59	Bivalves, ostracodes, ooids, intraclasts, Tubiphytes, encusting forams, fine-grained sand	Thin bedded, burrowed	Sandy bivalve intraclast packstone interbedded with silty mudstones, tan to light gray (f & w), siltstone partings (<1mm), alternating coarse and fine layers
3m					Gray siltstone to shale
	Intertidal	LH-58	Ostracodes, intraclasts		Recrystallized wackestone, light gray (f & w)
		LH-57	Recrystallized ostracode fragments	Brecciated top	Recrystallized mudstone, medium gray (f), light gray (w)
		LH-56	Encrusting forams, ostracodes, echinoid fragments, fine-grained sand	Beds thin upward	Ostracode wackestone, medium gray (f), dark gray (w)

Quaternary alluvium

Lower Waterfall Canyon Section, Robledo Mountains, New Mexico

UTM Base: 13S 323108E 3585382N
UTM Top: 323137 3585382

Interval: 30-56 m
Top: Strike: 015, Dip: 5W

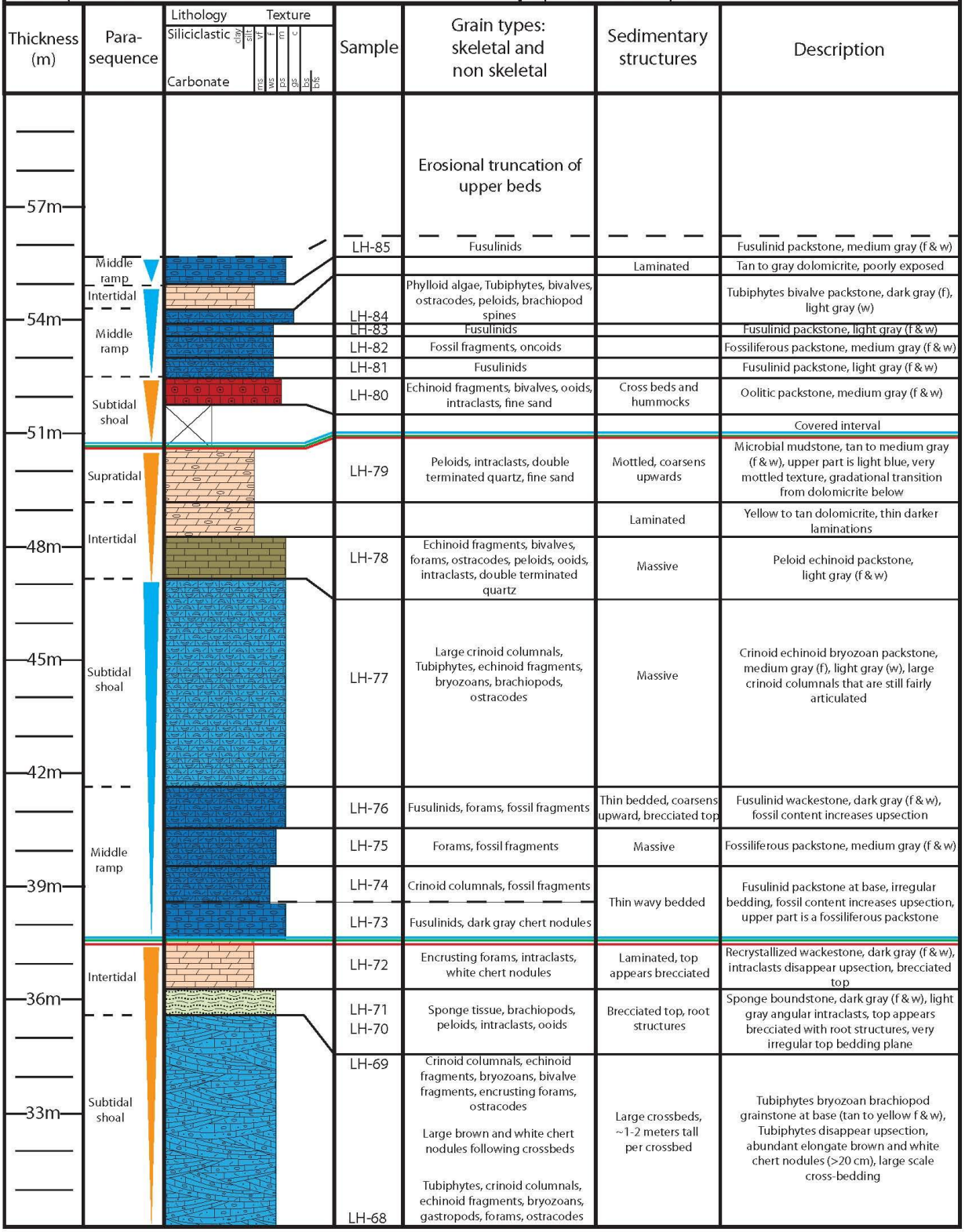

Thickness (m)	Para-sequence	Sample	Grain types: skeletal and non skeletal	Sedimentary structures	Description
			Erosional truncation of upper beds		
	Middle ramp	LH-85	Fusulinids		Fusulinid packstone, medium gray (f & w)
				Laminated	Tan to gray dolomicrite, poorly exposed
	Intertidal		Phylloid algae, Tubiphytes, bivalves, ostracodes, peloids, brachiopod spines		Tubiphytes bivalve packstone, dark gray (f), light gray (w)
54m		LH-84			
	Middle ramp	LH-83	Fusulinids		Fusulinid packstone, light gray (f & w)
		LH-82	Fossil fragments, oncoids		Fossiliferous packstone, medium gray (f & w)
		LH-81	Fusulinids		Fusulinid packstone, light gray (f & w)
	Subtidal shoal	LH-80	Echinoid fragments, bivalves, ooids, intraclasts, fine sand	Cross beds and hummocks	Oolitic packstone, medium gray (f & w)
51m					Covered interval
	Supratidal	LH-79	Peloids, intraclasts, double terminated quartz, fine sand	Mottled, coarsens upwards	Microbial mudstone, tan to medium gray (f & w), upper part is light blue, very mottled texture, gradational transition from dolomicrite below
	Intertidal			Laminated	Yellow to tan dolomicrite, thin darker laminations
48m		LH-78	Echinoid fragments, bivalves, forams, ostracodes, peloids, ooids, intraclasts, double terminated quartz	Massive	Peloid echinoid packstone, light gray (f & w)
	Subtidal shoal	LH-77	Large crinoid columnals, Tubiphytes, echinoid fragments, bryozoans, brachiopods, ostracodes	Massive	Crinoid echinoid bryozoan packstone, medium gray (f), light gray (w), large crinoid columnals that are still fairly articulated
45m					
42m		LH-76	Fusulinids, forams, fossil fragments	Thin bedded, coarsens upward, brecciated top	Fusulinid wackestone, dark gray (f & w), fossil content increases upsection
	Middle ramp	LH-75	Forams, fossil fragments	Massive	Fossiliferous packstone, medium gray (f & w)
39m		LH-74	Crinoid columnals, fossil fragments	Thin wavy bedded	Fusulinid packstone at base, irregular bedding, fossil content increases upsection, upper part is a fossiliferous packstone
		LH-73	Fusulinids, dark gray chert nodules		
	Intertidal	LH-72	Encrusting forams, intraclasts, white chert nodules	Laminated, top appears brecciated	Recrystallized wackestone, dark gray (f & w), intraclasts disappear upsection, brecciated top
36m		LH-71 LH-70	Sponge tissue, brachiopods, peloids, intraclasts, ooids	Brecciated top, root structures	Sponge boundstone, dark gray (f & w), light gray angular intraclasts, top appears brecciated with root structures, very irregular top bedding plane
	Subtidal shoal	LH-69	Crinoid columnals, echinoid fragments, bryozoans, bivalve fragments, encrusting forams, ostracodes Large brown and white chert nodules following crossbeds	Large crossbeds, ~1-2 meters tall per crossbed	Tubiphytes bryozoan brachiopod grainstone at base (tan to yellow f & w), Tubiphytes disappear upsection, abundant elongate brown and white chert nodules (>20 cm), large scale cross-bedding
33m		LH-68	Tubiphytes, crinoid columnals, echinoid fragments, bryozoans, gastropods, forams, ostracodes		

A.5

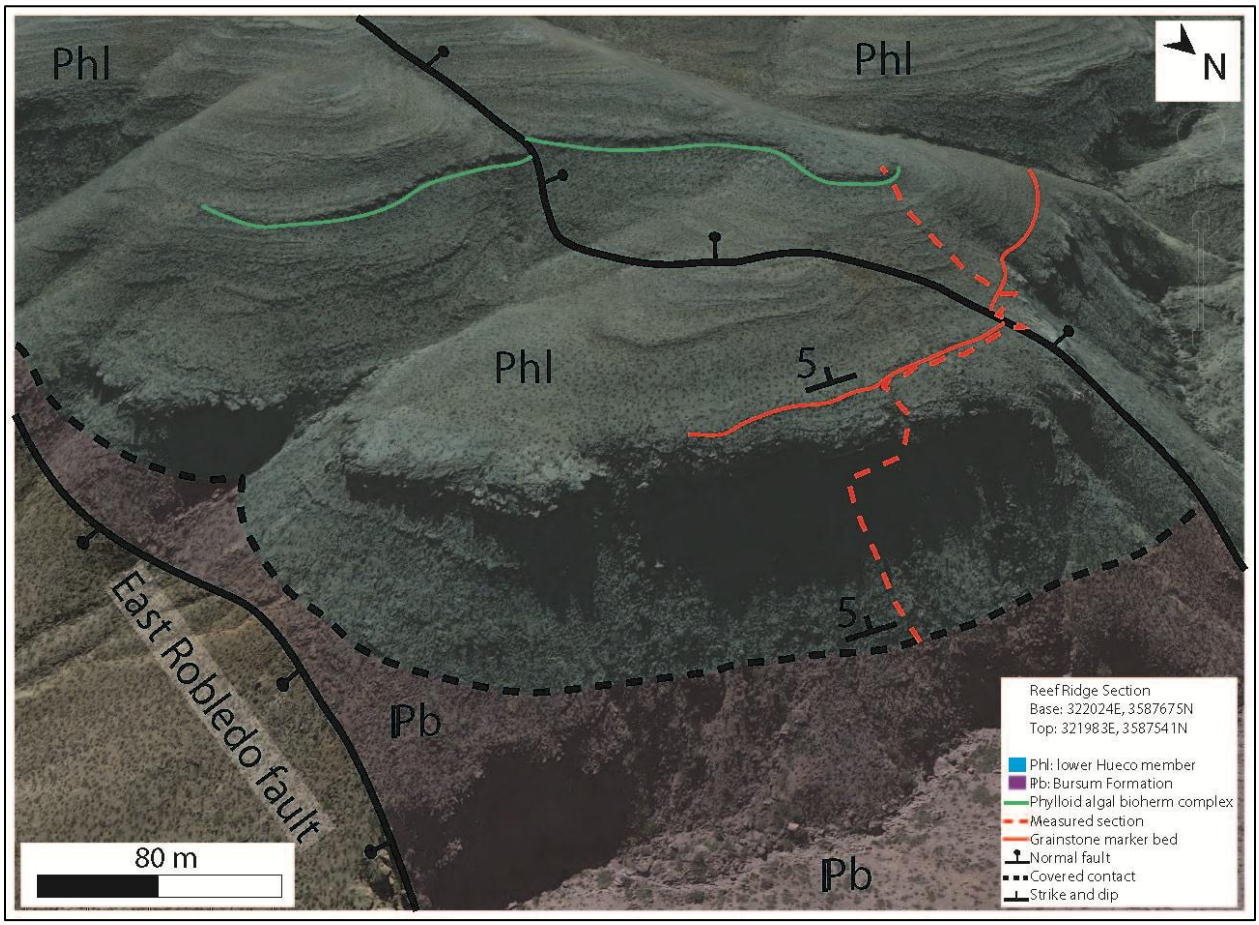

Oblique Aerial Photograph of the Reef Ridge Section Location.

Oblique aerial photograph overlain by the geologic units mapped by Seager et al. (2008), the transect of the measured stratigraphic section is shown by a red dashed line. Aerial photograph is courtesy of Google Earth.

Reef Ridge Section, Robledo Mountains, New Mexico

UTM Base: 13S 322024E, 3587675N,
UTM Top: 13S 321983E, 3587541N

Interval: 0-30 m
Base: Strike: 090, Dip: 5S

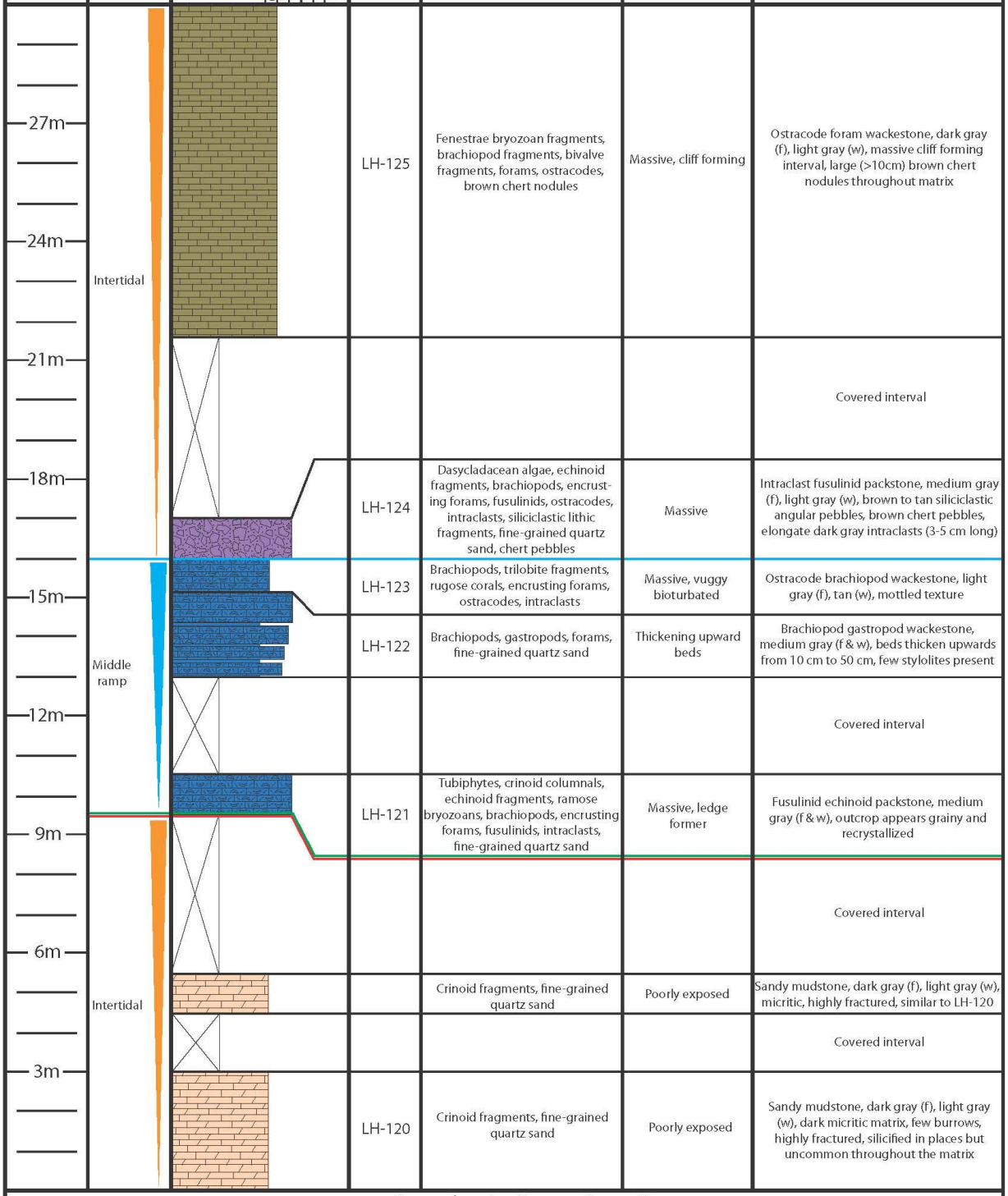

Sample	Grain types: skeletal and non skeletal	Sedimentary structures	Description
LH-125	Fenestrae bryozoan fragments, brachiopod fragments, bivalve fragments, forams, ostracodes, brown chert nodules	Massive, cliff forming	Ostracode foram wackestone, dark gray (f), light gray (w), massive cliff forming interval, large (>10cm) brown chert nodules throughout matrix
			Covered interval
LH-124	Dasycladacean algae, echinoid fragments, brachiopods, encrusting forams, fusulinids, ostracodes, intraclasts, siliciclastic lithic fragments, fine-grained quartz sand, chert pebbles	Massive	Intraclast fusulinid packstone, medium gray (f), light gray (w), brown to tan siliciclastic angular pebbles, brown chert pebbles, elongate dark gray intraclasts (3-5 cm long)
LH-123	Brachiopods, trilobite fragments, rugose corals, encrusting forams, ostracodes, intraclasts	Massive, vuggy bioturbated	Ostracode brachiopod wackestone, light gray (f), tan (w), mottled texture
LH-122	Brachiopods, gastropods, forams, fine-grained quartz sand	Thickening upward beds	Brachiopod gastropod wackestone, medium gray (f & w), beds thicken upwards from 10 cm to 50 cm, few stylolites present
			Covered interval
LH-121	Tubiphytes, crinoid columnals, echinoid fragments, ramose bryozoans, brachiopods, encrusting forams, fusulinids, intraclasts, fine-grained quartz sand	Massive, ledge former	Fusulinid echinoid packstone, medium gray (f & w), outcrop appears grainy and recrystallized
			Covered interval
	Crinoid fragments, fine-grained quartz sand	Poorly exposed	Sandy mudstone, dark gray (f), light gray (w), micritic, highly fractured, similar to LH-120
			Covered interval
LH-120	Crinoid fragments, fine-grained quartz sand	Poorly exposed	Sandy mudstone, dark gray (f), light gray (w), dark micritic matrix, few burrows, highly fractured, silicified in places but uncommon throughout the matrix

Pennsylvanian Bursum Formation

Reef Ridge Section, Robledo Mountains, New Mexico

UTM Base: 13S 322024E, 3587675N,
UTM Top: 13S 321983E, 3587541N

Interval: 30-60 m

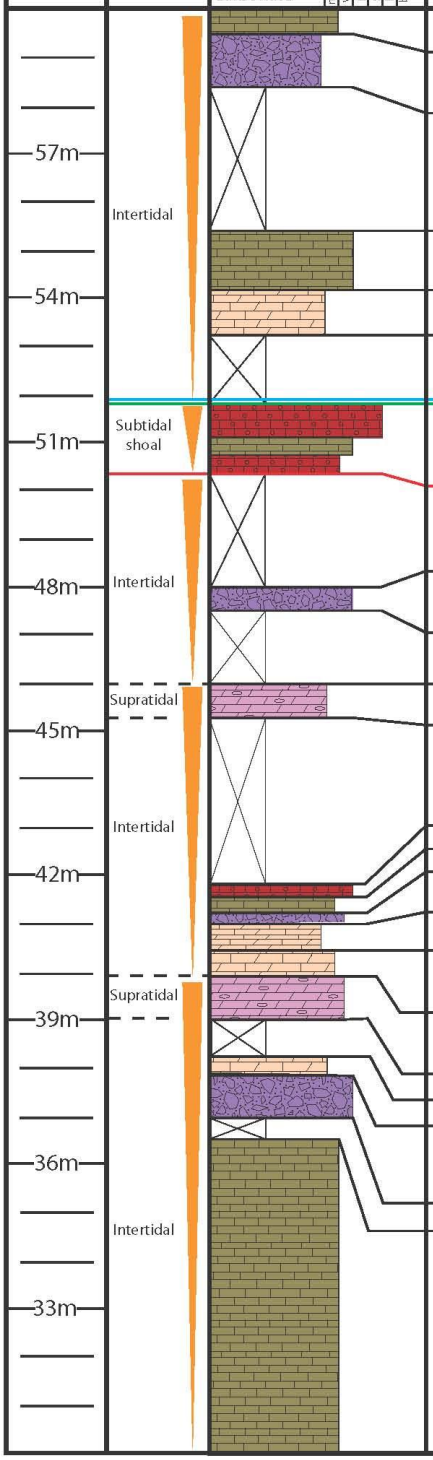

Thickness (m)	Para-sequence	Sample	Grain types: skeletal and non skeletal	Sedimentary structures	Description
			Ostracodes	Root structures	Ostracode wackestone, dark gray (f), light gray (w)
		LH-130	Brachiopod and bivalve fragments, ooids, intraclasts, fine-grained quartz sand	Ledge former, few stylolites	Sandy oolitic packstone, medium gray (f), tan (f)
57m					Covered interval
	Intertidal	LH-129	Encrusting forams, ostracodes	Massive	Foram ostracode wackestone, dark gray (f), light gray (w), micritic matrix, upper bedding plane has phylloid algae
54m					Sandy mudstone, brownish red (f), yellow to tan (w)
					Covered interval
51m	Subtidal shoal		Fine- to coarse-grained quartz sand, chert pebbles, carboante lithic fragments	Interbedded fine and coarse sandstones, some stylolites	Calcite cemented sandstone, dark brown (f), tan to brown (w), thin sandy mudstone between two sandstones, flat pebble yellow dolomitic fragments
					Covered interval
48m	Intertidal		Intraclasts		Intraclast packstone, dark gray (f), medium gray (w), tan, gray, and yellow elongate, sub-rounded intraclasts
					Covered interval
	Supratidal	LH-128	Stromatolites, fine-grained quartz sand	Wavy laminated	Stromatolitic mudstone, medium gray (f & w), appears recrystallized
45m					Covered interval
	Intertidal		Ooids, intraclasts, fine-grained sand		Sandy oolitic packstone, dark gray (f), tan (w)
			Ostracodes	Root structures	Ostracode wackestone, dark gray (f & w)
42m		LH-127	Fine-grained quartz sand, intraclasts	Wavy laminated	Sandy intraclast packstone, dark gray (f), tan (w), tan sandy burrows
			Brecciated stromatolites	Poorly exposed	Dolomicrite, tan (f & w), brecciated stromatolitic mats
	Supratidal		Monomictic intraclasts		Monomictic intraclast packstone dark gray intraclats in light gray matrix, all clasts are roughly the same color, size, and shape
39m			Stromatolites	Wavy laminated base, brecciated upper 20 cm	Stromatolitic mudstone, medium gray (f & w)
					Covered interval
				Poorly exposed	Dolomicrite, dark gray (f), tan (w)
36m		LH-126	Stromatolites, fusulinid fragments, ooids, intraclasts, carbonate lithic fragments, fine-grained quartz sand	Thin bedded, alternating coarse/fine beds	Intraclast grainstone, light gray (f), medium gray (w), alternating layers of intraclast rich beds and finer sandy layers, intraclasts are tan to gray and sub-rounded
	Intertidal				Covered interval
33m		LH-125	Fenestrae bryozoan fragments, brachiopod fragments, bivalve fragments, forams, ostracodes, brown chert nodules	Massive, cliff forming	Ostracode foram wackestone, dark gray (f), light gray (w), massive cliff forming interval, large (>10cm) brown chert nodules throughout matrix

Reef Ridge Section, Robledo Mountains, New Mexico

UTM Base: 13S 322024E, 3587675N,
UTM Top: 13S 321983E, 3587541N

Interval: 60-83 m
Top: Strike: 086, Dip: 5S

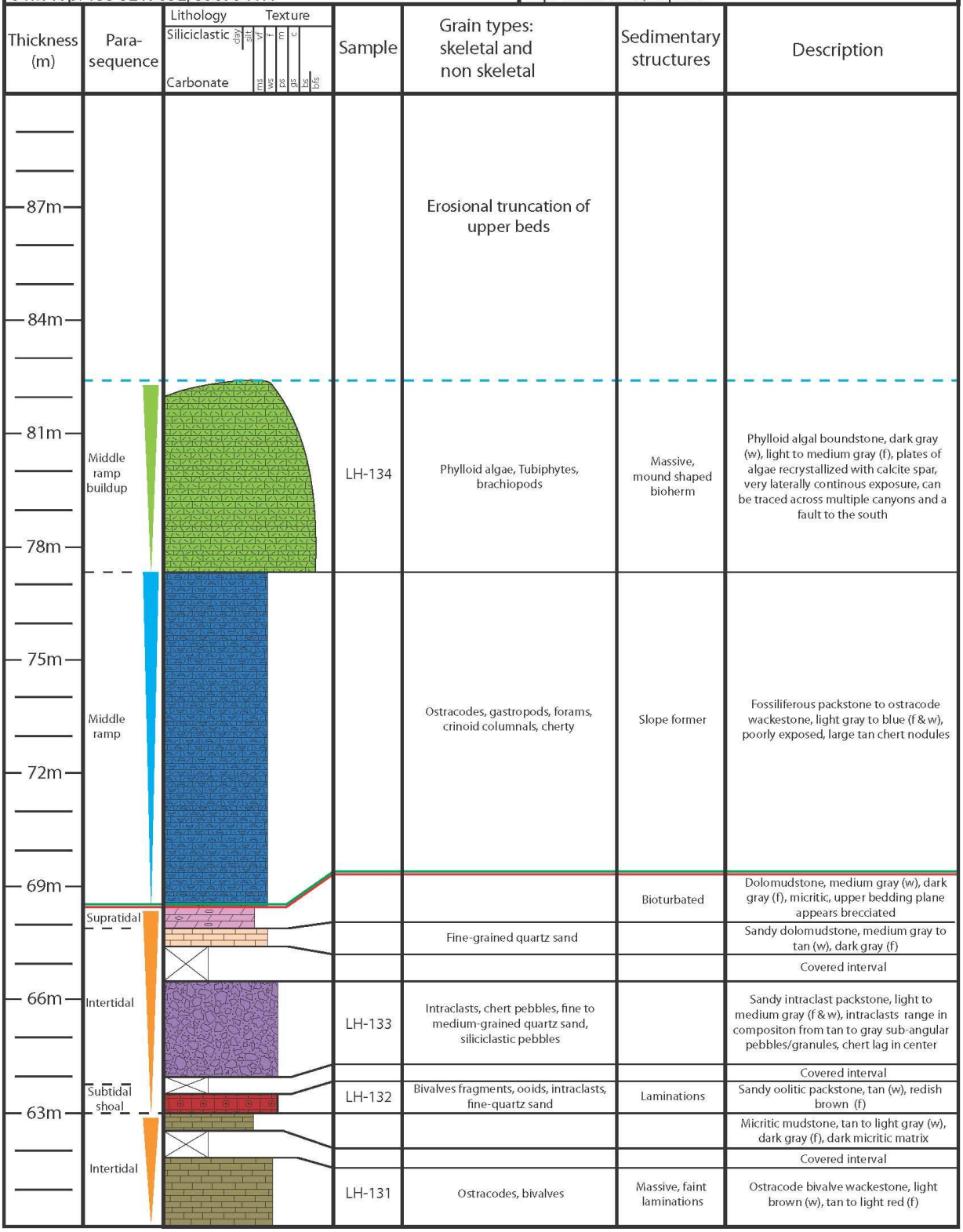

A.6

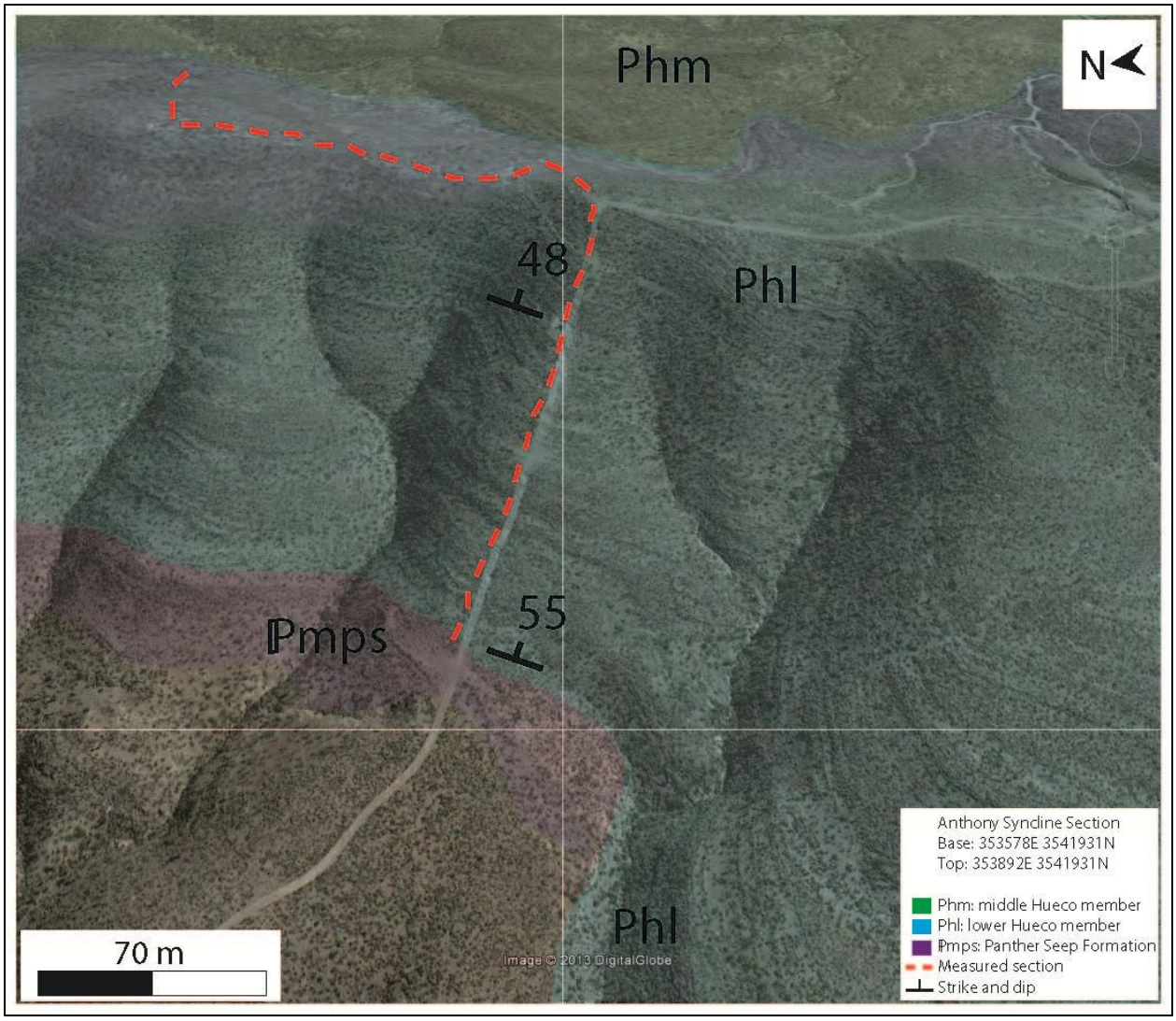

Oblique Aerial Photograph of the Anthony Syncline Section Location.

Oblique aerial photograph overlain by the geologic units mapped by Harbour (1972), the transect of the measured stratigraphic section is shown by a red dashed line. Aerial photograph is courtesy of Google Earth.

Anthony Syncline Section, Franklin Mountains, Texas

UTM Base: 13S 353578E 3541931N,
UTM Top: 353892E 3541931N

Interval: 0-50 m
Base: Strike: 035, Dip: 55E

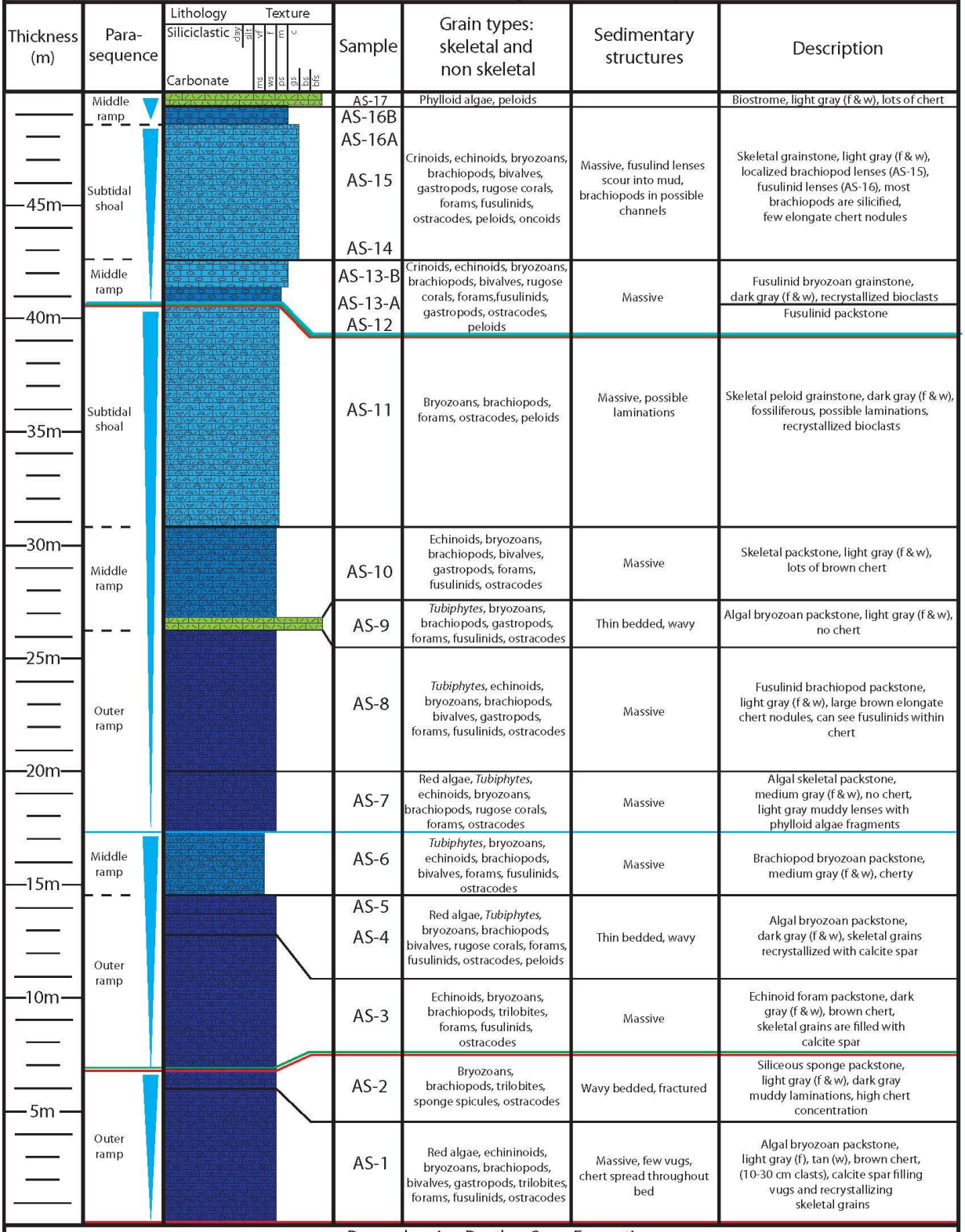

Sample	Grain types: skeletal and non skeletal	Sedimentary structures	Description
AS-17	Phylloid algae, peloids		Biostrome, light gray (f & w), lots of chert
AS-16B AS-16A AS-15 AS-14	Crinoids, echinoids, bryozoans, brachiopods, bivalves, gastropods, rugose corals, forams, fusulinids, ostracodes, peloids, oncoids	Massive, fusulind lenses scour into mud, brachiopods in possible channels	Skeletal grainstone, light gray (f & w), localized brachiopod lenses (AS-15), fusulinid lenses (AS-16), most brachiopods are silicified, few elongate chert nodules
AS-13-B AS-13-A AS-12	Crinoids, echinoids, bryozoans, brachiopods, bivalves, rugose corals, forams,fusulinids, gastropods, ostracodes, peloids	Massive	Fusulinid bryozoan grainstone, dark gray (f & w), recrystallized bioclasts Fusulinid packstone
AS-11	Bryozoans, brachiopods, forams, ostracodes, peloids	Massive, possible laminations	Skeletal peloid grainstone, dark gray (f & w), fossiliferous, possible laminations, recrystallized bioclasts
AS-10	Echinoids, bryozoans, brachiopods, bivalves, gastropods, forams, fusulinids, ostracodes	Massive	Skeletal packstone, light gray (f & w), lots of brown chert
AS-9	*Tubiphytes*, bryozoans, brachiopods, gastropods, forams, fusulinids, ostracodes	Thin bedded, wavy	Algal bryozoan packstone, light gray (f & w), no chert
AS-8	*Tubiphytes*, echinoids, bryozoans, brachiopods, bivalves, gastropods, forams, fusulinids, ostracodes	Massive	Fusulinid brachiopod packstone, light gray (f & w), large brown elongate chert nodules, can see fusulinids within chert
AS-7	Red algae, *Tubiphytes*, echinoids, bryozoans, brachiopods, rugose corals, forams, ostracodes	Massive	Algal skeletal packstone, medium gray (f & w), no chert, light gray muddy lenses with phylloid algae fragments
AS-6	*Tubiphytes*, bryozoans, echinoids, brachiopods, bivalves, forams, fusulinids, ostracodes	Massive	Brachiopod bryozoan packstone, medium gray (f & w), cherty
AS-5 AS-4	Red algae, *Tubiphytes*, bryozoans, brachiopods, bivalves, rugose corals, forams, fusulinids, ostracodes, peloids	Thin bedded, wavy	Algal bryozoan packstone, dark gray (f & w), skeletal grains recrystallized with calcite spar
AS-3	Echinoids, bryozoans, brachiopods, trilobites, forams, fusulinids, ostracodes	Massive	Echinoid foram packstone, dark gray (f & w), brown chert, skeletal grains are filled with calcite spar
AS-2	Bryozoans, brachiopods, trilobites, sponge spicules, ostracodes	Wavy bedded, fractured	Siliceous sponge packstone, light gray (f & w), dark gray muddy laminations, high chert concentration
AS-1	Red algae, echininoids, bryozoans, brachiopods, bivalves, gastropods, trilobites, forams, fusulinids, ostracodes	Massive, few vugs, chert spread throughout bed	Algal bryozoan packstone, light gray (f), tan (w), brown chert, (10-30 cm clasts), calcite spar filling vugs and recrystallizing skeletal grains

Pennsylvanian Panther Seep Formation

Anthony Syncline Section, Franklin Mountains, Texas

UTM Base: 13S 353578E 3541931N,
UTM Top: 353892E 3541931N

Interval: 50-100 m

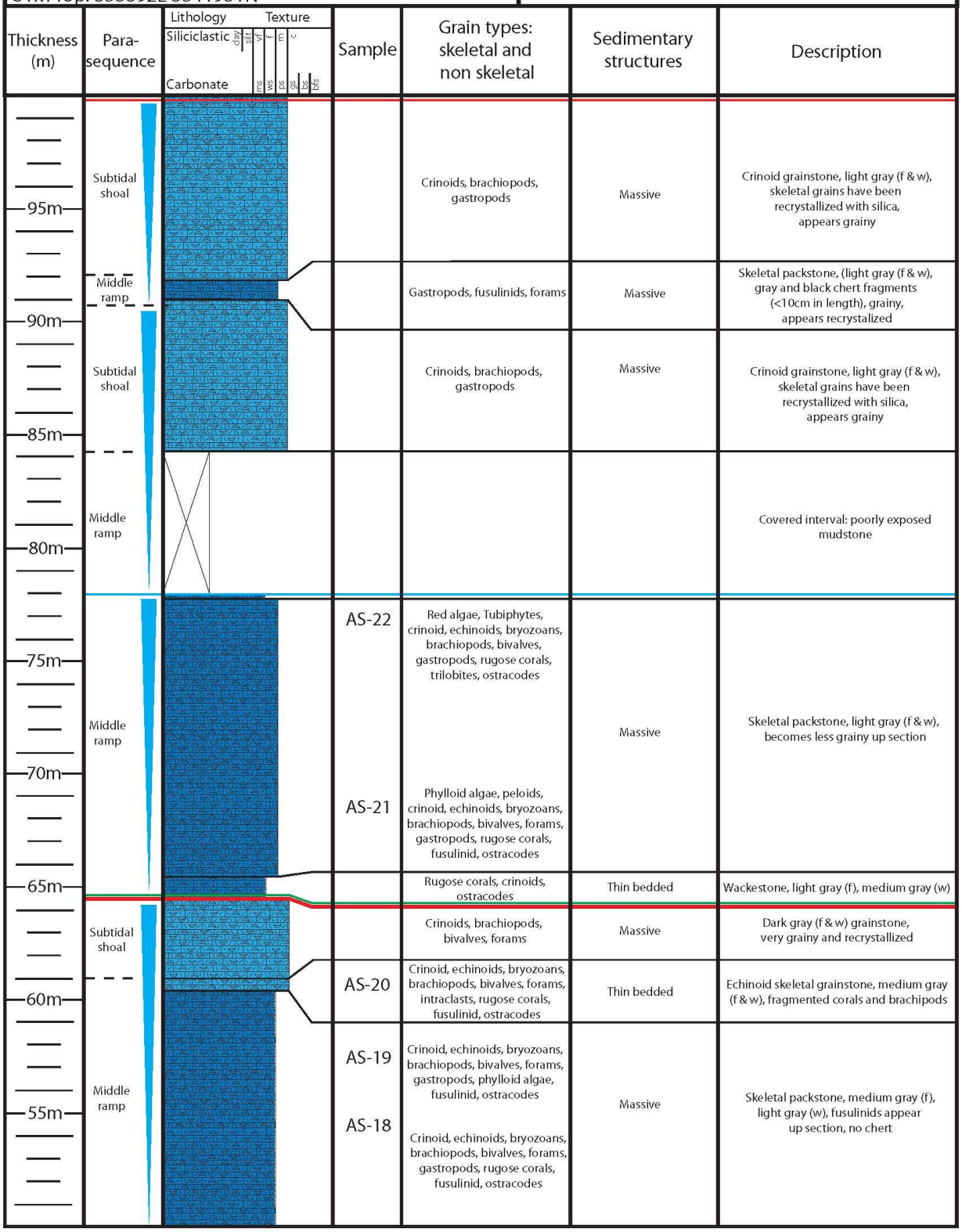

Anthony Syncline Section, Franklin Mountains, Texas

UTM Base: 13S 353578E 3541931N,
UTM Top: 353892E 3541931N

Interval: 100-150 m

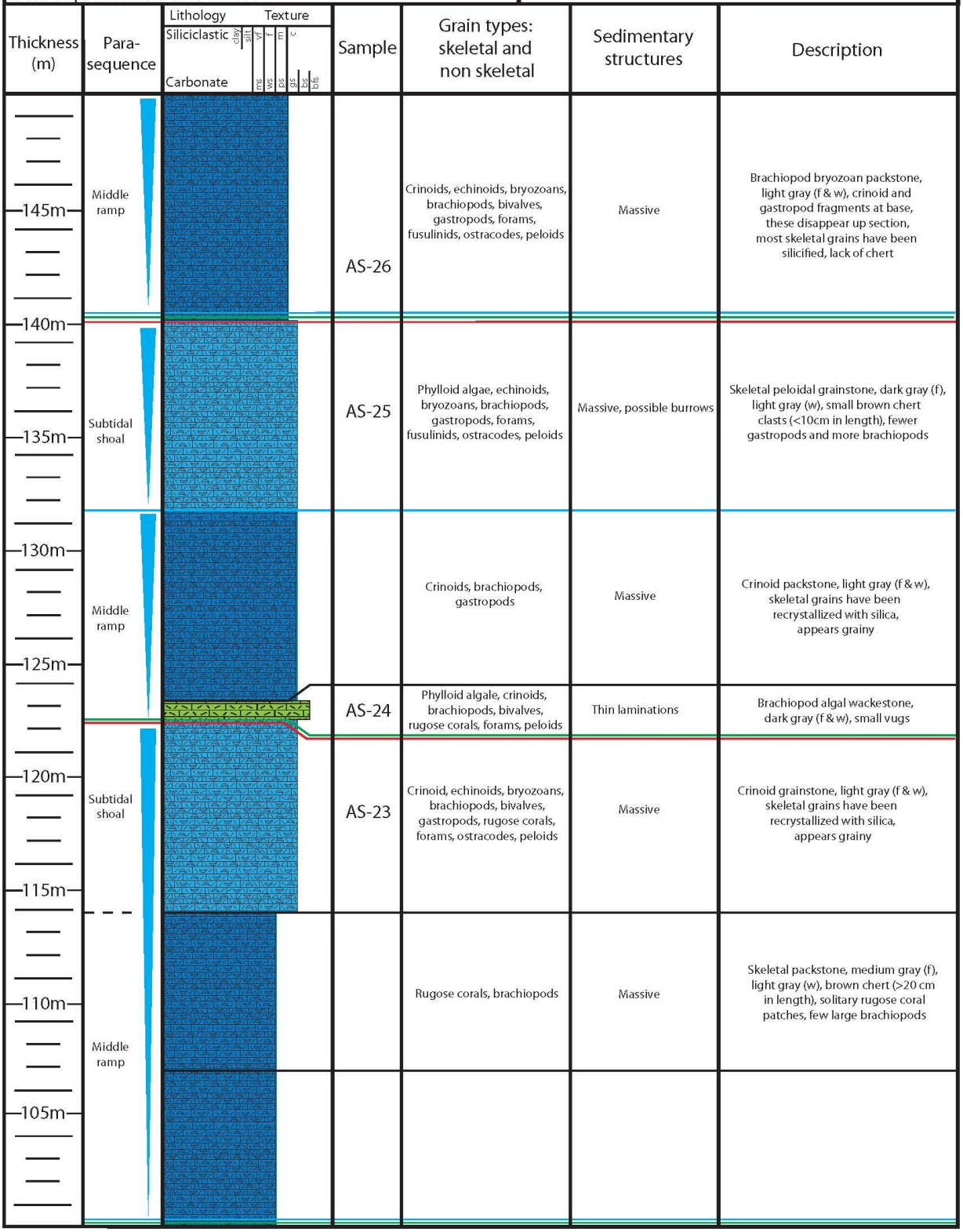

Anthony Syncline Section, Franklin Mountains, Texas

UTM Base: 13S 353578E 3541931N,
UTM Top: 353892E 3541931N

Interval: 150-200 m
Top: Strike: 039, Dip: 48E

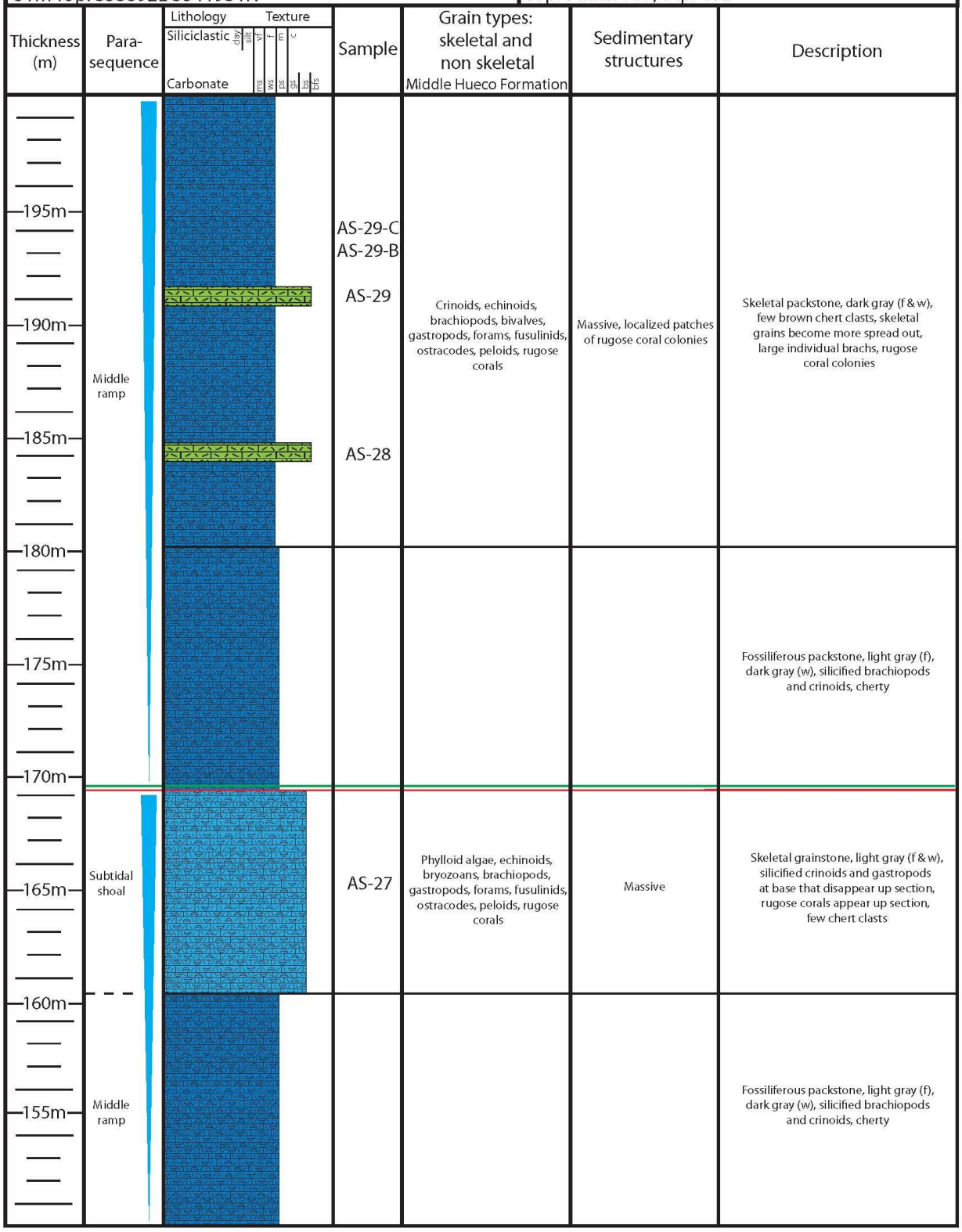

A.7

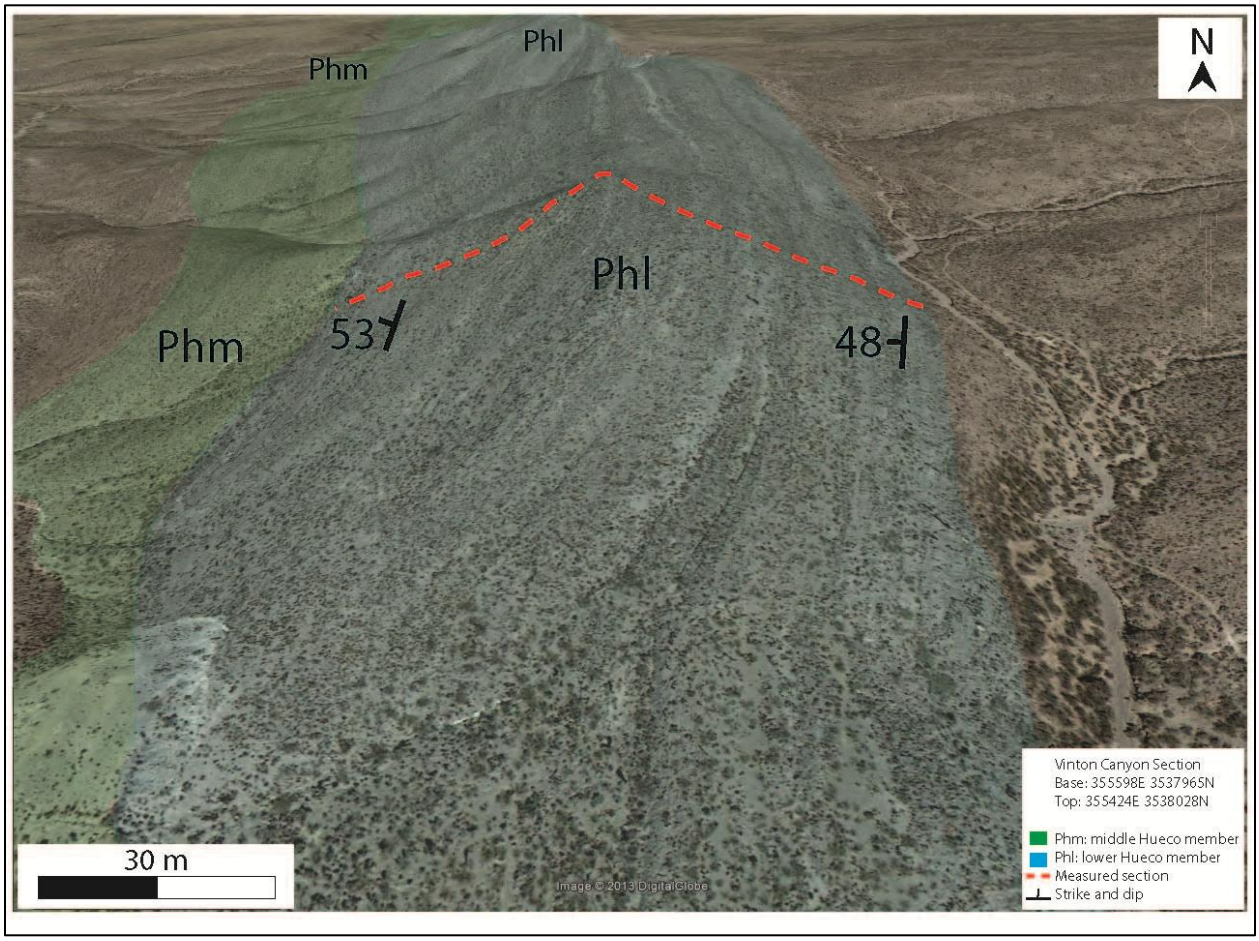

Oblique Aerial Photograph of the Vinton Canyon Section Location.

Oblique aerial photograph overlain by the geologic units mapped by Harbour (1972), the transect of the measured stratigraphic section is shown by a red dashed line. Aerial photograph is courtesy of Google Earth.

Vinton Canyon Section, Franklin Mountains, Texas

UTM Base: 13R 355598E 3537965N
UTM Top: 13R 355424E 3538028N

Interval: 0-50 m
Base: Strike: 010, Dip: 48W

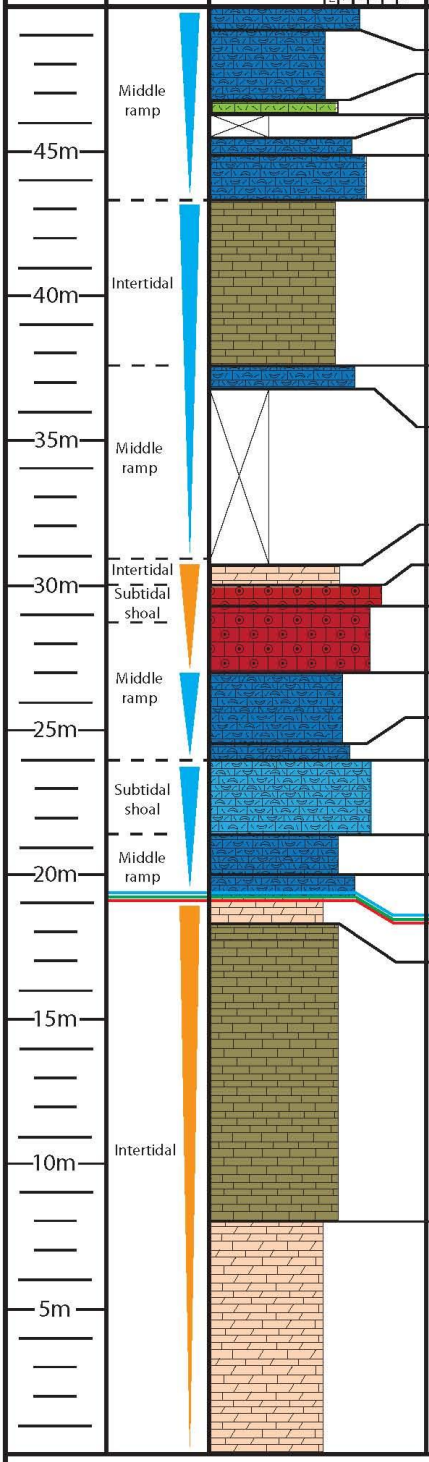

Thickness (m)	Para-sequence	Sample	Grain types: skeletal and non skeletal	Sedimentary structures	Description
	Middle ramp	VC-8, 4-6.5	Crinoids, echinoids, bryozoans, brachiopods, bivalves, ostracodes		Brachiopod echinoid packstone, dark gray (f), medium gray (w)
			Peloids, intraclast, ostracodes	Laminated	Peloidal mudstone, dark gray (f & w)
		4-3.2	Phylloid algae, brachiopod spines, encrusting forams, ostracodes		Phylloid algal bafflestone, dark gray (f), light gray (w)
45m		4-1.8	Green algae, ostracodes, gastropods, bivalves, forams	Wavy laminated	Algal gastropod packstone, dark gray (f), light gray (w)
		4-0	Peloids, intraclasts, ooids, bivalves, ostracodes, gastropods, forams	Massive	Peloid intraclast grainstone, medium gray (f & w)
	Intertidal	VC-7	Forams, ostracodes, peloids, bivalves	Massive, ledge former	Foram ostracode wackestone, medium gray (f & w), tan and orange chert nodules, becomes more fossiliferous up section
40m					
	Middle ramp	VC-6	Brachiopods, echinoid fragments, forams	Poorly exposed	Fossiliferous packstone, dark gray (f), medium gray (w), large brown and black chert nodules (>10cm), fetted odor
35m					Covered interval
			Forams, ostracodes, peloids, ooids, fine grained quartz sand	Bioturbated	Peloid ostracode grainstone, dark gray (f), medium gray (w), micritic matrix, no chert
	Intertidal Subtidal shoal	VC-5	Bivalve fragments, ostracodes, ooids, intraclasts, fine grained quartz sand	Ledge former, faint laminations	Oolitic grainstone, medium gray (f & w)
30m		VC-4	Forams, ostracodes, peloids, ooids, fine grained quartz sand	Bioturbated	Peloid ostracode grainstone, dark gray (f), medium gray (w), micritic matrix, no chert
	Middle ramp	VC-3	Crinoid columnals, echinoid fragments, gastropods, forams	Light gray laminations	Fossiliferous packstone, dark gray (f & w), large orange brown chert nodules (>10cm)
		VC-2	Crinoids, echinoids, bryozoans, brachiopods, ostracodes		Crinoid ostracode packstone, tan (f), light gray (w)
25m	Subtidal shoal	VC-1	Phylloid algae, echinoids, brachiopods, bivalves, gastropods, forams, ostracodes, peloids, diagenetic quartz	Massive	Fossiliferous grainstone, dark gray (f), medium gray (w), small brown chert nodules
	Middle ramp		Green algae, bivalves, forams	Poorly exposed	Algal cherty wackestone, light gray (f & w)
20m		01.VC-19	Crinoid columnals, echinoid fragments, bivalves, gastropods, forams	Poorly exposed	Echinoid bivalve packstone, medium gray (f), light gray (w), small chert nodules
		01.VC-18 01.VC-17	Intraclasts, peloids	Stylolites	Dolomudstone, medium gray (f), dark gray (w)
15m		01.VC-15	Forams, ostracodes, peloids	Massive, ledge former	Foram ostracode wackestone, medium gray (f & w), tan and orange chert nodules, upper 0.5m contains root structures
10m	Intertidal				
5m				Dark laminations	Micritic mudstone, dark gray (f), light gray to tan (w)

Quaternary alluvium

Vinton Canyon Section, Franklin Mountains, Texas

UTM Base: 13R 355598E 3537965N
UTM Top: 13R 355424E 3538028N

Interval: 50-100 m

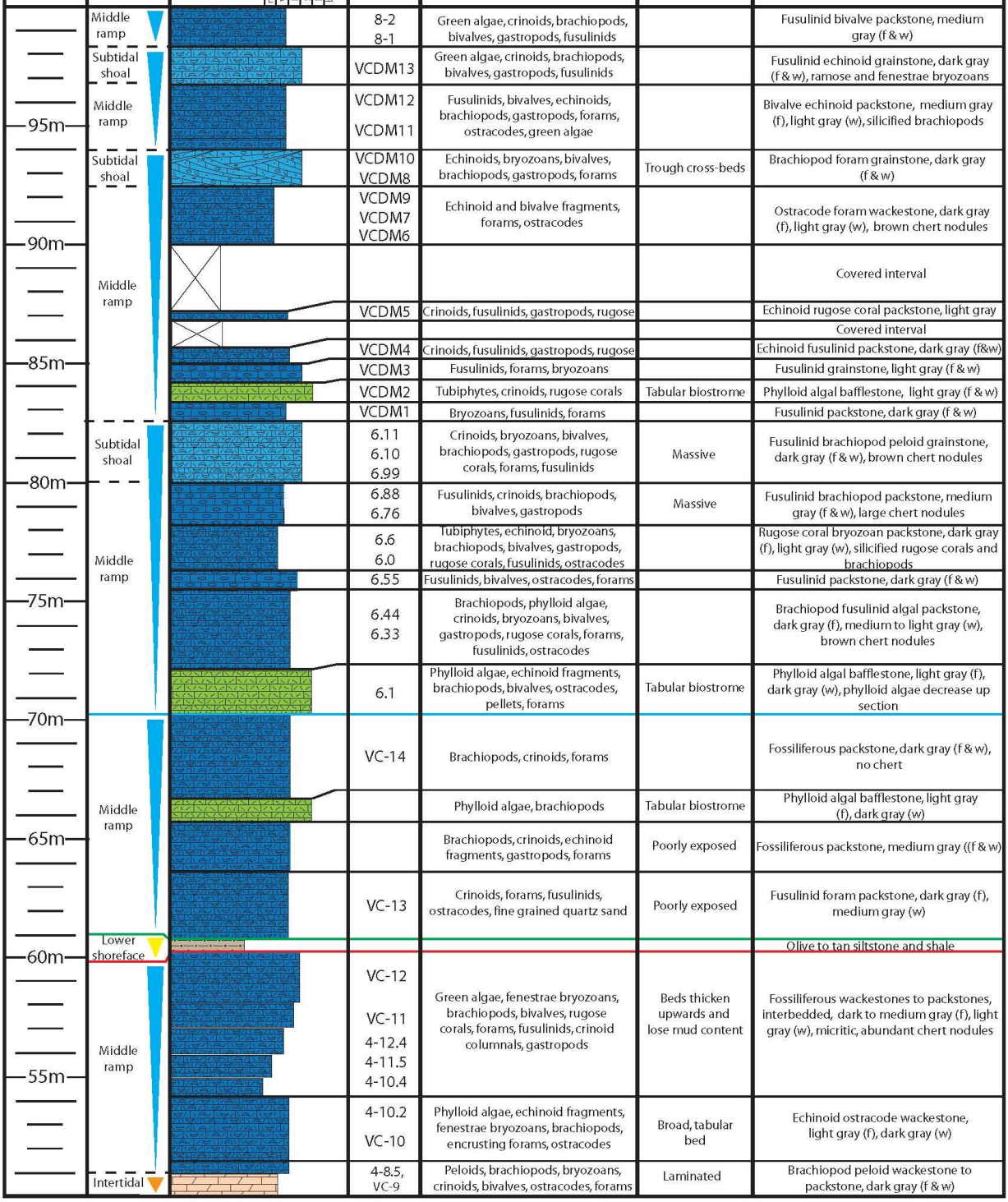

Thickness (m)	Para-sequence	Sample	Grain types: skeletal and non skeletal	Sedimentary structures	Description
	Middle ramp	8-2 8-1	Green algae, crinoids, brachiopods, bivalves, gastropods, fusulinids		Fusulinid bivalve packstone, medium gray (f & w)
	Subtidal shoal	VCDM13	Green algae, crinoids, brachiopods, bivalves, gastropods, fusulinids		Fusulinid echinoid grainstone, dark gray (f & w), ramose and fenestrae bryozoans
95m	Middle ramp	VCDM12 VCDM11	Fusulinids, bivalves, echinoids, brachiopods, gastropods, forams, ostracodes, green algae		Bivalve echinoid packstone, medium gray (f), light gray (w), silicified brachiopods
	Subtidal shoal	VCDM10 VCDM8	Echinoids, bryozoans, bivalves, brachiopods, gastropods, forams	Trough cross-beds	Brachiopod foram grainstone, dark gray (f & w)
		VCDM9 VCDM7 VCDM6	Echinoid and bivalve fragments, forams, ostracodes		Ostracode foram wackestone, dark gray (f), light gray (w), brown chert nodules
90m	Middle ramp				Covered interval
		VCDM5	Crinoids, fusulinids, gastropods, rugose		Echinoid rugose coral packstone, light gray
					Covered interval
		VCDM4	Crinoids, fusulinids, gastropods, rugose		Echinoid fusulinid packstone, dark gray (f&w)
85m		VCDM3	Fusulinids, forams, bryozoans		Fusulinid grainstone, light gray (f & w)
		VCDM2	Tubiphytes, crinoids, rugose corals	Tabular biostrome	Phylloid algal bafflestone, light gray (f & w)
		VCDM1	Bryozoans, fusulinids, forams		Fusulinid packstone, dark gray (f & w)
	Subtidal shoal	6.11 6.10 6.99	Crinoids, bryozoans, bivalves, brachiopods, gastropods, rugose corals, forams, fusulinids	Massive	Fusulinid brachiopod peloid grainstone, dark gray (f & w), brown chert nodules
80m		6.88 6.76	Fusulinids, crinoids, brachiopods, bivalves, gastropods	Massive	Fusulinid brachiopod packstone, medium gray (f & w), large chert nodules
	Middle ramp	6.6 6.0	Tubiphytes, echinoid, bryozoans, brachiopods, bivalves, gastropods, rugose corals, fusulinids, ostracodes		Rugose coral bryozoan packstone, dark gray (f), light gray (w), silicified rugose corals and brachiopods
		6.55	Fusulinids, bivalves, ostracodes, forams		Fusulinid packstone, dark gray (f & w)
75m		6.44 6.33	Brachiopods, phylloid algae, crinoids, bryozoans, bivalves, gastropods, rugose corals, forams, fusulinids, ostracodes		Brachiopod fusulinid algal packstone, dark gray (f), medium to light gray (w), brown chert nodules
		6.1	Phylloid algae, echinoid fragments, brachiopods, bivalves, ostracodes, pellets, forams	Tabular biostrome	Phylloid algal bafflestone, light gray (f), dark gray (w), phylloid algae decrease up section
70m		VC-14	Brachiopods, crinoids, forams		Fossiliferous packstone, dark gray (f & w), no chert
	Middle ramp		Phylloid algae, brachiopods	Tabular biostrome	Phylloid algal bafflestone, light gray (f), dark gray (w)
65m			Brachiopods, crinoids, echinoid fragments, gastropods, forams	Poorly exposed	Fossiliferous packstone, medium gray ((f & w)
		VC-13	Crinoids, forams, fusulinids, ostracodes, fine grained quartz sand	Poorly exposed	Fusulinid foram packstone, dark gray (f), medium gray (w)
	Lower shoreface				Olive to tan siltstone and shale
60m					
		VC-12	Green algae, fenestrae bryozoans, brachiopods, bivalves, rugose corals, forams, fusulinids, crinoid columnals, gastropods	Beds thicken upwards and lose mud content	Fossiliferous wackestones to packstones, interbedded, dark to medium gray (f), light gray (w), micritic, abundant chert nodules
	Middle ramp	VC-11 4-12.4 4-11.5 4-10.4			
55m		4-10.2 VC-10	Phylloid algae, echinoid fragments, fenestrae bryozoans, brachiopods, encrusting forams, ostracodes	Broad, tabular bed	Echinoid ostracode wackestone, light gray (f), dark gray (w)
	Intertidal	4-8.5, VC-9	Peloids, brachiopods, bryozoans, crinoids, bivalves, ostracodes, forams	Laminated	Brachiopod peloid wackestone to packstone, dark gray (f & w)

Vinton Canyon Section, Franklin Mountains, Texas

UTM Base: 13R 355598E 3537965N
UTM Top: 13R 355424E 3538028N

Interval: 100-128 m
Top: Strike: 014, Dip: 51W

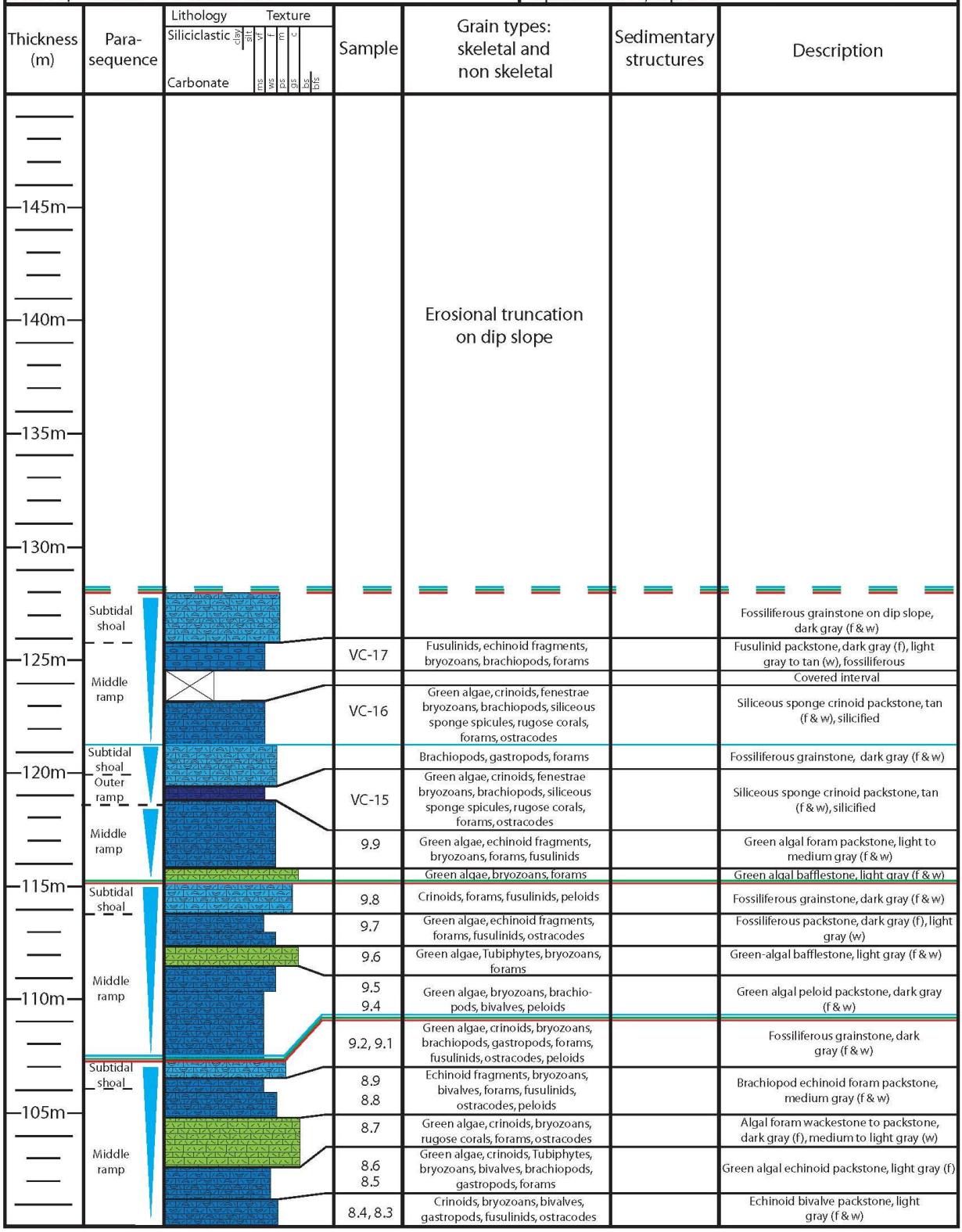

A.8

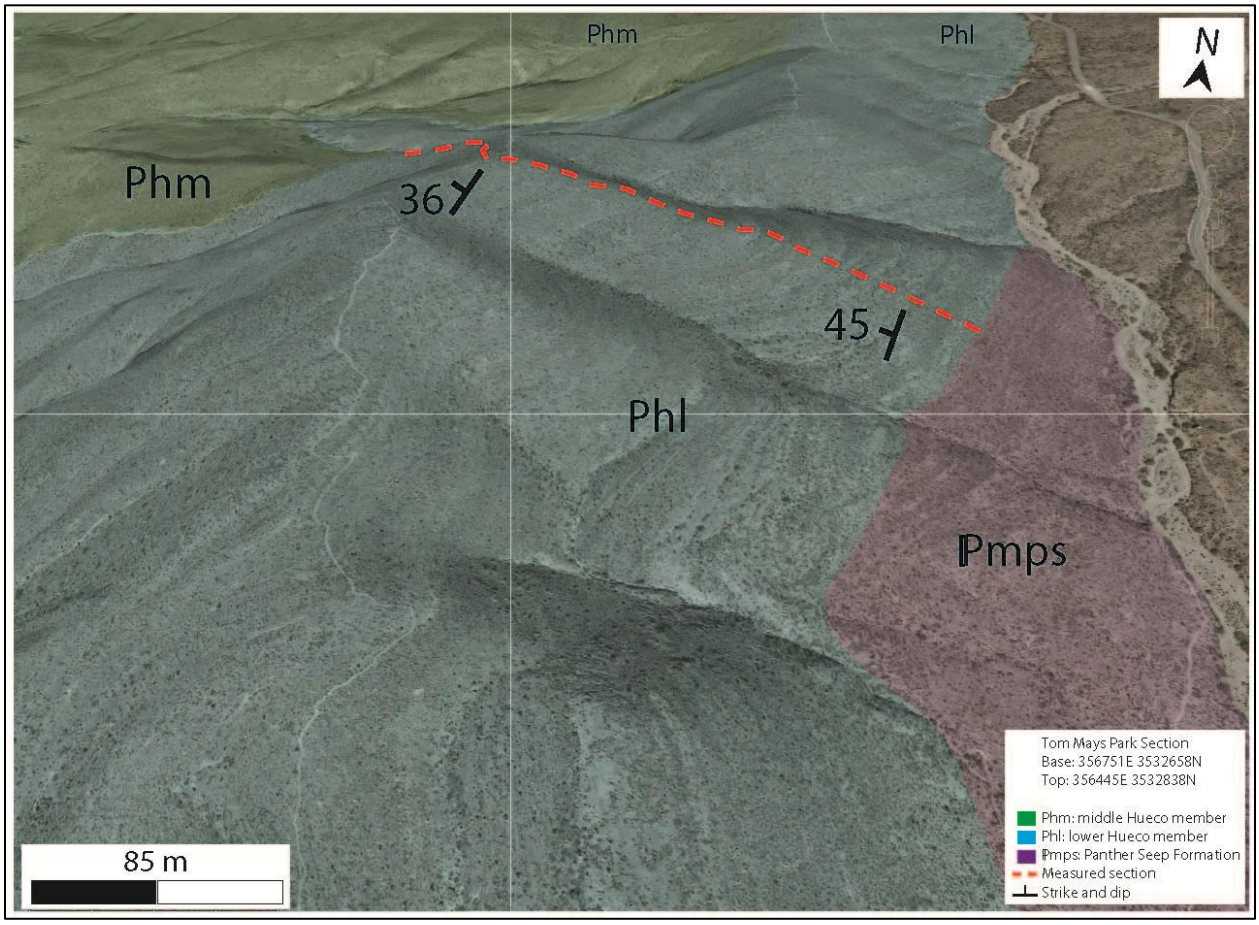

Oblique Aerial Photograph of the Tom Mays Park Section Location.

Oblique aerial photograph overlain by the geologic units mapped by Harbour (1972), the transect of the measured stratigraphic section is shown by a red dashed line. Aerial photograph is courtesy of Google Earth.

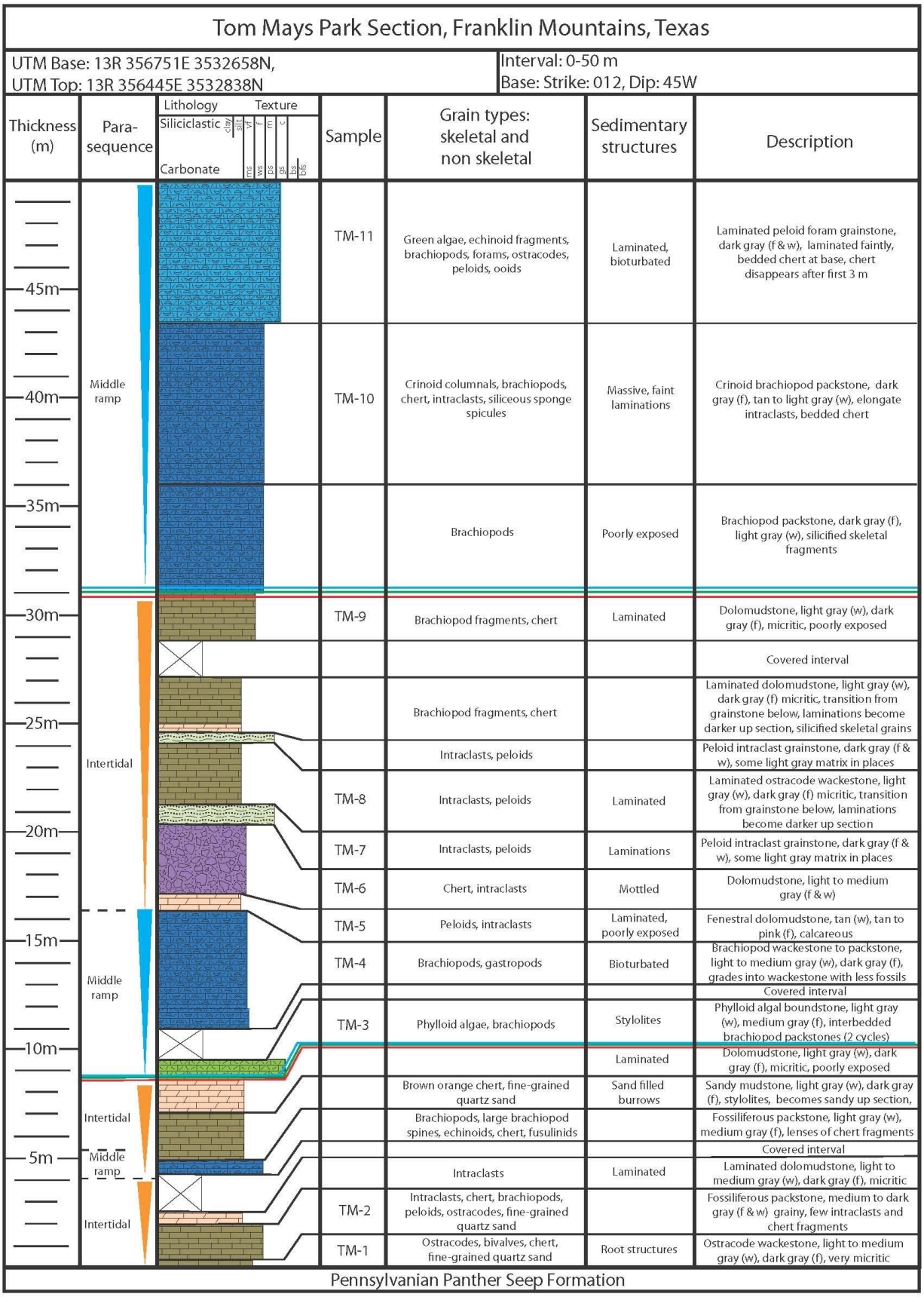
Tom Mays Park Section, Franklin Mountains, Texas
UTM Base: 13R 356751E 3532658N,
UTM Top: 13R 356445E 3532838N
Interval: 0-50 m
Base: Strike: 012, Dip: 45W
Thickness (m)
Para-sequence
Lithology
Texture
Siliciclastic
Carbonate
clay
silt
vf
f
m
c
mds
wks
pks
gs
bs
bls
Sample
Grain types: skeletal and non skeletal
Sedimentary structures
Description
45m
40m
35m
30m
25m
20m
15m
10m
5m
Middle ramp
Intertidal
Middle ramp
Intertidal
Middle ramp
Intertidal
TM-11
Green algae, echinoid fragments, brachiopods, forams, ostracodes, peloids, ooids
Laminated, bioturbated
Laminated peloid foram grainstone, dark gray (f & w), laminated faintly, bedded chert at base, chert disappears after first 3 m
TM-10
Crinoid columnals, brachiopods, chert, intraclasts, siliceous sponge spicules
Massive, faint laminations
Crinoid brachiopod packstone, dark gray (f), tan to light gray (w), elongate intraclasts, bedded chert
Brachiopods
Poorly exposed
Brachiopod packstone, dark gray (f), light gray (w), silicified skeletal fragments
TM-9
Brachiopod fragments, chert
Laminated
Dolomudstone, light gray (w), dark gray (f), micritic, poorly exposed
Covered interval
Brachiopod fragments, chert
Laminated dolomudstone, light gray (w), dark gray (f) micritic, transition from grainstone below, laminations become darker up section, silicified skeletal grains
Intraclasts, peloids
Peloid intraclast grainstone, dark gray (f & w), some light gray matrix in places
TM-8
Intraclasts, peloids
Laminated
Laminated ostracode wackestone, light gray (w), dark gray (f) micritic, transition from grainstone below, laminations become darker up section
TM-7
Intraclasts, peloids
Laminations
Peloid intraclast grainstone, dark gray (f & w), some light gray matrix in places
TM-6
Chert, intraclasts
Mottled
Dolomudstone, light to medium gray (f & w)
TM-5
Peloids, intraclasts
Laminated, poorly exposed
Fenestral dolomudstone, tan (w), tan to pink (f), calcareous
TM-4
Brachiopods, gastropods
Bioturbated
Brachiopod wackestone to packstone, light to medium gray (w), dark gray (f), grades into wackestone with less fossils
Covered interval
TM-3
Phylloid algae, brachiopods
Stylolites
Phylloid algal boundstone, light gray (w), medium gray (f), interbedded brachiopod packstones (2 cycles)
Laminated
Dolomudstone, light gray (w), dark gray (f), micritic, poorly exposed
Brown orange chert, fine-grained quartz sand
Sand filled burrows
Sandy mudstone, light gray (w), dark gray (f), stylolites, becomes sandy up section,
Brachiopods, large brachiopod spines, echinoids, chert, fusulinids
Fossiliferous packstone, light gray (w), medium gray (f), lenses of chert fragments
Covered interval
Intraclasts
Laminated
Laminated dolomudstone, light to medium gray (w), dark gray (f), micritic
TM-2
Intraclasts, chert, brachiopods, peloids, ostracodes, fine-grained quartz sand
Fossiliferous packstone, medium to dark gray (f & w) grainy, few intraclasts and chert fragments
TM-1
Ostracodes, bivalves, chert, fine-grained quartz sand
Root structures
Ostracode wackestone, light to medium gray (w), dark gray (f), very micritic
Pennsylvanian Panther Seep Formation

Tom Mays Park Section, Franklin Mountains, Texas

UTM Base: 13R 356751E 3532658N,
UTM Top: 13R 356445E 3532838N

Interval: 50-100 m

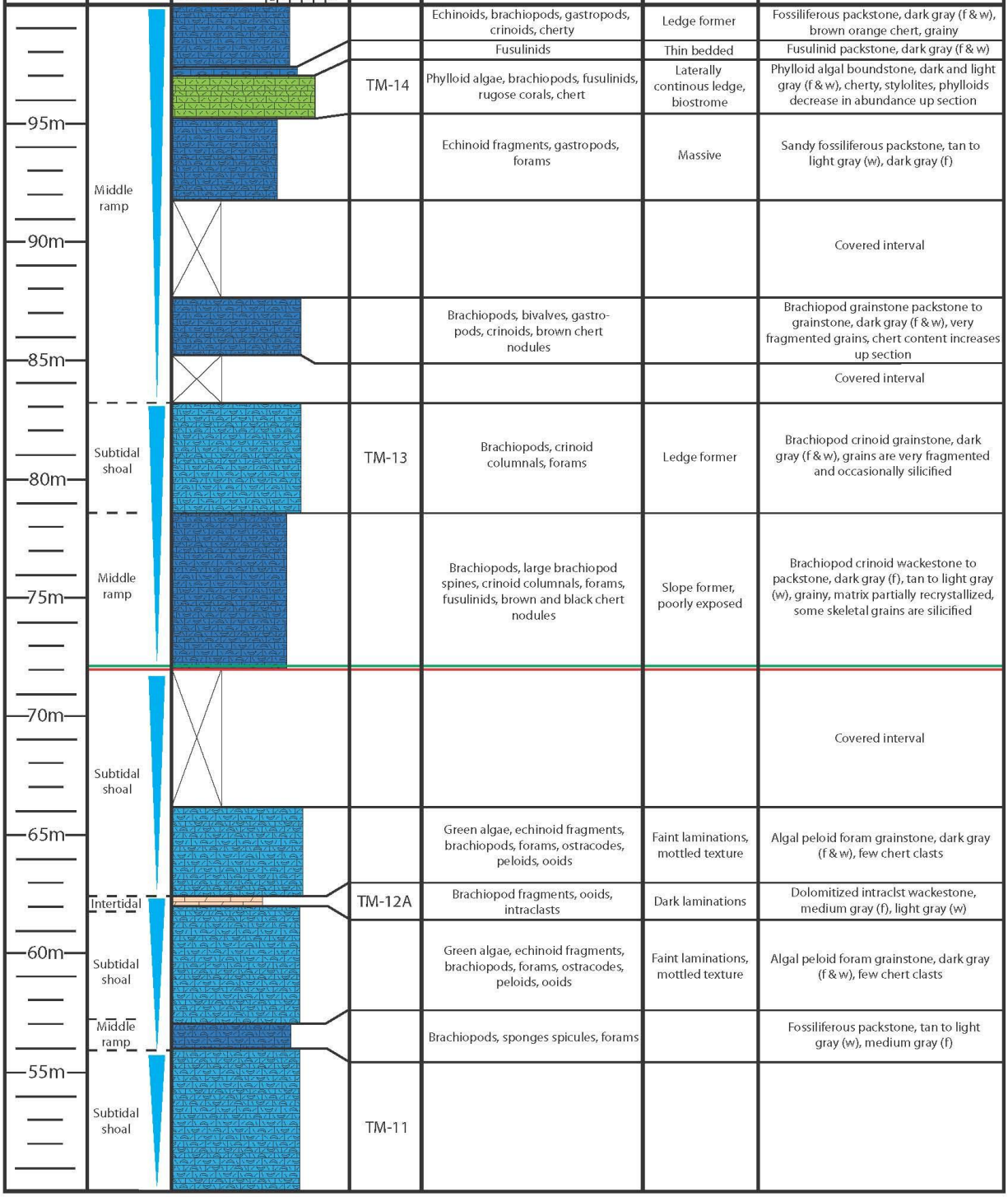

Tom Mays Park Section, Franklin Mountains, Texas

UTM Base: 13R 356751E 3532658N,
UTM Top: 13R 356445E 3532838N

Interval: 100-150 m

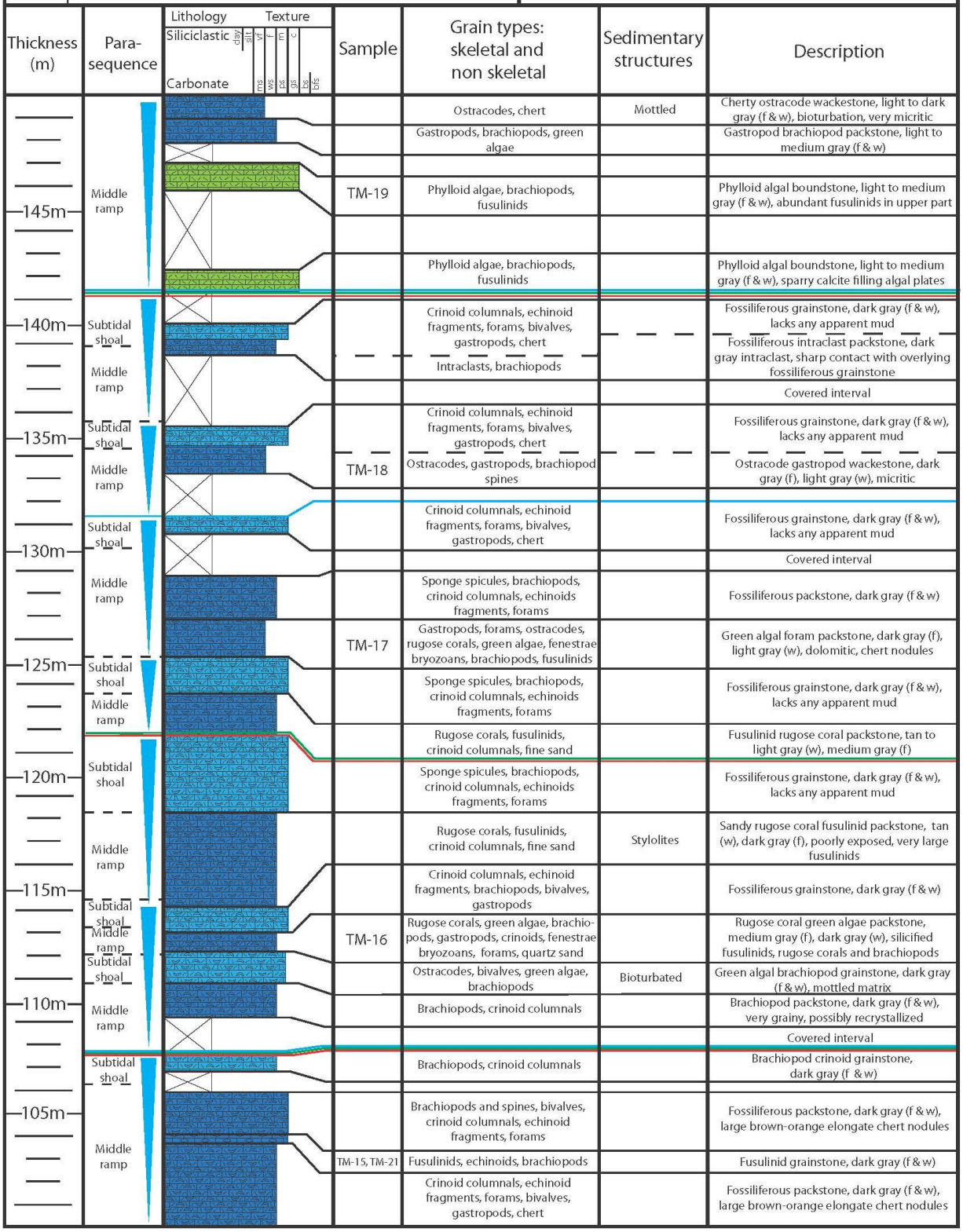

Tom Mays Park Section, Franklin Mountains, Texas

UTM Base: 13R 356751E 3532658N,
UTM Top: 13R 356445E 3532838N

Interval: 150-180m
Top: Strike: 018, 53W

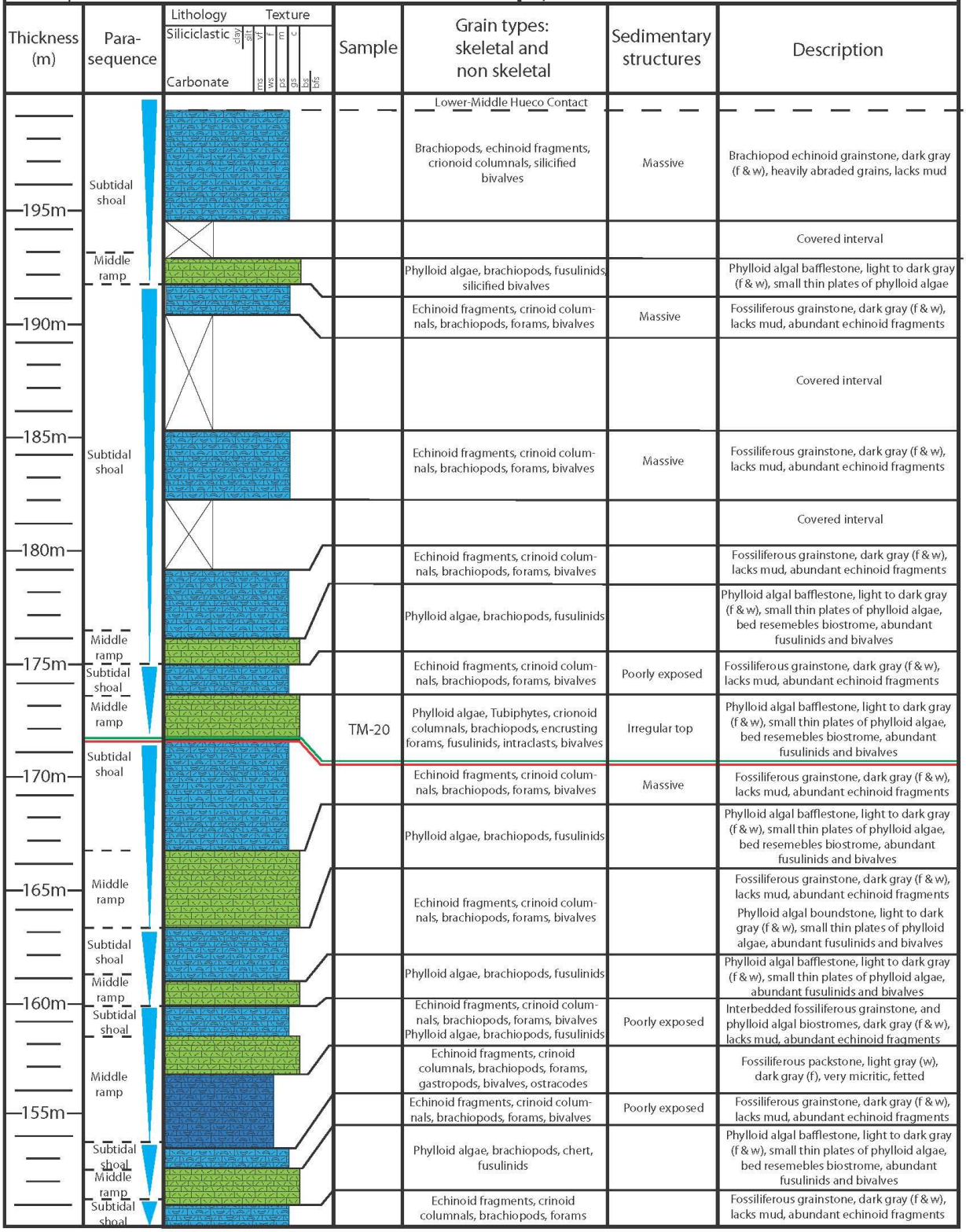

Thickness (m)	Para-sequence	Sample	Grain types: skeletal and non skeletal	Sedimentary structures	Description
			Lower-Middle Hueco Contact		
	Subtidal shoal		Brachiopods, echinoid fragments, crionoid columnals, silicified bivalves	Massive	Brachiopod echinoid grainstone, dark gray (f & w), heavily abraded grains, lacks mud
195m					Covered interval
	Middle ramp		Phylloid algae, brachiopods, fusulinids, silicified bivalves		Phylloid algal baffestone, light to dark gray (f & w), small thin plates of phylloid algae
			Echinoid fragments, crinoid columnals, brachiopods, forams, bivalves	Massive	Fossiliferous grainstone, dark gray (f & w), lacks mud, abundant echinoid fragments
190m					Covered interval
	Subtidal shoal		Echinoid fragments, crinoid columnals, brachiopods, forams, bivalves	Massive	Fossiliferous grainstone, dark gray (f & w), lacks mud, abundant echinoid fragments
185m					Covered interval
			Echinoid fragments, crinoid columnals, brachiopods, forams, bivalves		Fossiliferous grainstone, dark gray (f & w), lacks mud, abundant echinoid fragments
180m			Phylloid algae, brachiopods, fusulinids		Phylloid algal baffestone, light to dark gray (f & w), small thin plates of phylloid algae, bed resemebles biostrome, abundant fusulinids and bivalves
	Middle ramp		Echinoid fragments, crinoid columnals, brachiopods, forams, bivalves	Poorly exposed	Fossiliferous grainstone, dark gray (f & w), lacks mud, abundant echinoid fragments
175m	Subtidal shoal				
	Middle ramp	TM-20	Phylloid algae, Tubiphytes, crionoid columnals, brachiopods, encrusting forams, fusulinids, intraclasts, bivalves	Irregular top	Phylloid algal baffestone, light to dark gray (f & w), small thin plates of phylloid algae, bed resemebles biostrome, abundant fusulinids and bivalves
	Subtidal shoal		Echinoid fragments, crinoid columnals, brachiopods, forams, bivalves	Massive	Fossiliferous grainstone, dark gray (f & w), lacks mud, abundant echinoid fragments
170m			Phylloid algae, brachiopods, fusulinids		Phylloid algal baffestone, light to dark gray (f & w), small thin plates of phylloid algae, bed resemebles biostrome, abundant fusulinids and bivalves
	Middle ramp		Echinoid fragments, crinoid columnals, brachiopods, forams, bivalves		Fossiliferous grainstone, dark gray (f & w), lacks mud, abundant echinoid fragments Phylloid algal boundstone, light to dark gray (f & w), small thin plates of phylloid algae, abundant fusulinids and bivalves
165m					
	Subtidal shoal		Phylloid algae, brachiopods, fusulinids		Phylloid algal baffestone, light to dark gray (f & w), small thin plates of phylloid algae, abundant fusulinids and bivalves
	Middle ramp				
160m	Subtidal shoal		Echinoid fragments, crinoid columnals, brachiopods, forams, bivalves Phylloid algae, brachiopods, fusulinids	Poorly exposed	Interbedded fossiliferous grainstone, and phylloid algal biostromes, dark gray (f & w), lacks mud, abundant echinoid fragments
	Middle ramp		Echinoid fragments, crinoid columnals, brachiopods, forams, gastropods, bivalves, ostracodes		Fossiliferous packstone, light gray (w), dark gray (f), very micritic, fetted
155m			Echinoid fragments, crinoid columnals, brachiopods, forams, bivalves	Poorly exposed	Fossiliferous grainstone, dark gray (f & w), lacks mud, abundant echinoid fragments
	Subtidal shoal		Phylloid algae, brachiopods, chert, fusulinids		Phylloid algal baffestone, light to dark gray (f & w), small thin plates of phylloid algae, bed resemebles biostrome, abundant fusulinids and bivalves
	Middle ramp				
	Subtidal shoal		Echinoid fragments, crinoid columnals, brachiopods, forams		Fossiliferous grainstone, dark gray (f & w), lacks mud, abundant echinoid fragments

APPENDIX B

Tortugas Mountain Measured Stratigraphic Section

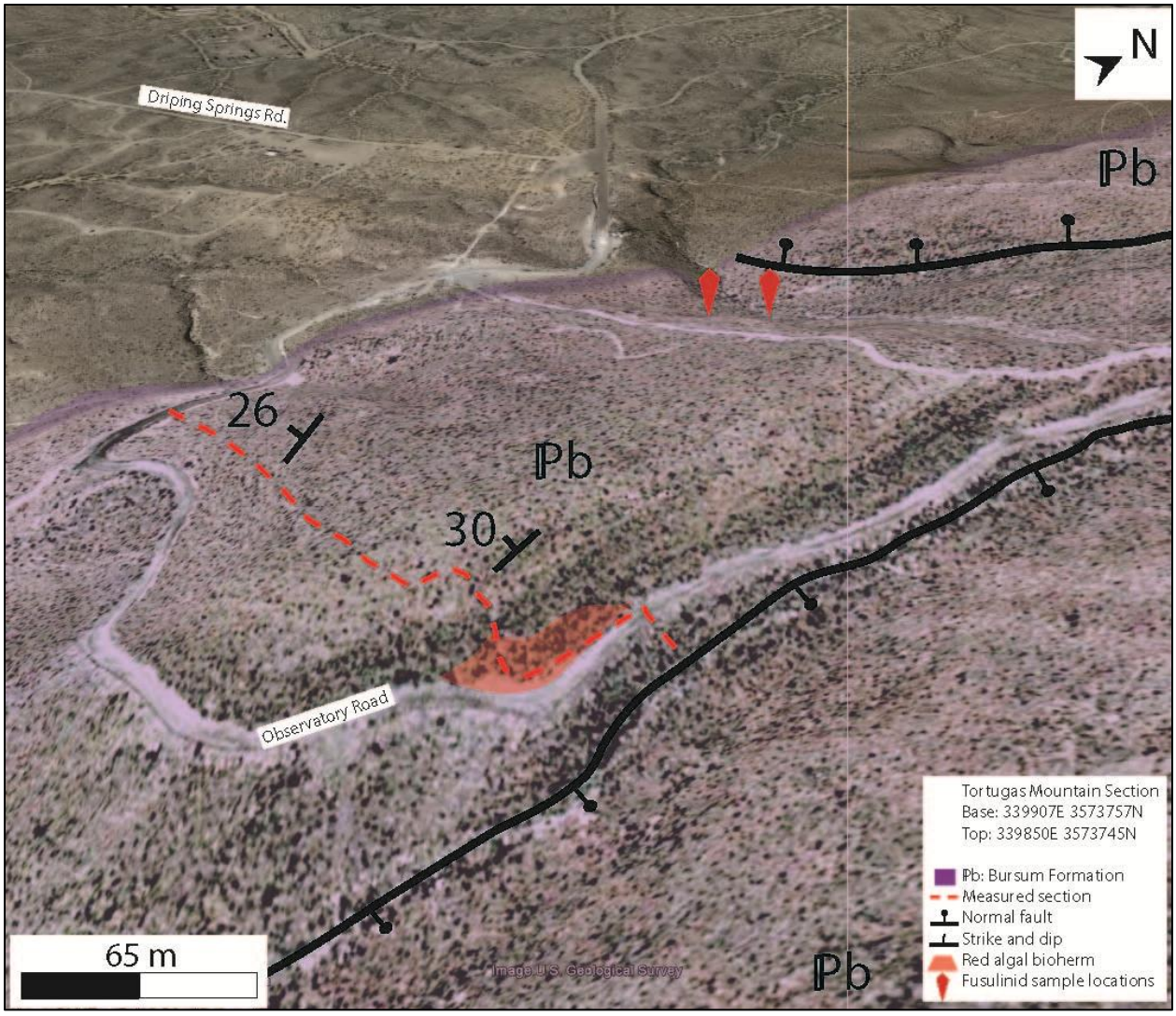

Oblique Aerial Photograph of the Tortugas Mountain Section Location.

Oblique aerial photograph overlain by the geologic units mapped by King and Kelley (1980), the transect of the measured stratigraphic section is shown by a red dashed line. Fusulinid samples were taken from the upper most beds at the base of the dip-slope and adjacent to another normal fault. Aerial photograph is courtesy of Google Earth.

Tortugas Mountain Measured Stratigraphic Section Key

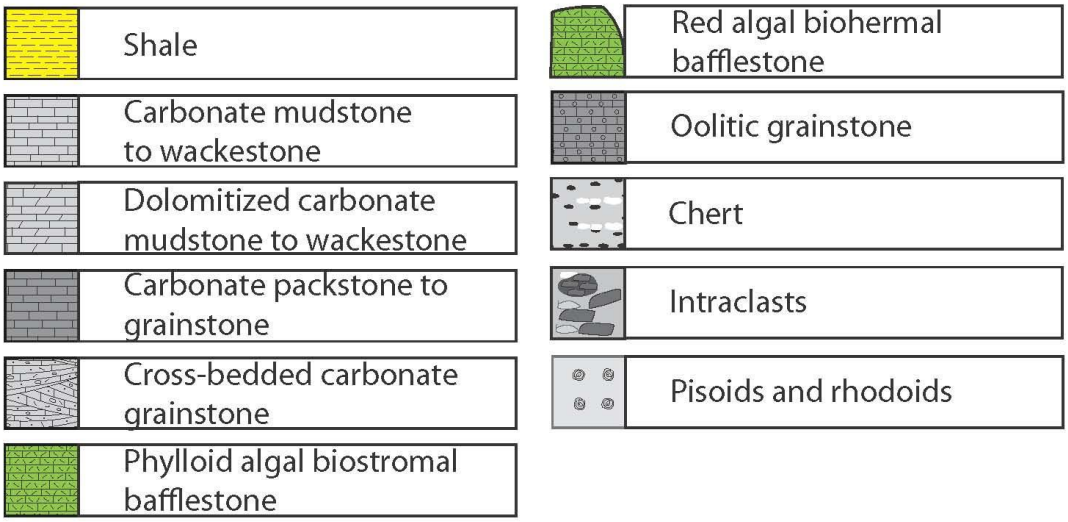

Tortugas Mountain Stratigraphic Section, Tortugas Mountain, New Mexico

UTM Base: 13S 339907E 3573757N ,
UTM Top: 339850E 3573745N

Interval 0 - 50 m
Measured by: Eric Stautberg and Evelyn Gannaway

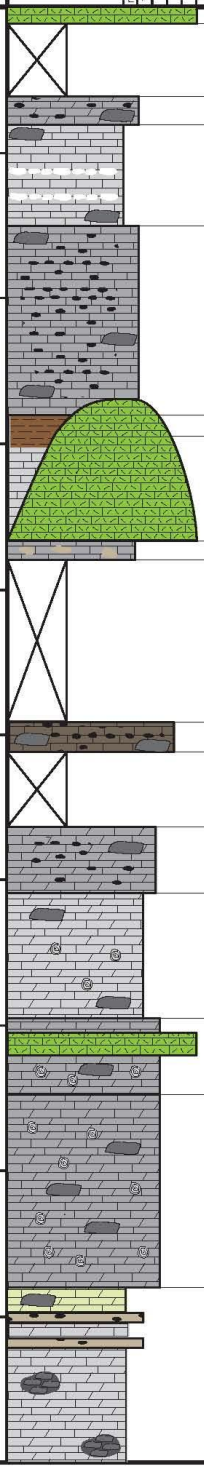

Height	Sample	Grain types: skeletal and non skeletal	Sedimentary structures	Description
				Covered interval: possible shaley interval
	A-14	Ostracodes, peloids, intraclasts		Medium gray (f),light gray (w), dolomitized
45m	A-13-B A-13-A	Chert, intraclasts	Bedded chert	Cherty mudstone, medium gray (f & w), two thin beds of white chert (10 cm thick), large blocky dark gray intraclasts in a light gray mud below chert, alternating dark and light layers 30-50 cm thick above chert
40m	A-12	Crinoid columnals, gastropods, peloids, intraclasts		Skeletal intraclast packstone, light gray (f), medium gray (w), becomes more grainy upsection, small chert fragments, some silicification of skeletal grains
			Thin bedded	Maroon, tan, gray fissle siltstone and shale
35m	A-11 A-10	Phylloid algae	Massive bioherm	Phylloid algal bioherm (bafflestone), dark gray (f & w), 4 m tall bioherm and roughly 30 m in length, vuggy porosity, onlapped but not overlapped by shale
		Chert		Small tan chert fragments
30m				Covered interval: road talus
25m	A-9	Peloids, intraclasts		Well sorted grains, (~.2 mm in diameter)
				Covered interval: road talus
	A-8	Bivalves, peloids, intraclasts	Thin muddy lenses	Bivalve intraclast packstone, medium gray (f & w), dolomitized, pebble sized intraclasts, heavily silicified
20m	A-7	Oncoids, intraclasts	Fenestral vugs filled with silica	Oncoid intraclast wackestone, medium gray (f & w), dolomitic, quartz cement
15m	A-6	Phylloid algae, peloids		Oncoid intraclast packstone with laminated peloidal algal bafflestone, micritized intraclasts, botryoidal cement
	A-5	Gastropods, oncoids, intraclasts	Wavy laminations	
10m	A-4	Crinoid columnals, bivalves, gastropods, oncoids, intraclasts	Light gray mottling throughout	Skeletal oncoid packstone, light gray (f & w), small disarticulated skeletal grains, granule-pebble sized intraclasts, botryoidal cement filling intraparticle porosity within oncoids
5m	A-3	Intraclasts		Dolomitic intraclast mudstone, light gray (f), medium gray (w) intraclast lenses near base, thin beds of intraclast and peloid wackestones overlain by a tan dolomudstone
	A-2	Forams, ostracodes, peloids intraclasts	Thin bedded	
	A-1	Intraclasts	Intraclast lenses	

Tortugas Mountain Stratigraphic Section, Tortugas Mountain, New Mexico

UTM Base: 13S 339907E 3573757N ,
UTM Top: 339850E 3573745N

Interval 50 - 77 m
Measured by: Eric Stautberg and Evelyn Gannaway

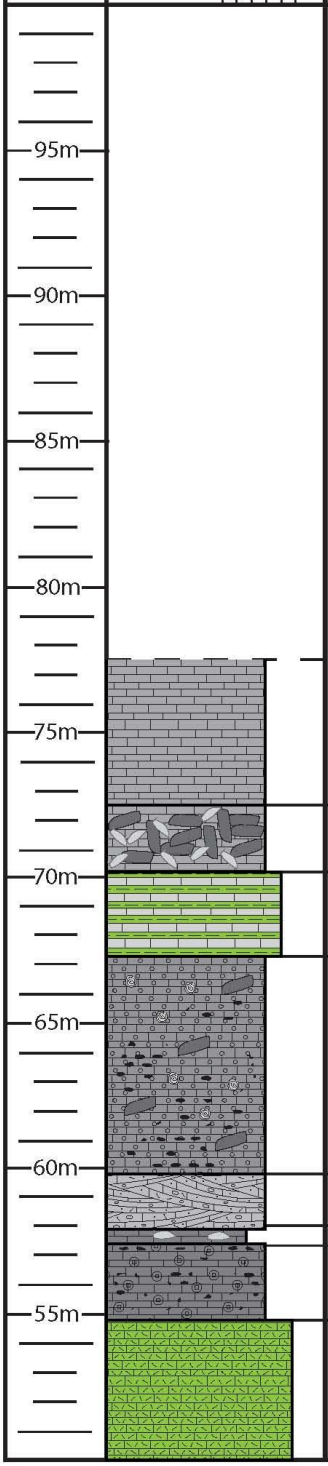

Sample	Grain types: skeletal and non skeletal	Sedimentary structures	Description
			Wackestone, medium gray (w), dark gray (w), grainy beds that become difficult to follow down the dip slope, grades into possible fusulinid bearing beds, dolomitized
	Intraclasts, rip-up clasts		Intraclast grainstone, large pebble sized intraclast, very angular,clasts range in color from light, medium, and dark gray
A-21	Cyanobacteria mats, echinoid fragments, rugose corals, ostracodes, peloids	Algal laminations, fenestral vugs, thin peloidal beds	Oolitic skeletal grainstone, medium gray (w), dark gray (f), thin algal laminations
A-20 A-19 A-18	Peloids, ooids, pisoids, intraclasts, crinoid columnals, echinoid fragments	Medium bedded, rip-up clasts, thin wavy laminations	Non-skeletal grainstones with thin beds of algal laminites, medium and light gray (f & w), micritized grains with algal coatings
A-22	Echinoids, ostracodes, peloids, ooids, intraclasts	Ripple cross-laminations, swaley	Oolitic grainstone, light gray (f & w), botryoidal fibrous cements
A-17	Ostracodes, peloids, intraclasts		Light gray (f & w), appears dolomitized
A-16-B A-16-A			Pisoid oncolite grainstone, dark gray muddy matrix, medium gray non skeletal grains
A-15	Phylloid algae	Massive bafflestone, fenestral vugs	Phylloid algal bafflestone, dark gray (w), medium gray (f), vugs filled with silica

CURRICULUM VITA

J. Eric Stautberg was born in Houston, Texas as the second son of Frank and Kathy Stautberg. He graduated from Foster High School in Richmond, Texas in the spring of 2006 and began attending Texas A&M University in College Station, Texas in the fall of 2006. He completed his Bachelors of Science in Engineering Geology in December of 2010. In the spring of 2011, Eric was nominated for and received the National Association of Geologic Teachers Field Internship through the United States Geological Survey. During the summer of 2011 he interned with the United States Geological Survey in Portland, Oregon in their Portland Field Office. In the fall of 2011, Eric began his Masters at New Mexico State University in Las Cruces, New Mexico. After 1 year at NMSU, Eric transferred to The University of Texas at El Paso in the fall of 2012 to continue his Master's degree. He completed his Masters of Science in Geological Sciences in December of 2013 and now works for the Anadarko Petroleum Corporation in Houston, Texas as an exploration geologist.

Permanent Address: 3405 N Shepherd
Apartment #905
Houston, Texas, 77018